DEVELOPMENT OF NEW MATERIALS FOR APPLICATIONS IN LIQUID CRYSTAL TECHNOLOGIES AND BIOFUEL PRODUCTION

Nicholas A. Zafiropoulos

A dissertation submitted to the faculty of the University of North Carolina at Chapel Hill in partial fulfillment of the requirements for the degree of Doctor of Philosophy in the Department of Chemistry.

Chapel Hill
2008

Approved by:

Professor Wenbin Lin

Professor Edward T. Samulski

Professor Michel R. Gagné

Professor Cynthia K. Schauer

Professor Sergei S. Sheiko

ABSTRACT

Nicholas A. Zafiropoulos: Development of New Materials for Applications in Liquid Crystal Technologies and Biofuel Production

(Under the direction of Wenbin Lin and Edward T. Samulski)

This work encompasses three distinct materials chemistries: solid support catalysts for biodiesel production, synthesis of molecular based liquid crystals for improved applications in liquid crystal display technologies, and mesoscopic behavior of high aspect ratio nanoscale metal-organic framework particles.

The production of biodiesel from waste biomass by the traditional two-step acid/base sequence is a costly and inefficient process. Solid supported acid catalysts were fabricated to reduce the free fatty acid content in waste greases in a process not requiring intensive and costly neutralization and aqueous workups. A high free fatty acid to methyl ester conversion was obtained for a variety of diarylammonium salts that served as homogeneous acid catalysts. The diarylamine was functionalized with appropriate moieties to enable incorporation into mesoporous silicas MCM-48 and SBA-15 as well as a more hydrophobic porous organic polymer. The efficacy of these heterogeneous acid catalysts was tested with greases containing up to 40 wt% free fatty acid and found to have greater than 98%

conversions. When combined with solid base catalysts, we were able to produce biodiesel in 99% yield from a high free fatty-acid containing feedstock.

Several 2,5-disubstituted oxadiazole based bent-core molecules were synthesized to explore new potential structures for biaxial nematic liquid crystals at room temperature. Structure-function behaviors dictated the thermal behaviors of these molecules measured using heat-stage facilitated optical microscopy and differential scanning calorimetry. Lower melting mesogens were judiciously chosen for exploration by sophisticated variable temperature ^{2}H-NMR experiments.

Lastly, Onsager predicted that anisotropic shapes could stabilize liquid crystalline behaviors. High aspect ratio metal-organic framework nanorods were synthesized and subsequently surface functionalized to minimize electrostatic and steric interparticle interactions. These particles were shown to self-assemble into nematic-like textures when subjected certain physical restraints on the macroscopic level. The ordered behavior was revealed through polarized luminescence studies dependent on the particles non-cubic crystalline space group.

ACKNOWLEDGEMENTS

It is a pleasure to thank the many people who made this thesis possible. Five years went a lot faster than envisioned when I first came to UNC, but being surrounded by great science, engaging faculty, and the tremendous support of my family and friends taught me to conquer and keep moving. At UNC I built a foundation for success.

I would like to sincerely thank my two advisors and friends, Professor Wenbin Lin and Professor Ed Samulski, for the opportunity to work in both of their labs. Wenbin's passion, diligence, acute sense for science, and late night chalkboard discussions kept me constantly thinking and developing new ideas. Ed's creativity, ambitiousness, and sophisticated and eloquent means of communicating science are just a few things I would like to develop for myself. Constantly juggling my time between two great mentors has only made me a stronger chemist and more importantly a stronger person.

I am indebted to Professor Lou Madsen at Virginia Tech for his ability to explain solid-state deuterium NMR as well as all the intricacies of an NMR probe. After spending many hours working on experiments together, I could not help but absorb his natural inquisition and genuine sincerity.

To Professor Theo Dingemans at the Delft University of Technology in The Netherlands I am incredibly thankful for our conversations on molecular liquid crystal design. His persistence and good humor are definitely contagious. Theo and Lou's curiosity in fact led

me to 12,000 feet atop a fairly steep rocky mountainside in Colorado and at the onset of a torrential down pour.

To Dr. Helen Ngo at the USDA I am very thankful for all her hard work in screening the designed catalysts for biodiesel production. Her analysis was integral to the success of this project.

My friends at UNC have really made my time here incredibly enjoyable, especially, Jason Kim, Dave Mihalcik, and Dee Jacobs. Jason is more than just my daily lunch partner; he is a great friend with lots of compassion. We pulled through a number of late nights in the lab, and though our projects are extremely different, I have learned so much from Jason inside and outside of Kenan B521. I can always count on Dave for traveling the many corners of the Triad to move other people's furniture. Dee has been another great friend since my first day at UNC. I attribute a lot of my organic chemistry knowledge to her.

Thanks to all my colleagues in the Lin and Samulski labs who have kept me in check with my work and allowed me the opportunity to learn from them.

I definitely want to thank Dana Holcomb for her love and support over these last four years. I thank you for making me get some much needed sleep, but most important for always being a trustworthy companion in life and keeping me grounded. Our time here has been exciting, and I look forward to what is in store for us after we leave Chapel Hill.

Lastly, I need to thank my family who has been there in support of me since I left for college nine years ago. They have more pride for me than I can imagine, and I thank them for their unending love and support.

TABLE OF CONTENTS

Page

LIST OF TABLES

Table

LIST OF FIGURES

Figure

LIST OF ABBREVIATIONS

5CB	4-cyano-4-*n*-pentylbiphenyl
AIBN	2,2'-azo-bis(isobutyronitrile)
BD	Biodiesel
BET	Brunauer, Emmett, Teller
BJH	Barrett, Joyner, Holenda
CaO	Calcium oxide
CD_3CO_2D	Acetic acid-d_4
$CDCl_3$	Chloroform-d_1
DCM	Dichloromethane
DG	Diglyceride
DMF	Dimethylformamide
DSC	Differential Scanning Calorimetry
DVB	1,4-Divinylbenzene
FAME	Fatty acid methyl ester
FFA	Free fatty acid
GC	Gas Chromatography
HMB	Hexamethylbenzene
HPLC	High Performance Liquid Chromatography

IR	Infrared Spectroscopy
K_2CO_3	Potassium carbonate
KOH	Potassium hydroxide
LB	Langmuir-Blodgett
LC	Liquid Crystal
LCD	Liquid Crystal Display
LLC	Lyotropic Liquid Crystal
MCM	Mobil Composition of Matter
MeOH	Methanol
MG	Monoglyceride
$MgSO_4$	Magnesium sulfate
mp	Melting point
MS	Mass Spectrometry
MSN	Mesostructured Networks
MW	Microwave
n	Director
N_B	Biaxial Nematic
NMOF	Nanoscale Metal-Organic Framework
NMR	Nuclear Magnetic Resonance
OLA	Oleic acid
POP	Porous organic polymer
PS	Polystyrene
PVA	Phenyl(vinyl-anilinium)

PVP	Poly(vinyl-pyrrolidone)
*rac*BINAP	2,2'-bis(diphenylphosphino)-1,1'-binaphthyl (racemic)
S	Order parameter
S_A	Smectic A
SBA	Santa Barbara Amorphous
S_C	Smectic C
SEM	Scanning Electron Microscopy
TBBA	Terephthal-bis(*p*-butylaniline)
*t*Boc	*tert*-butyloxycarbonyl
TEM	Transmission Electron Microscopy
TEOS	Tetraethyl orthosilicate
TfOH	Triflic acid
TG	Triglyceride
T_g	Glass transition temperature
TGA	Thermogravimetric Analysis
THF	Tetrahydrofuran
TLC	Thin Layer Chromatography
USD	US Dollar
UV	Ultraviolet
XRD	X-ray Diffraction
η	Biaxiality

CHAPTER 1

Homogeneous Esterification of Fatty Acids Using Diarylammonium Salts as Acid Catalysts

1.1 Biodiesel: History and Fundamentals

Biodiesel (BD) is defined as the simple methyl or ethyl esters of fatty acids that are typically derived from vegetable oils, animal fats, and waste greases. BD is an attractive alternative to petroleum diesel because of its lower viscosity and therefore improved engine performance. It is also considered a biodegradable and environmentally benign fuel. These advantages allow BD to transition into unmodified diesel engines and heating systems either in its neat form (B100) or as a blend with petroleum diesel. BD also reduces carbon monoxide and hydrocarbon particulates from diesel engine emissions.[1] The net-lifecycle carbon dioxide emissions from BD are about 60% less than its fossil derived counterpart since it is naturally produced from atmospheric carbon dioxide via photosynthesis.[1, 2] In comparison to fuel ethanol, another alternative fuel produced from corn and other starch-rich materials, BD production results in a lower release of nitrogen, phosphorus, and pesticide pollutants per net energy gain and is estimated to have a higher energy yield.[1]

Although biodiesel has been popularized only over the past decade as result of rising energy costs, the transesterification of vegetable oils (triglycerides) has been known for nearly 150 years by the work of Duffy and Patrick in the early 1850s. Rudolf Diesel, a

German inventor and mechanical engineer, displayed the first diesel engine powered by peanut oil at the World Fair in Paris, France in 1900. Rudolf Diesel was an environmentally conscious visionary as he noted in 1912, "the use of vegetable oils for engine fuels may seem insignificant today but such oils may become, in the course of time, as important as petroleum and the coal-tar products of the present time."

The petroleum industry is undeniably vital to the world's civilization, where total world consumption totals 30 billion barrels (4.8 km^3) of oil per year. The United States consumed 24% of the world's oil in 2004, and as nations become increasingly more developed over the coming years, the demand for oil will continue to rise. Petroleum is not only the most important fuel source but also provides feedstocks for a variety of important commodities such as plastics. This non-renewable natural resource is predicted to run out within the current century with the only temporary solution being exploration to untapped, accessibly challenged regions. Ultimately, this has driven these industries as well as the fuels industry to explore alternative, more natural raw materials. Biodiesel, the methyl or ethyl esters of short chain aliphatic fatty acids, is the best alternative to petroleum diesel, having a high boiling point and low vapor pressure. Similar to petroleum diesel, BD has a flash point of ~150 °C and a density of ~ 0.88 g/cm^3. This density is comparable to petroleum diesel. Overall, BD gives better lubricity and combustion, eventually leading to higher engine energy output.

The simplest method of producing biodiesel is by the direct transesterification of feedstocks comprised entirely of triglycerides (TG) with methanol in the presence of an acid, base or enzyme (lipase) catalyst to afford fatty acid methyl esters (FAME) and glycerol (Figure 1.1).[3] Currently, the most common commercial process for BD production is the

base-catalyzed transesterification of a refined vegetable oil with methanol. The vegetable oil feedstock is estimated to account for ~75% of the final BD cost,[4] which presently makes BD economically uncompetitive with petroleum diesel. To improve its economic competitiveness, one approach is to use less-expensive feedstocks such as waste-cooking oils or greases for the production of BD.[5]

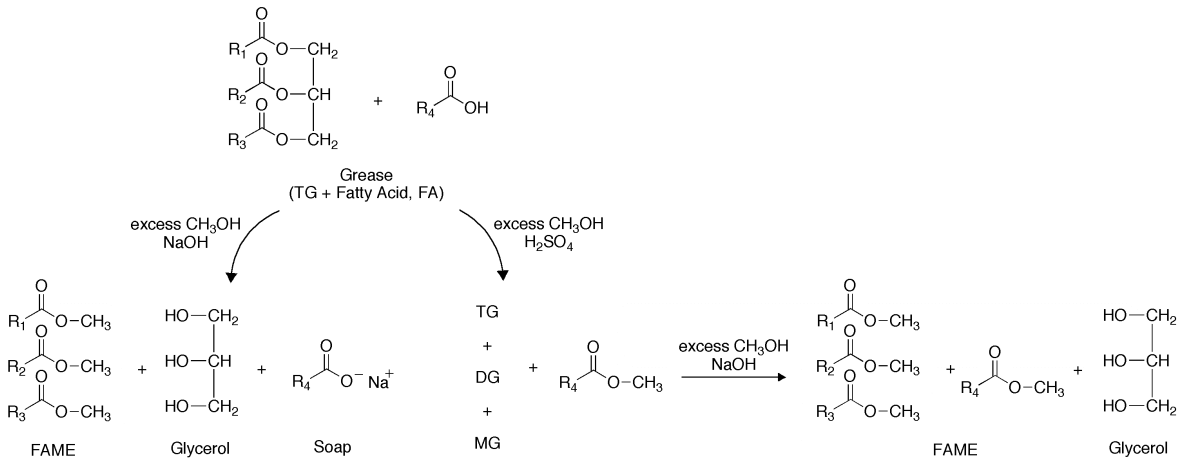

Figure 1.1. Acid- and base catalyzed esterification reactions.

Greases typically are composed of TG, diglycerides (DG), monoglycerides (MG), and free fatty acids (FFA) (8 – 40 wt%), and are categorized as either yellow (8 – 12 wt% FFA) or brown greases (>35 wt% FFA).[6] Yellow and brown greases are used as animal feeds, but this practice has been curtailed with the advent of mad cow disease in North America and Europe. As a result, there are mandates that all greases be disposed of properly or used in ways that pose no danger to human or animal health. One approach to their use is to convert this grease to biodiesel fuels. The FFA in greases, however, present a major problem in the base-catalyzed transesterification process since the FFA react with the base catalyst to form soaps, commonly referred to as the saponification reaction. This reaction process leads to loss of catalyst, ester product, and increase in processing costs.[7, 8]

In 2001, Canakci *et al*.[9] reported that grease feedstocks could be used for BD production after an aqueous acid pretreatment step that reduced the FFA content in the greases to <1 wt%. They first esterified the FFA to FAME with either ethanol or methanol using sulfuric acid. The pretreated greases were then subjected to base-catalyzed transesterification reactions to afford FAME and glycerol. A large amount of base was required, however, to neutralize the acid catalyst remaining in the pretreated greases using this two-step process, which increases the production cost of BD from greases. Other acids including HCl, BF_3, and H_3PO_4 also were examined, but they did not work as well as sulfuric acid.[10] There thus is a need to develop efficient catalysts that can reduce the FFA content in greases (<1 wt %) and can be easily removed from the treated greases.

1.2 Introduction to Acid Catalyzed Esterification

An exhaustive list of acids has been used to catalyze the Fischer esterification transformation – an acid-catalyzed nucleophilic acyl substitution by an alcohol. Production of the alkyl ester is a reversible process, *i. e*. this equilibrium can shift to the left via ester hydrolysis with the stoichiometric amount of water produced by the forward reaction. Excess of alcohols are thus used to drive the equilibrium to the ester formation based on Le Châtlier's principle. Acid catalysts play dual roles in the esterification reactions: (1) acid-catalyzed addition of the alcohol to the carbonyl and (2) acid-catalyzed dehydration (Figure 1.2).

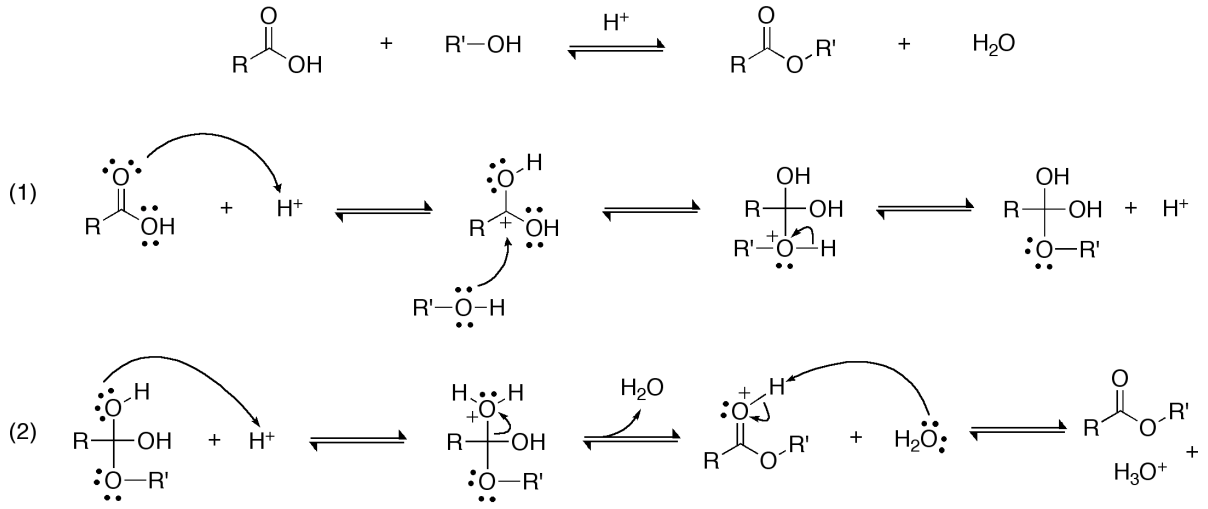

Figure 1.2. Key steps in acid-catalyzed Fischer esterification reactions.

A recent report by Tanabe *et al*. showed that diphenylammonium triflate (DPAT) and its bulkier derivatives catalyzed the esterification of carboxylic acids with equimolar amounts of sterically hindered alcohols in high yields.[11] Additionally, they have shown that azeotropic removal of water over the course of the reaction is not necessary to obtain high conversion. Ishihara *et al*. later reported a series of bulky diarylammonium arenesulfonates as mild yet highly active dehydrative ester condensation catalysts.[12, 13] Examples of the bulky diaryl-ammonium pentafluorobenzenesulfonates and tosylates are illustrated in Figure 1.3. The acidity of these salts arises from its superacid (pK_a (CD_3CO_2D) = -0.74) and weak base components.

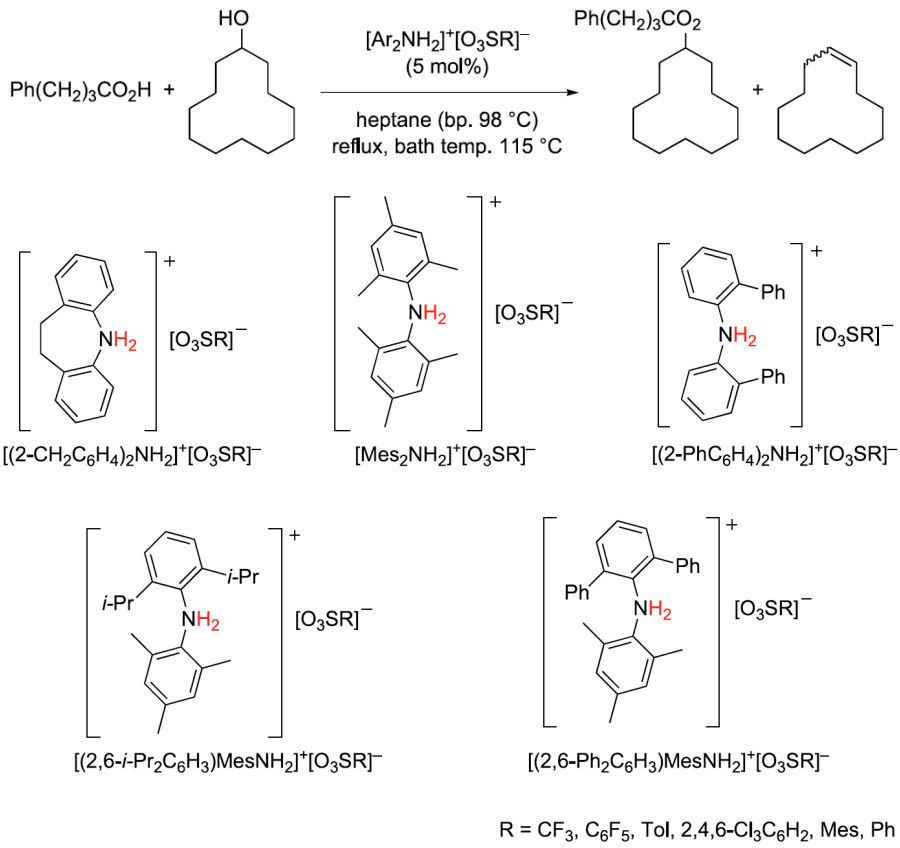

Figure 1.3. Diarylammonium salt catalyzed esterification of carboxylic acid with cyclic alcohol and structural examples of some bulky diarylammonium salts.

We have examined the use of such diarylammonium salts as catalysts for converting the FFA in greases to FAME. Structures of these homogeneous diarylammonium salts are shown in Figure 1.4. The homogeneous diarylammonium catalysts were shown to be highly efficient in reducing the FFA content of the grease to 0.5 – 1 wt%. We also incorporated these diarylammonium catalysts into insoluble porous polymers via free radical initiated polymerization and showed that the immobilized diarylammonium catalysts (see Chapter 2) are as effective as their homogeneous counterparts in reducing the FFA in greases. Once the FFA content of the greases was reduced to <1 wt%, the heterogeneous catalysts were removed by centrifugation and the greases were then subjected to base-catalyzed

transesterification.[12, 13] The work demonstrates the utility of diarylammonium catalysts in reducing the FFA content in greases and represents a promising alternative approach for the production of biodiesel from FFA containing feedstocks.

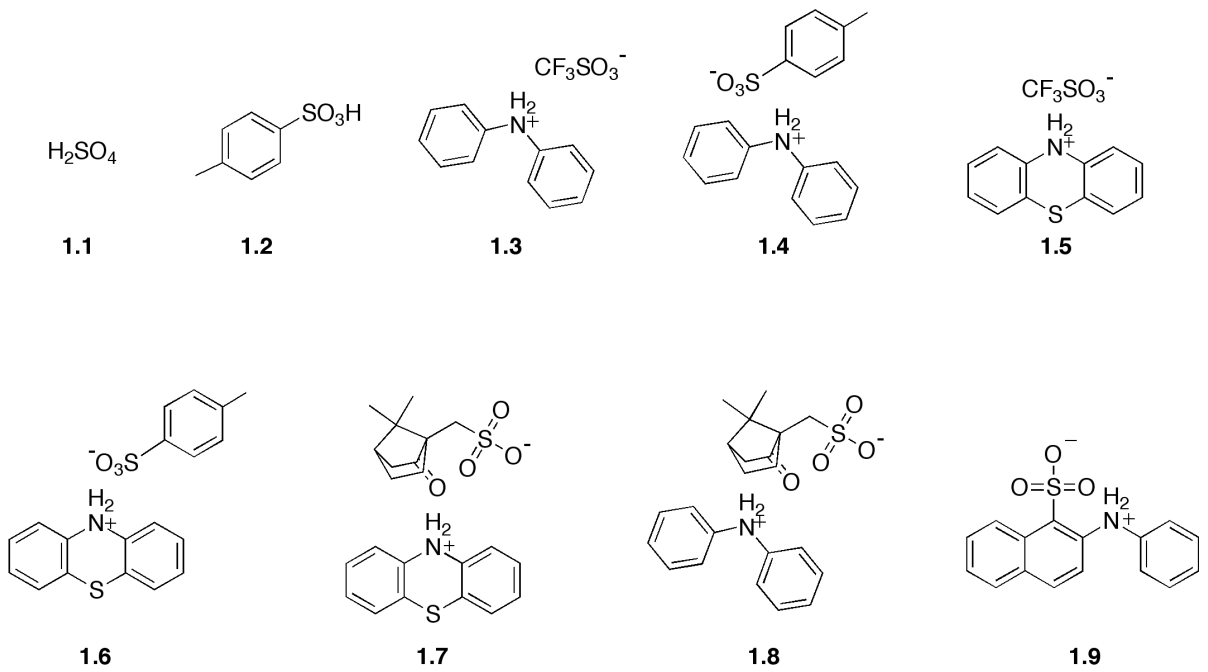

Figure 1.4. Structures of homogeneous diarylammonium catalysts.

1.3 Esterification of Oleic Acid Using Diarylammonium Catalysts

A series of diarylammonium salts **1.3** – **1.9** (Figure 1.4) was synthesized and tested as catalysts for the esterification of oleic acid with methanol. The newly synthesized catalysts were characterized by ^{1}H and ^{13}C NMR spectroscopy and their melting points determined. As shown in Table 1.1, oleic acid was effectively esterified in the presence of the arylammonium catalysts to afford methyl oleate. In general, the ammonium triflate salts **1.3** and **1.5** (Table 1.1) appear to be the more active catalysts. At a 0.5 mol% loading of **1.3** and **1.5**, oleic acid was esterified to methyl oleate >98% conversion with 2 equiv. of methanol at 95 °C in 2 h. On the other hand, the diarylammonium *p*-toluene sulphonate salts were less

effective esterification catalysts. For example, diphenylammonium tosylate (**1.4**) and phenothiazine tosylate (**1.6**) gave conversions of 93% and 80%, respectively, under identical conditions. We also examined other types of arylammonium compounds such as phenothiazinium camphorsulfonate (**1.7**), diphenylammonium camphorsulfonate (**1.8**), and 2-phenylamino-naphthalene-1-sulfonic acid (**1.9**). Oleic acid conversions to methyl oleate with catalysts **7** and 8 were only 77% and 87%, respectively, while **1.9** was ineffective.

Table 1.1. Esterification of Oleic Acid with Homogeneous Catalysts[a]

		wt% by HPLC	
Entry	catalyst (0.5 mol% loading)	methyl oleate	oleic acid
1	H_2SO_4 (**1.1**)	65	35
2	*p*-toluene sulphonic acid (**1.2**)	81	19
3	diphenylammonium triflate (**1.3**)	99	1.0
4	diphenylammonium tosylate (**1.4**)	93	7.1
5	phenothiazinium triflate (**1.5**)	98	2.0
6	phenothiazinium tosylate (**1.6**)	80	20
7	phenothiazine camphorsulfonate (**1.7**)	77	23
8	diphenylammonium camphorsulfonate (**1.8**)	87	13
9	2-Phenylamino-naphthalene-1-sulfonic acid (**1.9**)	4.5	95

[a] All reactions were performed with oleic acid (90% purity) and 2 equiv. of MeOH at 95 °C for 2 h.

For comparison, we also carried out control esterification experiments using sulfuric (**1.1**) and *p*-toluene sulphonic acid (**1.2**) as catalysts under the same conditions, obtaining 65% and 81% conversions, respectively. It was thus encouraging to find that the diarylammonium

catalysts **1.3** – **1.6** gave significantly higher esterification conversions than acids more commonly used as esterification catalysts.

Figure 1.5 shows the oleic acid to methyl oleate conversion curves catalyzed by the diarylammonium catalysts **1.3**, **1.5**, and **1.6** versus sulfuric acid. Since the diarylammonium tosylate compounds did not work as well as their triflate counterparts, we only examined the conversion profile for catalyst **1.6**, which gave the best yields for this catalyst type (Table 1.1). The reactions were performed with 1 mol% catalyst and 1 equiv. of methanol at 75 °C. Aliquots of the reactions were sampled to determine the percent conversion every 5 minutes over the first 2 h reaction and hourly thereafter. Figure 1.5 shows that the diarylammonium catalysts are highly active and the percent conversions varied with catalyst type. After 5.5 hours of reactions, catalyst **1.1**, **1.3**, **1.5**, and **1.6** gave a conversion of 68.5%, 89.6%, 79.1%, and 75.5%, respectively. The activities follow the trend of diphenylammonium triflate > phenothiazinium triflate > phenothiazinium tosylate > H_2SO_4. The arylammonium catalysts thus not only give higher conversions but also are more active than sulfuric acid.

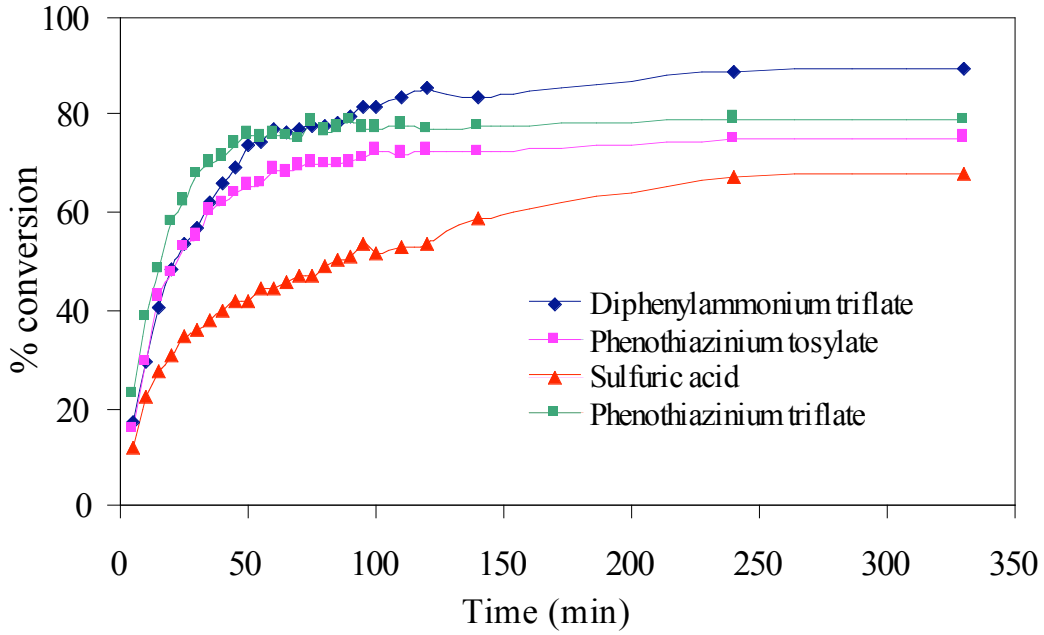

Figure 1.5. Oleic acid to methyl oleate conversion curves for different catalysts at 1 mol% loadings. All of the reactions were performed with 1:1 molar ratio of oleic acid and MeOH at 75 °C.

1.4 Homogeneous Diarylammonium-Catalyzed Esterification of FFA in Grease

Esterification experiments were carried out with greases containing 12 wt%, 21 wt%, and 40 wt% FFA. The reactions were run with different catalysts at various loadings and molar ratios of methanol. As shown in Table 1.2, for grease containing 12 wt% FFA, catalysts **1.3** – **1.6** gave a conversion of FFA to FAME of between 90 – 99% after a reaction time of 2 h at 95 °C. The conversion obtained with the ammonium catalysts is comparable to those obtained using sulfuric acid under similar conditions (Table 1.2). A catalyst loading of 2 to 3 mol% was needed to reduce the FFA content down to an acceptable level (<1 wt%). For example, using 10 equiv. of methanol and a 2 and 2.5 mol% catalyst loadings of **1.3** resulted

in a FFA conversion to FAME of 90% and 94% (with 1.2% and 0.73% FFA remaining), respectively (entries 3 and 6 in Table 1.2). As shown in Table 1.2 there also were minor changes in the glyceride composition of the grease when using these catalysts under the esterification conditions used in this study.

Table 1.2. Esterification of the FFA in Greases (12 wt% FFA) to FAME using Homogeneous Catalysts[a]

			percent composition by HPLC					
Entry	catalyst (mol% loading)	MeOH (eq.)[c]	FAME	FFA	TG	DG	MG	% conv. of FFA[d]
1	No catalyst	---	0	12	66.0	20.4	1.6	---
2	**1.1** (2.5)	10	18.3	0.9	54.8	22.4	3.6	93
3	**1.3** (2)	10	17.9	1.2	56.7	20.8	3.4	90
4	**1.5** (2)	20	17.2	1.1	59.4	19.6	2.7	91
5	**1.6** (2)[b]	20	14.7	0.4	61.7	21.6	1.6	97
6	**1.3** (2.5)	10	20.1	0.7	55.7	19.4	4.1	94
7	**1.4** (2.5)[b]	20	3.20	14	56.2	22.6	4.0	0
8	**1.5** (2.5)	20	17.3	0.9	60.4	19.1	2.3	93
9	**1.5** (3)	5	21.0	1.0	52.9	21.6	3.5	92
10	**1.6** (3)[b]	20	17.4	0	59.5	20.4	2.7	>99

[a] All reactions were performed at 95 °C for 2 h.

[b] Grease was filtered with Celite before used.

[c] Number of equivalents relative to the FFA that is present in greases.

[d] % conversion = $(FFA^i - FFA^f)/(FFA^i \times 100)$; [i=initial, f=final].

Triflate catalyst **1.5** (Table 1.2) also reduced the FFA content of the grease to a negligible level when a 2.5 – 3 mol% catalyst loading was used. With 20 equiv. of methanol, 2 mol% and 2.5 mol% of **1.5** gave a FFA conversion to FAME of 91% and 93% (with 1.1% and

0.85% FFA remaining), respectively. At 3 mol% loading, **1.5** gave a FFA conversion of 92% FAME when only 5 equiv. of methanol was used (entry 9, Table 1.2). For the tosylate complexes **1.4** and **1.6** (entries 5 and 7), the greases needed to be filtered with Celite before use to remove unknown impurities that inhibited esterification. As shown in Table 1.2, in the presence of 20 equiv. of methanol and 2 and 3 mol % of catalyst **1.6** (entries 5 and 10) gave a conversion of FFA to FAME of 96% and >99%, respectively. Catalyst **1.4**, did not work well under similar conditions in that the conversion of FFA to FAME was only 35% (entry 7).

We also examined the esterification of FFA to FAME in grease that contained 21 wt% FFA using catalysts **1**, **3** and **6.** The FFA content in the untreated grease could be reduced to <1 wt% with the arylammonium catalysts. As shown in Table 1.3, catalyst **1.3** worked the best for the esterification of FFA to FAME in this grease matrix. At 2.5 mol% of catalyst **1.3,** a FFA conversion to FAME of 94% was obtained using 10 equiv. of methanol, while with 3 mol% of catalyst **1.3** gave a 91% conversion of FFA to FAME with 5 equiv. of methanol (entries 4 and 8, Table 1.3).

Table 1.3. Esterification of FFA in Greases (21 wt% FFA) to FAME using Homogeneous Catalysts[a]

Entry	catalysts (mol% loading)	MeOH (eq.)[b]	percent composition by HPLC					% conv. of FFA[c]
			FAME	FFA	TG	DG	MG	
1	No catalyst	---	0	21.4	40.3	30.2	8.9	---
2	**1.1** (2.5)	10	16.5	1.35	56.3	22.8	2.9	94
3	**1.1** (3)	10	28.3	1.94	34.2	29.3	6.3	91
4	**1.3** (2.5)	10	32.3	1.3	32.3	23.9	10	94
5	**1.4** (2.5)	10	2.0	22.6	33.9	34.2	7.3	---
6	**1.5** (2.5)	10	25	2.47	37.6	28.9	6.1	88
7	**1.6** (2.5)	10	6.0	18	40	31.2	4.8	16
8	**1.3** (3)	5	25.6	1.8	36.6	27.8	8.2	92
9	**1.4** (3)	20	6.35	25.1	32.7	29.7	5.6	---
10	**1.5** (3)	10	33.4	1.3	31.9	24.3	9.1	94
11	**1.6** (3)	10	20.1	4.9	38.5	29.9	6.6	77

[a] All reactions were performed at 95 °C for 2 h.

[b] Number of equivalents relative to the FFA that is present in greases.

[c] % conversion = $(FFA^i - FFA^f)/(FFA^i \times 100)$.

When brown grease (40 wt% FFA) was used as a substrate for the esterification process, the grease had to be first filtered through Celite before use. As shown in Table 1.4, excellent conversions of FFA to FAME in this substrate was obtained at 3 mol% catalyst loading of **1.3** – **1.6** and 20 equiv. of methanol. The diarylammonium triflate catalysts reduced the FFA content to < 1 wt%. These results clearly show the utility of diarylammonium salts in catalyzing the conversion of FFA to FAME in greases with high a FFA content.

Table 1.4. Esterification of FFA Greases (40 wt% FFA) with Various Homogeneous Catalysts[a]

Entry	Catalysts (mol% loading)	MeOH (eq.)[b]	HPLC wt. %					% conv. of FFA[c]
			FAME	FFA	TG	DG	MG	
1	no catalyst	---	0	40	31.6	25	3.4	---
2	**1.1** (3)	20	49.1	1.0	17.5	24.6	7.8	98
3	**1.3** (3)	20	44.8	0.7	28.6	22.1	3.8	98
4	**1.4** (3)	20	42.9	2.0	25.7	23.2	6.2	95
5	**1.5** (3)	20	45.1	0.8	28.3	22.0	3.8	98
6	**1.6** (3)	20	45.2	1.5	22.2	23.6	7.44	96

[a]All reactions were performed at 95 °C for 2 h and the grease was filtered with Celite before used.

[b] Number of equivalents relative to the FFA that is present in greases.

[c]% conversion = $(FFA^i - FFA^f)/(FFA^i \times 100)$.

1.5 Concluding Remarks

We have successfully synthesized a family of diarylammonium catalysts for the esterification of FFA in greases containing between 12 – 40% FFA. The catalysts were highly effective for the esterification of FFA in greases, reducing the FFA contents to <1%. We have also incorporated these diarylammonium catalysts into insoluble porous polymers via free radical initiated polymerization. The immobilized diphenylammonium triflate catalysts were nearly as effective as their homogeneous counterparts in reducing the FFA content in greases to <1%. The heterogeneous diarylammonium catalysts were readily removed from the treated greases, which were then directly converted to FAME in subsequent base-catalyzed transesterification reactions. This work thus demonstrates the

utility of diarylammonium salts as catalysts in reducing the FFA content in greases. The two step process represents a promising alternative approach for the production of BD from FFA containing feedstocks.

1.6 Experimental Section

Materials. Oleic acid (90%), methanol, diphenylamine, aniline, and triflic acid, methanolic sodium methoxide solution were purchased from Aldrich Chemical (Milwaukee, WI). 4-Bromostyrene was purchased from Alfa Aesar (Ward Hill, MA). All other reagents used were of the highest purity available as obtainable from commercial suppliers. Greases with high FFA were from Kaluzny Bros. Inc. and Arlington International Inc. (Irving, TX).

Instrumentation. GC analysis of FAME was carried out with a Hewlett Packard HP 5890 instrument (Agilent, Wilmington DE) equipped with a capillary inlet (on column mode) and an FID detector. The GC capillary columns used were a HP DB-1HT column (15 m × 0.25 mm × 0.25 μm) and a HP DB-5HT column (15 m × 0.25 mm × 0.25 μm) with He carrier gas set at a linear velocity of 22 cm/sec at 100 °C. The oven temperature profile was: initial temperature 50 °C, hold 1 min; ramp at 15 °C/min to 180 °C; ramp at 7 °C/min to 230 °C. Dodecane was used as an external standard. GC/MS characterization was carried out with a capillary inlet (split mode) and an HP Model 5972 mass detector set to scan from 40 to 550 m/z at a rate of 1.5 scans/s. The capillary column used was a HP DB-5 column (30 m × 0.25 mm × 0.25 μm) with He carrier gas. The pressure was set at 8.0 psi at 50 °C. The injector and detector transfer line temperatures were set at 260 and 280 °C, respectively. The oven temperature profile was: initial temperature 100 °C; ramp at 10 °C/min to 250 °C; hold for 5 min; ramp at 10 °C/min. to 300 °C hold for 5 min.

Lipid mixtures were analyzed by HPLC with a Hewlett Packard HP 1050 instrument (Agilent, Wilmington DE). The lipid mixtures were separated on a Spherisorb CN (100 × 3.0mm, 3μ) column using a normal phase gradient of hexane/0.4% acetic acid and methyl t-butyl ether/0.4% acetic acid at a constant flow of 0.43 mL/min. Eluants from the column were detected by an evaporator light-scattering detector (ELSD ILA; All-tech, Deerfield, IL). The ELSD nebulizer temperature was set at 40 ºC and the nitrogen flow of 35 mL/min. All peaks were quantitated from standard curves constructed with reference compounds.[14]

NMR spectra were recorded on Bruker NMR 400 DRX (Bruker Instruments, Billerica, MA) and Varian (Varian, Palo Alto, CA) Gemini 200-MHz spectrometer. The ^{1}H-NMR spectra were referenced to the proton resonance resulting from incomplete deuteration of the deuterated chloroform (δ 7.26) and deuterated acetone (δ 2.09). Infrared spectra were obtained on a Nicolet (Nicolet Instruments, Lanham, MD) Magna-IR 560 spectrometer. Microwave reactions were performed with a CEM Discover–LabMate (CEM, Matthews, NC) microwave reactor. Nitrogen adsorption experiments were performed on a Quantachrome-1C (Quantachrome Instruments, Boynton Beach, FL) surface area analyzer at liquid nitrogen temperature. All the surface areas and pore volumes were calculated based on the Barrett, Joyner, and Halenda (BJH) method.[15]

Synthesis and Characterization of Diarylammonium Compounds. General procedure: The sulfonic acid (10 mmol) was added to a solution of the arylamine (10 mmol) in toluene (~20 mL) at room temperature (r.t.) under a nitrogen flow. The reaction mixture was stirred for 15 min. and the precipitated solid filtered and washed with hexane (~125 mL) to give the arylammonium sulfonate salts (Figure 1) in >90% yield.

Diphenylammonium triflate (**1.3**): (mp 169 - 170 ºC). ^{1}H NMR ($CDCl_3$, 200 MHz): δ 7.45 (m, 10H). ^{13}C NMR ($CDCl_3$, 50 MHz): δ 136.6 (s), 130.6 (s), 130.2 (s), 123.2 (s). The spectroscopic data are consistent with the literature values.

Diphenylammonium tosylate (**1.4**): mp 128 – 130 °C. ^{1}H NMR ($(CD_3)_2CO$, 200 MHz): δ 7.74 (m, 4H), 7.29 (m, 8H), 6.86 (m, 2H), 2.39 (s, -PhC*H*$_3$, 3H). ^{13}C NMR ($(CD_3)_2CO$, 50 MHz): δ 143.5 (s), 142.5 (s), 141.3 (s), 131.6 (s), 130.3 (s), 129.9 (s), 127.3 (s), 125.6 (s), 122.9 (s), 119.4 (s), 21.4 (s, Ph*C*H$_3$).

Phenothiazinium triflate (**1.5**): mp 100 - 104 °C. ^{1}H NMR ($(CD_3)_2CO$, 200 MHz): δ 7.0 – 6.6 (broad peak, 8H). ^{13}C NMR ($(CD_3)_2CO$, 50 MHz): δ 154.7 (s, -*C*F$_3$), 128.2 (m), 124.2 (m), 118.2 (s), 115.5 (s).

Phenothiazinium tosylate (**1.6**): mp 85 - 88 °C. ^{1}H NMR ($(CD_3)_2CO$, 200 MHz): δ 7.78 (d, -C*H*=C*H*-, 2H), 7.4 (d, -C*H*=C*H*-, 2H), 7.0 – 6.6 (broad peak, 8H), 2.42 (s, -PhC*H*$_3$, 3H). ^{13}C NMR ($(CD_3)_2CO$, 50 MHz): δ 144.2 (s), 138.9 (s), 130.4 (s), 127.5 (s), 21.5 (s, Ph*C*H$_3$).

Phenothiazinium camphorsulphonate (**1.7**): mp 136 - 138 °C. ^{1}H NMR ($(CD_3)_2CO$, 200 MHz): δ 7.1 – 6.9 (broad peak, 8H), 3.3 (dd, J_{para} = 60.8 Hz & 20 Hz, 2H), 2.41 (m, 2H), 2.1 (m, 3H), 1.45 (m, 2H), 1.11 (s, -C*H*$_3$, 3H), 0.92 (s, -C*H*$_3$, 3H). ^{13}C NMR ($(CD_3)_2CO$, 50 MHz): δ 218.9 (s, *C*=O), 126 (m), 116 (m), 59.1 (s), 49.3 (m), 43.3 (m), 27.3 (s), 26.6 (s), 19.9 (m, -(*C*H$_3$)$_2$).

Diphenylammonium camphorsulphonate (**1.8**): mp 111 – 117 °C. ^{1}H NMR ($(CD_3)_2CO$, 200 MHz): δ 7.21 (m, 8H), 6.86 (m, 2H), 3.3 (dd, J_{para} = 60.8 Hz & 20 Hz, 2H), 2.45 (m, 2H), 2.0 (m, 3H), 1.45 (m, 2H), 1.12 (s, -C*H*$_3$, 3H), 0.90 (s, -C*H*$_3$, 3H). ^{13}C NMR ($(CD_3)_2CO$, 50 MHz): δ 213.9 (s, *C*=O), 143.9 (s), 131.6 (s), 130.1 (s), 125.7 (s), 122.1 (s), 118.8 (s), 59 (s), 48.7 (m), 43.2 (m), 27.4 (s), 25.9 (s), 20.1 (m, -(*C*H$_3$)$_2$).

2-Phenylamino-naphthalene-1-sulfonic acid (**1.9**): mp 220 – 240 °C. ^{1}H NMR ($(CD_3)_2CO$, 200 MHz): δ 6.83 (d, 1H), 6.4 (d, 1H), 6.12 (d, 1H), 5.87 (m, 3H), 5.72 (m, 4H), 5.44 (m, 1H). ^{13}C NMR ($(CD_3)_2CO$, 50 MHz): δ 143.5 (s), 140.5 (s), 138.3 (m), 137.4 (s), 134.5 (s), 130.6 (m), 129.7 (s), 127.3 (m), 125.8 (s), 125.2 (s), 124.1 (s), 121.1 (s).

2,6-dimethyl-N-(4-vinylphenyl)aniline. In a glove box a 10 mL thick-walled pressure vial equipped with silicone seal cap was charged with NaO^{t}Bu (0.139 g, 1.40 mmol), $Pd(OAc)_2$ (4.5 mg, 0.020 mmol), and *rac*BINAP (24.9 mg, 0.040 mmol). 2,6-Dimethylaniline (0.13 mL, 1.0 mmol), 4-bromostyrene (0.13 mL, 1.0 mmol), and distilled toluene (1 mL) were added via a syringe to the sealed tube, and the mixture was sonicated for 30 minutes. The reaction vessel was then subjected to microwave irradiation under the following conditions: power, 300 W; pressure, 100 psi; temperature, 140 °C; reaction time, 10 minutes. The color of the reaction mixture changed from red to dark brown. The mixture was diluted with ethyl acetate and filtered. The filtrate was concentrated in vacuo, and the residue was purified by flash column chromatography on SiO_2 using hexane and 50:1 hexane:EtOAc to give the desired product as a yellow oil (0.169 g, 75.9 %). ^{1}H NMR ($CDCl_3$, 400 MHz): δ 7.20 (d, 2H), 7.11 (d, 2H), 7.01 (d, 2H), 6.45 (t, 1H), 6.56 (q, 1H), 5.51 (d, 1H), 5.01 (d, 1H), 2.12 (s, 6H). MS m/z = 223.2 ([M^+]).

3,5-dimethyl-N-(4-vinylphenyl)aniline. In a glove box a 10 mL thick-walled pressure vial equipped with silicone seal cap was charged with NaO^{t}Bu (0.139 g, 1.40 mmol), $Pd(OAc)_2$ (4.5 mg, 0.020 mmol), and *rac*BINAP (24.9 mg, 0.040 mmol). 3,5-Dimethylaniline (0.13 mL, 1.0 mmol), 4-bromostyrene (0.13 mL, 1.0 mmol), and distilled toluene (1 mL) were added via a syringe to the sealed tube, and the mixture was sonicated for 30 minutes. The reaction vessel was then subjected to microwave irradiation under the following conditions:

power, 300 W; pressure, 100 psi; temperature, 140 °C; reaction time, 10 minutes. The color of the reaction mixture changed from red to dark brown. The mixture was diluted with ethyl acetate and filtered. The filtrate was concentrated in vacuo, and the residue was purified by flash column chromatography on SiO_2 using hexane and 50:1 hexane:EtOAc to give the desired product as a yellow oil (0.167 g, 74.8 %). ^{1}H NMR ($CDCl_3$, 400 MHz): δ 7.30 (d, 2H), 6.99 (d, 2H), 6.70 (s, 2H), 6.40 (q, 1H), 6.59 (s, 1H), 5.67 (d, 1H), 5.09 (d, 1H), 2.26 (s, 6H). MS m/z = 223.2 ([M^+]).

2,4,6-trimethyl-N-(4-vinylphenyl)aniline. In a glove box a 10 mL thick-walled pressure vial equipped with silicone seal cap was charged with NaO^{t}Bu (0.139 g, 1.40 mmol), $Pd(OAc)_2$ (4.5 mg, 0.020 mmol), and *rac*BINAP (24.9 mg, 0.040 mmol). 2,4,6-Trimethylaniline (0.14 mL, 1.0 mmol), 4-bromostyrene (0.13 mL, 1.0 mmol), and distilled toluene (1 mL) were added via a syringe to the sealed tube, and the mixture was sonicated for 30 minutes. The reaction vessel was then subjected to microwave irradiation under the following conditions: power, 300 W; pressure, 100 psi; temperature, 140 °C; reaction time, 10 minutes. The color of the reaction mixture changed from red to dark brown. The mixture was diluted with ethyl acetate and filtered. The filtrate was concentrated in vacuo, and the residue was purified by flash column chromatography on SiO_2 using hexane and 50:1 hexane:EtOAc to give the desired product as a yellow oil (0.198 g, 83.6 %). ^{1}H NMR ($CDCl_3$, 400 MHz): δ 7.20 (d, 2H), 6.92 (s, 2H), 6.59 (q, 1H), 6.42 (d, 2H), 5.50 (d, 1H), 4.99 (d, 1H), 2.29 (s, 3H), 2.15 (s, 6H). MS m/z = 237.1 ([M^+]).

2,6-difluoro-N-(4-vinylphenyl)aniline. In a glove box a 10 mL thick-walled pressure vial equipped with silicone seal cap was charged with NaO^{t}Bu (0.277 g, 2.80 mmol), $Pd(OAc)_2$ (9.0 mg, 0.040 mmol), and *rac*BINAP (49.8 mg, 0.080 mmol). 2,6-difluoroaniline (0.23 mL,

2.0 mmol), 4-bromostyrene (0.27 mL, 2.0 mmol), and distilled toluene (1 mL) were added via a syringe to the sealed tube, and the mixture was sonicated for 30 minutes. The reaction vessel was then subjected to microwave irradiation under the following conditions: power, 300 W; pressure, 100 psi; temperature, 140 °C; reaction time, 15 minutes. The color of the reaction mixture changed from red to dark brown. The mixture was diluted with diethyl ether and extracted once with HCl (1 M, 40 mL) and sat. $NaHCO_3$ (40 mL). Organics were dried over $MgSO_4$ and concentrated in vacuo, and the residue was purified by flash column chromatography on SiO_2 using hexane and 50:1 hexane:EtOAc to give the desired product as a yellow oil (0.358 g, 76.0 %). ^1H NMR ($CDCl_3$, 400 MHz): δ 7.29 (d, 2H), 7.10 (d, 2H), 6.95 (t, 1H), 6.74 (d, 2H), 6.63 (q, 1H), 5.58 (d, 1H), 5.08 (d, 1H). MS m/z = 231.2 ([M^+]).

Catalytic Reactions. *Esterification of Oleic Acid*: A mixture of oleic acid (90%, 100 mg, 0.35 mmol), methanol (230 mg, 7.1 mmol), and diphenylammonium triflate (1.1 mg, 3.5 μmol) was mixed in a 4 mL vial with a Teflon cap. The vial was capped tightly and heated at 95 °C for 2 h. The reaction mixture went from colorless to a dark red color. The mixture was allowed to cool to rt and ~5 mL of hexane added to transfer the mixture into a 25 mL one neck round bottom flask. The solvents were evaporated under reduced pressure and the crude product analyzed by GC and HPLC.

Esterification of Free Fatty Acid in Greases using Homogeneous Catalyst: A mixture of grease (12 wt% FFA, 1g, 0.43 mmol based on the FFA content), methanol (0.18 g, 5.6 mmol), and diphenylammonium triflate (1.8 mg, 5.8 μmol) was mixed in a 4 mL vial with a Teflon cap. The vial was capped tightly and heated at 95 °C for 2 h. The reaction went from light yellow to a dark brown color. The mixture was allowed to cool to rt and transferred with hexane (~5 mL) into a 25 mL one neck round bottom flask. The solvents were

evaporated under reduced pressure. 10 μL of crude product was pipetted into a 2 mL vial and ~1.5 mL of hexane was added. The mixture was passed through a syringe filter and analyzed by HPLC.

1.7 References

1. Graboski, M. S.; McCormick, R. L., Combustion of fat and vegetable oil derived fuels in diesel engines. *Progress in Energy and Combustion Science* **1998,** 24, (2), 125-164.

2. Hill, J.; Nelson, E.; Tilman, D.; Polasky, S.; Tiffany, D., From the Cover: Environmental, economic, and energetic costs and benefits of biodiesel and ethanol biofuels. *Proceedings of the National Academy of Sciences* **2006,** 103, (30), 11206-11210.

3. Knothe, G.; Van Gerpen, J.; Krahl, J., The Biodiesel Handbook. *AOCS Press* **2005**.

4. Haas, M. J.; McAloon, A. J.; Yee, W. C.; Foglia, T. A., A process model to estimate biodiesel production costs. *Bioresource Technology* **2006,** 97, (4), 671-678.

5. Zhang, Y.; Dube, M. A.; McLean, D. D.; Kates, M., Biodiesel production from waste cooking oil: 2. Economic assessment and sensitivity analysis. *Bioresource Technology* **2003,** 90, (3), 229-240.

6. Kulkarni, M. G.; Dalai, A. K., Waste Cooking Oil-An Economical Source for Biodiesel: A Review. *Industrial & Engineering Chemistry Research* **2006,** 45, (9), 2901-2913.

7. Haas, M. J.; Scott, K. M.; Michalski, P. J.; Runyon, S., US Patent 6,855,838 B2. **2005**.

8. Lotero, E.; Liu, Y.; Lopez, D. E.; Suwannakarn, K.; Bruce, D. A.; Goodwin, J. G., Synthesis of Biodiesel via Acid Catalysis. *Industrial & Engineering Chemistry Research* **2005,** 44, (14), 5353-5363.

9. Canakci, M.; Gerpen, J. V., *Trans. ASAE* **2001,** 44, 1429.

10. Hoydonckx, H. E.; De Vos, D. E.; Chavan, S. A.; Jacobs, P. A., Esterification and Transesterification of Renewable Chemicals: Catalytic Conversion of Renewables. Guest Editors: Herman van Bekkum and Pierre Gallezot. *Topics in Catalysis* **2004,** 27, 83-96.

11. Wakasugi, K.; Misaki, T.; Yamada, K.; Tanabe, Y., Diphenylammonium triflate (DPAT): efficient catalyst for esterification of carboxylic acids and for transesterification of carboxylic esters with nearly equimolar amounts of alcohols. *Tetrahedron Letters* **2000,** 41, (27), 5249-5252.

12. Mbaraka, I. K.; Radu, D. R.; Lin, V. S. Y.; Shanks, B. H., Organosulfonic acid-functionalized mesoporous silicas for the esterification of fatty acid. *Journal of Catalysis* **2003,** 219, (2), 329-336.

13. Wang, P. S.; Tat, M. E.; Van Gerpen, J., *J. Am. Oil Chem. Soc.* **2005,** 82, 845.

14. Foglia, T. A.; Jones, K. C.; Nuñez, A.; Phillips, J. G.; Mittelbach, M., Comparison of Chromatographic Methods for the Determination of Bound Glycerol in Biodiesel. *Chromatographia* **2004,** 60, (5), 305-311.

15. Barrett, E. P.; Joyner, L. G.; Halenda, P. P., The Determination of Pore Volume and Area Distributions in Porous Substances. I. Computations from Nitrogen Isotherms. *Journal of the American Chemical Society* **1951,** 73, (1), 373-380.

CHAPTER 2

Esterification of Fatty Acids using Diarylammonium Salts Supported onto Various Solids

2.1 A Background to Heterogeneous Catalysis and its Application to Biodiesel Production

2.1.1 Heterogeneous Catalysis for Biodiesel Production

Increasing biodiesel consumption has driven an obligatory response by scientists and engineers to develop new processes for producing biodiesel in high capacities, simplified operations, high yields, and the absence of special chemical requirements and waste streams.[11] To be economically viable and competitive with petroleum-based diesel fuel, the two costs associated with the price of biodiesel need to be addressed: the cost of raw materials and the cost of processing. Chapter 1 highlights the use of diphenylammoniun triflate as an acid catalyst in the conversion of high FFA-containing grease feedstock to pure biodiesel in a two-step process. We will show in this chapter the immobilization of those catalysts to various solid supports and their catalytic activity for esterification of FFA to FAME.

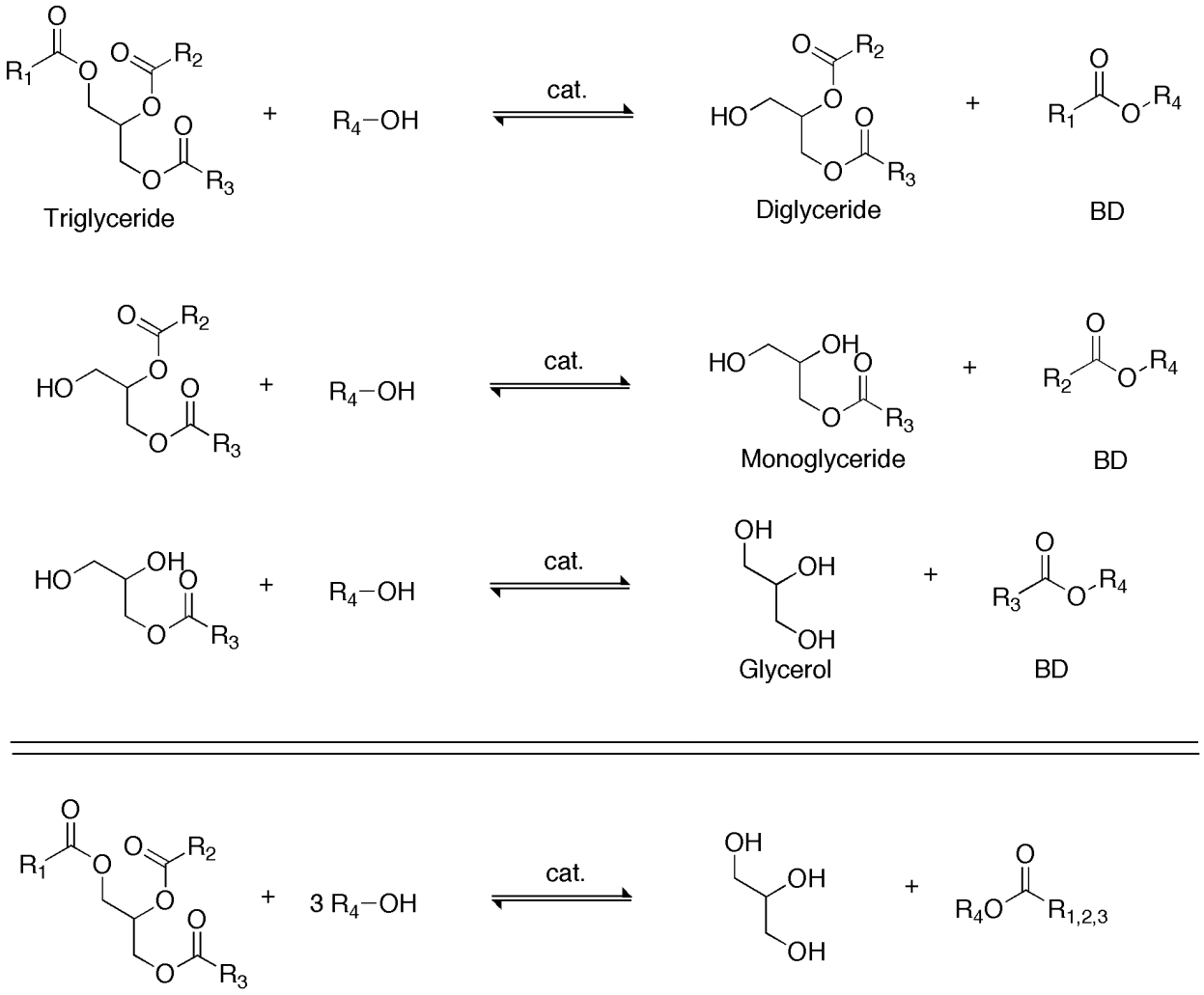

Figure 2.1. Stepwise transesterification of triglyceride with alcohol, yielding glycerol and FAME.

The leading commercial process for FAME production is achieved using sodium hydroxide or sodium methoxide homogeneous catalyst systems in either a batch or continuous mode.[11] A stepwise reaction mechanism for triglyceride transesterification is illustrated in Figure 2.1.[2] In general, this is a reversible acid- or base-catalyzed reaction that sequentially converts TG to DG and then to MG. The final step is liberation of three equivalents of alkyl esters and one equivalent of glycerol. Transesterification by base catalysis begins by formation of an alkoxide nucleophile that attacks the carbonyl carbon of the fatty acid (Figure 2.2). Rearrangement of the

glyceride occurs, and the methyl (or ethyl) ester releases from the glycerol backbone. An alkoxide ion forms as a result, which immediately becomes protonated to form the alcohol (or diglyceride), and regenerates the catalyst. The final reaction mixture (after all TG has been converted to FAME and glycerol) is now highly basic. The most costly drawback to this process is the need for acidic neutralization and aqueous washing steps. In order to reduce the saponification side reaction, any trace amounts of FFA must either be neutralized first or removed from the feedstock.

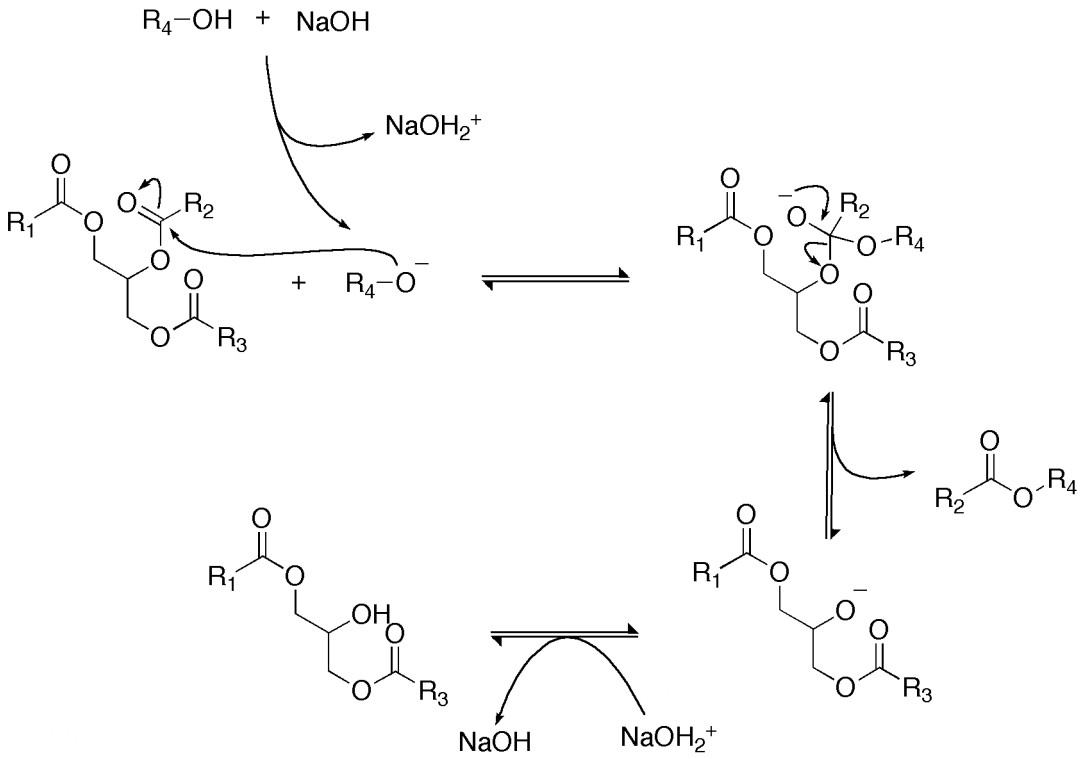

Figure 2.2. Reaction mechanism for the transesterification of triglyceride to diglyceride.

Solid metal oxides such as tin, magnesium and zinc oxides have been reported to act as base catalysts for transesterification reactions.[2] It was however later shown that the transesterification reaction was in fact catalyzed by leached metal cations homogeneously. The mixed oxide of zinc and aluminum were reported by Chodrage *et al*. to catalyze transesterification at high

temperature and pressure.[11] The Na/NaOH/γ-Al_2O_3 heterogeneous bases were used for converting soybean oil to useable biodiesel in appreciable quantities.[12] No mention was however made about the recycle and reuse of these catalysts. Cantrell *et al*. also reported that basic solids of Mg–Al calcined hydrotalcites, which are derived from hydrotalcites of the general formula $[Mg^{2+}_{(1-x)}Al^{3+}_{x}(OH)_2]^{x+}(CO_3)^{2-}$, showed moderate activities for trans-esterification.[13, 14]

Another approach is to incorporate known organic bases onto a support. Mesoporous silicas represent ideal candidates as catalyst supports. These solids are robust under harsh conditions, have large surface areas, have tunable pore sizes, and their surfaces are tailorable. Figure 2.3 highlights some organic bases that exhibit high catalytic activity for transesterification.[2] Sercheli *et al*. successfully immobilized alkylguanidines onto polystyrene beads, MCM-41 and zeolite Y.[15] Because of the unhindered diffusion and hydrophobic surface, the polystyrene alkyl-guanidine outperformed both other supports; conversion was still inferior to that of the homogeneous equivalents.[15]

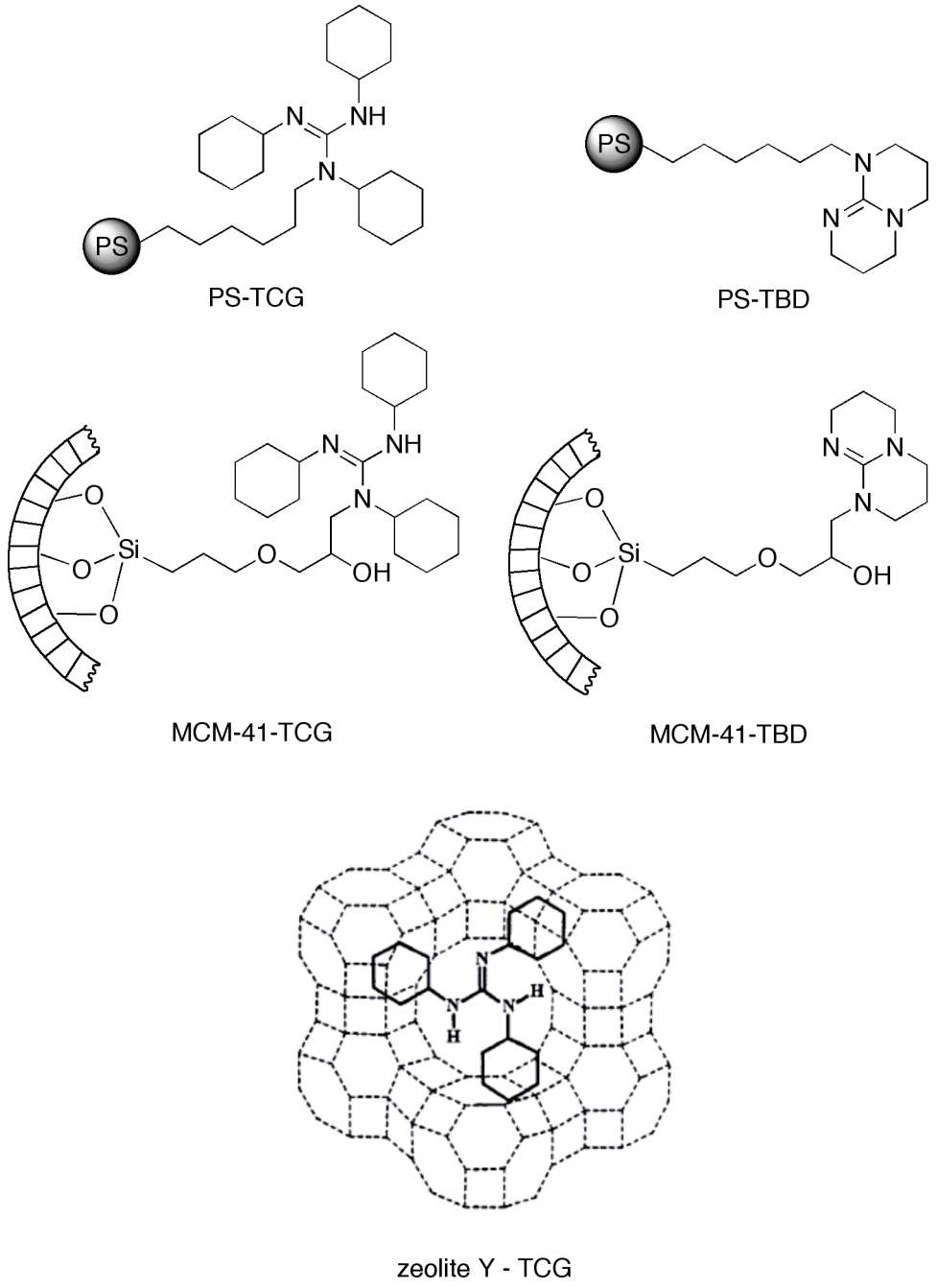

Figure 2.3. Organic bases TCG (1,2,3-tricyclohexylguanidine) and TBD (1,5,7-triazabicyclo-[4.4.0]dec-5-ene) supported on polystyrene, MCM-41 and zeolite Y.

Acid catalysts such as sulfuric acid, hydrofluoric acid, and *p*-toluensulfonic acid are commonly used for converting the FFA in high free fatty acid-containing feedstocks to biodiesel then followed by the standard base-catalyzed transesterification of the remaining glycerides to FAME.

The development of solid acid catalysts remedies issues associated with extensive neutralizations and aqueous washings required to purify the final biodiesel/glycerol mixture.[16, 17]

Many acid catalysts, including Nafion-NR50, Amberlyst-15, sulfated zirconia, and sulphonated sugar (Figure 2.4), have been examined for catalyzing esterification over the last decade. Nafion-NR50 is a copolymer of tetrafluoroethane and perfluoro-2-(fluorosulphonyl-ethoxy)propyl vinyl ether. Amberlyst-15 is a styrene-based sulphonic acid while sulfated zirconia is a metal oxide modified with sulfate ions to form a highly acidic or superacidic catalyst.[18-20] Gadi Rothenberg *et al*.[17] observed that amongst Nafion, Amberlyst and sulfated zirconia, the sulfated zirconia demonstrated the highest thermal stability and best catalytic performance for the conversion of fatty acid to its ethyl esters. M. Toda *et al*. prepared sulphonated sugars via the pyrolysis of D-glucose (Figure 2.5).[21] The incomplete carbonization results in small polycyclic aromatic carbon rings in which sulphonite groups (-SO_3H) are introduced by exposure to sulfuric acid. The solid sulphonated carbon catalyst was at least more than half as effective as sulfuric acid for the esterification reaction, and there was no loss of activity after repeated reactions.

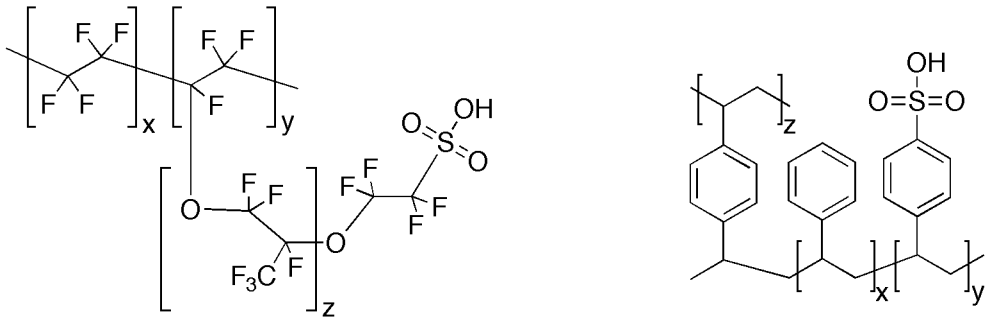

Nafion Amberlyst

Figure 2.4. Molecular structures of sulfated polymers, Nafion and Amberlyst-15.

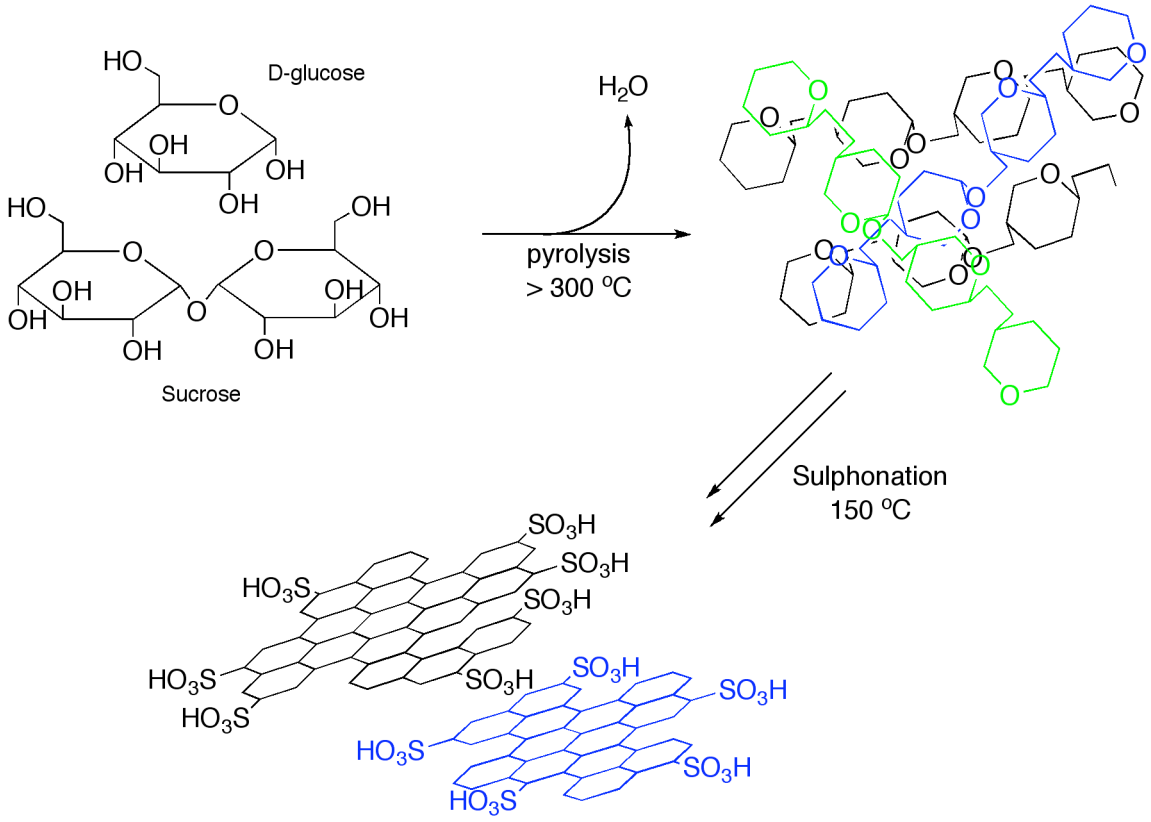

Figure 2.5. Synthetic procedure for the making of a solid acid catalyst derived from various sugar sources.

More recently, Lin *et al*. at Iowa State University has discovered acid-base mesoporous calcium oxide silica nanoparticles (Figure 2.6) that cooperatively convert a high FFA-containing feedstock into biodiesel in one step.[22] The combination of high surface, large pore size, and short diffusion lengths across individual particles, makes these supported catalysts attractive for large substrates and reactants, such as triglycerides and long-chain fatty acids. In these multifunctional materials, the Lewis acid and basic (CaO) sites are responsible for the esterification of high FFA feedstocks and the transesterification of lower FFA containing biomass oils. This catalyst shows no decrease in reactivity after recycling 20 times.

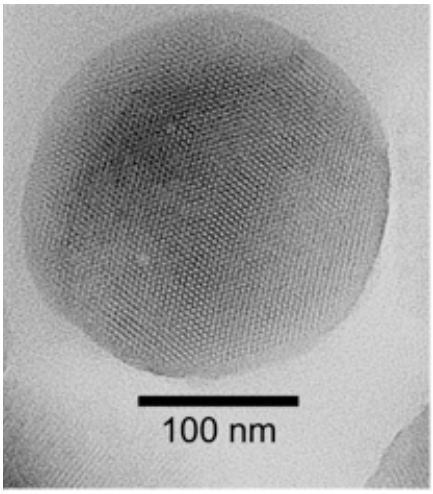

Figure 2.6. TEM image of a MCM-41 mesoporous silica nanoparticle.

2.2 Synthesis and Catalytic Performance of Solid Acid Catalysts for Biodiesel Production

2.2.1 Synthesis of Porous 1,4-Divinylbenzene/Phenyl(Vinylanilinium) Copolymers.

One problem associated with homogeneous catalysts is the difficulty of their recovery and/or reuse after the catalytic reaction. This represents a drawback when homogeneous acid catalysts are used for pretreatment of greases because the remaining acid catalyst has to be neutralized with base before the reaction mixture can be used in subsequent base-catalyzed transesterification reactions. To overcome this drawback, we immobilized the diarylammonium salts onto a porous highly crosslinked organic polymers to prepare potential heterogeneous diarylammonium catalysts. An insoluble polymer resin was made by free radical initiated polymerization of 1,4-divinylbenzene (DVB) with desired co-monomers at elevated temperature in the presence of a porogen.[23] Since the diphenylammonium triflates worked the best for the conversion of FFA to FAME in high FFA containing greases (see Chapter 1), we focused our

attention to the preparation of porous DVB/phenyl(vinyl-anilinium) triflate (DVB/PVA-OTf) copolymers.

We examined two different methods for the synthesis of DVB/PVA-OTf copolymers. In the first approach, we synthesized a porous DVB/4-bromostyrene copolymer (Poly-DVB/BrPh), which provided an insoluble platform with accessible bromophenyl moieties (Figure 2.7). The bromophenyl group was subsequently aminated with aniline under Pd-coupling conditions[24, 25] using a microwave synthesis approach to give a 1,4-divinylbenzene/phenyl(vinylaniline) *(Poly-DVB/PVA-1) copolymer*. After a thorough rinsing of the solid with various solvents and solutions, the polymer with pendant diphenylamines was reacted with a dilute solution of triflic acid in dichloromethane/1,4-dioxane solvent mixture to afford the heterogeneous catalyst **2.10** (Figure 2.7). The resulting solid was dark brown in color, suggesting protonation of the secondary amine. This synthetic scheme relies on the Pd-catalyzed amination reaction to install the phenyl(vinylaniline) moieties, which presents a significant challenge in quantifying the number of active sites in the copolymers since Pd-coupling reaction efficiency is less than unity.

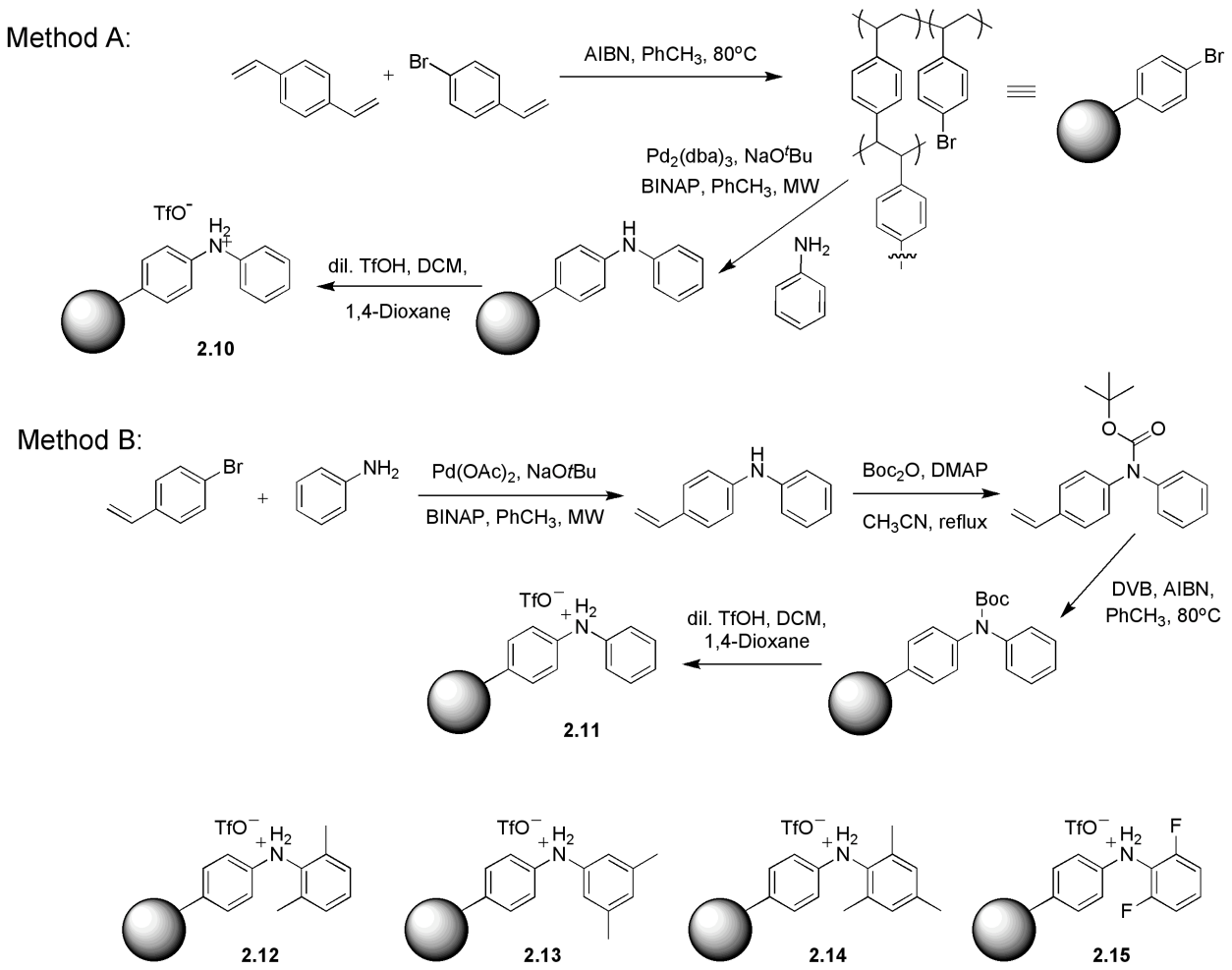

Figure 2.7. Synthetic routes for porous Poly-DVB/PVA-OTf copolymers.

The second synthetic approach utilized a pre-synthesized vinyl analogue of diphenylamine as a co-monomer in the polymerization with DVB (Figure 2.7). Because this copolymerization reaction gave a quantitative yield, it is much easier to quantify the number of the diarylammonium active sites in the porous copolymers prepared by the second approach. Pd-catalyzed N-arylation of aniline with 4-bromostyrene was performed under microwave reaction conditions to afford *N-phenyl-4-vinylaniline*. This secondary diarylamine however inhibits the copolymerization reaction by trapping free radicals. We therefore carried out the copolymerization reaction with the *t*Boc-protected *N-phenyl-4-vinylaniline*. The protected

monomer was readily co-polymerized with DVB (1:4 molar ratio) to give a quantitative yield of *Poly-DVB/PVA-2*. After Soxhlet extraction of the polymer solid with methanol, the resin was treated with dilute triflic acid to simultaneously remove the ^{t}Boc protecting group and protonate the diarylamine to generate the heterogeneous catalyst **2.11** (Figure 2.7).

The use of a toluene porogen and rigid diarylamine comonomer allowed the synthesis of highly porous crosslinked copolymers. Nitrogen sorption isotherms were taken on the porous copolymers to estimate their surface areas and pore sizes. All of the four copolymers, Poly-DVB/BrPh, **2.10**, Poly-DVB/PVA-2-Boc, and **2.11**, exhibit very high surface areas (Figure 2.8). As expected, the surface area slightly decreased from 840 m^2/g for Poly-DVB/BrPh to 730 m^2/g for **2.10**, as a result of the increasing steric bulk after the N-arylation of Poly-DVB/BrPh and subsequent protonation with triflic acid. Interestingly, for the DVB/PVA-OTf copolymers made by the second approach, we observed an increase in surface area as the Poly-DVB/PVA-2-Boc underwent deprotection and protonation steps. Poly-DVB/PVA-2-Boc and **2.11** had surface areas of 850 m^2/g and 1000 m^2/g, respectively. These results are all summarized in Table 2.1. This result is consistent with a slightly larger size of the *t*Boc protection group over the triflate anion. We have also synthesized several derivatives of the polymer-immobilized diarylammonium triflate **2.12** – **2.15** by AIBN-initiated copolymerization of DVB with substituted N-(4-vinylphenyl)aniline. These derivatives did not require *t*Boc protection in order to be copolymerized with DVB. The resulting solids however retained similar porous structures. The nitrogen sorption isotherms showed that these porous polymers are highly meso- and macroporous (Figure 2.8 and Table 2.1). Given the high porosity and large pore size of the copolymers, the diarylammonium protonated sites were expected to be readily accessible to the substrates in heterogeneously catalyzed esterification reactions.

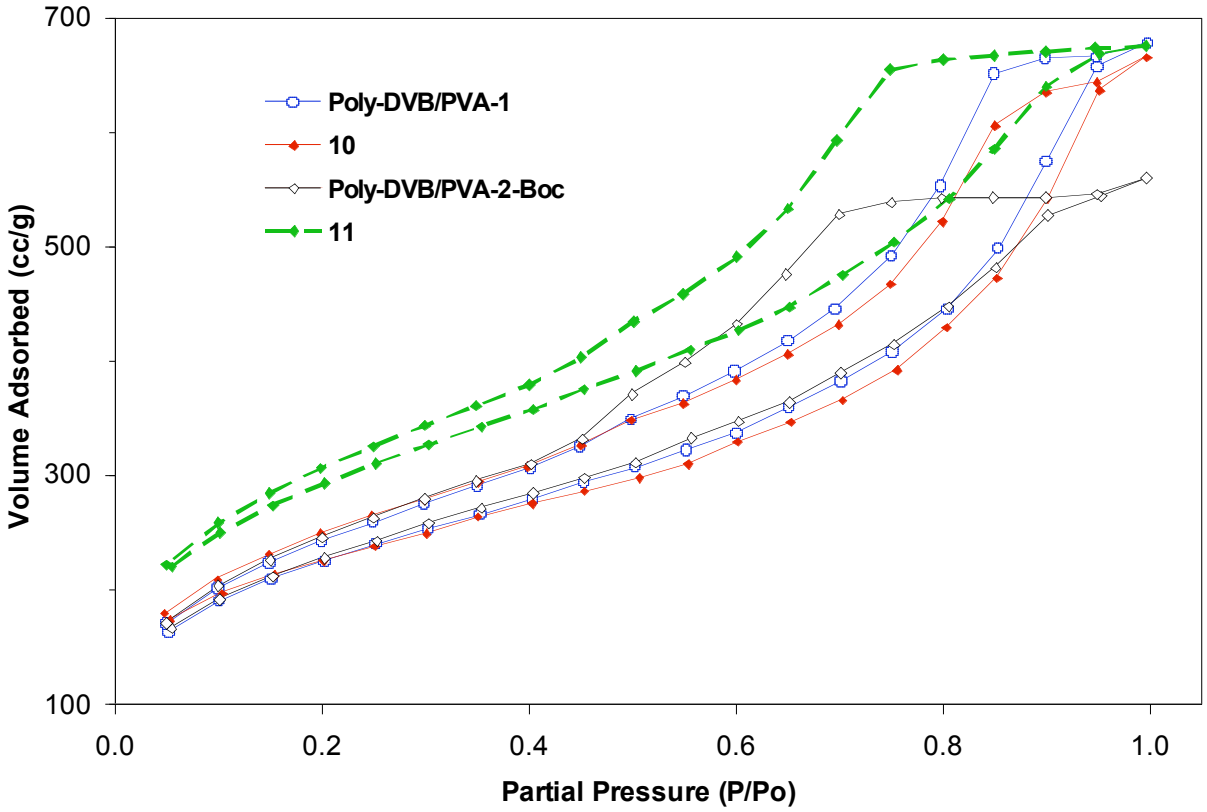

Figure 2.8. Nitrogen sorption isotherms of porous copolymers after 6 h of heating at 100 °C.

Table 2.1. Nitrogen Sorption Isotherm Data for Porous Copolymers.

	Surface Area (m^2/g)	Pore Volume (cc/g)
POP/2,6-PVA	1241	1.19
POP/2,6-PVA-OTf, **2.12**	883	0.88
POP/3,5-PVA	1360	1.20
POP/3,5-PVA-OTf, **2.13**	977	0.89
POP/2,4,6-PVA	837	0.78
POP/2,4,6-PVA-OTf, **2.14**	1278	1.22
POP/2F-PVA	754	0.64
POP/2F-PVA-OTf, **2.15**	869	0.71

2.2.2 Synthesis of Diarylammonium Triflate Immobilized onto SBA-15 and MCM-48 Mesoporous Silicas

We explored alternative immobilization of the diphenylammonium triflate acid catalyst onto a more robust, highly porous slicas MCM-48 and SBA-15. MCM-48, as mentioned previously, is a network of interconnected three-dimensional channels with extremely high surface areas and pore sizes in the range of 2 – 3 nm. We also chose to explore the immobilization on SBA-15 that possesses one-dimensional open channels of 5 – 9 nm in diameter. We anticipate the larger pore size to facilitate the transport of substrates to the catalytic sites decorating all of the channels.

In order to decorate the surface of either MCM-48 or SBA-15, we pre-synthesized an alkoxy silyl analogue of diphenylamine (Figure 2.9). Pd-catalyzed N-arylation of 4-(trimethoxysilyl)aniline with 4-bromostyrene afforded 4-(*tert*-butoxydimethoxysilyl)-*N*-phenylaniline. We discovered that the *t*-butoxide anion of sodium *t*-butoxide base required for the transformation displaces a methoxide and inhibit and shutdown the Pd catalytic cycle.

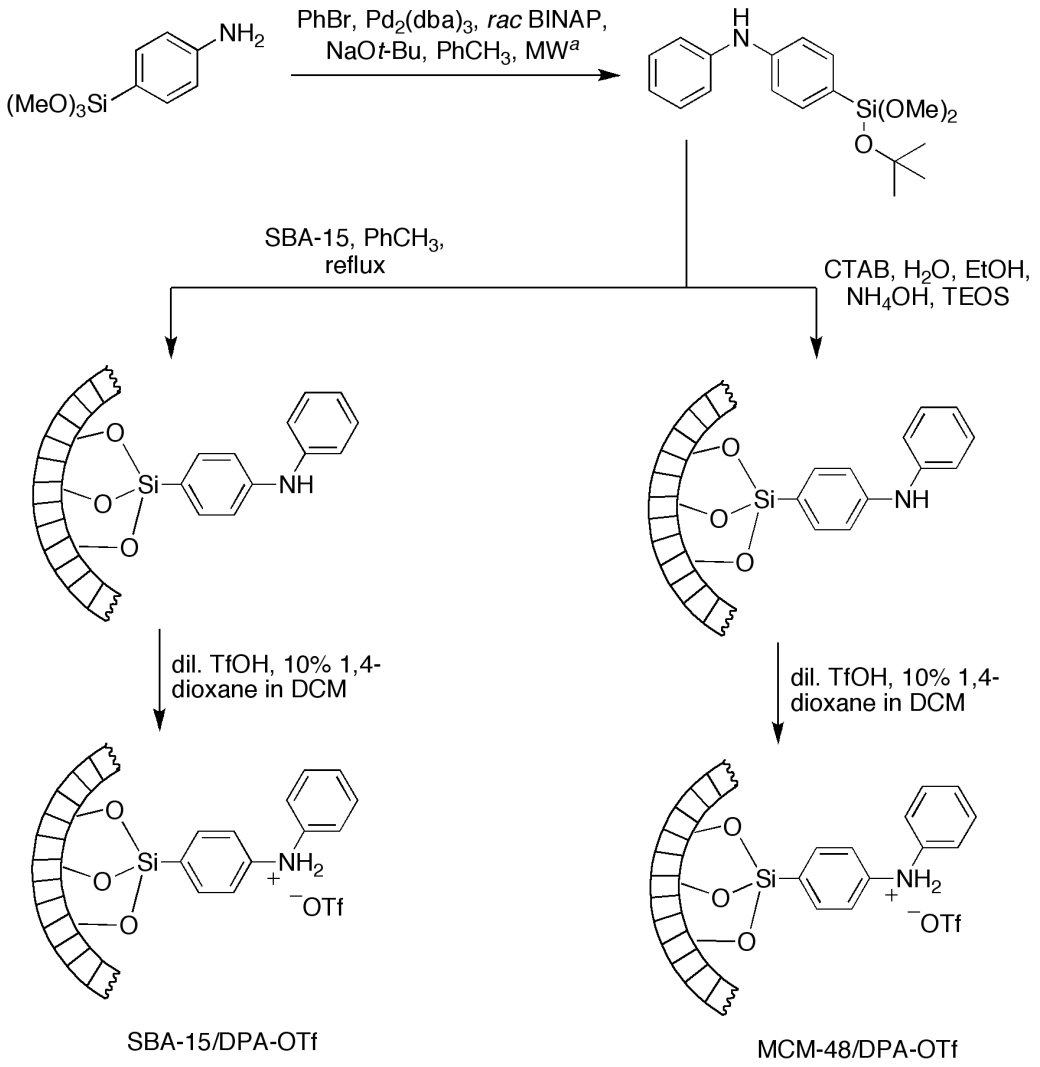

Figure 2.9. Synthetic routes for the production of diphenylammoniun salt immobilization onto meosoporous silicas. [a] Microwave (MW) conditions: Solvent, toluene; temperature, 140 °C; power, 300W; pressure, 100 psi; cooling, off; stirring, off; run time, 2:00 min; hold time, 10:00min.

Our first approach utilized the method of co-condensation of 4-(*tert*-butoxy-dimethoxysilyl)-*N*-phenylaniline and TEOS at 1.5 mol% loading (with respect to Si) to make MCM-48 mesoporous silica (Figure 2.9); with the established mixture: cetyltrimethylammonium bromide (CTAB), H_2O, ethanol, ammonium hydroxide (NH_4OH), tetraethyl orthosilicate (TEOS), and

catalyst at a weighted ratio of 0.76 : 35.3 : 11.6 : 3.5 : 1.0 : 0.025. After mesoporous silica formed, the surfact and co-solvents were removed by a mild neutral extraction with 1 wt% NaCl in methanol. The resulting immobilized diphenylamine onto MCM-48 (MCM-48/PVA) had a concentration of 0.44 mmol PVA/g, which was then subsequently reacted with a dilute solution of triflic acid in dichloromethane/1,4-dioxane solvent mixture to afford the active MCM-48/PVA-OTf.

The second approach utilized SBA-15 as the catalyst support. SBA-15 was made by a previously reported synthesis. The pendant silanols on the surface of SBA-15 channels were used in the hydrolysis of our 4-(*tert*-butoxydimethoxysilyl)-*N*-phenylaniline at 10 wt% loading under refluxing toluene conditions. The final solid SBA-15/PVA had a concentration of 0.28 mmol PVA/g, which was then subsequently reacted in a similar fashion to MCM-48 to afford the active SBA-15/PVA-OTf.

Nitrogen sorption isotherms were taken on each of the mesoporous silicas to estimate their BJH[26] surface areas and pore sizes. Both MCM-48/PVA-OTf and SBA-15/PVA-OTf exhibit very high surface areas (Figure 2.10 and Table 2.2). Interestingly, when MCM-48/PVA underwent protonation with triflic acid, we saw a slight increase in surface area from 274 m^2/g to 281 m^2/g, and a decrease in pore size from 2.5 nm to 1.4 nm. As for SBA-15/PVA-OTf, the original SBA-15 had a surface area of 961 m^2/g, but after subsequent modifications SBA-15/PVA-OTf had a surface area and pore size diameter of 578 m^2/g and 4.9 nm, respectively. The diphenylammonium protonated sites of both MCM-48 and SBA-15 mesoporous silicas were expected to be readily accessible to FFAs and alcohol during the heterogeneous esterification transformation.

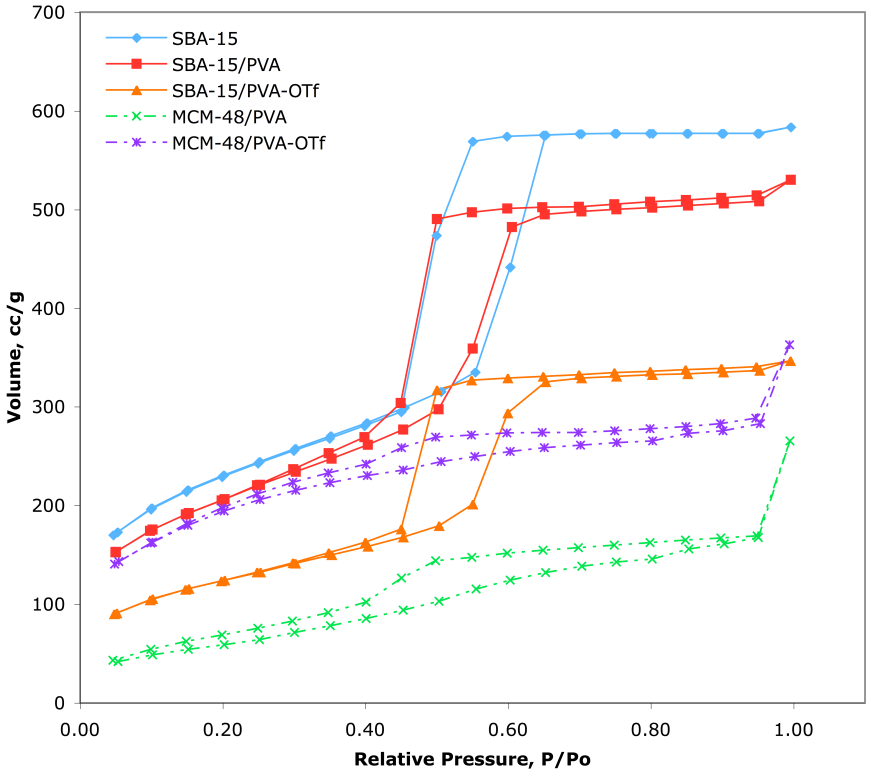

Figure 2.10. Nitrogen sorption isotherms of mesoporous silicas after 6 h of heating at 100 °C.

Table 2.2. Nitrogen Sorption Isotherm Data for Mesoporous Silicas.

	Surface Area (m^2/g)	Pore Volume (cc/g)	Pore Size (nm)
MCM-48/PVA	274	0.45	2.5
MCM-48/PVA-OTf	281	0.49	1.4
SBA-15	961	0.93	5.7
SBA-15/PVA	902	0.85	4.9
SBA-15/PVA-OTf	578	0.57	4.9

2.2.3 Esterification of the FFA in Greases by Porous Divinylbenzene/Diarylammonium Triflate Copolymers Catalysts.

We first examined the catalytic activity of heterogeneous catalyst **2.10** for the esterification of oleic acid and FFA in greases. The reactions were carried out under similar conditions to the homogeneous catalyst systems. In the presence of 2 mol% of **2.10**, an oleic acid to methyl oleate conversion of >99% was obtained when a mixture of oleic acid and 5 equiv. of methanol was heated at 95 °C for 2 hours (Table 2.3, entry 1). Solid catalyst **2.10** also worked well in converting the FFA to FAME in FFA-containing greases. In the presence of 7.5 mol% of this catalyst and 20 equiv. of methanol, the greases containing 12 and 21 wt% FFA were reduced to 0.45 wt% and 1.1 wt%, respectively (entries 2 and 3). This result corresponds to a FFA conversion to FAME of 96% and 95%, respectively. For the brown grease with 40 wt% FFA, 15 mol% of **2.10** gave a >99% conversion of FFA to FAME in the presence of 20 equiv. of methanol (entry 4). Since we assumed complete arylation of all the phenyl bromide moieties in Poly-DVB/BrPh when calculating catalyst loadings, we apparently over-estimated the amount of the PVA-1-OTf active sites and thus underestimated the activity of **2.10** in all our experiments. We therefore carried out parallel experiments with catalyst **2.11** to obtain a better estimate of the catalytic activity for the immobilized diarylammnonium catalysts.

Table 2.3. Esterification of the FFA in Greases using Heterogeneous Poly-DVB/PVA-OTf Catalysts[a]

entry	substrates	catalyst (mol%)	MeOH (eq.)[b]	Wt.% by HPLC					% conv. of FFA[c]
				FAME	FFA	TG	DG	MG	
1	oleic acid (90% purity)	**2.10** (2)	5	99	1.0	---	---	---	99
2	grease (12 wt% FFA)	**2.10** (7.5)	20	23	0.5	47.9	21.9	6.7	96
3	grease (21 wt% FFA)	**2.10** (7.5)	20	24	1.1	32.4	30.5	12	95
4	grease (40 wt% FFA)	**2.10** (15)	20	49	0	24.6	21	5.4	>99
5	oleic acid (90% purity)	**2.11** (0.5)	5	99	<1.0	---	---	---	>99
6	grease (12 wt% FFA)	**2.11** (2.5)	20	20.3	0.4	52.9	22.6	3.8	97
7	grease (12 wt% FFA)[d]	**2.11** (2.5)	20	22.4	1.4	54.9	17.3	4.0	88
8	grease (21 wt% FFA)	**2.11** (5)	20	29.3	0.7	39.9	24.3	5.8	97
9	grease (40 wt% FFA)	**2.11** (5)	20	50.6	1.3	24.5	19.2	4.4	97
10	oleic acid (90% purity)	**2.12** (1)	5	84	16	---	---	---	84
11	grease (12 wt% FFA)[e]	**2.12** (2.5)	20	16.6	1.1	67.9	12.8	1.6	91
12	grease (40 wt% FFA)	**2.12** (5.0)	20	53	1.0	26.1	17.7	2.2	98
13	oleic acid (90% purity)	**2.13** (1)	5	97	3	---	---	---	97
14	grease (12 wt% FFA)[e]	**2.13** (2.5)	20	17.9	0.7	66.8	13.1	1.5	94
15	grease (40 wt% FFA)	**2.13** (5)	20	44.1	6.4	25.4	20.4	3.7	84
16	oleic acid (90% purity)	**2.14** (1)	5	99	1	---	---	---	99
17	grease (12 wt% FFA)[e]	**2.14** (2.5)	20	10.4	3.1	77	9.5	0	74
18	grease (40 wt% FFA)	**2.14** (5)	20	40	8.75	26.5	21.4	3.32	78
19	grease (12 wt% FFA)[e]	**2.15 (5)**	20	10.3	6.1	75.3	8.3	0	51

[a]All reactions were performed at 95 °C for 2 h.

[b]Number of equivalents relative to FFA.

[c]% conversion = $(FFA^i\text{-}FFA^f)/(FFA^i \times 100)$.

[d]Reaction was performed at 50g scale in a stainless steel reactor.

[e]wt% composition of grease before esterification: 12.5 FFA, 79.4 TG, 9.0 DG, 0 MG. Note, there were only about 6 wt%FFA obtained from Darling International, we have intentionally added another 6 wt% OLA.

As expected, **2.11** had a much higher apparent activity than **2.10**. With only a 0.5 mol% loading of **2.11**, we were able to completely convert oleic acid to methyl oleate by treatment with 5 equiv. of MeOH (Table 2.3, entry 5). For the grease containing 12 wt% FFA, only 2.5 mol% of **2.11** was needed to attain a 97% conversion of FFA to FAME (with the final FFA content of 0.41%) (entry 6). As for the greases with 21 wt% and 40 wt% FFA, 5 mol% and 7.5 mol% of **2.11** gave an FFA to FAME conversion of 97% and >99%, respectively (entries 7 and 8). The results indicate that the porous phenyl(vinylanilinium) triflate/divinylbenzene copolymer catalysts are very effective in converting FFA to FAME in greases with high FFA content. These immobilized catalyst also caused change in the glyceride content of the grease much as the homogeneous counterparts but again their transesterification activity was low compared to their esterification activity. We also examined time-dependent oleic acid to methyl oleate conversion curves catalysts **2.10** and **2.11**. As shown in Figure 2.11, both heterogeneous catalysts **2.10** and **2.11** have an esterification activity similar sulfuric acid.

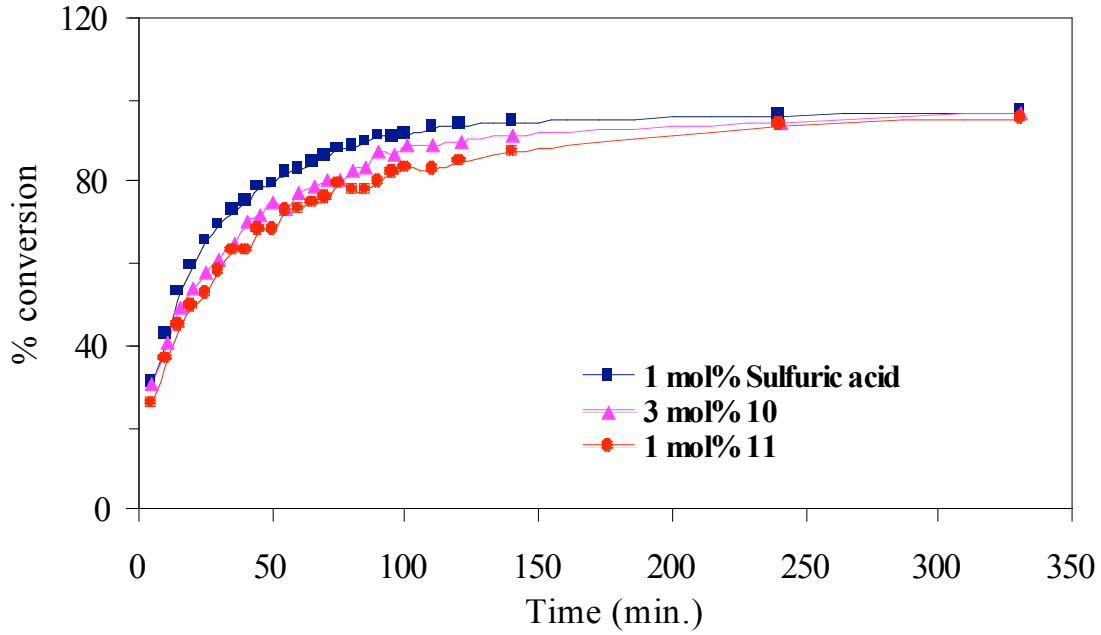

Figure 2.11. Conversion curves of esterification of oleic acid by solid catalysts. All reactions were performed at an oleic acid:MeOH mol ratio of 1:10 at 95 °C.

The derivatives of **2.11** were synthesized to explore potential electron-donating and -withdrawing effects on the acidic nature of the parent diarylammonium triflate. Methylated analogues, **2.12**, **2.13** and **2.14**, with an anticipated electron-donating effect all showed a slight decrease in the conversion of oleic acid to methyl oleate (Table 2.3). When these catalysts were tested on greases containing 12 and 40 wt% FFA, **2.13** and **2.14** exhibited lower activities in converting FFA to FAME. Surprisingly, **2.12** reduced the FFA content to ~1.0 wt% for both greases. Catalyst **2.15** was a much less active esterification catalyst than **2.11**; with 5 mol% of **2.15**, an FFA to FAME conversion of 51% was obtained after a 2 h reaction at 95 °C.

2.2.4 Esterification of the FFA in Greases by Mesoporous MCM-48 and SBA-15/Diarylammonium Triflate Catalysts.

We also explored the catalytic activity of the mesoporous silica heterogeneous catalysts based on the MCM-48 and SBA-15 solid supports for the esterification of oleic acid and FFA-containing greases. The conditions used for the homogeneous catalyst system were applied for MCM-48/PVA-OTf. An oleic acid to methyl oleate conversion of 98.1% was obtained in the presence of 15 mol% MCM-48/PVA-OTf and 10 equivalents of methanol at 95 °C for 2 h (Table 2.4, entry 5). This same solid catalyst at 15 mol% loading and with 20 equivalents of methanol was also successful in converting FFA-containing (12 – 40 wt%) yellow and brown greases. The FFA to FAME conversions for these greases was 96% on average (Table 2.4, entries 6 – 8). This result corresponds to a FFA conversion to FAME of 96% and 95%, respectively. Because MCM-48 materials typically have smaller pore features, we also explored in parallel the catalytic activity of diphenylammonium triflate found in SBA-15/PVA-OTf.

Table 2.4. Esterification of the FFA in Grease using Heterogeneous Poly-DVB/PVA-OTf Catalysts.

				Wt.% by HPLC					
entry	substrates	catalyst (mol%)	MeOH (eq.)[b]	FAME	FFA	TG	DG	MG	% conv. [a]
1	oleic acid (90% purity)	SBA-15/PVA-OTf (2.5)[c]	10	>99	0	---	---	---	>99
2	grease (12 wt% FFA)	SBA-15/PVA-OTf (7.5) [c]	20	16.8	0.62	60.8	19.3	2.33	95.0
3	grease (21 wt% FFA)	SBA-15/PVA-OTf (15) [c]	20	30.6	1.92	43.8	23.5	0	91.0
4	grease (40 wt% FFA)	SBA-15/PVA-OTf (2.5) [c]	20	56.1	0.59	25.5	17.7	0	98.5
5	oleic acid (90% purity)	MCM-48/PVA-OTf (15) [d]	10	98.1	1.89	---	---	---	98.1
6	grease (12 wt% FFA)	MCM-48/PVA-OTf (15) [d]	20	16.6	0.52	63.1	19.7	0	96.0
7	grease (21 wt% FFA)[d]	MCM-48/PVA-OTf (15) [d]	20	28.2	1.36	43.9	24.8	1.72	94.0
8	grease (40 wt% FFA)	MCM-48/PVA-OTf (15) [d]	20	51.9	0.77	22.9	18.5	5.87	98.1

[a] All reactions were performed at 95 °C for 2 h.
[b] Number of equivalents relative to FFA.
[c] 0.28 mmol/g
[d] 0.44 mmol/g
[e] % conversion = $(FFA^i\text{-}FFA^f)/(FFA^i \times 100)$.

As expected, SBA-15/PVA-OTf outperformed MCM-48/PVA-OTf. The amount of catalyst loading required to obtain high FFA conversion was lower. We believe the larger pore size allowed efficient grafting of PVA to the silica surface. With only a 2.5 mol% loading of SBA-15/PVA-OTf, we were able to completely convert oleic acid to methyl oleate by treatment with 10 equivalents of methanol (Table 2.4, entry 1). For the yellow greases containing 12 and 21 wt% FFA, 7.5 and 15 mol%, respectively, loadings were needed to attain modest 95% and 91% conversions of FFA to FAME (entries 2 and 3). The same catalyst proved to be more successful for the grease with 40 wt% FFA. A 2.5 mol% loading gave a FFA to FAME conversion of 98.5% (entry 4). We have shown the immobilization of PVA to MCM-48 and SBA-15 mesoporous silicas to be very effective in converting FFA to FAME in greases with high FFA

content. Additionally, we examined the time-dependent conversion of oleic acid to methyl oleate. These results are illustrated as conversion curves in Figure 2.12. These catalysts perform slightly less than sulfuric acid. Porous organic polymers **2.10** and **2.11** are better heterogeneous catalysts. It is possible the more hydrophobic nature of the porous polymer facilitates the transport of the long-chain fatty acids and the FAME product.

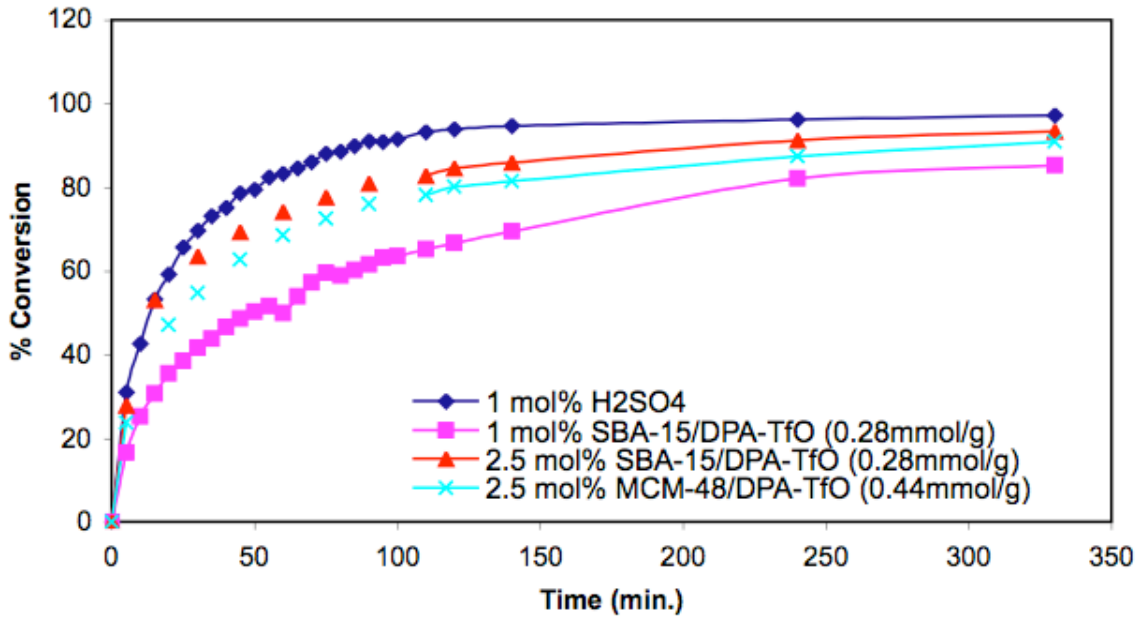

Figure 2.12. Conversion curves of esterification of oleic acid by mesoporous solid catalysts. All reactions were performed at an oleic acid:MeOH mol ratio of 1:10 at 95 °C.

2.2.5 Catalyst Re-Use Experiments

We have also demonstrated that catalyst **2.11** could be recycled and re-used for at least 3 cycles. As shown in Table 2.5, the grease with 12% FFA was used for this study. At 2.5 mol% loading of **2.11**, an 88% conversion of FFA to FAME was obtained for the first run of the reaction. The solid catalyst was recovered by filtration and then re-activated with triflic acid. A 92% conversion of FFA to FAME was obtained for the second run of reaction at 2.5 mol% of

2.11. In the third run, an 87% conversion of FFA to FAME was achieved under the same conditions with the re-activated **2.11**. However, when the re-activated catalyst was used for the fourth time under similar reaction conditions, a significant drop in the catalyst activity (~47% FFA to FAME conversion) was observed.

Table 2.5. Catalyst re-used in yellow grease esterification reaction.[a]

entry	Catalysts[b]	MeOH (eq.)[c]	HPLC wt. %					% conv. of FFA[d]
			FAME	FFA	TG	DG	MG	
1	no catalyst	---	0	12	66.0	20.4	1.6	---
2	First use	20	22.4	1.4	54.9	17.3	4.0	88
3	Second use	20	14.6	1.0	64.6	19.8	0	92
4	Third use	20	12.6	1.6	63.2	20.5	2.1	87

[a] All reactions were performed at 95 °C for 2h with 2.5mol% catalyst loading.
[b] Catalyst **2.11** was re-activated by treating with 5 equiv. of 0.1 M TfOH in dioxane at rt for about 20 h. The catalyst was then washed with dioxane (5 × 8mL).
[c] Number of equivalents relative to FFA.
[d] % conversion = $(FFA^i\text{-}FFA^f)/(FFA^i \times 100)$.

2.2.6 Transesterification of Pretreated Greases with Homogeneous Base Catalyst

Since the FFA in greases could be converted to FAME with the heterogeneous diarylammonium catalysts, it was important to show that the pretreated greases could be directly used for FAME production using well-established base-catalyzed transesterification processes. As seen in Table 2.6, **2.11** reduced the FFA content of the grease from 12 wt% (initial) to 0.9 wt% (after pretreatment (entry 1)). After removal of solid catalyst **2.11** by simple filtration (and removal of volatile solvents), this pretreated grease was subjected to base-catalyzed transesterification. In the presence of 0.3 wt% sodium methoxide ($NaOCH_3$) catalyst, between 4.4 and 8.5 equiv. of methanol (relative to the fatty acyl equivalents in the grease) were needed to completely convert all of the glycerides in the grease to FAME at 50 °C within 2 h. The final

mixture contained >98 wt% FAME and less than 2 wt% FFA (entry 4). About half of the residual FFA in the final ester product is carried over from the pretreated grease. It is established that $NaOCH_3$ does not catalyze the esterification FFA to FAME.[27]

Table 2.6. Transesterification of Pretreated Greases with 0.3 wt% Sodium Methoxide[a]

			HPLC wt%				
entry	Sample	MeOH (eq.)[b]	FAME	FFA	TG	DG	MG
1	pretreated grease[c]		20.5	0.9	52.4	22.1	4.1
2	after transesterification	3	90.9	1.6	5.5	2.0	0
3	after transesterification	4.4	95.9	1.5	2.6	0	0
4	after transesterification	8.5	98.1	1.9	0	0	0
5	pretreated grease[d]		18.4	0.9	57	20.2	3.4
6	after transesterification	5.8	80.1	1.4	11.8	4.95	1.7
7	after transesterification	7.2	90.6	1.3	6.1	2.0	0
8	after transesterification	11.2	98.6	1.4	0	0	0
9	pretreated grease[d]		22.8	1.8	57.3	14.5	3.6
10	after transesterification	11.7	97.4	2.6	0	0	0
11	pretreated grease[e]		24.2	0.7	54.9	15.7	4.5
12	after transesterification	3	99	1.0	0	0	0

[a] All the transesterification reactions were run with 0.3 wt% NaOMe catalyst at 50 °C for 2h.

[b] Numbers of equiv. of MeOH were calculated relative to the equivalent moles of FFA in pretreated greases.

[c] The pretreated grease was vacuum dried to remove water and MeOH from the pretreatment (esterification) step (Method **A**).

[d] Catalyst **2.11** was removed from the pretreated greases by centrifugation, i.e., methanol and water carried over from the esterification step were not removed from the pretreated greases (method **B**).

[e] The esterification reaction of FFA to FAME in grease was performed at 50g scale in a 600mL stainless steel reactor. Catalyst **2.11** was removed from the pretreated greases by centrifugation, and the mixture was transferred to a separator funnel to separate the lipid mixtures from the methanol/water phase (method **C**).

We also examined the transesterification reactions using pretreated greases containing residual methanol and water of reaction from the acid-catalyzed pretreatment (esterification) step. In

these experiments, the solid catalyst **2.11** was removed from the pretreated grease by centrifugation. Interestingly, similar results were obtained and the water generated from the pretreatment (esterification) step did not seem to adversely affect the transesterification reactions of the glycerides. For the pretreated grease with 0.95 wt% final FFA content, transesterification with 5.8, 7.2, and 11.2 equiv. of MeOH (relative to the fatty acyl equivalents in the grease) in the presence of 0.3 wt% $NaOCH_3$ gave a final FAME content of 80.1, 90.6, and 98.6 wt%, respectively (Table 2.6, entries 6-8). The reaction product with 11.2 equiv. of MeOH (including the carried-over MeOH) had a final FFA content of 1.43 wt% with no glycerides left in the mixture. The base-catalyzed transesterification reaction also worked well for the pretreated grease with containing 1.78 wt% FFA. With 0.3 wt% $NaOCH_3$ and 11.7 equiv. of MeOH (including the carried-over MeOH), the final product contained 97.4 wt% FAME, 2.62 wt% FFA (no remaining glycerides) (Table 2.6, entry 10). Interestingly, when the lipid mixture was separated from the MeOH/water layer, only 3 equiv. of MeOH and 0.3 wt% $NaOCH_3$ are needed to reduce all of the glycerides in the pretreated grease to 99 wt% FAME (Table 2.6, entry 12).

2.2.7 Transesterification of Pretreated Greases with Heterogeneous Base Catalyst

In addition to our extensive work on this novel insoluble porous polymer acid diphenylammonium triflate catalyst for the esterification of FFA in waste greases, we also utilized the same technology to immobilize a strong organic base. 1,5,7-Triazabicyclo[4.4.0]dec-5-ene (or TBD) is a known strong organic guanidine base with a pKa = 26. It is commonly used in catalytic amounts for Michael reactions, Wittig reactions, Henry reactions and in transesterification. In particular, it has served as the base catalyst for the transesterification of pure vegetable oil to biodiesel in near quantitative yields.[15] These findings supported our efforts

to synthesize a TBD/vinyl monomer that would allow for facile copolymerization with DVB (Figure 2.13). The free proton of TBD underwent standard S_N2 reaction conditions with 4-vinylbenzyl chloride to afford the final TBD-styrene monomer. This monomer was then readily polymerized with DVB (1:4 molar ratio) to give a quantitative yield of *Poly-DVB/TBD*. After Soxhlet extraction of the polymer solid with methanol, the resin was ready for use as a solid supported base catalyst.

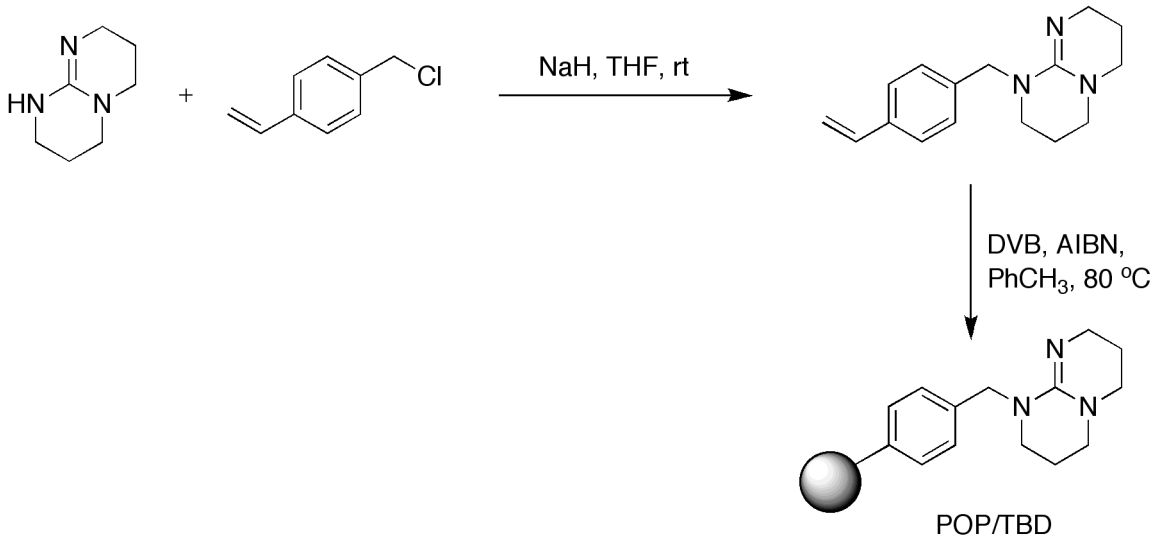

Figure 2.13. Synthetic routes for porous Poly-DVB/TBD copolymers.

The use of a toluene porogen and rigid TBD monomer allowed the synthesis of highly porous crosslinked copolymers by AIBN initiated polymerization. Our work indicates that POP/TBD is an active catalyst for transesterification of glycerides to FAME. At 95 °C, glycerides from pre-treated greases were nearly completely converted to FAME in the presence of 10% POP/TBD loading after 4 hours of reaction (Figure 2.14). Ideally, supported acid and base catalysts can be used in the same reactor (e.g., in two catalyst beds) for a single-step BD synthesis.

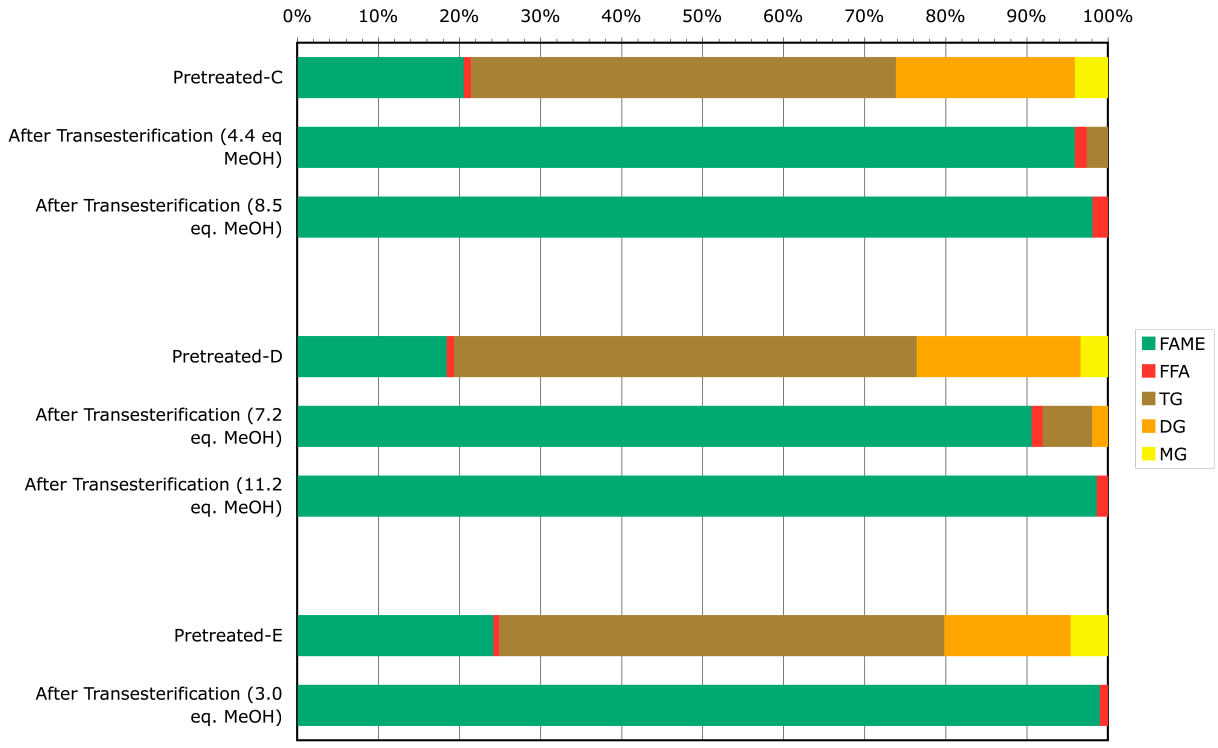

Figure 2.14. Transesterification of a variety of pretreated greases with Poly-DVB/TBD at 10 mol% loading, 95 °C, for 4 h, and varying amounts of methanol.

2.3 Concluding Remarks

We have successfully synthesized a family of diarylammonium catalysts for the esterification of FFA in greases containing between 12 – 40% FFA. The catalysts were highly effective for the esterification of FFA in greases, reducing the FFA contents to <1%. We have also incorporated these diarylammonium catalysts into insoluble porous polymers via free radical initiated polymerization. The immobilized diphenylammonium triflate catalysts were nearly as effective as their homogeneous counterparts in reducing the FFA content in greases to <1%. The heterogeneous diarylammonium catalysts were readily removed from the treated greases, which were then directly converted to FAME in subsequent base-catalyzed transesterification reactions

with standard alkali bases as well as immobilized guanidine base catalyst Poly-DVB/TBD. This work thus demonstrates the utility of diarylammonium salts as catalysts in reducing the FFA content in greases. The two-step process (illustrated in Figure 2.15) represents a promising alternative approach for the production of BD from FFA containing feedstocks.

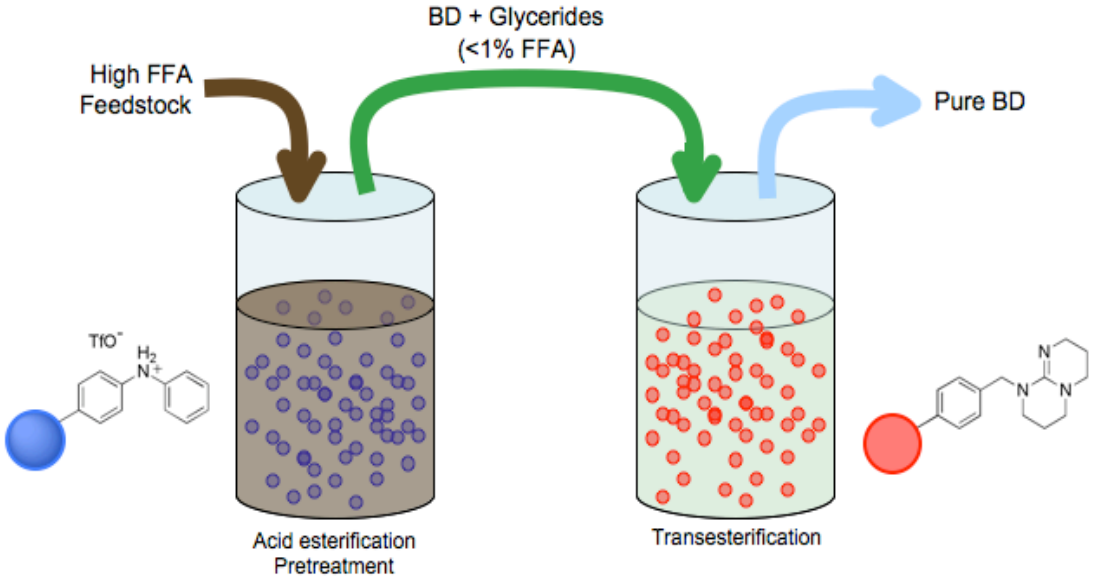

Figure 2.15. Two-step process for the production of pure biodiesel.

2.4 Experimental Section

Materials. Oleic acid (90%), methanol, diphenylamine, aniline, and triflic acid, methanolic sodium methoxide solution were purchased from Aldrich Chemical (Milwaukee, WI). 4-Bromostyrene was purchased from Alfa Aesar (Ward Hill, MA). All other reagents used were of the highest purity available as obtainable from commercial suppliers. Greases with high FFA were from Kaluzny Bros. Inc. and Arlington International Inc. (Irving, TX).

Instrumentation. GC analysis of FAME was carried out with a Hewlett Packard HP 5890 instrument (Agilent, Wilmington DE) equipped with a capillary inlet (on column mode) and an FID detector. The GC capillary columns used were a HP DB-1HT column (15 m × 0.25 mm ×

0.25 μm) and a HP DB-5HT column (15 m × 0.25 mm × 0.25 μm) with He carrier gas set at a linear velocity of 22 cm/sec at 100 °C. The oven temperature profile was: initial temperature 50 °C, hold 1 min; ramp at 15 °C/min to 180 °C; ramp at 7 °C/min to 230 °C. Dodecane was used as an external standard. GC/MS characterization was carried out with a capillary inlet (split mode) and an HP Model 5972 mass detector set to scan from 40 to 550 m/z at a rate of 1.5 scans/s. The capillary column used was a HP DB-5 column (30 m × 0.25 mm × 0.25 μm) with He carrier gas. The pressure was set at 8.0 psi at 50 °C. The injector and detector transfer line temperatures were set at 260 and 280 °C, respectively. The oven temperature profile was: initial temperature 100 °C; ramp at 10 °C/min to 250 °C; hold for 5 min; ramp at 10 °C/min. to 300 °C hold for 5 min.

Lipid mixtures were analyzed by HPLC with a Hewlett Packard HP 1050 instrument (Agilent, Wilmington DE). The lipid mixtures were separated on a Spherisorb CN (100 × 3.0mm, 3μ) column using a normal phase gradient of hexane/0.4% acetic acid and methyl t-butyl ether/0.4% acetic acid at a constant flow of 0.43 mL/min. Eluants from the column were detected by an evaporator light-scattering detector (ELSD ILA; All-tech, Deerfield, IL). The ELSD nebulizer temperature was set at 40 °C and the nitrogen flow of 35 mL/min. All peaks were quantitated from standard curves constructed with reference compounds (4).

NMR spectra were recorded on Bruker NMR 400 DRX (Bruker Instruments, Billerica, MA) and Varian (Varian, Palo Alto, CA) Gemini 200-MHz spectrometer. The ^{1}H-NMR spectra were referenced to the proton resonance resulting from incomplete deuteration of the deuterated chloroform (δ 7.26) and deuterated acetone (δ 2.09). Infrared spectra were obtained on a Nicolet (Nicolet Instruments, Lanham, MD) Magna-IR 560 spectrometer. Microwave reactions were performed with a CEM Discover–LabMate (CEM, Matthews, NC) microwave reactor. Nitrogen

adsorption experiments were performed on a Quantachrome-1C (Quantachrome Instruments, Boynton Beach, FL) surface area analyzer at liquid nitrogen temperature. All the surface areas and pore volumes were calculated based on the Barrett, Joyner, and Halenda (BJH) method.[26]

Synthesis of POP Heterogeneous Acid Catalysts. *Porous 1,4-divinylbenzene/4-bromostyrene (Poly-DVB/BrPh) copolymer*. A 20 mL thick-walled pressure vial equipped with a magnetic stir bar and septum was charged with 2,2'-azobis(2-methylpropionitrile) (AIBN, 44.2 mg, 0.27 mmol), 1,4-divinylbenzene (DVB, 2.58 mL, 2.36 g, 18.1 mmol), 4-bromostyrene (0.42 mL, 0.59 g, 3.2 mmol), and toluene (3.0 mL, 1:1 total monomer volume). The stirred mixture was degassed and purged with argon gas three times. The septum was replaced with a screw cap, and the vial was immersed in an oil bath at 80 °C for 12 hours. At the end of the reaction, the solidified mixture was dried in vacuo for 6 hours. The solid polymer was ground and purified by Soxhlet extraction with methanol for 24 hours. The polymer resin was dried in vacuo to give a white solid with a loading of 1.1 mmol *BrPh* per gram of polymer. IR (cm^{-1}): 2920.2 (b), 1599.0 (w), 1512.2 (s), 1487.1 (s), 1442.8 (s), 1406.1 (s), 1338.6 (w), 1309.7 (w), 1288.5 (w), 1072.4 (s), 1026.1 (s), 1008.8 (s), 987.6 (s), 902.7 (vs), 823.6 (vs), 794.7 (vs), 744.5 (s), 707.9 (vs), 692.4 (s), 603.7 (s).

Porous 1,4-divinylbenzene/Phenyl(vinylaniline) (Poly-DVB/PVA-1) copolymer. In a glove box, a 10 mL thick-walled pressure vial equipped with a silicone seal cap was charged with the above *Poly-DVB/BrPh copolymer (1.46 g,* 1.61 mmol *BrPh*), tris(dibenzylideneacetone)-dipalladium (Pd_2dba_3, 14.8 mg, 0.016 mmol), racemic-2,2'-bis(diphenylphosphino)-1,1'-binaphthyl (*rac*BINAP, 30.1 mg, 0.048 mmol), and NaO^{t}Bu (0.223 g, 2.25 mmol) (6). Aniline (0.15 mL, 1.61 mmol) and distilled toluene (4.0 mL) were added via a syringe to the sealed vial, and the mixture was sonicated for 30 minutes. The reaction vessel was subjected to microwave

irradiation under the following conditions: power 300 W; pressure, 100 psi; temperature, 140 °C; reaction time, 25 min. After the mixture was cooled, the contents were centrifuged, the organic layer decanted, and the solid residue sonicated with THF (10 mL) for 30 min. After centrifugation, THF was decanted and a mixture of triethylamine/THF 1:1, (10 mL) added. After 30 min. of stirring, the mixture was centrifuged and the solvents removed to afford 1.51 g of *porous Poly-DVB/PVA-1 copolymer*. IR (cm^{-1}): 2864.3 (b), 1604.8 (s), 1506.4 (s), 1481.3 (s), 1419.6 (w), 1265.3 (w), 1163.1 (w), 1018.4 (s), 1010.7 (s), 987.6 (s), 964.4 (s), 877.6 (s), 823.6 (s), 794.7 (vs), 754.2 (vs), 727.2 (s), 707.9 (vs), 688.6 (vs), 669.3 (s), 661.6 (w), 646.2 (s), 605.7 (vs).

Porous 4-divinylbenzene/Phenyl(vinylanilinium) triflate copolymer, **2.10**. 0.75g of the above *Poly-DVB/PVA-1* polymer was treated with 14.3 mL of a 0.4 M solution of triflic acid in 10% 1,4-dioxane in dichloromethane (10 equiv.) at r.t. for 6 hours. The mixture was centrifuged, and the remaining solid rinsed and centrifuged five times with EtOAc (10mL) and then dried in vacuo to afford 0.80 g of **2.10** as a pale brown solid (1.0 mmol/g loading). IR (cm^{-1}): 2920.2 (b), 1705.1 (vs), 1597.1 (w), 1485.2 (w), 1446.6 (s), 1421.5 (w), 1371.4 (s), 1298.1 (s), 1236.4 (vs), 1170.8 (s), 1045.4 (vs), 1026.1 (s), 1008.8 (w), 875.7 (w), 825.5 (s), 796.6 (vs), 707.9 (vs), 690.5 (vs), 638.4 (vs), 603.7 (s).

N-phenyl-4-vinylaniline. In a glove box, a 10 mL thick-walled pressure vial equipped with a silicone seal cap was charged with NaO^tBu (0.694 g, 7.00 mmol), $Pd(OAc)_2$ (22.5 mg, 0.10 mmol), and *rac*BINAP (124.5 mg, 0.20 mmol). Aniline (0.46 mL, 5.0 mmol), 4-bromostyrene (0.65 mL, 5.0 mL), and distilled toluene (5 mL) were added via a syringe, and the mixture sonicated for 30 minutes. The reaction vessel was then subjected to microwave irradiation under the following conditions: power, 300 W; pressure, 100 psi; temperature, 140 °C; reaction time,

25 minutes. The color of the reaction mixture changed from red to dark brown. The mixture was diluted with ethyl acetate and filtered. The filtrate was concentrated in vacuo, and the residue purified by flash column chromatography on silica using hexane and 50:1 hexane:EtOAc to give the desired product as a pale yellow solid. ^{1}H NMR ($CDCl_3$, 400 MHz): δ 7.31(d, 2H), 7.24 (d, 2H), 7.03 (d, 2H), 7.00 (d, 2H), 6.90 (t, 1H), 6.64 (q, 1H), 5.74 (s, 1H), 5.60 (d, 1H), 5.10 (d, 1H). MS *m*/*z* = 195.1 ([M^+]).

Tert-butyl phenyl(4-vinylphenyl)carbamate. A 25 mL round bottom 2-neck flask equipped with a magnetic stir bar and a reflux condenser was flame-dried and charged with *N*-phenyl-4-vinylaniline (218.3 mg, 1.12 mmol), di-*tert*-butyl dicarbonate (Boc_2O, 378.0 mg, 1.68 mmol), and 4-(dimethylamino)pyridine DMAP (13.6 mg, 0.11 mmol). Anhydrous acetonitrile (1 mL) was added and the mixture stirred at reflux for 24 hours. After the reaction mixture cooled to r.t. water was added (25 mL). The product was extracted with EtOAc (30 mL) three times and the combined organic layers were washed three times with water (20 mL), dried over $MgSO_4$, and filtered. The solvent was removed in vacuo, and the residue was purified by flash column chromatography on silica using hexane and 50:1 hexane:EtOAc to give the desired product as a pale yellow solid (186.2 mg, 56.3 %). ^{1}H NMR ($CDCl_3$, 400 MHz): δ 7.4 - 7.1(m, 8H), 6.90 (t, 1H), 6.65 (q, 1H), 5.68 (d, 1H), 5.20 (d, 1H), 1.42 (s, 9H). MS *m*/*z* = 295.2 ([M^+]).

Boc-protected porous 1,4-divinylbenzene/Phenyl(vinylaniline), (Poly-DVB/DVA-2-Boc) copolymer. A 20 mL screw-capped glass vial equipped with magnetic stir bar and septum was charged with AIBN (11.3 mg, 0.069 mmol), DVB (0.66 mL, 0.60 g, 4.61 mmol) and *tert-butyl phenyl(4-vinylphenyl)carbamate* (0.15 g, 0.508 mmol), and toluene (0.7 mL, 1:1 total monomer volume). The mixture was degassed and purged three times with argon gas, the septum replaced with a screw cap, and the vial immersed in an oil bath at 80 °C for 12 hours. At the end of the

reaction, the solidified reaction mixture was dried in vacuo for 6 hours. The solid polymer was ground and purified by Soxhlet extraction with methanol for 24 hours. The residue was dried in vacuo to give a white solid of *Poly-DVB/DVA-2-Boc* (0.74 g, 0.68 mmol/g loading). IR (cm^{-1}): 2910.6 (b), 1627.9 (vs), 1583.6 (w), 1508.3 (w), 1491.0 (w), 1440.8 (w), 1367.5 (w), 1332.8 (b), 1161.5 (vs), 1053.1 (s), 1016.5 (s), 987.6 (s), 900.8 (s), 825.5 (s), 794.7 (vs), 758.0 (vs), 729.1 (vs), 707.9 (w), 694.4 (s), 680.9 (vs).

Porous 1,4-divinylbenzene (DVB)/Phenyl(vinylanilinium) triflate copolymer, **2.11**. *Poly-DVB/DVA-2-Boc* (0.70 g, 0.48 mmol) was treated with 20 mL of 0.125 M triflic acid in 10% 1,4-dioxane in dichloromethane (5 equiv.) for the simultaneous deprotection and amine protonation. The mixture was allowed to stir at room temperature for 6 hours and then centrifuged. The solid was rinsed and centrifuged with EtOAc (20 mL, 5×) and the solid residue dried in vacuo to afford **2.11** as a dark brown solid (0.73 g, 0.68 mmol/g loading). IR (cm^{-1}): 2912.5 (b), 1734.0 (s), 1597.1 (s), 1508.3 (s), 1485.2 (w), 1444.7 (w), 1435.0 (w), 1371.4 (w), 1298.1 (s), 1232.5 (vs), 1170.8 (s), 1045.4 (w), 1026.1 (s), 889.2 (w), 825.5 (s), 790.8 (vs), 706.0 (vs), 692.4 (s), 638.4 (vs), 601.8 (vs).

2,6-dimethyl-N-(4-vinylphenyl)aniline. In a glove box a 10 mL thick-walled pressure vial equipped with silicone seal cap was charged with NaO^{t}Bu (0.139 g, 1.40 mmol), $Pd(OAc)_2$ (4.5 mg, 0.020 mmol), and *rac*BINAP (24.9 mg, 0.040 mmol). 2,6-Dimethylaniline (0.13 mL, 1.0 mmol), 4-bromostyrene (0.13 mL, 1.0 mmol), and distilled toluene (1 mL) were added via a syringe to the sealed tube, and the mixture was sonicated for 30 minutes. The reaction vessel was then subjected to microwave irradiation under the following conditions: power, 300 W; pressure, 100 psi; temperature, 140 °C; reaction time, 10 minutes. The color of the reaction mixture changed from red to dark brown. The mixture was diluted with ethyl acetate and

filtered. The filtrate was concentrated in vacuo, and the residue was purified by flash column chromatography on SiO_2 using hexane and 50:1 hexane:EtOAc to give the desired product as a yellow oil (0.169 g, 75.9 %). ^{1}H NMR ($CDCl_3$, 400 MHz): δ 7.20 (d, 2H), 7.11 (d, 2H), 7.01 (d, 2H), 6.45 (t, 1H), 6.56 (q, 1H), 5.51 (d, 1H), 5.01 (d, 1H), 2.12 (s, 6H). MS m/z = 223.2 ([M^+]).

3,5-dimethyl-N-(4-vinylphenyl)aniline. In a glove box a 10 mL thick-walled pressure vial equipped with silicone seal cap was charged with NaO^{t}Bu (0.139 g, 1.40 mmol), $Pd(OAc)_2$ (4.5 mg, 0.020 mmol), and *rac*BINAP (24.9 mg, 0.040 mmol). 3,5-Dimethylaniline (0.13 mL, 1.0 mmol), 4-bromostyrene (0.13 mL, 1.0 mmol), and distilled toluene (1 mL) were added via a syringe to the sealed tube, and the mixture was sonicated for 30 minutes. The reaction vessel was then subjected to microwave irradiation under the following conditions: power, 300 W; pressure, 100 psi; temperature, 140 °C; reaction time, 10 minutes. The color of the reaction mixture changed from red to dark brown. The mixture was diluted with ethyl acetate and filtered. The filtrate was concentrated in vacuo, and the residue was purified by flash column chromatography on SiO_2 using hexane and 50:1 hexane:EtOAc to give the desired product as a yellow oil (0.167 g, 74.8 %). ^{1}H NMR ($CDCl_3$, 400 MHz): δ 7.30 (d, 2H), 6.99 (d, 2H), 6.70 (s, 2H), 6.40 (q, 1H), 6.59 (s, 1H), 5.67 (d, 1H), 5.09 (d, 1H), 2.26 (s, 6H). MS m/z = 223.2 ([M^+]).

2,4,6-trimethyl-N-(4-vinylphenyl)aniline. In a glove box a 10 mL thick-walled pressure vial equipped with silicone seal cap was charged with NaO^{t}Bu (0.139 g, 1.40 mmol), $Pd(OAc)_2$ (4.5 mg, 0.020 mmol), and *rac*BINAP (24.9 mg, 0.040 mmol). 2,4,6-Trimethylaniline (0.14 mL, 1.0 mmol), 4-bromostyrene (0.13 mL, 1.0 mmol), and distilled toluene (1 mL) were added via a syringe to the sealed tube, and the mixture was sonicated for 30 minutes. The reaction vessel was then subjected to microwave irradiation under the following conditions: power, 300 W; pressure, 100 psi; temperature, 140 °C; reaction time, 10 minutes. The color of the reaction

mixture changed from red to dark brown. The mixture was diluted with ethyl acetate and filtered. The filtrate was concentrated in vacuo, and the residue was purified by flash column chromatography on SiO_2 using hexane and 50:1 hexane:EtOAc to give the desired product as a yellow oil (0.198 g, 83.6 %). ^{1}H NMR ($CDCl_3$, 400 MHz): δ 7.20 (d, 2H), 6.92 (s, 2H), 6.59 (q, 1H), 6.42 (d, 2H), 5.50 (d, 1H), 4.99 (d, 1H), 2.29 (s, 3H), 2.15 (s, 6H). MS *m*/*z* = 237.1 ([M^+]).

2,6-difluoro-N-(4-vinylphenyl)aniline. In a glove box a 10 mL thick-walled pressure vial equipped with silicone seal cap was charged with NaO^{t}Bu (0.277 g, 2.80 mmol), $Pd(OAc)_2$ (9.0 mg, 0.040 mmol), and *rac*BINAP (49.8 mg, 0.080 mmol). 2,6-difluoroaniline (0.23 mL, 2.0 mmol), 4-bromostyrene (0.27 mL, 2.0 mmol), and distilled toluene (1 mL) were added via a syringe to the sealed tube, and the mixture was sonicated for 30 minutes. The reaction vessel was then subjected to microwave irradiation under the following conditions: power, 300 W; pressure, 100 psi; temperature, 140 °C; reaction time, 15 minutes. The color of the reaction mixture changed from red to dark brown. The mixture was diluted with diethyl ether and extracted once with HCl (1 M, 40 mL) and sat. $NaHCO_3$ (40 mL). Organics were dried over $MgSO_4$ and concentrated in vacuo, and the residue was purified by flash column chromatography on SiO_2 using hexane and 50:1 hexane:EtOAc to give the desired product as a yellow oil (0.358 g, 76.0 %). ^{1}H NMR ($CDCl_3$, 400 MHz): δ 7.29 (d, 2H), 7.10 (d, 2H), 6.95 (t, 1H), 6.74 (d, 2H), 6.63 (q, 1H), 5.58 (d, 1H), 5.08 (d, 1H). MS *m*/*z* = 231.2 ([M^+]).

Porous 1,4-divinylbenzene/2,6-dimethyl-N-(4-vinylphenyl)aniline (Poly-DVB/2,6-PVA) copolymer. A 20 mL scintillation vial equipped with a magnetic stir bar and a septum was charged with AIBN (12.7 mg, 0.077 mmol), 1,4-divinylbenzene (DVB) (0.74 mL, 0.68 g, 5.20 mmol), 2,6-dimethyl-N-(4-vinylphenyl)aniline (0.169 g, 0.759 mmol), and toluene (0.8 mL, 1:1 total monomer volume). The mixture was degassed and purged three times with argon gas. The

septum was replaced with a screw cap, and the vial was immersed into oil bath at 80 °C for 12 hours with stirring. At the end of the reaction, the reaction mixture had solidified and was dried in vacuo for 6 hours. The solid polymer was ground and purified via soxhlet extraction with methanol as the solvent for 24 hours. The residue was dried in vacuo to give a white solid of *Poly-DVB/2,6-PVA* (0.888 g, 0.90 mmol/g). IR (cm^{-1}): 2916.4 (s), 2183.4 (w), 2164.1 (b), 2021.4 (b), 1979.0 (w), 1955.8 (w), 1708.9 (w), 1597.1 (vs), 1508.3 (w), 1446.6 (w), 1307.7 (b), 1165.0 (s), 987.6 (s), 902.7 (s), 829.4 (s), 794.7 (vs), 767.7 (s), 709.8 (vs).

Porous 1,4-divinylbenzene/3,5-dimethyl-N-(4-vinylphenyl)aniline, (Poly-DVB/3,5-PVA) copolymer. A 20 mL scintillation vial equipped with a magnetic stir bar and a septum was charged with AIBN (12.5 mg, 0.073 mmol), DVB (0.73 mL, 0.67 g, 5.13 mmol), 3,5-dimethyl-N-(4-vinylphenyl)aniline (0.167 g, 0.748 mmol), and toluene (0.8 mL, 1:1 total monomer volume). The mixture was degassed and purged three times with argon gas. The septum was replaced with a screw cap, and the vial was immersed into oil bath at 80 °C for 12 hours with stirring. At the end of the reaction, the reaction mixture had solidified and was dried in vacuo for 6 hours. The solid polymer was ground and purified via soxhlet extraction with methanol as the solvent for 24 hours. The residue was dried in vacuo to give a white solid of *Poly-DVB/3,5-PVA* (0.891 g, 0.90 mmol/g). IR (cm^{-1}): 2916.4 (w), 2183.4 (w), 2164.1 (s), 2021.4 (w), 1979.0 (b), 1955.8 (b), 1708.9 (s), 1597.1 (w), 1508.3 (s), 1446.6 (w), 1323.2 (s), 1157.3 (s), 1010.7 (s), 987.6 (vs), 902.7 (s), 833.3 (vs), 794.7 (vs), 709.8 (vs).

Porous 1,4-divinylbenzene/2,4,6-trimethyl-N-(4-vinylphenyl)aniline, (Poly-DVB/2,4,6-PVA) copolymer. A 20 mL scintillation vial equipped with a magnetic stir bar and a septum was charged with AIBN (14.9 mg, 0.091 mmol), DVB (0.87 mL, 0.79 g, 6.09 mmol), 2,4,6-trimethyl-N-(4-vinylphenyl)aniline (0.198 g, 0.836 mmol), and toluene (0.8 mL, 1:1 total

monomer volume). The mixture was degassed and purged three times with argon gas. The septum was replaced with a screw cap, and the vial was immersed into oil bath at 80 °C for 12 hours with stirring. At the end of the reaction, the reaction mixture had solidified and was dried in vacuo for 6 hours. The solid polymer was ground and purified via soxhlet extraction with methanol as solvent for 24 hours. The residue was dried in vacuo to give a white solid of *Poly-DVB/2,4,6-PVA* (0.990 g, 0.84 mmol/g). IR (cm^{-1}): 2916.4 (b), 2152.6 (w), 2021.4 (b), 1979.0 (w), 1708.9 (w), 1604.8 (w), 1508.3 (s), 1485.2 (s), 1442.8 (w), 1311.6 (w), 987.6 (s), 902.7 (vs), 829.4 (vs), 794.7 (vs), 709.8 (vs).

Porous 1,4-divinylbenzene/2,6-difluoro-N-(4-vinylphenyl)aniline (Poly-DVB/2,6-2F-PVA) copolymer. A 20 mL scintillation vial equipped with a magnetic stir bar and a septum was charged with AIBN (24.8 mg, 0.151 mmol), DVB (1.44 mL, 1.32 g, 10.13 mmol), 2,6-difluoro-N-(4-vinylphenyl)aniline (0.330 g, 1.415 mmol), and toluene (1.5 mL, 1:1 total monomer volume). The mixture was degassed and purged three times with argon gas. The septum was replaced with a screw cap, and the vial was immersed into oil bath at 80 °C for 12 hours with stirring. At the end of the reaction, the reaction mixture had solidified and was dried in vacuo for 6 hours. The solid polymer was ground and purified via soxhlet extraction with methanol as the solvent for 24 hours. The residue was dried in vacuo to give a white solid of *Poly-DVB/2F-PVA* (1.65 g, 0.857 mmol/g). IR (cm^{-1}): 2916.4 (s), 2160.3 (w), 2021.4 (b), 1967.4 (w), 1600.9 (s), 1512.2 (vs), 1489.1 (s), 1446.6 (s), 1311.6 (w), 1234.4 (w), 1003.0 (vs), 987.6 (s), 902.7 (s), 829.4 (s), 794.7 (vs), 709.8 (vs), 613.4 (vs).

Activation of Porous polymers to generate Poly-DVB/PVA-OTf analogs (**2.11**-**2.14**). The above polymers were activated in a similar fashion as **2.10** by treating with 15 mL of 0.23 M solution of triflic acid in 10% 1,4-dioxane in dichloromethane (5 equiv.). The mixture was

allowed to stir at room temperature for 6 hours and then centrifuged. The solid was rinsed and centrifuged with EtOAc (5 x 20 mL) and then dried in vacuo to afford activated polymer. IR for **2.11** (cm^{-1}): 2920.2 (s), 2156.4 (w), 2029.1 (b), 1971.2 (w), 1600.9 (w), 1508.3 (vs), 1485.2 (w), 1446.6 (s), 1288.4 (s), 1226.7 (vs), 1172.7 (s), 1030.0 (vs), 987.6 (w), 902.7 (w), 825.5 (s), 790.8 (vs), 705.9 (vs), 636.5 (vs). IR for **2.12** (cm^{-1}): 2920.2 (s), 2160.3 (w), 2017.5 (b), 1971.3 (w), 1708.9 (w), 1597.1 (s), 1508.3 (s), 1485.2 (w), 1446.6 (s), 1288.4 (s), 1226.7 (vs), 1172.7 (vs), 1026.1 (vs), 825.5 (s), 790.8 (vs), 706.0 (vs), 636.5 (vs). IR for **2.13** (cm^{-1}): 2920.2 (w), 2360.9 (w), 1604.8 (w), 1508.3 (s), 1485.2 (w), 1446.6 (s), 1280.7 (s), 1226.7 (s), 1172.7 (s), 1030.0 (vs), 898.8 (w), 825.5 (s), 794.7 (vs), 706.0 (vs), 636.5 (s), 628.8 (s). IR for **2.14** (cm^{-1}): 2916.4 (s), 2160.3 (w), 2021.4 (b), 1967.4 (w), 1600.9 (s), 1512.2 (vs), 1489.0 (s), 1446.6 (s), 1311.6 (w), 1234.4 (w), 1003.0(vs), 987.6 (s), 902.7 (s), 829.4 (s), 794.7 (vs), 709.8 (vs), 613.4 (vs). IR for **2.15** (cm^{-1}): 2912.5 (w), 1600.9 (s), 1512.2 (vs), 1489.1 (s), 1450.5 (s), 1300.0 (w), 1234.4 (s), 1172.7 (w), 1122.6 (w), 1003.0 (vs), 983.7 (s), 902.7 (s), 825.5 (s), 794.7 (vs), 706.0 (vs), 605.6 (s).

Synthesis of Mesoporous Silica Heterogeneous Catalysts. *4-(tert-butoxydimethoxysilyl)-N-phenylaniline*. In a glove box a 10 mL thick-walled pressure vial equipped with silicone seal cap was charged with 4-(trimethoxysilyl)aniline (593.0 mg, 2.50 mmol), NaO^{t}Bu (347.0 mg, 3.5 mmol), $Pd_2(dpa)_3$•$CHCl_3$ (23.0 mg, 0.0025 mmol), and *rac*BINAP (46.7 mg, 0.075 mmol). Bromobenzene (0.26 mL, 2.5 mmol) and distilled toluene (6 mL) were added via syringe to the sealed tube, and the mixture was sonicated for 30 minutes. The reaction vessel was then subjected to microwave irradiation under the following conditions: power, 300 W; pressure, 100 psi; temperature, 140°C; reaction time, 25 minutes. The color of the reaction mixture changed from dark brown to dark red. The mixture was diluted with hexanes and filtered. The filtrate

was concentrated in vacuo, and the residue was purified by flash column chromatography on SiO_2 using hexane and 50:1 hexane:EtOAc to give the desired product as a yellow liquid (535.8 mg, 64 %). ^{1}H NMR ($CDCl_3$, 400 MHz): δ 7.51 (d, 2H), 7.27 (t, 2H), 7.11 (d, 2H), 7.04 (d, 2H), 6.95 (t, 1H), 5.28 (broad s, 1H), 3.55 (s, 6H), 1.33 (s, 9H).

Synthesis of MCM-48/PVA-OTf. A solution of cetyltrimethylammonium bromide CTAB (7.8 g), H_2O (360 mL), EtOH (150 mL), and ammonia (39 mL) was stirred for 10 minutes at room temperature. To this solution tetraethylorthosilicate TEOS (10.2 g) and 4-(*tert*-butoxydimethoxysilyl)-*N*-phenylaniline (250.0 mg, 0.75 mmol) were added and allowed to stir for 4 hours at room temperature. Final solid was filtered and rinsed thoroughly with water and EtOH, sequentially. Surfactant was removed by neutral extraction (three times) with a 1 wt% NaCl in MeOH (200 mL) for 6 hours at room temperature. Solid was filtered, rinsed thoroughly with water and EtOH, and air dried (after each extraction) to afford MCM-48/PVA (2.5 g). Dried solid (2.2 g, 0.44 mmol/g) was treated with a triflic acid solution (10 equiv., 0.5 M 10% 1,4-dioxane in DCM). After suspension was stirred for 2 hours at room temperature, contents were centrifuged and solvents decanted. The activated solid MCM-48/PVA-OTf was rinsed and centrifuged five times to remove excess TfOH.

Synthesis of SBA-15/PVA-OTf. SBA-15 was prepared according to a previously reported synthesis.[28] A 25 mL round bottom flask was charged with SBA-15 silica (3.2 g), 4-(*tert*-butoxydimethoxysilyl)-*N*-phenylaniline (0.321 g, 0.97 mmol), and toluene (10 mL) and set to reflux for 18 hours under inert atmosphere. After reaction, contents were brought to room temperature and centrifuged. Solvents were decanted and solid was rinsed with toluene (10 mL x 3) and EtOAc (10 mL x 3) to afford SBA-15/PVA (3.5 g, 0.28 mmol/g) in quantitative yield. SBA-15/PVA (1.8 g) was activated with triflic acid (10 equiv., 0.5 M 10% 1,4-dioxane in DCM)

by stirring at room temperature for 2 hours. Contents were then centrifuged and solvents decanted. The activated solid SBA-15/PVA-OTf was rinsed and centrifuged five times to remove excess TfOH.

Synthesis of POP Heterogeneous Base Catalyst. *1-(4-vinylbenzyl)-2,3,4,6,7,8-hexahydro-1H-pyrimido[1,2-a]pyrimidine (TBD-styrene).* A 50 mL, 2-neck round-bottom flask equipped with Argon inlet was flame dried and then charged with sodium hydride (0.265 g, 11.0 mmol) and anhydrous THF (16 mL). To this suspension was added drop-wise a solution of TBD (1.56 g, 11.0 mmol) in anhydrous THF (4 mL). Upon addition hydrogen gas evolved, and solution remained cloudy. After all TBD was added, reaction mixture was evacuated and purged (x3). After 1 hour, 4-vinylbenzyl chloride (1.57 mL, 10.0 mmol) was added, and resulting mixture allowed to stir at rt for 48 h. At the end of the reaction, mixture was centrifuged (3000 rpm) and rinsed thoroughly with dichloromethane. Contents were dried in vacuo to afford the final TBD-styrene monomer (1.51 g, 59% yield). ^{1}H NMR ($CDCl_3$, 400 MHz): δ 7.34 (d, 2H), 7.23 (d, 2H), 6.79 (dd, 1H), 5.76 (d, 1H), 5.19 (d, 1H), 4.57 (s, 2H), 3.40 (t, 2H), 3.16 (t, 2H), 3.10 (t, 2H), 3.00 (t, 2H), 1.90 (p, 2H).

Porous 1,4-divinylbenzene/1,5,7-triazabicyclo[4.4.0]dec-5-ene (or TBD) (Poly-DVB/TBD) copolymer. A 20 mL thick-walled pressure vial equipped with a magnetic stir bar and septum was charged with 2,2'-azobis(2-methylpropionitrile) (AIBN, 18.9 mg, 0.12 mmol), 1,4-divinylbenzene (DVB, 1.09 mL, 1.00 g, 7.7 mmol), TBD-styrene (0.25 g, 0.98 mmol), and toluene (1.2 mL, 1:1 total monomer volume). The stirred mixture was degassed and purged with argon gas three times. The septum was replaced with a screw cap, and the vial was immersed in an oil bath at 80 °C for 12 hours. At the end of the reaction, the solidified mixture was dried in vacuo for 6 hours. The solid polymer was ground and purified by Soxhlet extraction with

methanol for 24 hours. The polymer resin was dried in vacuo to give an off-white solid with a loading of 0.81 mmol TBD per gram of polymer.

Catalytic Reactions. *Esterification of Free Fatty Acid in Greases with Heterogeneous Catalysts*. A mixture of grease (12 wt% FFA, 5g, 2.1 mmol based on the FFA content), methanol (1.4 g, 0.043 mol), and **2.11** (0.68mmol/g, 78 mg, 0.053mmol) was mixed in a 25mL 3-neck round bottom flask equipped with a thermometer and a reflux condenser. The reaction mixture was placed into a mineral oil bath set at 95 °C (90 °C internal temperature) for 2 h. The reaction turned from light yellow to a dark brown color. The mixture was cooled to r.t. and an aliquot (~10 μL) of the product taken for HPLC analysis.

The esterification reaction was also carried out in the same fashion as above in a 50 g scale with a 600 mL high pressure stainless steel vessel (Parr Instrument, Moline IL) equipped with a mechanical stirrer and an electric heating mantle equipped with temperature controller. The vessel was sealed and purged with 40 psi N_2 (3× for 15 min each). The N_2 gas in the reactor was removed and the mixture was heated to 95 °C for ~2 h. The mixture was cooled to r.t., and the product was taken for HPLC analysis.

The crude transesterified product was isolated in one of three ways. In method A, the crude product was vacuum filtered to remove the solid catalysts from the lipid mixture. Hexane (~10 mL) was added to wash the excess lipids from the solid catalyst and the mixture transferred to a 50 mL one neck round bottom flask. The solvent was removed under reduced pressure and the residue (dark brown viscous liquid) was dried under vacuum at r.t. for ~1 h. The brown liquid product was ready for subsequent reactions. In method B, the crude mixture and the solid catalyst were pipetted into a 25 mL test tube. The test tube was capped tightly and centrifuged at 3000 rpm for 45 min. The liquid mixture was carefully decanted to a second test tube and

centrifuged, and the clear supernatant used for subsequent reactions. Method C was similar to method B except that after the centrifugation step to remove the solid catalysts, the reaction mixture was then transferred into a 125mL separatory funnel where the lipid mixture and the methanol/water layer were separated. The lipid mixture settled to bottom and was drained off for subsequent reaction.

Transesterification of Pretreated Greases with Sodium Methoxide and Poly-DVB/TBD. The oil phase, [250 mg, 0.28 mmol (<1 wt.% FFA) relative to equivalent moles of FFA in pretreated greases], methanol (180 mg, 5.6 mmol), and 5.5N sodium methoxide in methanol (2.5 μL, 0.3 wt.%, relative to the equivalent moles of FFA in pretreated greases) were mixed in a 4 mL vial with a Teflon cap. The vial was capped tightly and heated at 50°C for ~2 h. The reaction mixture went from brown to light yellow in color. The mixture was allowed to cool to r.t. and two phases were observed. The mixture was transferred with hexane into a 60 mL separator funnel and ~5 mL of 1N HCl added to the mixture to neutralize the base. The hexane layer was washed with water (~30 mL, 2×), dried with $MgSO_4$, and solvent removed under reduced pressure. The light yellow liquid product was analyzed by HPLC.

Catalyst re-use experiments. Catalyst **2.11** (100 mg) recovered from the above experiment was used in the catalyst re-use experiments. The residual dark brown solid catalyst was treated with 5 equiv. of 0.1 M TfOH in dioxane (~3.9 mL) at r.t. for ~20 h. The solid was centrifuged, washed with dioxane (5 × 8 mL), and dried under vacuum for ~20 h at r.t. The freshly re-activated catalyst, yellow grease (12 wt.% FFA), and methanol were then recharged for a subsequent esterification reaction. This process was repeated for subsequent re-use cycles.

2.5 References

1. Augustine, Heterogeneous Catalysis.

2. Mbaraka, I.; Shanks, B., Conversion of oils and fats using advanced mesoporous heterogeneous catalysts. *Journal of the American Oil Chemists' Society* **2006,** 83, (2), 79-91.

3. Kim, G.-J.; Shin, J.-H., The catalytic activity of new chiral salen complexes immobilized on MCM-41 by multi-step grafting in the asymmetric epoxidation. *Tetrahedron Letters* **1999,** 40, (37), 6827-6830.

4. Beck, J. S.; Vartuli, J. C.; Roth, W. J.; Leonowicz, M. E.; Kresge, C. T.; Schmitt, K. D.; Chu, C. T. W.; Olson, D. H.; Sheppard, E. W.; et al., A new family of mesoporous molecular sieves prepared with liquid crystal templates. *Journal of the American Chemical Society* **1992,** 114, (27), 10834-10843.

5. Jacobsen, E. N.; Zhang, W.; Muci, A. R.; Ecker, J. R.; Deng, L., Highly enantioselective epoxidation catalysts derived from 1,2-diaminocyclohexane. *Journal of the American Chemical Society* **1991,** 113, (18), 7063-7064.

6. Miyashita, A.; Yasuda, A.; Takaya, H.; Toriumi, K.; Ito, T.; Souchi, T.; Noyori, R., Synthesis of 2,2'-bis(diphenylphosphino)-1,1'-binaphthyl (BINAP), an atropisomeric chiral bis(triaryl)phosphine, and its use in the rhodium(I)-catalyzed asymmetric hydrogenation of .alpha.-(acylamino)acrylic acids. *Journal of the American Chemical Society* **1980,** 102, (27), 7932-7934.

7. Noyori, R.; Takaya, H., BINAP: an efficient chiral element for asymmetric catalysis. *Accounts of Chemical Research* **1990,** 23, (10), 345-350.

8. Takeshi Ohkuma, H. T. Y. H. R. N., Asymmetric Hydrogenation of Ketones with Polymer-Bound BINAP/Diamine Ruthenium Catalysts. *Advanced Synthesis & Catalysis* **2001,** 343, (4), 369-375.

9. Hu, A.; Ngo, H. L.; Lin, W., Chiral Porous Hybrid Solids for Practical Heterogeneous Asymmetric Hydrogenation of Aromatic Ketones. *Journal of the American Chemical Society* **2003,** 125, (38), 11490-11491.

10. Hu, A.; Yee, G. T.; Lin, W., Magnetically Recoverable Chiral Catalysts Immobilized on Magnetite Nanoparticles for Asymmetric Hydrogenation of Aromatic Ketones. *Journal of the American Chemical Society* **2005,** 127, (36), 12486-12487.

11. Bournay, L.; Casanave, D.; Delfort, B.; Hillion, G.; Chodorge, J. A., New heterogeneous process for biodiesel production: A way to improve the quality and the value of the crude glycerin produced by biodiesel plants. *Catalysis Today* **2005,** 106, (1-4), 190-192.

12. Kim, H.-J.; Kang, B.-S.; Kim, M.-J.; Park, Y. M.; Kim, D.-K.; Lee, J.-S.; Lee, K.-Y., Transesterification of vegetable oil to biodiesel using heterogeneous base catalyst. *Catalysis Today* **2004,** 93-95, 315-320.

13. Cantrell, D. G.; Gillie, L. J.; Lee, A. F.; Wilson, K., Structure-reactivity correlations in MgAl hydrotalcite catalysts for biodiesel synthesis. *Applied Catalysis A: General* **2005,** 287, (2), 183-190.

14. DiSerio, M.; Ledda, M.; Cozzolino, M.; Minutillo, G.; Tesser, R.; Santacesaria, E., Transesterification of Soybean Oil to Biodiesel by Using Heterogeneous Basic Catalysts. *Industrial & Engineering Chemistry Research* **2006,** 45, (9), 3009-3014.

15. Sercheli, R.; Matheus Vargas, R.; Schuchardt, U., Alkylguanidine-catalyzed heterogeneous transesterification of soybean oil. *Journal of the American Oil Chemists' Society* **1999,** 76, (10), 1207-1210.

16. Schuchardt, U.; Sercheli, R.; Vargas, R. M., Transesterification of vegetable oils: a review. *Journal of the Brazilian Chemical Society* **1998,** 9, 199-210.

17. Anton A. Kiss, A. C. D., Gadi Rothenberg, Solid Acid Catalysts for Biodiesel Production -- Towards Sustainable Energy. *Advanced Synthesis & Catalysis* **2006,** 348, (1-2), 75-81.

18. Harmer, M. A.; Farneth, W. E.; Sun, Q., High Surface Area Nafion Resin/Silica Nanocomposites: A New Class of Solid Acid Catalyst. *Journal of the American Chemical Society* **1996,** 118, (33), 7708-7715.

19. Harmer, M. A.; Sun, Q., Solid acid catalysis using ion-exchange resins. *Applied Catalysis A: General* **2001,** 221, (1-2), 45-62.

20. Harmer, M. A.; Sun, Q.; Vega, A. J.; Farneth, W. E.; Heidekum, A.; Hoelderich, W. F., Nafion resin-silica nanocomposite solid acid catalysts. Microstructure-processing-property correlations. *Green Chemistry* **2000,** 2, (1), 7-14.

21. Toda, M.; Takagaki, A.; Okamura, M.; Kondo, J. N.; Hayashi, S.; Domen, K.; Hara, M., Green chemistry: Biodiesel made with sugar catalyst. *Nature* **2005,** 438, (7065), 178-178.

22. Lin, V. S.-Y.; Nieweg, J. A.; Kern, C.; Trewyn, B. G.; Wiench, J. W.; Pruski, M., Acid-Base Mesoporous Calcia-Silica Catalysts for Cooperative Conversion of Bio-based Feedstocks into Biodiesel. *Prepr. Symp. Am. Chem. Soc, Div. Fuel Chem.* **2006,** 51, 426-427.

23. Santora, B. P.; Gagne, M. R.; Moloy, K. G.; Radu, N. S., Porogen and Cross-Linking Effects on the Surface Area, Pore Volume Distribution, and Morphology of Macroporous Polymers Obtained by Bulk Polymerization. *Macromolecules* **2001,** 34, (3), 658-661.

24. Jensen, T. A.; Liang, X.; Tanner, D.; Skjaerbaek, N., Rapid and efficient microwave-assisted synthesis of aryl aminobenzophenones using Pd-catalyzed amination. *J Org Chem* **2004,** 69, (15), 4936-47.

25. Weigand, K.; Pelka, S., Microwave-assisted Pd(0)-catalyzed amination of aryl halides on solid support. *Mol Divers* **2003,** 7, (2-4), 181-4.

26. Barrett, E. P.; Joyner, L. G.; Halenda, P. P., The Determination of Pore Volume and Area Distributions in Porous Substances. I. Computations from Nitrogen Isotherms. *Journal of the American Chemical Society* **1951,** 73, (1), 373-380.

27. Christie, W. W., Lipid Analysis: Isolation, Separation, Identification, and Structural Analysis of Lipids. **2003,** 205.

28. Zhao, D.; Sun, J.; Li, Q.; Stucky, G. D., Morphological Control of Highly Ordered Mesoporous Silica SBA-15. *Chemistry of Materials* **2000,** 12, (2), 275-279.

CHAPTER 3

Synthesis of Novel Bent-Core Molecules as Potential Biaxial Nematics

3.1 General History and Significance

The first noted observance of liquid crystal-like behavior nearly 120 years ago was by Freidrich Reinitzer,[1] a French botanist, as he was extracting cholesterol from carrots in order to determine its chemical formula. After further exploration, he recognized cholesterol benzoate to have two distinct melting points: this substance first melted into a cloudy liquid at 145.5 C and then further melted to a transparent liquid at 178.5 °C (Figure 3.1). Georges Friedel in 1922 described and coined the three most important features of cholesteric liquid crystals:

- The existence of at least two melting points.
- The reflection of circularly polarized light.
- The ability to rotate the polarization direction of light (birefringence).

The study and application of liquid crystals remained as a novelty material for nearly 80 years after the first discovery. It was not until the early 1970s, researchers began to utilize the physical properties – low viscosity, high elasticity, variable dielectric anisotropy, magnetic susceptibility and rapid stimulus response – of these materials in applications such as simple digital displays found in watches and calculators. But as technology boomed, liquid crystals found themselves ubiquitous in small and large display technologies; in fact

the liquid crystal display (LCD) world market has seen revenue grow to a 33.5 billion dollar (USD) industry over the past thirty years.[2,3] In 1991 Pierre-Gilles de Gennes received the Nobel Prize in physics for making the connection between ordered phenomena found in simple finite systems and complex forms of matter, particularly liquid crystals and polymers.[4]

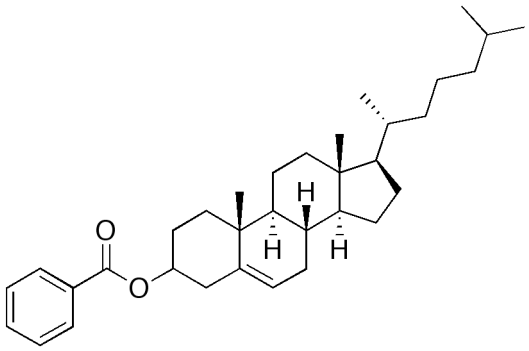

Crystalline $\xrightarrow{145.5\ ^{o}C}$ Cholesteric $\xrightarrow{178.5\ ^{o}C}$ Isotropic

Figure 3.1. Molecular structure and phase map for cholesterol benzoate. Note that phase map indicates two melting points, the intermediate phase being liquid crystalline.

Once the electronics industry caught up to the potential and available physical properties of liquid crystals, the collaborative efforts of organic chemists stimulated by physicists and electrical engineers produced a myriad of liquid crystals with unanticipated characteristics. In this section we present work on molecules based on a 2,5-disubstituted 1,3,4-oxadiazole. The library of organic compounds we synthesized employing this heterocycle are termed non-linear or bent-core liquid crystals. Non-linearity in these molecular structures arises from an exocyclic bond angle across the disubstituted oxadiazole of 134°. In 2004, the Samulski group first reported unequivocal experimental evidence for the existence of the elusive biaxial nematic (N_B) phase.[5] We specifically focused our efforts on judicious structural modifications to the parent molecule that would enable a biaxial nematic to exist at

LCD working temperatures, and to gain an understanding of the extreme sensitivity of this phase.

3.2 Molecular Liquid Crystals – Introduction

The most common phases of condensed matter are the solid and liquid states. These phases are characterized by their intermolecular interactions and the mobility of individual molecules relative to one another. A crystalline solid exemplifies limited to no mobility of individual molecules in this three dimensional periodic arrangement. The arrangement of molecules in this state of matter shows both positional (organization of molecules into a lattice network) and orientational (overall alignment of molecules in defined directions). On the other extreme, a liquid is characterized by a molecule's facile rotation resulting in complete randomness of position and orientation. As the name implies, a liquid crystal (or *mesophase*) is an intermediate phase possessing flow-like properties of a liquid but organizational behavior of a solid, most often orientational ordering (before positional ordering) in the fluid.[4, 6]

Liquid crystals (LC) can be categorized into two separate classes, lyotropic and thermotropic. The first is a two-component liquid crystalline phase that is determined based on solvent-solute interactions and relative amounts of each component. The competing effects of hydrophobic and hydrophilic interactions of amphiphilic molecules in an aqueous environment can stabilize ordered arrangements, depending on water/amphiphile ratio. The two most common LC phases for lyotropics are the hexagonal and lamellar phases. Both of these phases exhibit long-range orientational order. In a hexagonal phase, the amphiphiles assemble to form cylindrical structures over indefinite lengths, which can then assemble into

a hexagonal arrangement. At higher concentrations of amphiphile in water, a lamellar phase exists where amphiphiles organize into bilayer sheets separated by water over long-range distances.

Thermotropic liquid crystals are compounds whose phase behavior is temperature dependent. Most liquid crystals will exhibit reversible mesophase behavior (enantiotropic liquid crystals); those whose phase behaviors differ upon heating and cooling are commonly referred to as monotropics. The next level of categorization for thermotropic liquid crystals is defined by their molecular architectures. This level puts liquid crystals into three different classes: columnar discotics, calamitics and bent-cores. Thermotropic liquid crystals of all types have two distinguishable molecular components that give rise to molecular shape anisotropy. In the example shown in Figure 3.2, terephthal-bis (*p*-butylaniline) (TBBA) has both a rigid core, responsible for generating required excluded-volume interactions, and flexible tails, which facilitate the transition and stabilization of the intermediate LC phase. The idealized structure calamitics is a prolate ellipsoid and is merely a statistical representation of the mesogen.[7]

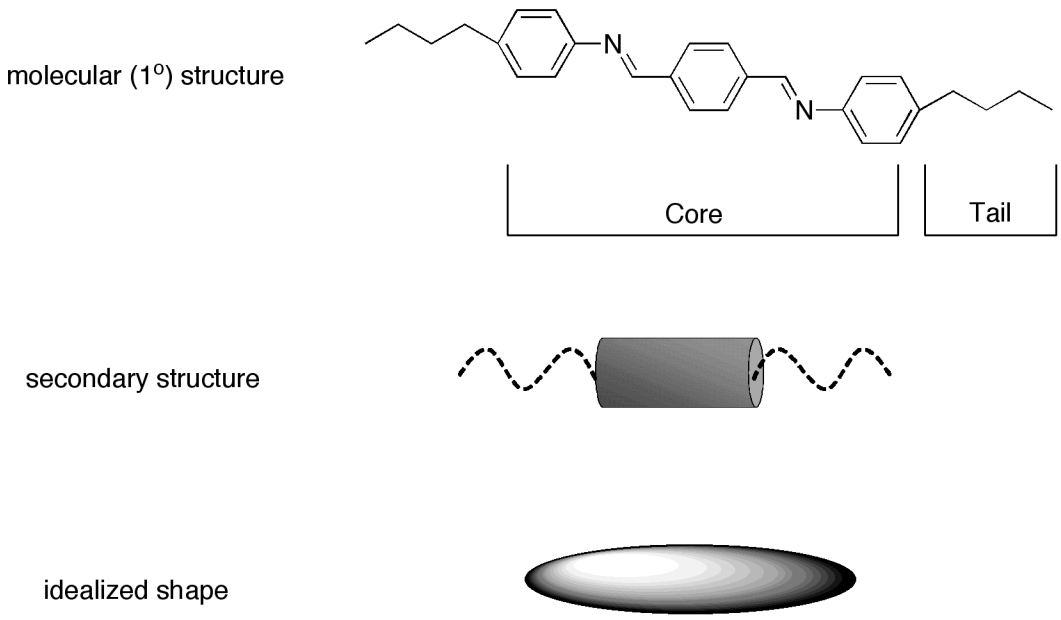

Figure 3.2. Identification of core and tail components of terephthal-bis (*p*-butylaniline) (TBBA) as its primary molecular structure. Additional images show secondary and idealized structures for this rod-shaped liquid crystal.

The potential for these rod-like structures to organize over the long-range is dictated by the core and tail functionalities. The least organized liquid crystalline phase is the uniaxial nematic phase comprised of cylindrical shape molecules where the symmetry axis tends to align along a preferred direction while the molecules undergo diffusional motion typical of liquids. This preferred direction is called the director and is commonly denoted as a unit vector **n**. Cylindrical symmetry describes this phase because the liquid crystal molecular symmetry is blurred by fast isomerization fast and hindered rotation about its long axis. However, this latter rotation can become impeded by extreme structural shapes, leading to a biaxial nematic phase. A pictorial representation (Figure 3.3) illustrates a uniaxial nematic phase with long-range, orientational order but lack of positional order, i.e. the long-axes are

oriented, but their centers of mass are isotropically distributed. For comparison an isotropic distribution of the molecular axes is illustrated in Figure 3.3a and denotes a liquid phase.

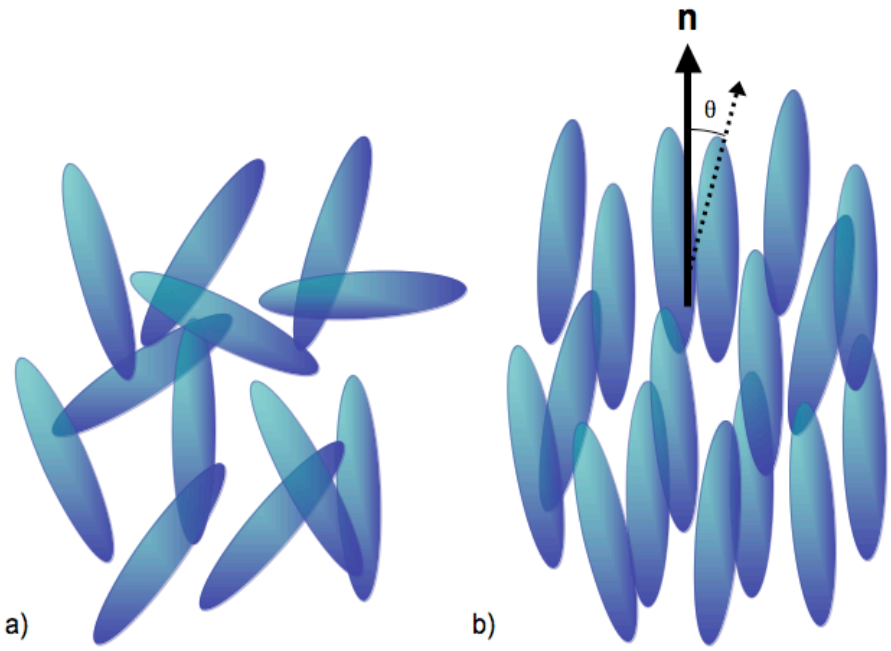

Figure 3.3. Schematic of an idealized prolate ellipsoid representing both isotropic liquid (a) and nematic (b) phases. The long-range orientational order of the nematic phase is indicated by the director **n**.

Depending on the molecular structure of the liquid crystal, the idealized prolate shapes can also assemble into higher ordered, stratified phases, commonly referred to as smectics (Figure 3.4). In addition to long-range orientational ordering, the centers of mass can possess translational ordering, which give rise to layered arrangements. Individual molecules in smectics can freely diffuse within the strata. The simplest of the smectic phases is the smectic A (S_A) where the director is orthogonal to the layers. If the director is tilted with respect to the layer (at an angle θ), the phase is called a smectic C (S_C). There are higher and more complicated levels of organization that give rise to different LC phases, however, these are not relevant to this work and therefore will not be discussed.

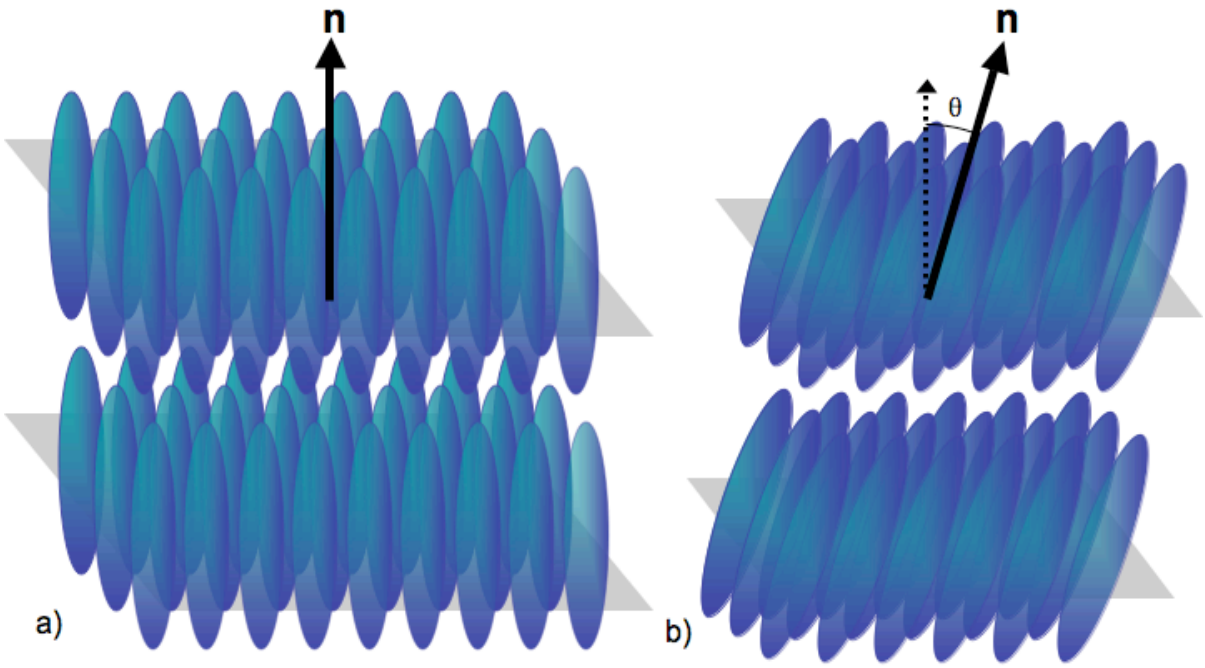

Figure 3.4. Schematic picture of (a) smectic A (S_A) and (b) tilted smectic C (S_C) phases.

Finally, the ordering behavior of liquid crystals is quantified by defining an order parameter (S), which is a reflection of the degree of orientational ordering of the molecule's "symmetry" axis. The order parameter appears in brackets to indicate an average over many molecules equivalently or the average over time for a single molecule. If the molecules are perfectly oriented where $\theta \equiv 0$, the term that is averaged assume the maximized value of $S = 1$. When there is no orientational order (isotropic liquid), $S = 0$ and all molecules at a given time are adopting all orientations. Liquid crystal order parameters fall in between 0 and 1 with the least ordered nematic having S in the range from 0.25 to 0.75, smectics exhibit S ranging from 0.5 to 0.85. The order parameter is usually measured on a macroscopically aligned sample using techniques such as X-ray diffraction[7] and nuclear magnetic resonance (NMR)[8].

Order Parameter:

$$S = \left\langle \frac{3}{2}\cos^2\theta - \frac{1}{2} \right\rangle$$

Isotropic	$S = 0.0$
Nematic	$S = 0.25 - 0.75$
Smectics	$S = 0.5 - 0.85$
Highest order	$S = 1.0$

There are several techniques used to characterize and identify liquid crystal phases. We will briefly discuss each technique employed in this work below.

Polarized optical microscopy.[9-11] This technique in conjunction with a heating stage is the most well and known and widely used method for identifying phases and transitions. For this technique a sample is placed between two crossed polarizers. In a polarizing microscope, the light source most often found below the sample stage where un-polarized light becomes linearly polarized as it passes through the first polarizer. The incident polarized light then passes through the sample at rates dependent on the refractive index of the sample. Light, which has passed through the sample, exits through a second polarizer (also known as the analyzer) in line with the stage and first polarizer. The analyzer and polarizer both have the ability to rotate 360°; in order to observe the birefringent nature of a liquid crystalline material – two independent refractive indices, the polarizer and analyzer are situated 90° with respect to each other. In the absence of any sample or with an isotropic material with a single refractive index (light cannot refract), the observation to the viewer in this orthogonal state is a complete dark state. The reason why liquid crystal textures are visible under this setup is because as light enters a LC sample, the light's velocity decreases by the inverse index of refraction (*n*). Isotropic materials have one single index of refraction, so as polarized light enters these samples, it will travel at the same velocity through the entire

sample. As for an anisotropic material, the index of refraction varies as a function of direction relative to the sample's symmetry axes, therefore, the index of refraction parallel to the director has one value $n_{\parallel}$ while the index of refraction perpendicular will have a second value $n_{\perp}$. The process of decomposing polarized light into two perpendicular components as they grow out of phase as it travels through a sample is known as birefringence.[12, 13] This phenomenon is dependent on the thickness of the sample and is defined as such:

$$\Delta n = \frac{\Gamma}{t} = n_{\parallel} - n_{\perp}$$

where Γ is the optical retardation or the phase difference between the two components of polarized light as they exit the sample, and t is the sample thickness. Light behaves differently as a result of the supramolecular structure of a liquid crystalline phase. Nematic and smectics have very distinguishable features used in the identification of their textures.[14]

Differential Scanning Calorimetry (DSC).[15] This thermoanalytical technique is very useful accurately identify the phase map of a liquid crystal. This is accomplished by measuring the difference in the amount of heat required to increase the temperature of the LC sample and the reference as a function of temperature. By keeping, the sample and reference at the sample temperature through the courses of heating and cooling (typically at a rate of 5 to 10 °C min^{-1}, when the LC undergoes an endothermic phase transition, heat is required by the sample, which is measured by a compensatory amount of heat to the reference. In addition to DSC analysis for liquid crystals, this technique is also very important in measuring subtle glass transition temperatures (T_g) and in evaluating the purity of a sample.

Temperature Dependent Nuclear Magnetic Resonance (NMR).[7, 8] The intricacies of this technique are more complicated. But this method for analyzing supramolecular organizations of liquid crystals in the presence of a magnetic field as well as a function of

temperature is well developed. NMR allows for the extraction of order parameters and will be discussed later in this chapter.

Temperature Dependent X-ray diffraction.[7] This method of supramolecular analysis also enables the extraction of translational order and order parameters. A magnetic or electric field is commonly applied to a bulk LC material. By observing a LC under these field constraints and as a function of temperature, molecular tilt angles and interlayer spacings can be obtained.

3.3 Introduction to Biaxial Nematic Liquid Crystals

Nearly 40 years ago, in 1970, Freiser[16] published a molecular field approximation predicting a second-order transition from a uniaxial nematic phase to a biaxial nematic (N_b). By reducing the molecular symmetry from $D_{\infty h}$ (cylindrical) to D_{2h} (board-like), the formation of a biaxial nematic is stabilized (Figure 3.5). The point at which a uniaxial nematic undergoes a second-order transition to the biaxial phase is known as the Landau point.[16] The secondary orientation axis is of interest in applications such as opto-electronics and display technologies. It is predicted that rotation of the secondary axis in a sandwiched LC cell will occur at a faster switching rates, ultimately leading to a more efficient device.

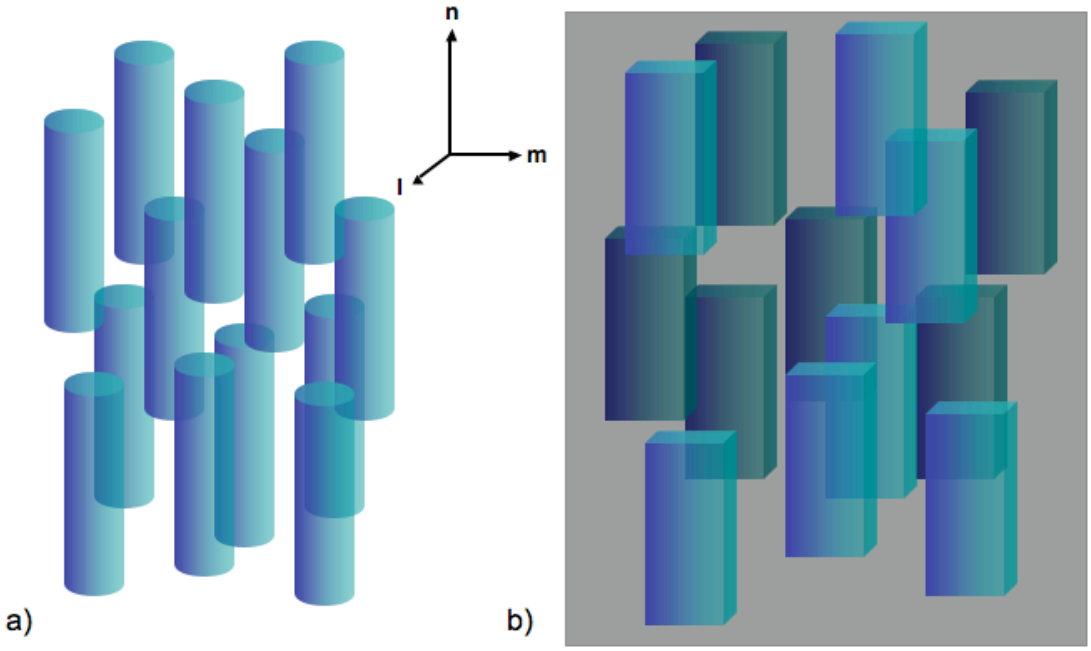

Figure 3.5. a) The organization of molecular cylinders in a uniaxial nematic phase with director **n**. b) The organization of molecular orthorhombics in a biaxial nematic phase with directors **n** and **m**.

Since the prediction of phase biaxiality, organic chemists interested in liquid crystals have sought multiple efforts to molecular engineer compounds to possess the appropriate phase symmetries. It took almost 20 years since Freiser's seminal prediction for claim of a biaxial nematic to surface. Following this claim, several other biaxial LCs were reported.[17-19]

A variety of new phases and applications have evolved since the advent of bent-core mesogens. There have been some claims for a biaxial nematic phase, however, the report was later proven not to be truly biaxial rather the phase biaxiality was induced by an external stimulus.[20] This leads to the criteria required for a stable biaxial nematic: rotation about the long axis is hindered in the (biaxial) nematic phase. As illustrated in Figure 3.5a, a molecule with free rotation in the melt will appear cylindrical in shape. If a molecule were board-like in shape, then rotation about the long-axis becomes hindered and, therefore, in principle will

show the properties of a N_b phase – 3 different refractive indices (Figure 3.5b). The first reported thermotropic liquid crystal with undisputed evidence of phase biaxiality in both the nematic and smectic A phases was by Leube and Finkelmann in 1991.[21] In order to hinder the rotation of a low molecular weight liquid crystal with no parent biaxial character in the nematic phase, they covalently attached the molecule to a polymethacrylate backbone through a flexible spacer (Figure 3.6).

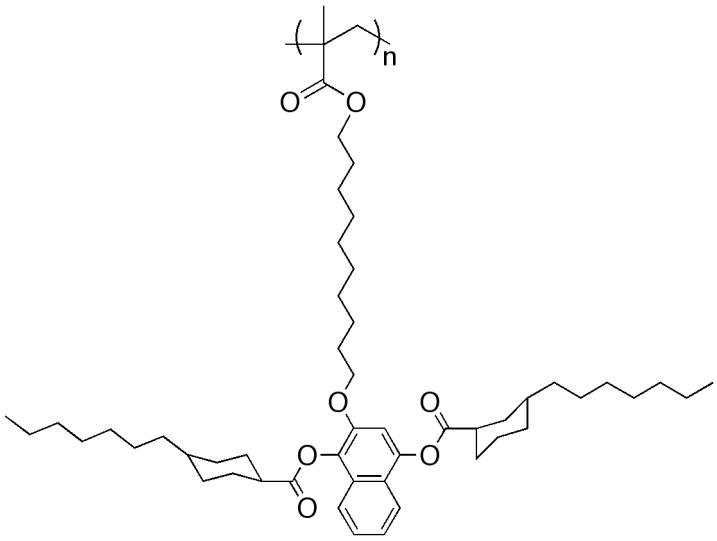

Figure 3.6. Molecular structure of a N_b polymer. A liquid crystal is covalently attached to polymethacrylate through an alkyl spacer in order to hinder its rotation.

To synthesize a molecule with shape biaxiality is not as arduous of an endeavor as demonstrating phase biaxiality. Bent-core mesogens are the newest class of thermotropic liquid crystals, following calamitics and discotics. Several shapes are recognized as promoting shape biaxiality, for instance the following (Figure 3.7) core functionalities have predetermined exocyclic bond angles and have appeared in the literature to give bent-core mesogenic architectures:

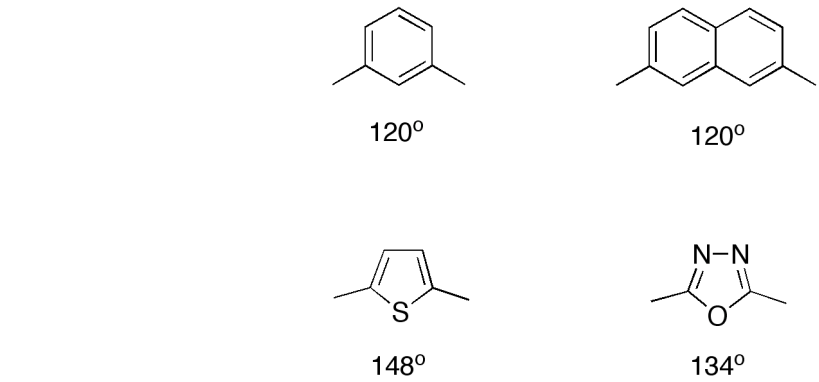

Figure 3.7. Functional moieties with shape biaxial promoting abilities and their corresponding exocyclic bond angles.

The bent nature of these mesogens could provide the appropriate hindered rotation in the nematic phase to stabilize a biaxial state as illustrated in Figure 3.8.

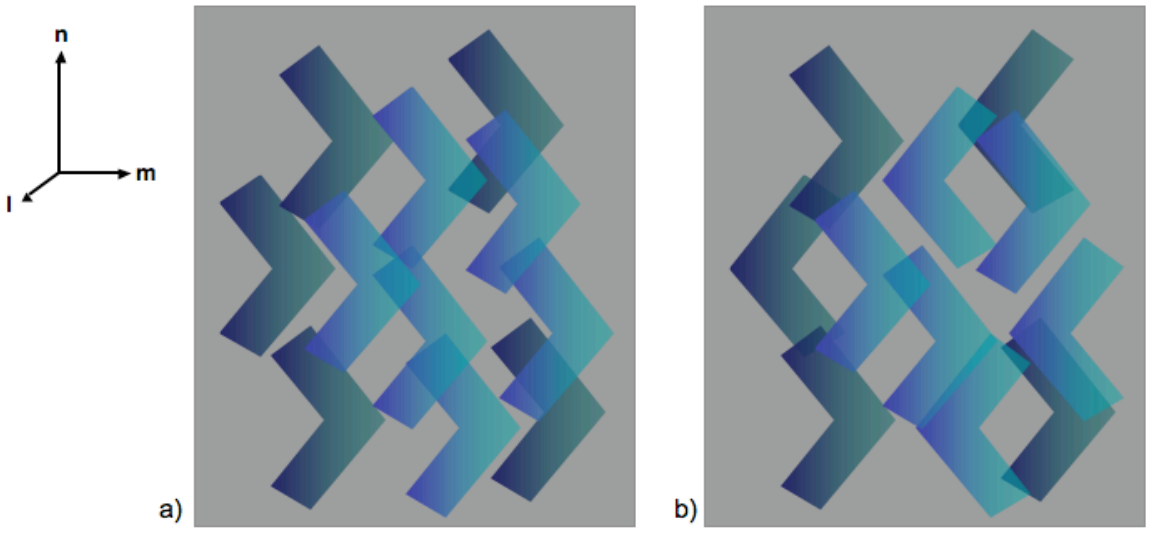

Figure 3.8. The organization of molecular bent-cores in a biaxial nematic phase of polar (a) and apolar (b) fashions with directors **n** and **m**.

Recently, simulations on bent-core mesogens concluded that N_b are in fact.[22] It was not until the Samulski group presented ^{2}H-NMR evidence in 2004, as well as XRD[23] and conoscopy, to finally prove the existence of a low molecular weight thermotropic biaxial

nematic.[5] The molecules synthesized were based on a nonlinear oxadiazole. The 2,5-disubstituted oxadiazole as seen in Figure 3.9 has a large electric dipole moment (~ 5D) that is coincident with the orthogonal secondary axis of the symmetric molecule. It is believed that the bent structure in conjunction with the added intermolecular associations from the strong dipole moment gives rise to the stable N_b with a secondary order parameter $\eta = 0.11$.

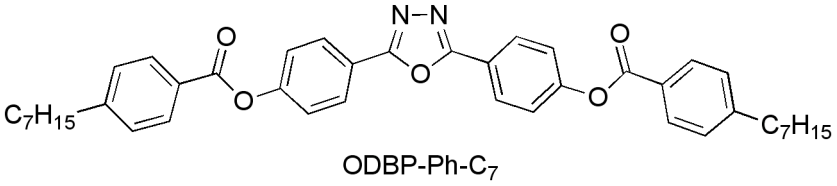

ODBP-Ph-C_7

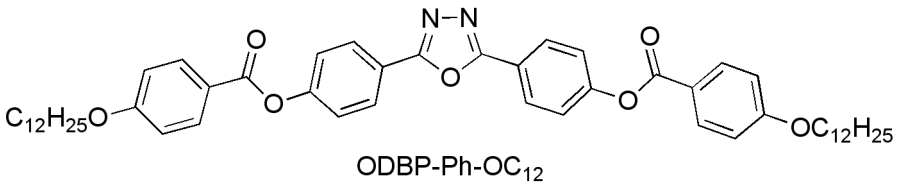

ODBP-Ph-OC_{12}

Figure 3.9. Molecular structures of the two bent-core biaxial nematics liquid crystals, ODBP-Ph-C_7 and ODBP-Ph-OC_{12}.

In addition to the strong evidence for biaxiality in the nematic phase obtained by conoscopy for these mesogens, where surface-induced biaxiality cannot be ruled out, it was the experiment in which ^{2}H-labeled samples are rotated about an axis perpendicular to the magnetic field ~200Hz that provided the conclusive evidence.

In order to extract the phase biaxiality by NMR, we take advantage of the diamagnetic anisotropy $\Delta X = X_{ZZ} - \frac{1}{2}(X_{XX} + Y_{YY})$,[24] which anchors the primary director $\boldsymbol{n}$ (Z axis in a phase-fixed x,y,z coordinate system) along the magnetic field $\mathbf{B}_0$. This macroscopic tensorial property (X_{ij}) is used to construct the order parameter of the nematic phase as a symmetric traceless tensor Q_{ij} where

$$X_{ij} = \begin{pmatrix} X_{XX} & 0 & 0 \\ 0 & X_{YY} & 0 \\ 0 & 0 & X_{ZZ} \end{pmatrix}$$

and where Q_{ij} can be written in the form of the two order parameters q and η

$$Q_{ij} = G\begin{pmatrix} -\frac{1}{2}q(1-\eta) & 0 & 0 \\ 0 & -\frac{1}{2}q(1+\eta) & 0 \\ 0 & 0 & q \end{pmatrix}$$

For phase biaxiality to exist $Q_{XX} \neq Q_{YY}$ and therefore η is non-zero. G is a normalization constant generally chosen to ensure Q_{ZZ}= 1 for a perfectly ordered nematic. In the traceless tensor, q represents the scalar order parameter Q_{ZZ}, which on the microscopic scale is a good approximation of S defined previously.

Since the natural abundance of deuterium is about 0.015%, in order to obtain ^{2}H NMR spectrum, a LC sample must either be synthetically made with meticulously chosen deuteron positions or the sample doped with a high symmetry deuterium probe molecule.[25] In the cases where ODBP mesogens were explored, hexamethylbenzene-d_{18} (HMB) was chosen as a high-melting probe molecule with D_{6h} symmetry. The symmetry of the liquid crystalline phase is revealed by the limited diffusion of the probe molecule. Having 18 deuterons per molecule, allows spectrum to be obtained with as little as 1 weight % probe and satisfactory signal-to-noise. To extract η from a spinning spectrum, the nematogen must first be looked at in a non-spinning, static case where the mesogen exhibits a pair of lines split by ν_Q, where ν_Q is proportional to the nuclear quadrupole tensor component q_{ZZ}. q_{ZZ} is the motionally averaged component of the partially averaged quadrupole tensor $\boldsymbol{q}$ parallel to $\boldsymbol{n}$ while q_{XX} and

q_{YY} are the perpendicular components.[5] These are the components that determine the biaxiality parameter $\eta = (q_{XX} - q_{YY})/q_{ZZ}$.

Now the sample is rotated at a rate which will isotropically orient the primary director ***n*** in a plane that is tangent to the field direction and perpendicular to the rotation axis. When spun, ***n*** experiences the torque due to the magnetic field but additionally a viscous torque. The resulting spectrum is a two-dimensional (2D) "powder" pattern, which is an indication of a weighted average of the quadrupolar splitting of the planar distribution of ***n***. A biaxial nematic is predicted to have different magnetic susceptibilities in three directions; the first two determines the third. In a spun sample where the *Y* and *Z* components are uniformly in a plane distributed and *X* aligns along the rotation axis in order to minimize the magnetic free energy (Figure 3.10). To obtain a planar distribution of ***n***, samples are typically spun at rate greater than 150 Hz.

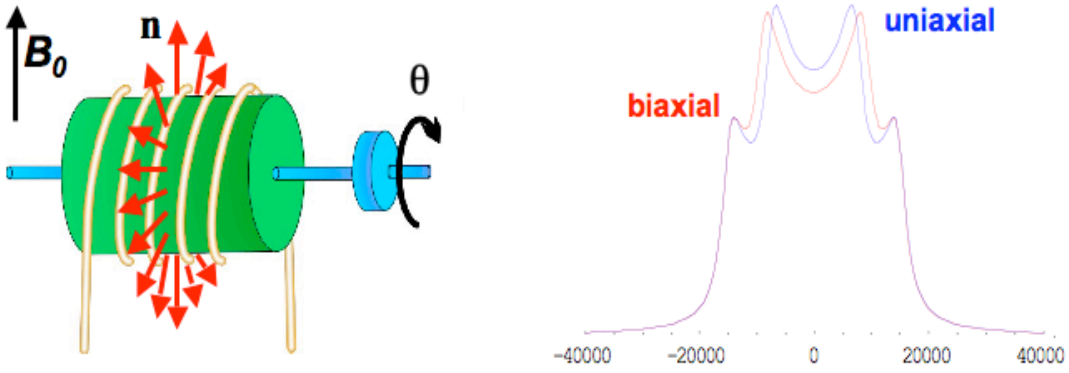

Figure 3.10. Pictorial representation of an isotropic distribution of directors ***n*** in plane parallel to the magnetic field $\mathbf{B}_0$ and the corresponding 2D powder patterns of uniaxial and biaxial nematic phases.

The next step towards determining η for a mesogen is to simulate the powder pattern. We follow the methods of Goldfarb *et al.*[26] and Fan *et al.*[27] In the spinning state ***n*** makes an

angle θ with $\mathbf{B}_0$, and the transition frequency ν' of a given NMR line as a function of θ is given by

$$\nu'(\theta) = \nu_0 \pm \tfrac{1}{4}\nu_Q[(3\cos^2\theta - 1) + \tfrac{1}{2}\eta\sin^2\theta],$$

where ν_0 is the ^{2}H Larmor frequency including the chemical shift. The 2D powder pattern $S(\nu)$ is then calculated as an integral over Lorentzian lines with

$$S(\nu) = \frac{1}{\pi}\int_0^{2\pi} \frac{T_2}{\{1 + 4\pi^2 T_2^2[\nu - \nu'(\theta)]^2\}} d\theta,$$

where T_2 is the spin-spin relaxation time. According to the experimental conditions for the rotated spectrum and the ν_Q obtained from the static spectrum at equivalent temperatures a η value can be determined. Because we are rotating the samples at such high speeds, we needed to address the issues of rotational averaging. This required theory derived by Photinos *et al*. and was applied to the simulated data.[28] The 2D powder pattern was also simulated using the convolution of Gaussian line shape function,

$$S(\nu) = J[0,z]C[e^{-[(\nu-E)^2/2\sigma^2]} + e^{-[(\nu+E)^2/2\sigma^2]}]$$

$$+\sum_{i=1}^{\infty} J[i,z]C[e^{-[(\nu-E+2\omega_s)^2/2\sigma^2]} + e^{-[(\nu-E-2\omega_s)^2/2\sigma^2]} + e^{-[(\nu+E+2\omega_s)^2/2\sigma^2]} + e^{-[(\nu+E-2\omega_s)^2/2\sigma^2]}]$$

where $E = \nu_Q(1+\eta)/8, z = \nu_Q(3-\eta)/16\omega_s$, C is an overall scalar factor, ω_S is the rotation rate in Hz, and σ is the spectral line half-width in Hz. Typically a simulated 2D powder pattern is fitted to the experimental spectrum by visual inspection with the known parameters from the experiment, but in the end a least-squares regression is used ensure a best fit for a given biaxiality η.

3.3.1 Application of Uniaxial and Biaxial Nematics

The most conceivable application for biaxial nematics is in the field display technologies. An LCD is comprised of an array of LC pixels that operate in an ON/OFF or bright/dark state (Figure 3.11).[3, 29] Blue, green and red filters are commonly applied to individual pixels in order to obtain the desired color. In a standard pixel the liquid crystalline material is sandwiched between two polarizers at 90° to each other and two conductive and transparent substrates coated with an alignment material (alignment parallel to adjacent polarizer). The alignment material is used to rotate the director over 90° from top to bottom of the cell. A light source is used to generate plane-polarized light by the first polarizer. So as polarized light passes through the device, its plane of polarization will rotate as it passes through the cell to exit from the second orthogonal polarizer. This scenario affords the "bright" state. The impedance of polarized light – the "dark" state – is accomplished by applying an electric field across the pixel and reorienting the directors perpendicular to the substrate, effectively removing the birefringence of the sample and disabling the rotation of light as it passes through the cell and encounters the second polarizer.

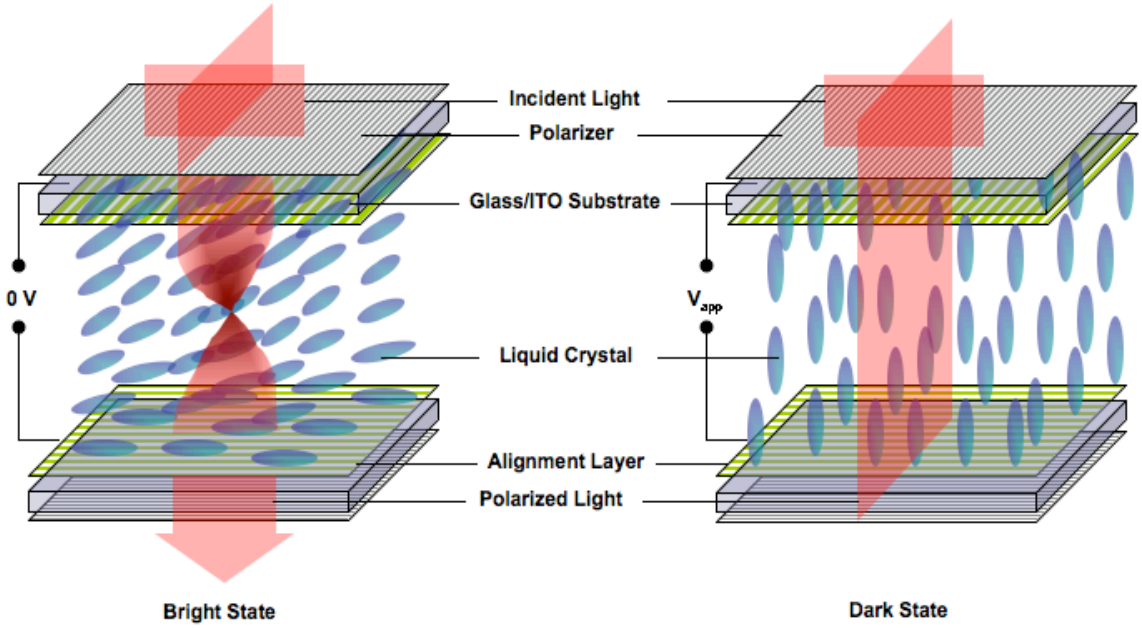

Figure 3.11. Schematic of a uniaxial nematic-based pixel in a bright and dark state with all pixel components appropriately labeled.

In a pixel engineered around a biaxial nematic, the long axes of director **n** align perpendicular to the substrate. When no electric field is present, free rotation of the secondary director **m** allows light to pass through the sample. To obtain a dark state pixel (Figure 3.12), an electric field is applied in the plane of the cell, causing the secondary axes **m** to reorient in a polar or apolar manner coincident with the applied field. Polarized light orthogonal to the alignment of director **m**, results in no light transmittance and therefore a dark state.

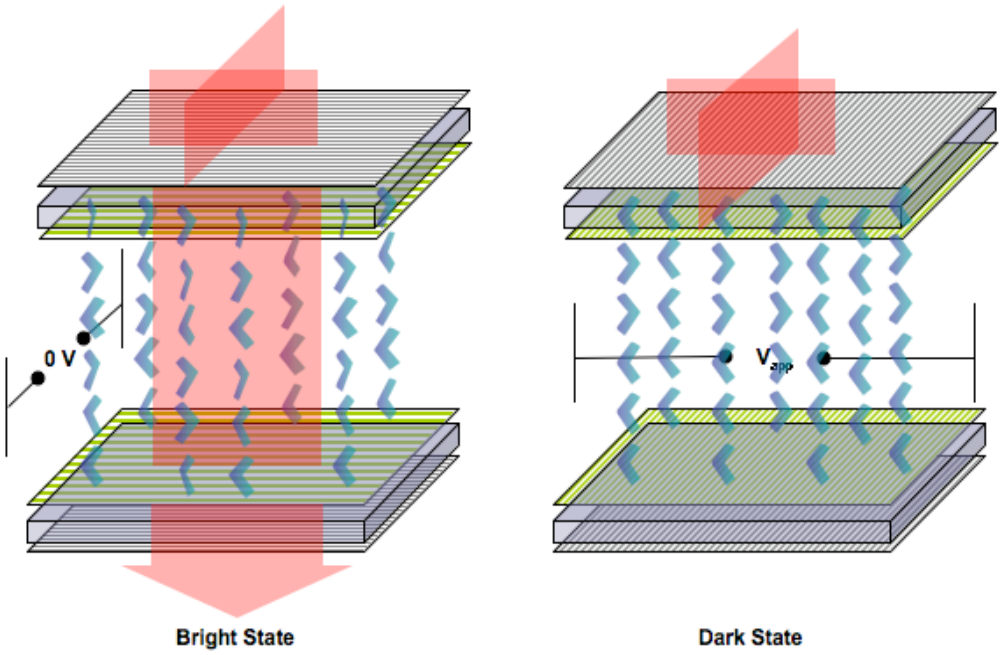

Figure 3.12. Schematic of a hypothetical biaxial nematic-based pixel in bright and dark states.

3.4 Research Objectives

Examples of biaxial nematic mesogens in the literature that provide undeniable evidence are limited to a few example; in lyotropic systems formed from mixed rod-core micellar aggregates and in thermotropics by covalently linked rod/disc structures. Though both of these examples reported evidence for biaxiality, it was not until the Samulski group first reported in 2004 unequivocal experimental evidence for a low molecular weight, biaxial nematic mesogen, ODBP-Ph-C_7.[5] This mesogen belongs to the new class of bent-core liquid crystalline materials. The bent-core or 'boomerang' structures have received a considerable amount of attention as of late, due in part to advent and potential for new applications for liquid crystals.

Bent-core mesogens based on the ODBP moiety may see themselves in device applications if the nematic phase can be reduced to a more thermally accessible range. Currently, what we will refer to as the parent structure, ODBP-Ph-OC_7 has a nematic range between 173 and 222 °C (Figure 3.13). These temperatures are well outside the usable range for display technologies. In addition to their potential uses in devices, by lowering the nematic onset temperatures, and thusly raising the viscosities, this would enable more controlled ^{2}H-NMR analysis at lower critical rotation rates of the biaxial order parameter as a function of temperature.

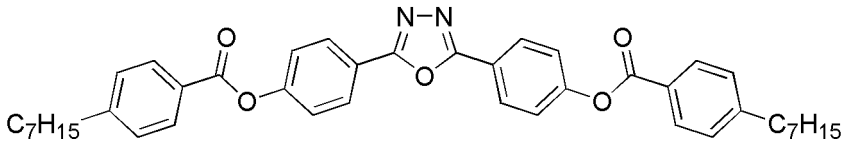

Figure 3.13. Parent structure, ODBP-Ph-C_7 having nematic range between 173 and 222 °C.

In order to obtain a suitable biaxial nematic, we need to explore both core and peripheral modifications that will lower the nematic onset temperature and most importantly retain the biaxial integrity of the nematic phase. In this work we will investigate oxadiazole versus oxazole core variants; more exhaustively, we will alter the peripheries of these molecules, exploring unsymmetric analogues, various isomers to the normal alkyl chains, and anomalous siloxane derivatives. These novel liquid crystals were characterized using Nuclear Magnetic Resonance (NMR), Differential Scanning Calorimetry (DSC), polarized optical microscopy to study and identify phase behaviors, and interference microscopy (conoscopy) to study phase symmetries.

3.5 Synthesis of Derivatives

The synthetic strategy to produce liquid crystal compounds with C_{2v} symmetry – 180° axis of rotation through center of molecule combined with mirror plane in the aromatic plane – requires synthesis of the symmetric 2,5-oxadiazole bisphenol (ODBP). ODBP and its unsymmetric analogue 2,5-oxazole bisphenol were synthesized in similar fashions (Figure 3.14); a methoxy benzhydrazide is reacted with a methoxy benzoyl chloride to afford the diahydrazide, which can subsequently be dehydrated using phosphorus oxychloride ($POCl_3$) to yield the 1,3,4-oxadiazole heterocycle. The final dimethyl ether can be deprotected with boron tribromide (BBr_3) to give the bisphenol ODBP.

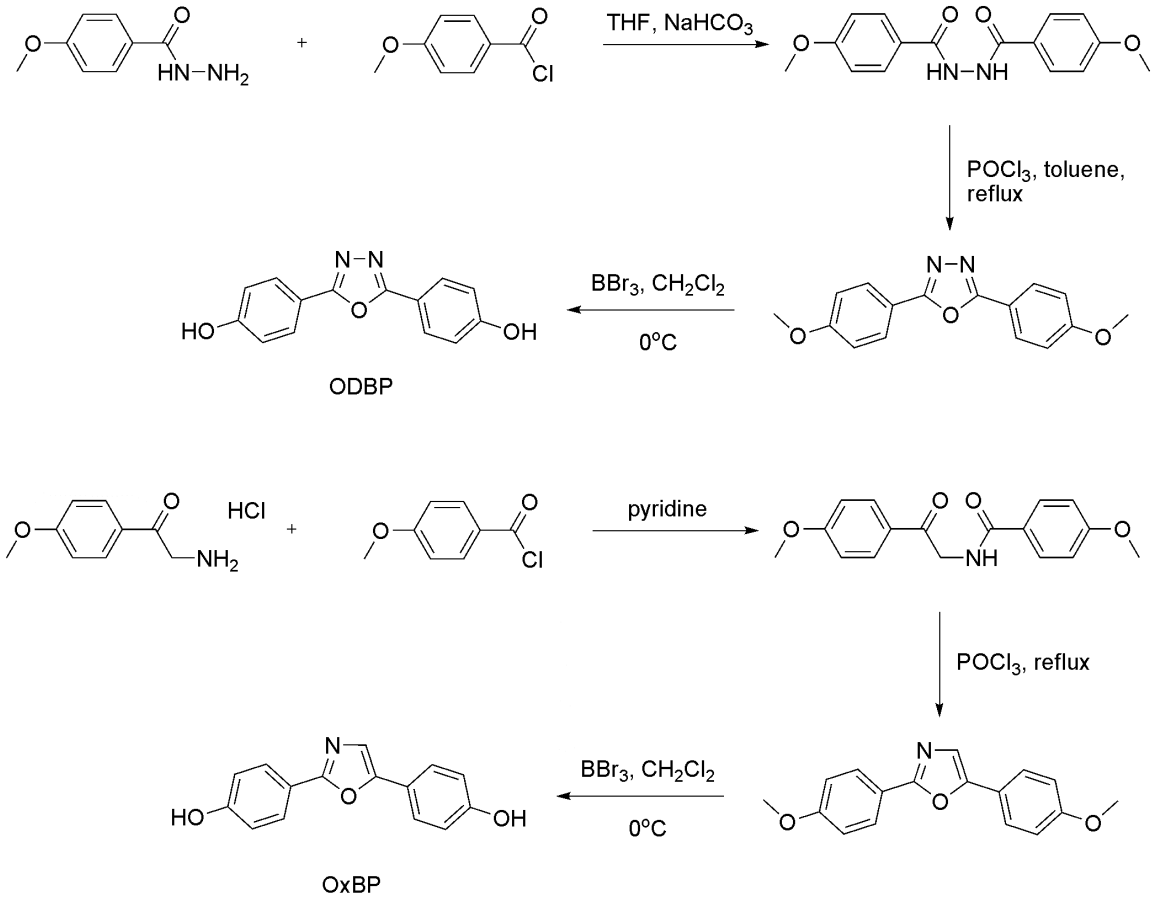

Figure 3.14. Synthesis of 4,4'-(1,3,4-oxadiazole-2,5-diyl)diphenol, ODBP, and 4,4'-(oxazole-2,5-diyl)diphenol, OxBP, cores structures.

To elongate the mesogenic core, we employed two different coupling conditions to attach benzoic acid derivatives to ODBP (Figure 3.15). A standard procedure is to *in situ* generate the acid chloride of the carboxylic acid, which when added to the phenol in slight excess will form the ester linkage. Alternatively, certain benzoic acid derivates required milder coupling conditions. In these instances, a common carbodiimide, 1-ethyl-3-(3-dimethylaminopropyl) carbodiimide hydrochloride (EDC) or dicyclohexyl carbodiimide (DCC) in conjunction with catalytic amounts of 4-dimethyl-aminopyridine (DMAP) will yield esters from benzoic acids and phenols.

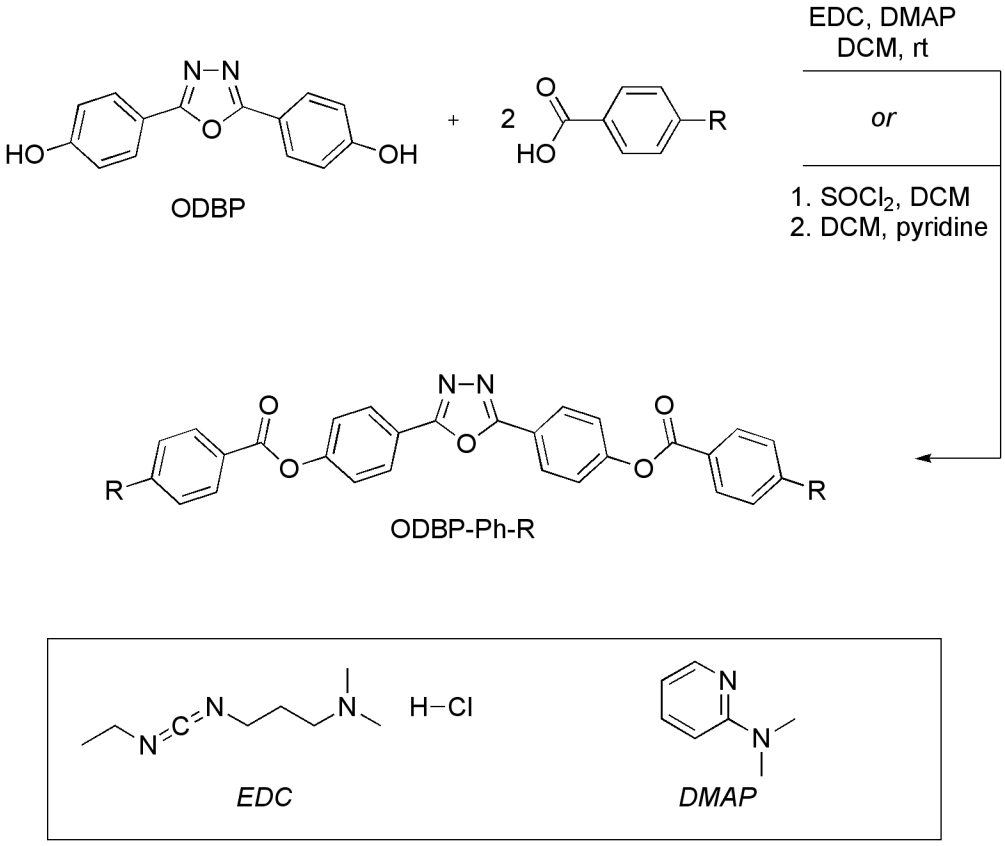

Figure 3.15. Coupling strategies for attaching generic benzoic acids to ODBP core to give ODBP-Ph-R final product.

The first series of compounds we synthesized were similar to ODBP-Ph-C_7 as seen in Figure 3.13; but now we have replaced the *p*-septyl with *p*-butyloxy. Additionally, we modified the core slightly by utilizing the oxazole core over oxadiazole. The synthesis of these compounds starts with *p*-butyloxy benzoic acid and ODBP and OxBP cores, as shown in Figure 3.16. We generated the acid chloride of *p*-butyloxybenzoic acid *in situ* with thionyl chloride, which we then added to ODBP and OxBP in the presence to pyridine, which serves as both an acid scavenger and co-solvent. This afforded both 4,4'-(1,3,4-oxadiazole-2,5-diyl)bis(4,1-phenylene) bis(4-butoxybenzoate (ODBP-Ph-OC_4) and 4,4'-(oxazole-2,5-diyl)bis(4,1-phenylene) bis(4-butoxybenzoate) (OxBP-Ph-OC_4), both of which were recrystallized twice from dichloromethane and methanol.

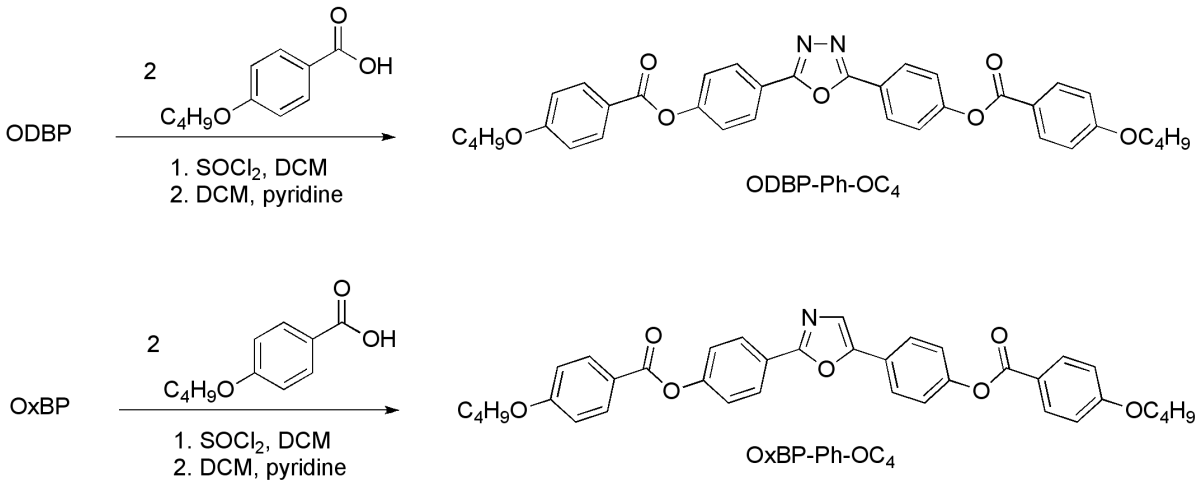

Figure 3.16. Synthesis of ODBP-Ph-OC_4 and OxBP-Ph-OC_4.

Isomers of normal alkyl chains are known to pack less efficiently than their straight-chain counterparts, leading to lower thermal behaviors, such as melting points. We transferred this observation to our peripheral side-chains of the parent compound by incorporating a dimethyl substituted α-carbon of a pentyloxy and nonyloxy side chain (Figure 3.17). This benzoic acid derivative was not commercially available, so was synthesized from 2-methylhexan-2-ol

and 4-fluorobenzonitrile; these components were coupled using potassium hexamethyldisilizane (KHMDS) in THF. The benzonitrile was then oxidized under basic conditions to afford the desired benzoic acid. This tertiary ether is susceptible to the harsh acidic conditions via the thionyl chloride coupling route, so the milder carbodiimide DCC along with catalytic DMAP were utilized to afford ODBP-Ph-Odm6.

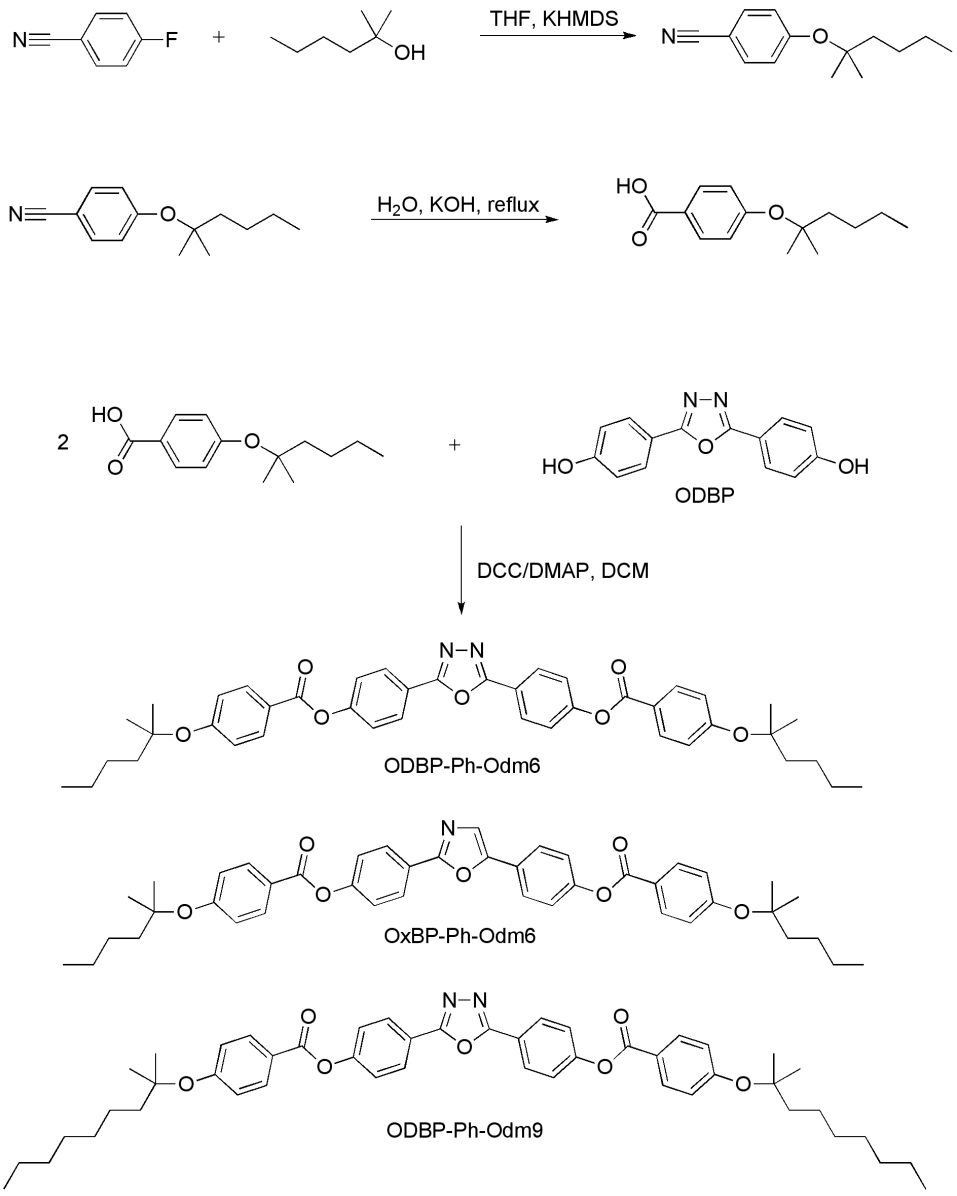

Figure 3.17. Synthetic strategy for the branched isomer variant of *n*-hexyloxy and *n*-nonyloxy to yield ODBP-Ph-Odm6, OxBP-Ph-Odm6 and ODBP-Ph-Odm9.

It is known in the literature that siloxanes, specifically terminal disiloxanes, have low surface energies, owing to their ability to depress thermal properties. Our final target ODBP-Ph-Odps prior to Pt-catalyzed hydrosilation was a bis terminal vinyl intermediate (Figure 3.18). We obtained this product by first reacting *p*-hydroxybenzoic acid with allyl bromide in an S_N2 like fashion to selectively afford the allyl-phenyl ether.

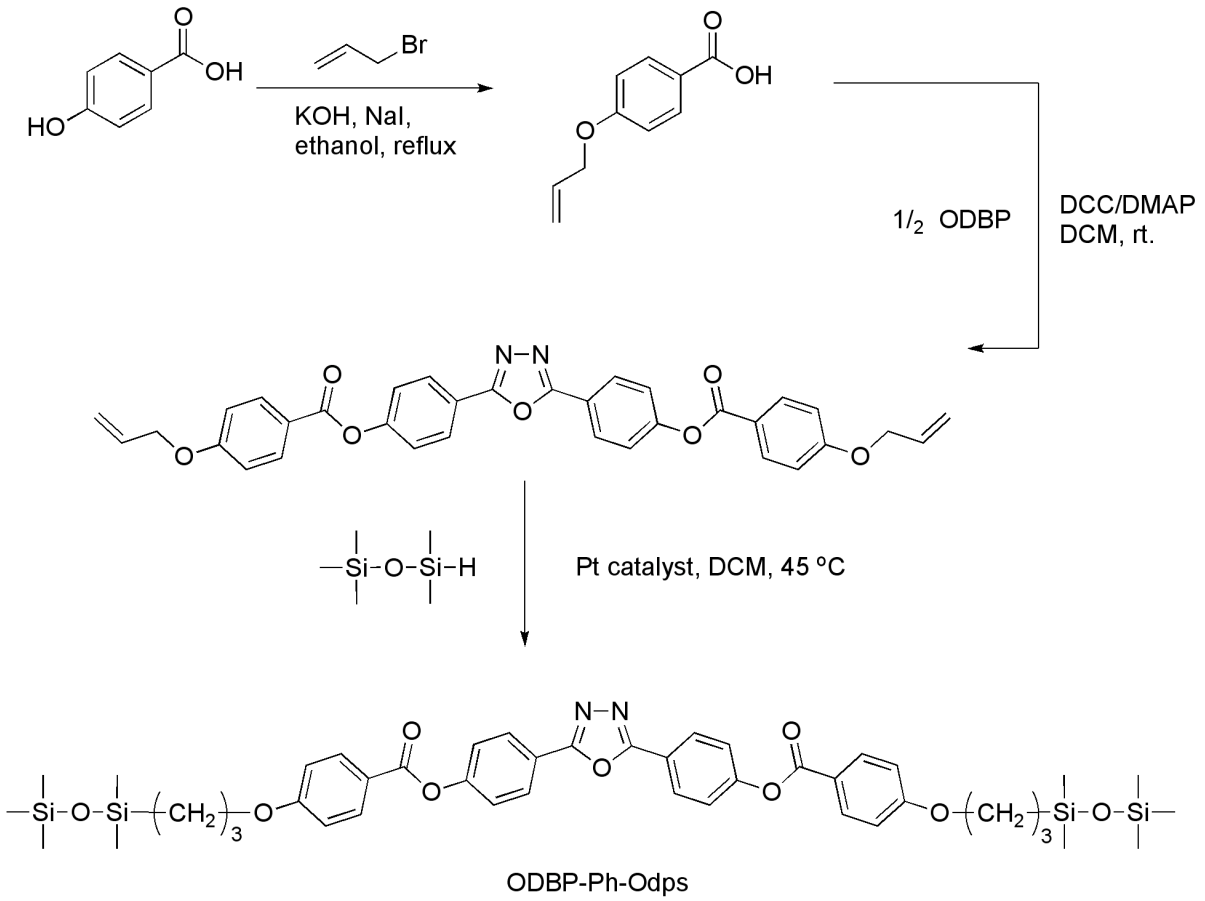

Figure 3.18. Synthetic strategy for the production of ODBP-Ph-Odps.

In order to obtain liquid crystals with lower transition temperatures, we embarked on synthesis of unsymmetric molecules – each peripheral side-chain is chemically different. Our target molecule includes a normal pentyloxy side-chain, and the side-chain observed in ODBP-Ph-Odm6. The molecular length of this molecule is nearly equivalent to its

symmetric parents, ODBP-Ph-OC_5 and ODBP-Ph-Odm6; but we wanted to explore the non-symmetric packing side-chain interactions.

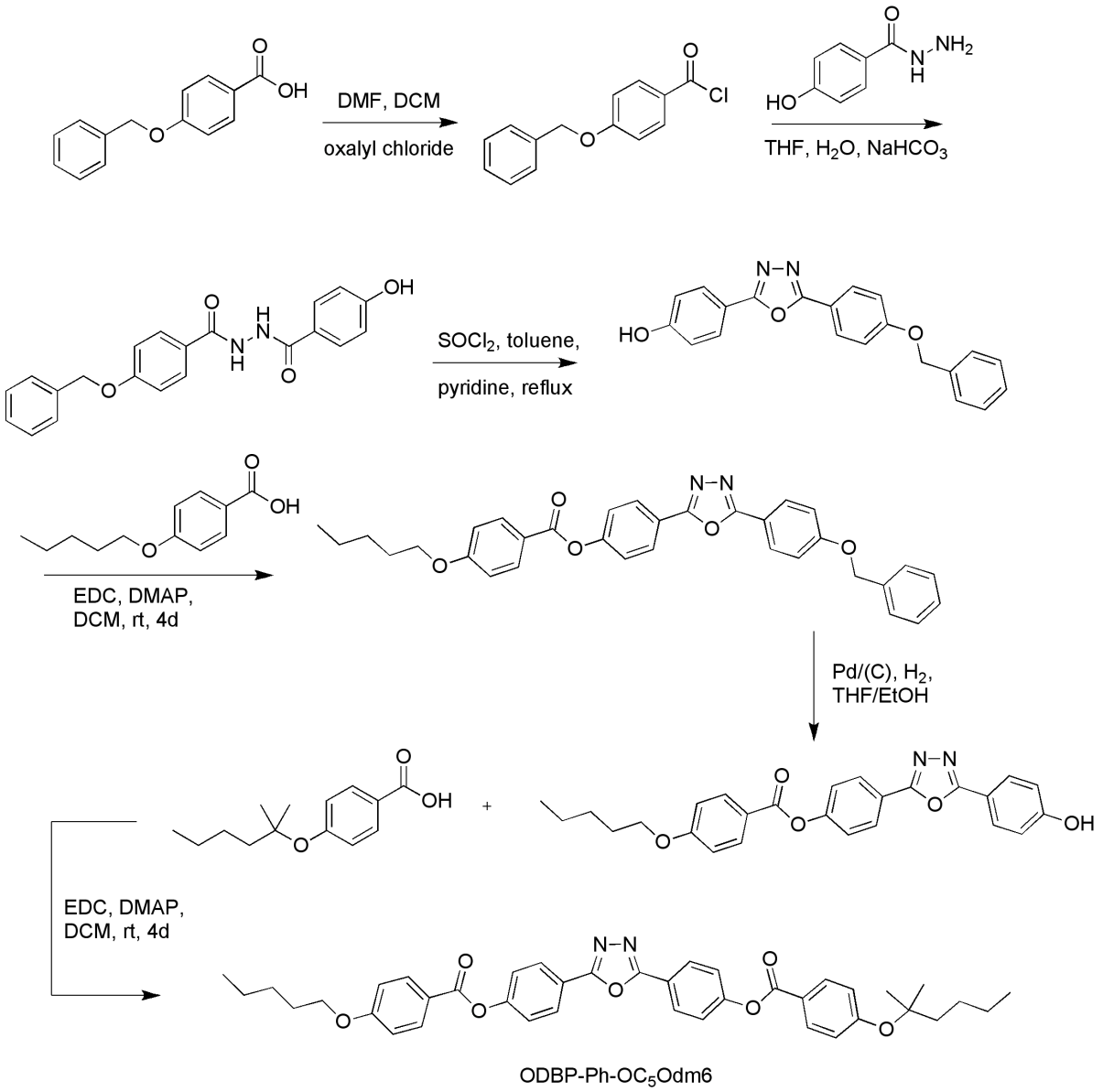

Figure 3.19. Synthetic strategy for the production of the symmetric mesogen ODBP-Ph-OC_5Odm6.

To synthesize an unsymmetric compound, this required an unsymmetric core starting material as illustrated in Figure 3.19. We began with a benzyl protected *p*-hydroxy benzoic acid, which we coupled to *p*-hydroxybenzhydrazide. This afforded an unsymmetric

dihydrazide, which when dehydrated with thionyl chloride ($SOCl_2$) in the presence of pyridine, results in facile ring closing to give the desired 2,5-substituted oxadiazole functionality. This hydroxy-benzyloxy compound is a key intermediate for the synthesis of unsymmetric liquid crystals: coupling is performed with the one available phenol followed by mild benzyl deprotection. The resulting second phenol is then coupled to a differing benzoic acid derivative.

Another functionality we wanted to explore in the development of liquid crystals with lower transition temperatures was a benzyloxy ether linkage. The benzyloxy group introduces an axis of rotation that can significantly depress overall thermal behaviors. As a no-hydrocarbon control, we attached *p*-benzyloxybenzoic acid to ODBP in a single step coupling reaction (Figure 3.20) to afford ODBP-Ph-OBn. This compound serves as a control for the seven-membered aromatic system ODBP-Ph-OBnC_4 whose synthesis is shown in Figure 3.20. *p*-Butylbenzyl alcohol is commercially available, but in order to generate the desired ether linkage, this alcohol was converted to a benzyl bromide by a halogen exchange reaction facilitated by carbon tetrabromide (CBr_4) and triphenylphosphine (PPh_3). The same sequences of reactions can be applied to the methyl benzoate, base-assisted hydrolysis of the methyl ester and DCC/DMAP coupling to ODBP, to finally yield ODBP-Ph-OBnC_4 as seven-membered liquid crystal.

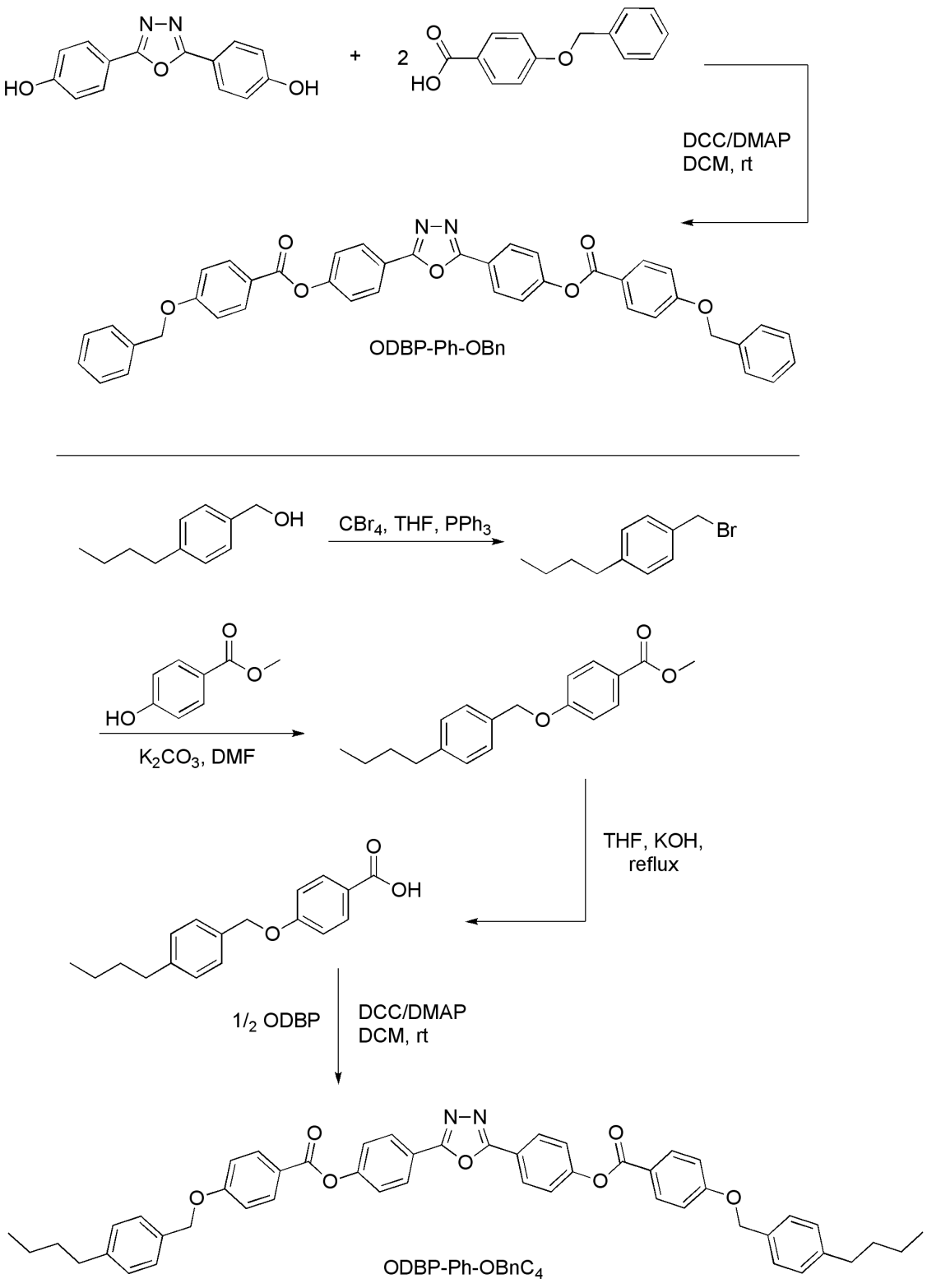

Figure 3.20. Synthetic strategy for the production of ODBP-Ph-OBn (upper) and ODBP-Ph-$OBnC_4$ (lower).

In the parent structure ODBP-Ph-C_7, the connection between the ODBP core and the terminal side-chains is an ester linkage. All molecules discussed up until now included at least an ester linkage; ODBP-Ph-OBnC_4 demonstrated a combination of ester and ether linkage between core benzenes. This final series was constructed solely based upon the benzyloxy ether functionality. Step-wise use of S_N2 reaction conditions – phenol and benzyl bromide – makes synthesis of the compounds ODBP-OBn, ODBP-OBnC_4, ODBP-OBn-OBn, ODBP-OBnOC_8 shown in Figures 3.20 – 3.24 straightforward.

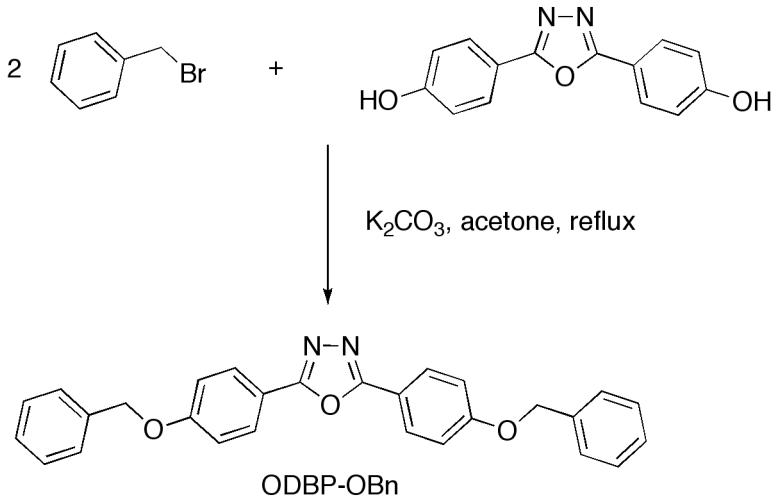

Figure 3.21. Synthetic strategy for the synthesis of ODBP-OBn.

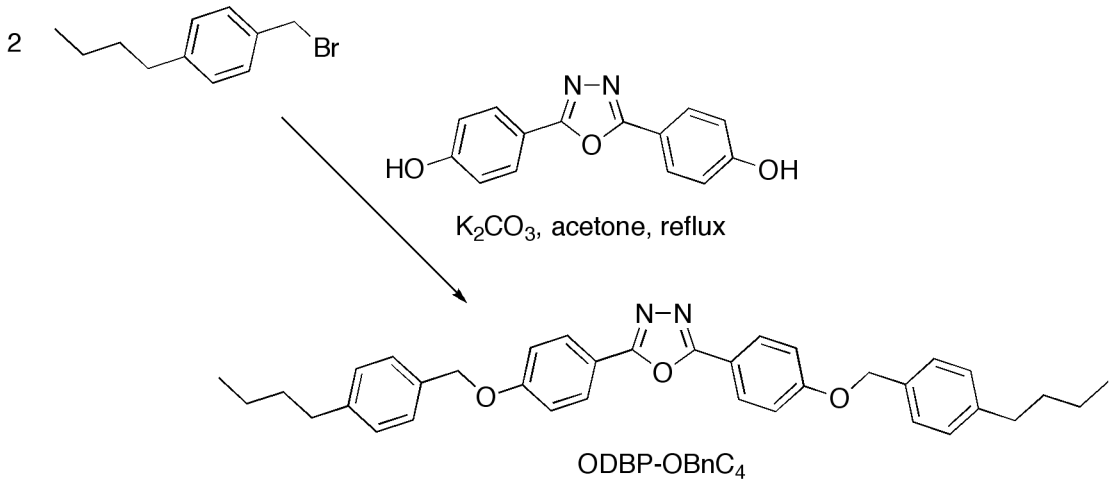

Figure 3.22. Synthetic strategy for the synthesis of ODBP-OBnC_4.

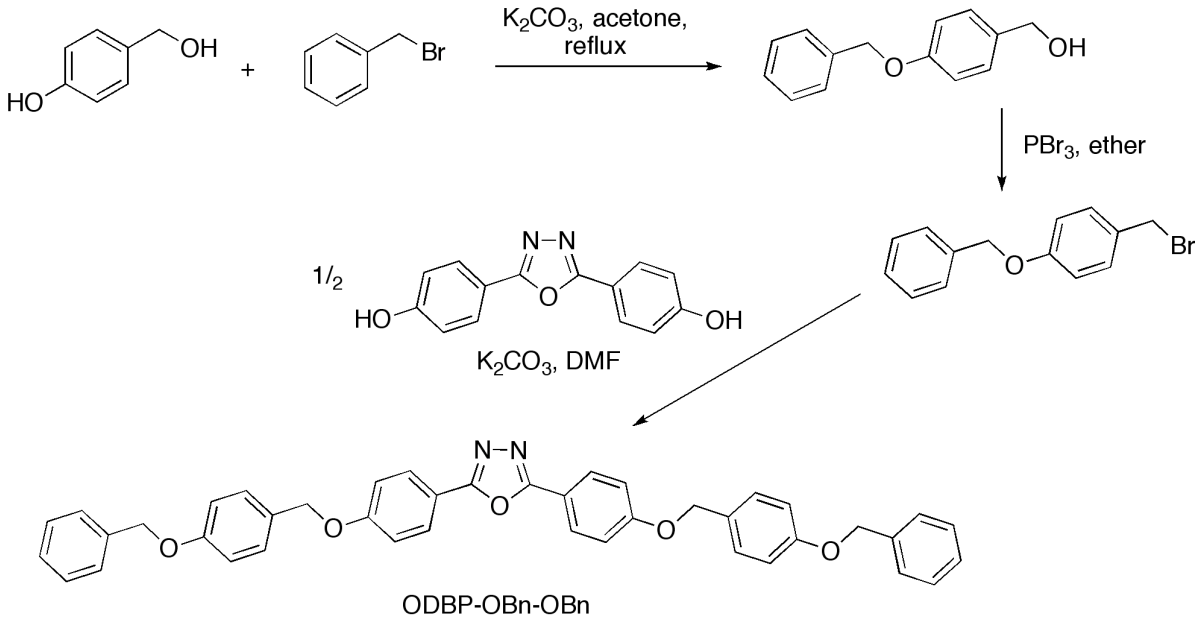

Figure 3.23. Synthetic strategy for the synthesis of ODBP-OBn-OBn.

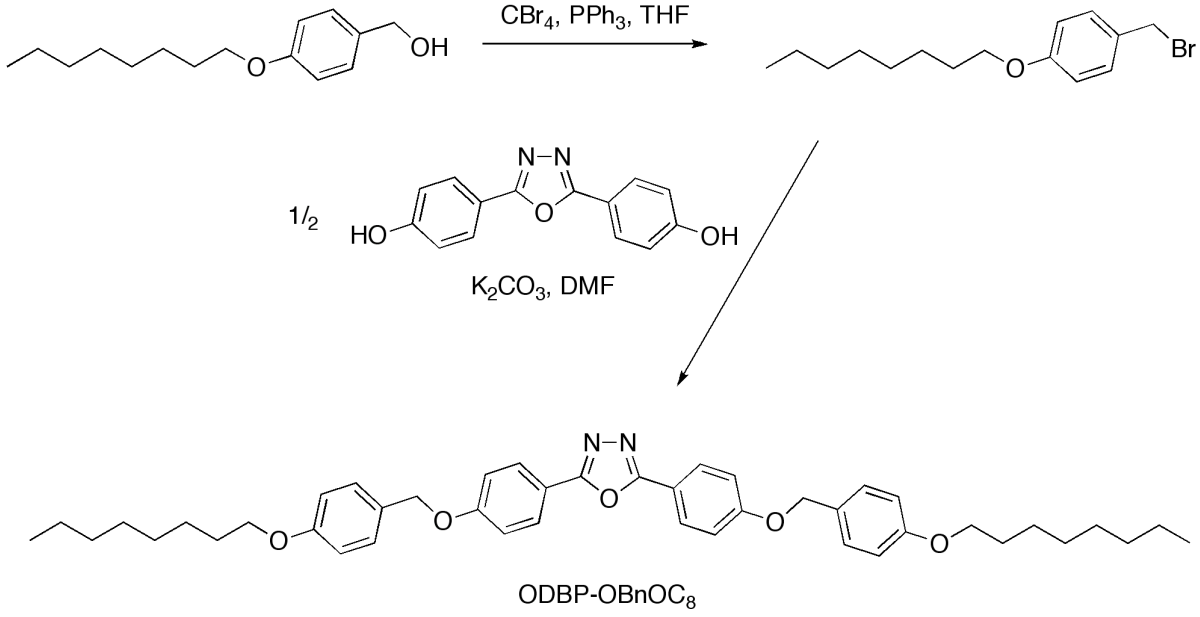

Figure 3.24. Synthetic strategy for the synthesis of ODBP-OBnOC$_8$.

3.6 Results and Discussion

The structures of all compounds were confirmed by proton Nuclear Magnetic Resonance (^{1}H-NMR); all were soluble in deuterated chloroform ($CDCl_3$). Thermal behaviors of each compound were analyzed by differential scanning calorimetry (DSC) and optical microscopy. Optical microscopy accompanied with a heating stage allowed for controlled and detailed observation of the phase transitions as well as the identification of phase textures. We judiciously chose liquid crystals with the appropriate nematic phase transition temperatures to perform solid-state ^{2}H-NMR analyses in order to measure the phase biaxiality of our nematogens.

3.6.1 Thermal Characterization

The transition phase maps for all of these compounds were either determined by DSC or optical microscopy at heating and cooling rates of 10 °C min^{-1}. The reported transition temperatures were recorded upon heating of the sample; we have noted instances where a supercooling exists and the heating and cooling temperatures are not the same. All phase transitions are summarized in Table 3.1.

Table 3.1. Transition temperatures (°C) for all ODBP and OxBP based compounds. Temperatures listed as a pair indicate transitions upon cooling and heating, respectively. (• indicates phase observed)

Entry	K	S_1	S_2	S_A	N	I
ODBP-Ph-OC_4	•				193 • 280	•
OxBP-Ph-OC_4	•				191 • 226	•
ODBP-Ph-Odm6	•				119/126	•
OxBP-Ph-Odm6	•				68/85	•
ODBP-Ph-Odm9	•				82/122	•
ODBP-Ph-Odps	•				135	•
ODBP-Ph-OC_5Odm6	•				138 • 176	•
ODBP-Ph-OBn	•				116/179	•
ODBP-Ph-OBnC_4	•				158 • 290	•
ODBP-OBn	•				135/195	•
ODBP-OBn-OBn	•				180/195	•
ODBP-OBnC_4	•				145/160	•
ODBP-OBnOC_8	•	120 •	125 •	128 •		155 •

It is obvious from the summary of phase behaviors that all compounds synthesized were not infact liquid crystalline, however, it is still interesting to note and pay close attention to how detrimental an innocuous modification to the chemical structure can have on the thermal behavior of the compound. This goes to show the sensitivity of the liquid crystalline phases of these bent-core structures. ODBP-Ph-OC_4 exhibited a nematic phase between 193 and

280 °C. Even though this compound did not suppress the T_{KN} (transition temperature for the crystalline to nematic phase) of the parent structure ODBP-Ph-C_7, when compared to the oxazole equivalent OxBP-Ph-OC_4, we saw a 54 °C depression in the T_{NI}. We suspect that the non-orthogonal direction of the dipole moment across the oxazole heterocycle influences the behavior of the intermolecular interactions, which are stronger when this dipole moment is coincident with the transverse molecular director.

A similar dipolar directional influence was seen for the non-liquid crystalline ODBP-Ph-Odm6 and OxBP-Ph-Odm6, whose melting points, 119 °C and 68 °C, respectively, are significantly lower than the parent structures T_{NI} = 222 °C. The terminal hydrocarbon proved to be detrimental to the phase map of these two compounds. In order to promote and push a liquid crystalline material using dimethyl-substituted functionality, we extended the carbon chain by three carbons to give ODBP-Ph-Odm9. Again, we observed no mesophase behavior; in fact the melting point (82 °C) upon heating was slightly lower than ODBP-Ph-Odm6.

Apart from the all-hydrocarbon tail containing compounds, we also synthesized a molecule with terminal disiloxanes. Siloxanes are known in the literature to dramatically lower transition temperatures while retaining the original mesophases. For the case of ODBP-Ph-Odps, whose terminus is composed of a propyloxy spacer and disiloxane, there was no sign of liquid crystallinity; the material had a melting point of 135 °C.

We wanted to explore the effects of a liquid crystal with ODBP core having different terminal side chains. Goodby reported in 2005,[30] the synthesis of a variety of combinations of C_nO-Ph-ODBP-Ph-OC_m whose $n \neq m$. The results of this study showed that the nematic onset temperature was particularly sensitive to the structural modification. Instead, we used

the previous results of our symmetric ODBP-Ph-Odm6 to synthesize the unsymmetric ODBP-OC_5Odm6 where one side-chain is pentyloxy and the other is of equivalent length but the α-carbon is dimethyl substituted. This gave us a liquid crystal with a nematic phase ranging from 138 °C to 176 °C. The nematic phase was characterized at 170 °C using an optical microscope equipped with crossed polarizers and a CCD camera (Figure 3.25).

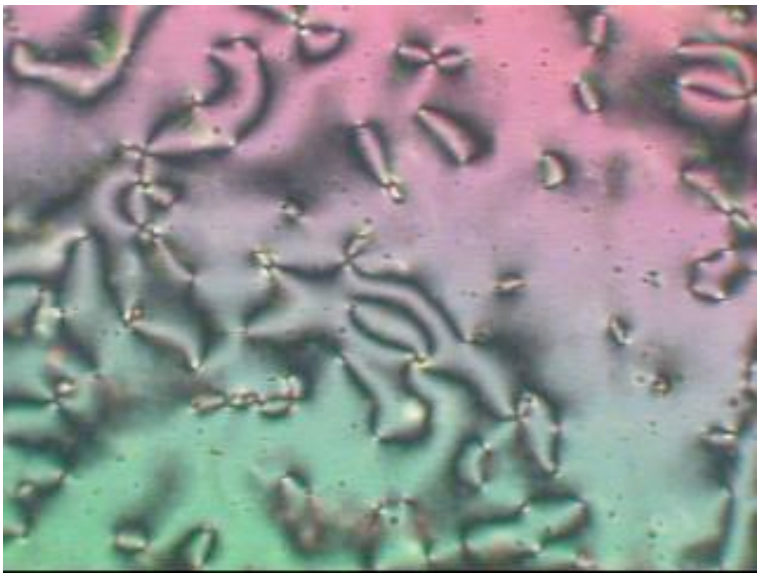

Figure 3.25. ODBP-Ph-OC_5Odm6 at 170 °C shows a typical nematic Schlieren texture with mostly two-brush disclinations (image obtained at 10X magnification).

Typically, the introduction of more aromatics to a molecule will increase its melting point. But when the aromatic is in the form of benzyloxy ether, rotation about the carbon-oxygen bond can significantly influence the occupied space of the tail. We began with the synthesis of a non-aliphatic control ODBP-Ph-OBn. This compound was not liquid crystalline, but the seven-membered ring system had a fairly lower melting point at 116 °C upon cooling and 179 °C upon heating. This 63 °C hysteresis suggests ODBP-Ph-OBn has a strong propensity to become a liquid crystal by introducing pendant aliphatic side-chains. ODBP-Ph-OBnC_4 with a butyl tail has a very wide nematic range (132 °C). The nematic phase was

characterized by optical microscopy between crossed polarizers, and its texture is seen in Figure 3.26.

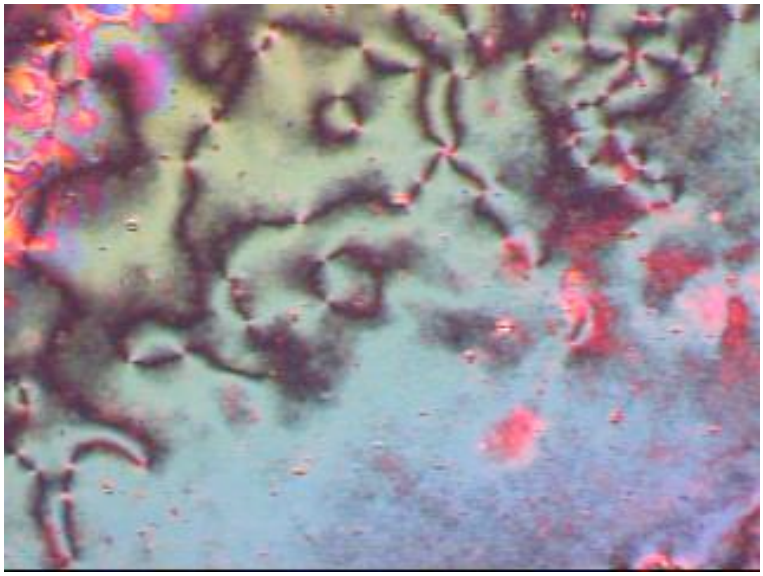

Figure 3.26. ODBP-Ph-OBnC_4 at 170 °C shows a typical nematic texture with mostly two-brush disclinations.

The final set of compounds was synthesized without the ester linkage; rather we simplified the molecule by employing a series of benzyloxy ether linkages. The high rotational flexibility of these bulkier groups was expected to play a pressing role in lowering the thermal behavior of these ODBP-core compounds. Neither ODBP-OBn nor ODBP-OBn-OBn possess pendant side chains but will serve as non-aliphatic controls. ODBP-OBn has a melting point of 195 °C upon heating (with a 60 °C hysteresis) while ODBP-OBn-OBn has the same melting point but a smaller hysteresis of 15 °C. ODBP-OBnC_4 was synthesized with the intention of stabilizing a mesophase, instead it exhibited a melting point of 160 °C upon cooling. By increasing the tail to octyloxy, we were able to stabilize a sequence of ill-defined smectic phases. Upon cooling the sample, at 155 °C the bulk material transitions from the isotropic directly into a smectic A phase, indicative by the formation of batonets

(Figure 3.27). The behavior of this liquid crystal was unusual as the smectic A phase was persisted by a series of two other smectic phases.

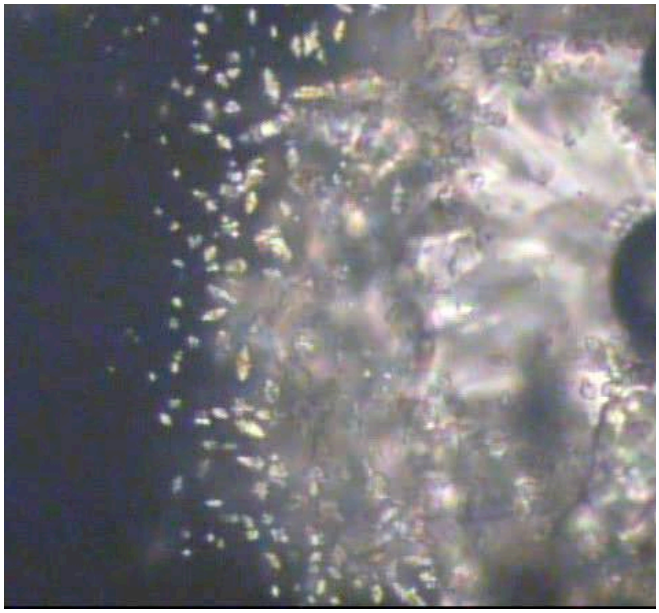

Figure 3.27. ODBP-OBnOC$_8$ at 154 °C shows batonets forming at the nematic-isotropic transition (20x magnification).

It becomes apparent that simple modifications to the core and tails of these molecular structures are very influential to the thermal properties of these ODBP bent-core compounds. Oxazole substitution appears to influence the stability of the phase as result of a loss in symmetry brought upon by the non-orthogonal dipole moment across the heterocycle. As for the tail-modified compounds, it is not obvious why a dimethyl substitution of an alkyl-aryl ether seen in the symmetric ODBP-Ph-Odm6, OxBP-Ph-Odm6 and ODBP-Ph-Odm9 lowered the transition temperatures tremendously; but we presume the modification limits the possible degrees of freedom of the aliphatic chain and contorts the side-chain in an orientation far from co-linear with the molecule. As we expected, employment of benzyloxy ether to the core as well as the periphery demonstrated in ODBP-Ph-OBnC$_4$ and ODBP-

$OBnC_4$ a substantial drop in mesophase transition temperatures. Continued efforts are being explored by the Samulski group to achieve the ultimate goal of a room temperature biaxial nematic liquid crystal.

3.6.2 ^{2}H-NMR Analysis of Nematic Phases of ODBP-Ph-$OBnC_4$ and ODBP-Ph-OC_5dm6

We have shown ODBP-Ph-$OBnC_4$ and ODBP-Ph-OC_5Odm6 to both have lower nematic onset temperatures with broad nematic ranges, making them strong candidates for ^{2}H-NMR analysis. Our goal was to determine the biaxiality ($Q_{XX} \neq Q_{YY}$) for these mesogens according to the procedure described in the introduction to this chapter.

When the original report of unambiguous evidence towards a biaxial nematic liquid crystal appeared in the literature, there was initial skepticism of the NMR data. As a result, we performed several control experiments strengthening our argument for ODBP-Ph-C_7 reported $\eta = 0.1$ biaxiality. The first being ^{2}H-NMR analysis of 4-cyano-4-*n*-pentylbiphenyl (5CB) with about 1 wt% hexamethylbenzene-d_{18}. 5CB is one of the most common and well-studied calamitic liquid crystal (Figure 3.28). It is a room temperature liquid crystal with only a nematic phase that exists at room temperature. This compound has a molecular structure with clearly one director coincident with the symmetry axis of this $D_{\infty h}$ uniaxial nematic liquid crystal. This experiment was performed in addition to previously reported TBBA (Figure 3.28), another nematic widely considered and proven to be uniaxial at temperatures and viscosities comparable to ODBP-Ph-C_7.[31]

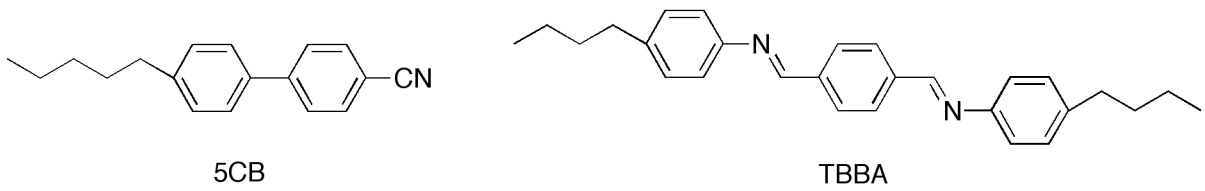

5CB TBBA

Figure 3.28. Molecular structures of uniaxial nematics, 4-cyano-4-*n*-pentyldiphenyl (5CB) and terephthalylidene-bis-butylanilene (TBBA).

5CB is not a perdeuterated compound, so the experiment was conducted by doping the sample with 1-2 wt% hexamethylbenzene-d_{18} to serve as a high symmetry (D_{6h}) solute probe molecule. The first experiment involved obtaining the NMR spectrum in the static case at a range of temperatures from 297.8 K to 307 K (Figure 3.29). The ^{2}H-labeled compound transitions to the isotropic indicated by both a single and split peaks at 306 K. As this sample cools, we observe a pair of lines split by ν_Q, where ν_Q is proportional to the motionally averaged component of the partially averaged quadrupole tensor $\boldsymbol{q}$ parallel to the major director $\boldsymbol{n}$. This splitting continues until the sample reaches room temperature at 25 °C.

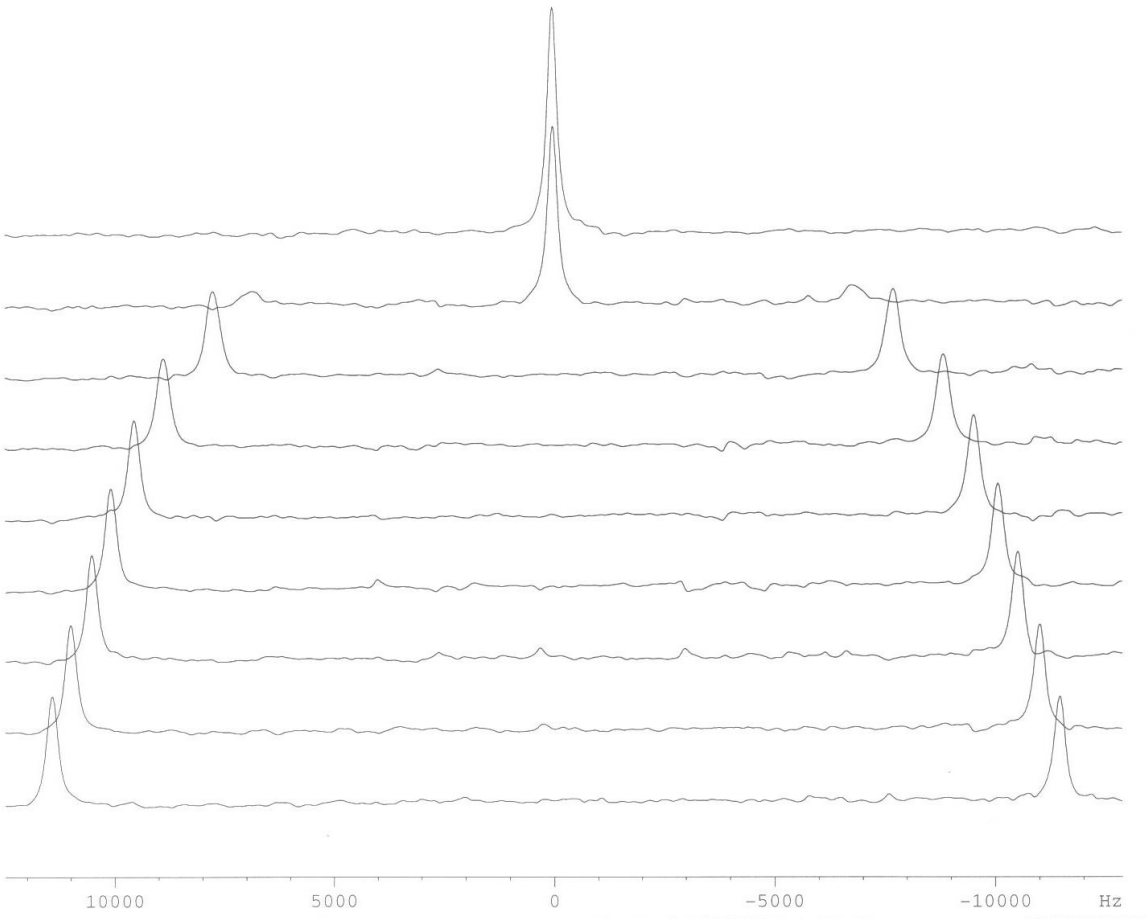

Figure 3.29. NMR data for a static sample of 5CB upon cooling at temperatures ranging from 297.8 K (lower) to 307 K (upper) incremented by one degree.

When rotating this nematic about an axis normal to the magnetic field B_0 at a rate of 190 Hz at 298 K (25 °C), a two-dimensional "powder" pattern – a weighted average of the quadrupolar spectra for a planar distribution of $\boldsymbol{n}$ – is generated. Unlike a biaxial nematic where we would expect to see a secondary alignment of the *X* component to minimize the magnetic free energy, instead, we observed an anticipated uniaxial nematic with equivalent *X* and *Y* components. This is apparent in Figure 3.30 where we have fitted quantitatively by theory,[28] and the fit yields a measured biaxiality parameter $\eta = 0.00 \pm 0.03$.

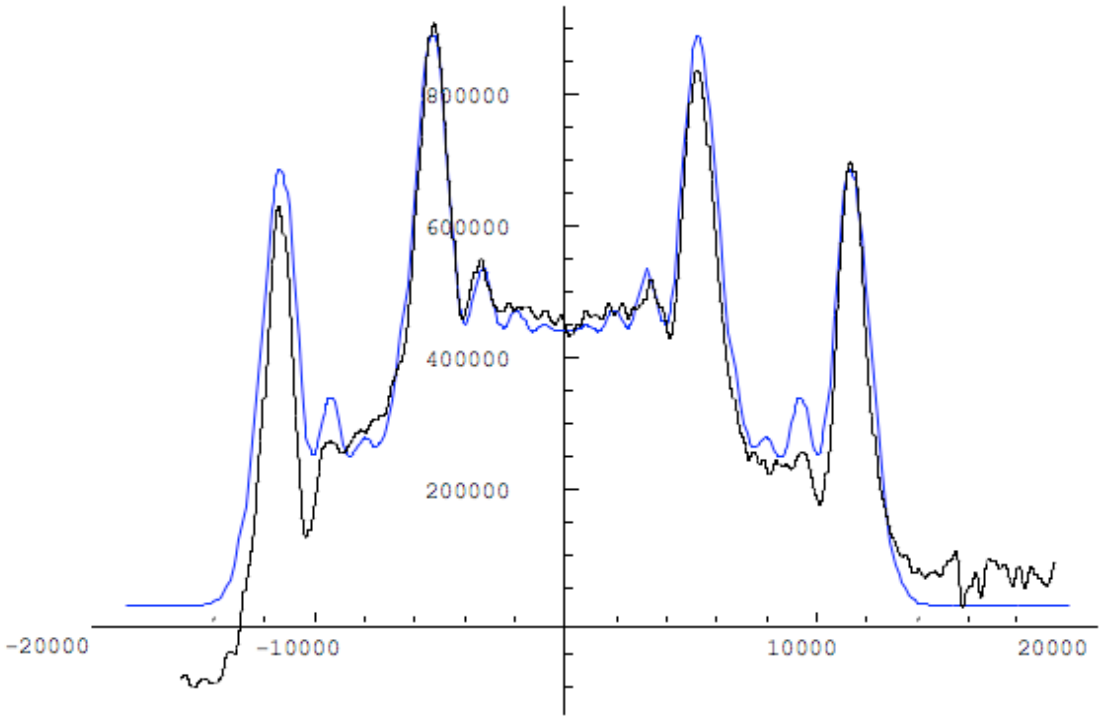

Figure 3.30. NMR data (black) and simulation (blue) for a rotating uniaxial nematic 5CB (x-axis is in Hz). Best fit obtained with biaxiality $\eta = 0.00 \pm 0.03$.

Of the series of compounds synthesized and shown to exhibit suitable nematic phases for characterization by ^{2}H-NMR spectroscopy were ODBP-Ph-OBnC$_4$ and ODBP-Ph-OC$_5$Odm6. The symmetric ODBP-Ph-OBnC$_4$ mesogen has an extraordinarily large nematic range, which initially appeared to be a strong candidate for analysis. However, upon attempting to heat a sample with about 2 wt% HMB-d_{18} while in the probe, we noticed in our signal an unidentified central peak that persisted upon cooling. Because of the extremely high temperature in order to bring the liquid crystal into the isotropic phase and completely dissolve the probe molecule, which also has a reported boiling point of 264 °C, we began to see signs of decomposition and loss of signal. Perhaps the HMB-d_{18} at near 300 °C catalyzed decomposition of ODBP-Ph-OBnC$_4$ or escaped out of the glass bulb; but upon observation of the sample after attempted experiments, there was an obvious discoloration in the sample.

We then chose to explore ODBP-Ph-OC_5Odm6 as a potential biaxial nematic. With a lower nematic onset temperature, we began our experiments by measuring the splitting as a function of temperature. In Figure 3.31 we have plotted the quadrupolar splitting versus temperature, which decreases with increasing temperature. At 460 K the sample becomes completely isotropic. Next, we rotated the sample at 160 Hz and at 119 °C (the temperature is lower than the reported nematic phase as a result of 2 wt% of the solute probe molecule HMB-d_{18}). We chose the lower ended of the nematic range where we would most likely observe nematic phase behavior. When the observed powder pattern of ODBP-Ph-OC_5Odm6 (Figure 3.32) was fitted quantitatively according to theory, we obtained a value for $\eta = 0.05 \pm 0.03$. This data suggests ODBP-Ph-OC_5Odm6 is in fact a N_b with a secondary order parameter not quite as large as the parent ODBP-Ph-C_7 $\eta = 0.11$. Further studies in the Samulski lab include the exploration of the N_b across a range of temperatures and spinning rates in the nematic phase, allowing for more conclusive NMR experiments.

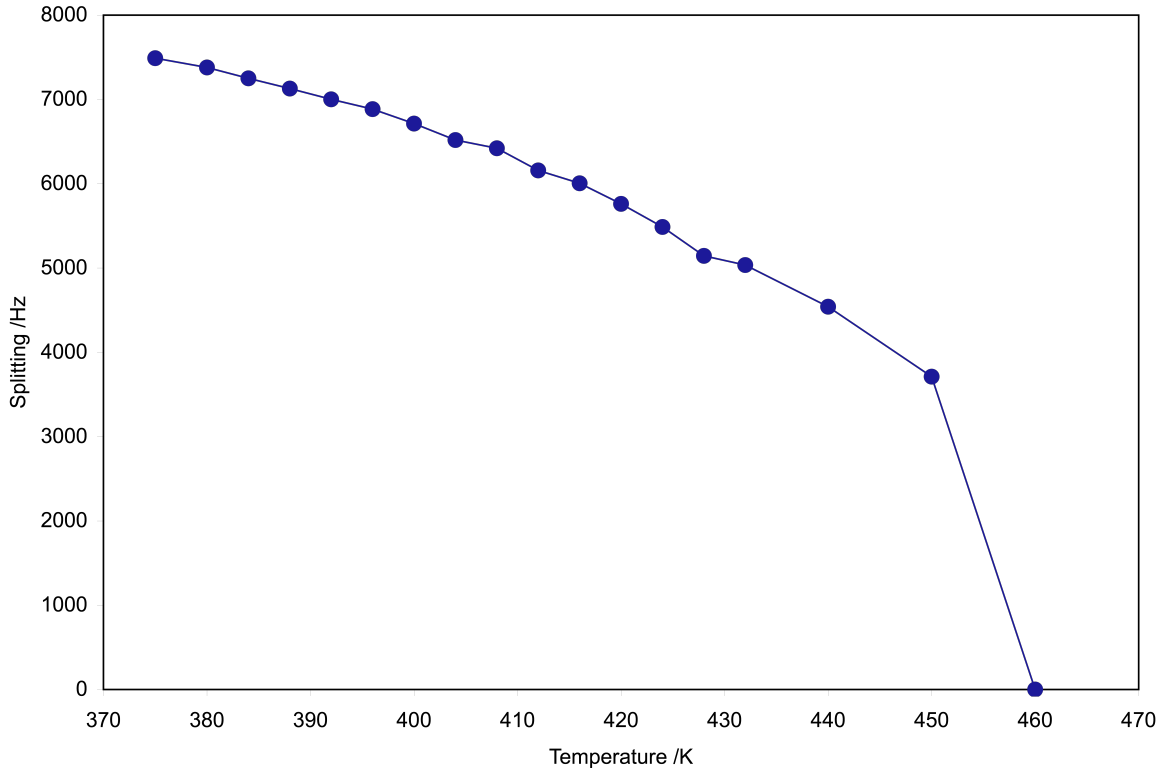

Figure 3.31. Quadrupolar splitting as a function of temperature for a static sample of ODBP-Ph-OC_5Odm6 upon cooling from the isotropic.

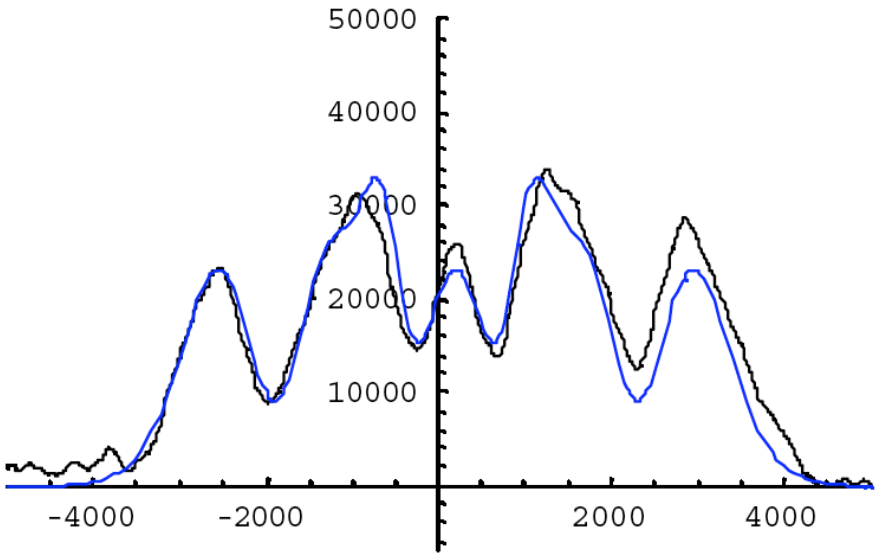

Figure 3.32. NMR data (black) and simulation (blue) for a rotating biaxial nematic ODBP-Ph-OC_5Odm6 (x-axis is in Hz). Best fit obtained with biaxiality $\eta = 0.05 \pm 0.03$.

3.7 Concluding Remarks

After an extensive exploration in potential tail and core modifications to the parent ODBP-Ph-C_7 biaxial nematic, the most well-suited synthetic endeavor towards lowering the nematic onset temperature was the incorporation of a benzyloxy ether extension to the core to afford the nematic mesogen ODBP-Ph-OBnC_4. Unfortunately, this modification also increased the molecules' T_{NI} to give a nematic range of nearly 150 °C, well above the boiling point of the deuterated HMB probe molecule. In another instance where we synthesized an unsymmetric compound with one side-chain being a pentyloxy and the other a tertiary ether of identical chain length, ODBP-Ph-OC_5Odm6 exhibited a nematic phase, which proved by ^{2}H-NMR analysis to be biaxial. To conclude, the biaxial nematic phase as well as the overall phase behavior of bent-cores based on the ODBP core are extremely sensitive to even innocuous chemical modifications.

3.8 Experimental Section

General. Tetrahydrofuran (THF) and toluene were dried over and distilled from sodium/benzophenone prior to use. Pyridine was dried over and distilled from calcium hydride. Dichloromethane (CH_2Cl_2) was dried through molecular sieves. All other solvents and reagents were purchased from Aldrich and used without further purification. All of the reactions were carried out under argon with the use of standard inert-atmosphere Schlenk techniques. NMR spectra were recorded on a Bruker NMR 400 DRX spectrometer. ^{1}H-NMR were recorded at 400 MHz and referenced to the proton resonance resulting from the incomplete deuteration of chloroform (δ 7.26) and dimethylsulfoxide (δ 2.50). Transition temperatures were determined by using a PerkinElmer Sapphire differential scanning

calorimeter (DSC), calibrated with indium (99.99%) (m.p., 156.5 °C, ΔH = 28.315 J/g) and tin (99.99%) (m.p., 232.0 °C, ΔH = 54.824 J/g). The second heating (10 °C min^{-1}) as well as the cooling scans (10 °C min^{-1}) were recorded. In order to prevent the LCs from subliming out of the sample pans we used high-pressure DSC sample capsules (Seiko, AL 15). Mesophases were identified with a Nikon Microphot-FX polarizing microscope with orthoscopic and conoscopic equipment and a linkam hotstage.

^{2}H-NMR of ODBP-Ph-OBnC_4 and ODBP-Ph-OC_5dm6.

Sample Preparation. Samples were prepared for ^{2}H-NMR by packing the LC material as a solid into a glass bulb. The glass bulb contains up to about 25 mg of sample and typically 1-2 wt% of the solute probe molecule HMB. To remove all oxygen and ensure the sample is completely contained within the bulb, the sample was slowly heated under vacuum and then subsequently sealed by flame torch under liquid nitrogen.

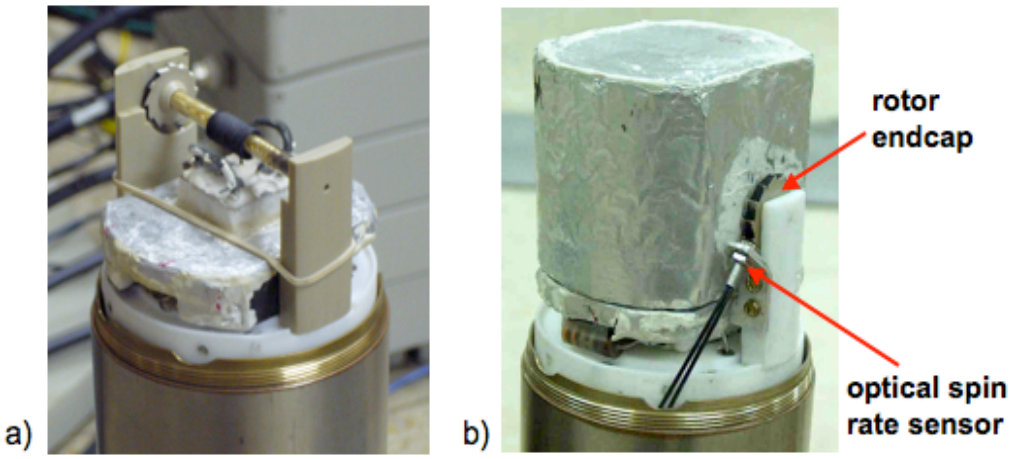

Figure 3.33. Pictures of modified high-temperature solids probe with a) rotation device and b) fumed silica oven.

NMR Setup. A Bruker ^{2}H static solids probe (72 mm OD) was modified, according to an already reported schematic,[31] to include a rotation stage enclose in a fumed silica high

temperature oven (Figures 3.33 and 3.34). A typical variable temperature static spectrum was obtained by first heating the sample, while in the probe, into the isotropic and then slowly cooled by one or two degree increments as the sample passes through the T_{NI}. A rotation spectrum was obtained by heating the sample into the lower temperature regime of the nematic phase. The act of spinning at this high temperature can induce a ± 2 °C uncertainty. After about 10k pulse-acquire scans, we obtained a 2D powder pattern that we fit using MATHEMATICA 6.0 according the previously discussed functions with varying values of η, and then minimized with a non-linear least-squares fit.

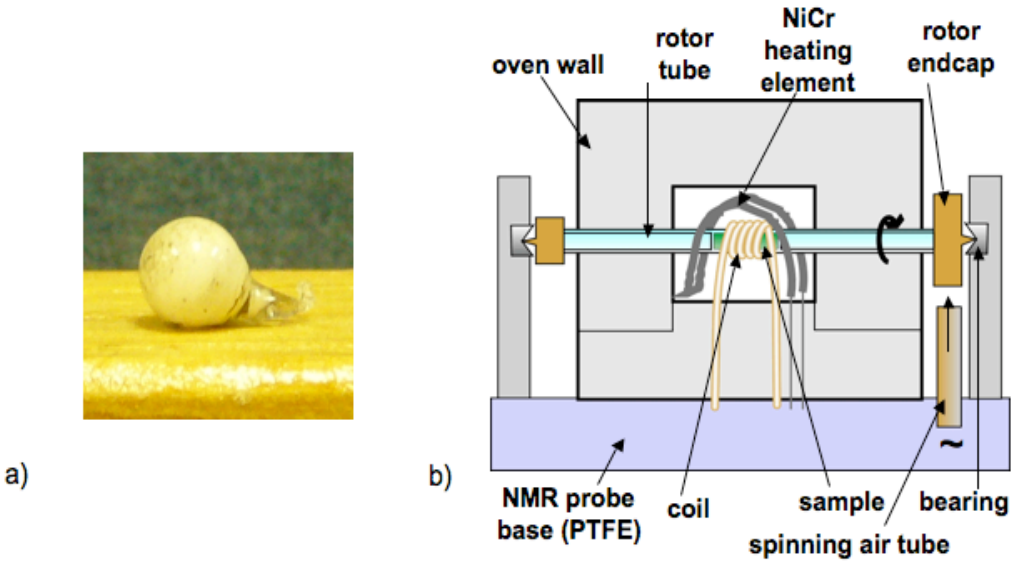

Figure 3.34. a) Picture of glass bulb containing ODBP mesogen and HMB probe molecule. b) Schematic of all components to modified solids probe.

Synthesis of ODBP-OC$_n$Bn Series

Synthesis of 4,4'-(1,3,4-oxadiazole-2,5-diyl)diphenol, ODBP. *Synthesis of 4-methoxy-N'-(4-methoxybenzoyl)benzohydrazide*. 4-methoxybenzohydrazide (7.00 g, 42.1 mmol) and $NaHCO_3$ (3.54 g, 42.1 mmol) were dissolved in a anhydrous THF/water mixture (20 and 50

mL, respectively). To this solution 4-methoxybenzoyl chloride (7.19 g, 42.1 mmol) was added as a solution in THF (20 mL). Upon addition a precipitate formed immediately and allowed to stir at room temperature for under Ar atmosphere for 30 minutes. The solid was then filtered and rinsed throuroughly with water and dried to give the dihydrazide in 97% yield (12.24 g). This product was carried over to the ring closing dehydration reaction without purification.

Synthesis of 2,5-bis(4-methoxyphenyl)-1,3,4-oxadiazole. A 250 mL 2-neck, round-bottom flask equipped with Ar inlet and condensor was charged with a mixture of 4-methoxy-*N*'-(4-methoxybenzoyl)benzohydrazide (9.41 g, 31.3 mmol), $POCl_3$ (50 mL), and anhydrous toluene (90 mL) and set to reflux under Ar atmosphere for 6 hours. At the end of the allotted time, excess $POCl_3$ and toluene were distilled off and the remaining crude product was recrystallized from hot ethanol to give 2,5-bis(4-methoxyphenyl)-1,3,4-oxadiazole in 70% yield (6.20 g). ^{1}H NMR ($CDCl_3$): δ 8.07 (d, 4H), 7.03 (d, 4H), 4.04 (s, 6H).

Synthesis of ODBP. A 250 mL 1-neck, round-bottom flask was charged with 2,5-bis(4-methoxyphenyl)-1,3,4-oxadiazole (6.20 g, 22.0 mmol), dissolved with minimal amount of anhydrous DCM (20 mL) and cooled over a water/ice bath. To this solution was added BBr_3 (7.1 mL, 75.0 mmol) at 0 °C and allowed to reach room temperature overnight. At the end of the reaction, ice was added to the mixture, and a precipitate formed immediately. The slurry was then filtered and rinsed thoroughly with water to remove boronic acid. The final crude product was recrystallized in ethanol to give ODBP in 75% yield (4.19 g). ^{1}H NMR (DMSO): δ 10.29 (s, 2H), 7.92 (d, 4H), 6.95 (d, 4H).

Synthesis of 4,4'-(oxazole-2,5-diyl)diphenol, OxBP. *Synthesis of 4-methoxy-N-(2-(4-methoxyphenyl)-2-oxoethyl)benzamide*. 2-amino-1-(4-methoxyphenyl)-ethanone hydro-

chloride (3.00 g, 14.9 mmol) and 4-methoxybenzoyl chloride (2.54 g, 14.9 mmol) were added to a 250 mL round-bottom flask, which was then charged with anhydrous pyridine (30 mL). The mixture was stirred for 30 minutes at room temperature and then set to reflux for 45 minutes. After the reaction was cooled to room temperature, water (20 mL) was added directly to the flask, and a white precipitate formed immediately. This was filtered and rinsed thoroughly with water and finally dried to give the dihydrazide in 82% yield (3.65 g). This product was carried over to the ring closing dehydration reaction without purification.

Synthesis of 2,5-bis(4-methoxyphenyl)oxazole. A 100 mL 1-neck, round-bottom flask equipped with Ar inlet and condensor was charged with a mixture of 4-methoxy-*N*-(2-(4-methoxyphenyl)-2-oxoethyl)benzamide (3.65 g, 12.2 mmol) and $POCl_3$ (30 mL) and set to reflux under Ar atmosphere for 12 hours. At the end of the allotted time, the dark green reaction mixture was slowly added to about 300 mL ice/water bath. Upon addition, a precipitate formed, was rinsed with water and recrystallized from hot ethanol to give 2,5-bis(4-methoxyphenyl)oxazole in 74 % yield (2.54 g). ^{1}H NMR ($CDCl_3$): δ 8.17 (d, 2H), 7.78 (d, 2H), 7.42 (d, 2H), 7.13 (d, 2H), 7.10 (s, 1H), 3.99 (s, 3H), 4.02 (s, 3H).

Synthesis of OxBP. A 250 mL 1-neck, round-bottom flask was charged with 2,5-bis(4-methoxyphenyl)oxazole (1.00 g, 3.55 mmol), dissolved with minimal amount of anhydrous DCM (10 mL) and cooled over a water/ice bath. To this solution was added BBr_3 (1.2 mL, 12.44 mmol) at 0 °C and allowed to reach room temperature overnight. At the end of the reaction, ice was added to the mixture, and a precipitate formed immediately. The slurry was then filtered and rinsed thoroughly with water to remove boronic acid. The final crude product was recrystallized in ethanol to give OxBP in 61% yield (0.55 g). ^{1}H NMR (DMSO): δ 7.98 (d, 2H), 7.65 (d, 2H), 7.18 (s, 1H), 6.81 (d, 4H).

Synthesis of ODBP-Ph-OC_4. A 25 mL 2-neck round-bottom flash equipped with Ar inlet was charged with 4-butoxybenzoic acid (100.0 mg, 0.515 mmol) and cooled by a water/ice bath. To this solid was added $SOCl_2$ in excess (1.5 mL). After 45 minutes of stirring, remaining $SOCl_2$ was distilled off and diluted with anhydrous DMF. In a separate 25 mL round-bottom flask, ODBP (52.5 mg, 0.206 mmol) and NaH (10.0 mg, 0.221 mmol) were dissolved into DCM (5 mL) and set to reflux for 12 hours. The reaction was then brought to room temperature and solvents were removed in vacuo. The crude solid was chromatographed on silica-gel with hexanes, acetone, DCM (10:1:1). The final product ODBP-Ph-OC_4 was obtained in 45% yield (53.9 mg). ^{1}H NMR ($CDCl_3$): δ 8.20 (d, 2H), 8.15 (d, 2H), 7.25 (d, 2H), 7.24 (d, 2H), 4.08 (t, 4H), 1.77 (p, 4H), 1.45 (sextet, 4H), 0.95 (t, 6H).

Synthesis of OxBP-Ph-OC_4. A 25 mL 2-neck round-bottom flash equipped with Ar inlet was charged with 4-butoxybenzoic acid (95.5 mg, 0.494 mmol) and cooled by a water/ice bath. To this solid was added $SOCl_2$ in excess (1.5 mL). After 45 minutes of stirring, remaining $SOCl_2$ was distilled off and diluted with anhydrous DMF. In a separate 25 mL round-bottom flask, OxBP (50.0 mg, 0.197 mmol) and NaH (10.0 mg, 0.221 mmol) were dissolved into DCM (5 mL) and set to reflux for 12 hours. The reaction was then brought to room temperature and solvents were removed in vacuo. The crude solid was chromatographed on silica-gel with hexanes, acetone, DCM (10:1:1). The final product ODBP-Ph-OC_4 was obtained in 42% yield (50.1 mg). ^{1}H NMR ($CDCl_3$): δ 8.18 (d, 2H), 8.14 (d, 4H), 7.76 (d, 2H), 7.43 (s, 1H), 7.33 (d, 2H), 7.29 (d, 2H), 6.96 (d, 4H), 4.05 (t, 4H), 1.80 (p, 4H), 1.50 (sextet, 4H), 0.98 (t, 6H).

Synthesis of ODBP-Ph-Odm6 and OxBP-Ph-Odm6. *Synthesis of 4-(2-methylhexan-2-yloxy)benzonitrile*. A 50 mL 2-neck round-bottom flask equipped with Ar inlet was charged

with 4-fluorobenzonitrile (1.010 g, 8.34 mmol), 2-methylhexan-2-ol (1.066 g, 9.17 mmol) and anhydrous THF (25 mL). The mixture was brought to 0 °C after which a solution of KHMDS (0.5 M, 18.3 mL) was added dropwise over the course of 45 minutes. The solution changed from colorless to dark orange. The reaction mixture was allowed to stir for 2 hours as it reached room temperature before being worked up. The mixture was diluted with additional DCM and washed once with saturated NH_4Cl. The isolated aqueous layer was washed once with DCM. The organics were combined and dried over $MgSO_4$, filtered and reduced; the final crude 4-(2-methylhexan-2-yloxy)benzonitrile product was a yellow oil and used for the next step without further purification.

Synthesis of 4-(2-methylhexan-2-yloxy)benzoic acid. A solution of 4-(2-methylhexan-2-yloxy)benzonitrile (197.1 mg, 0.907 mmol), deionized water (1.0 mL) and NaOH (6 N, 1.0 mL) was refluxed for 18 hours under Ar atmosphere. The reaction was cooled to room temperature and neutralized with a solution of HCl (6 N). A white precipitate crashed out of solution, was filtered and rinsed thoroughly with water. The final benzoic acid was isolated in 72% yield (158.7 mg). ^1H NMR ($CDCl_3$): δ 8.00 (d, 2H), 7.00 (d, 2H), 1.69 (t, 2H), 1.41 (p, 2H), 1.35 (s, 6H), 1.33 (sextet, 2H), 0.90 (t, 3H).

Synthesis of ODBP-Ph-Odm6. A solution of 4-(2-methylhexan-2-yloxy)benzoic acid (35.5 mg, 0.150 mmol), ODBP (15.3 mg, 0.060 mmol) and DCM (10 mL) was prepared in a 25 mL round-bottom flask equipped with Ar inlet. To this mixture was added 1,3-dicyclohexylcarbodiimide (DCC, 31.9 mg, 0.155 mmol) and 4-dimethylaminopyridine (DMAP, 4.6 mg, 0.0376 mmol). The reaction mixture was allowed to stir for 48 hours at room temperature. Upon completion, a white precipitate had formed, was filtered. The filtrate was rinsed with 10% HOAc (10 mL), rinsed with saturated NaCl (20 mL), and finally

the organics were dried over $MgSO_4$. The final product ODBP-Ph-Odm6 was isolated as a white solid after being recrystallized from DCM/MeOH in 68% yield (26.7 mg). ^{1}H NMR ($CDCl_3$): δ 8.20 (d, 4H), 8.10 (d, 4H), 7.39 (d, 4H), 7.06 (d, 4H), 1.69 (t, 4H), 1.47 (m, 4H), 1.41 (m, 12H), 1.33 (sextet, 4H), 0.91 (t, 6H).

Synthesis of OxBP-Ph-Odm6. A solution of 4-(2-methylhexan-2-yloxy)benzoic acid (35.5 mg, 0.150 mmol), OxBP (15.3 mg, 0.060 mmol) and DCM (10 mL) was prepared in a 25 mL round-bottom flask equipped with Ar inlet. To this mixture was added 1,3-dicyclohexylcarbodiimide (DCC, 31.9 mg, 0.155 mmol) and 4-dimethylaminopyridine (DMAP, 4.6 mg, 0.0376 mmol). The reaction mixture was allowed to stir for 48 hours at room temperature. Upon completion, a white precipitate had formed, was filtered. The filtrate was rinsed with 10% HOAc (10 mL), rinsed with saturated NaCl (20 mL), and finally the organics were dried over $MgSO_4$. The final product ODBP-Ph-Odm6 was isolated as a white solid after being recrystallized from DCM/MeOH in 59% yield (24.5 mg). ^{1}H NMR ($CDCl_3$): δ 8.16 (d, 2H), 8.11 (d, 4H), 7.76 (d, 2H), 7.43 (s, 1H), 7.33 (d, 2H), 7.29 (d, 2H), 7.06 (d, 4H), 1.72 (t, 4H), 1.57 (m, 4H), 1.43 (m, 12H), 1.34 (sextet, 4H), 0.92 (t, 6H).

Synthesis of ODBP-Ph-Odm9. *Synthesis of 4-(2-methylnonan-2-yloxy)benzonitrile*. A 50 mL 2-neck round-bottom flask equipped with Ar inlet was charged with 4-fluorobenzonitrile (0.602 g, 4.97 mmol), 2-methylnonan-2-ol (0.866 g, 5.47 mmol) and anhydrous THF (25 mL). The mixture was brought to 0 °C after which a solution of KHMDS (0.5 M, 10.9 mL) was added dropwise over the course of 45 minutes. The solution changed from colorless to dark orange. The reaction mixture was allowed to stir for 2 hours as it reached room temperature before being worked up. The mixture was then diluted with additional DCM and washed once with saturated NH_4Cl. The isolated aqueous layer was washed once with

DCM. The organics were combined and dried over $MgSO_4$, filtered and reduced; the final crude 4-(2-methylhexan-2-yloxy)benzonitrile product was passed through a short silica-gel column with hexanes, DCM, and ethyl acetate (10:1:1) and to afford 4-(2-methylnonan-2-yloxy)benzonitrile as a yellow oil (1.23 g). This product was used for the next step without further purification.

Synthesis of 4-(2-methylnonan-2-yloxy)benzoic acid. A solution of 4-(2-methylnonan-2-yloxy)benzonitrile (1.212 g, 4.67 mmol), ethylene glycol (30.0 mL) and KOH (1.3 g) was refluxed for 24 hours under Ar atmosphere. The reaction was cooled to room temperature and neutralized with a solution of HCl (2 N). A white precipitate crashed out of solution, was filtered and rinsed thoroughly with water. The final benzoic acid was isolated in 86% yield (1.12 g). ^{1}H NMR ($CDCl_3$): δ 8.00 (d, 2H), 7.00 (d, 2H), 1.67 (t, 2H), 1.43 (m, 2H), 1.27 (m, 8H), 0.86 (t, 3H).

Synthesis of ODBP-Ph-Odm9. A solution of 4-(2-methylnonan-2-yloxy)benzoic acid (42.7 mg, 0.153 mmol), ODBP (15.6 mg, 0.061 mmol) and DCM (10 mL) was prepared in a 25 mL round-bottom flask equipped with Ar inlet. To this mixture was added 1,3-dicyclohexylcarbodiimide (DCC, 32.6 mg, 0.158 mmol) and 4-dimethylaminopyridine (DMAP, 4.7 mg, 0.0384 mmol). The reaction mixture was allowed to stir for 48 hours at room temperature. Upon completion, a white precipitate had formed, was filtered. The filtrate was rinsed with 10% HOAc (10 mL), rinsed with saturated NaCl (20 mL), and finally the organics were dried over $MgSO_4$. The final product ODBP-Ph-Odm6 was isolated as a white solid after being recrystallized from DCM/MeOH in 74% yield (35.0 mg). ^{1}H NMR ($CDCl_3$): δ 8.22 (d, 4H), 8.15 (d, 4H), 7.39 (d, 4H), 7.07 (d, 4H), 1.67 (t, 4H), 1.43 (m, 4H), 1.27 (m, 16H), 0.86 (t, 6H).

Synthesis of ODBP-Ph-Odps. *Synthesis of 4-(allyloxy)benzoic acid*. A 50 mL, one-neck round-bottom flask equipped with condenser and Ar inlet was charged with 4-hydroxybenzoic acid (0.50 g, 3.62 mmol), allyl bromide (0.33 mL, 3.80 mmol), KOH (0.508 g, 9.05 mmol), NaI (7.6 mg, 0.0507 mmol) and ethanol (6 mL) and then set to reflux for 12 hours. After completion of the reaction, the mixture was acidified with 2 M HCl. A white precipitate formed, which was filtered, rinsed with water and finally recrystallized from ethanol to give 4-(allyloxy)benzoic acid in 76% yield (0.49 g).). ^{1}H NMR ($CDCl_3$): δ 8.03 (d, 2H), 6.94 (d, 2H), 6.05 (d of p, 1H), 5.42 (d of d, 1H), 5.31 (d of d, 1H), 4.59 (d of t, 2H).

Synthesis of 4,4'-(1,3,4-oxadiazole-2,5-diyl)bis(4,1-phenylene) bis(4-(allyloxy)benzoate). A solution of 4-(allyloxy)benzoic acid (26.3 mg, 0.148 mmol), ODBP (15.0 mg, 0.059 mmol) and DCM (10 mL) was prepared in a 25 mL round-bottom flask equipped with Ar inlet. To this mixture was added 1,3-dicyclohexylcarbodiimide (DCC, 31.4 mg, 0.152 mmol) and 4-dimethylaminopyridine (DMAP, 4.5 mg, 0.0367 mmol). The reaction mixture was allowed to stir for 48 hours at room temperature. Upon completion, a white precipitate had formed, was filtered. The filtrate was rinsed with 10% HOAc (10 mL), rinsed with saturated NaCl (20 mL), and finally the organics were dried over $MgSO_4$. The final product ODBP-Ph-Oallyl was isolated as a white solid after being recrystallized from DCM/MeOH in 71% yield (24.1 mg). ^{1}H NMR ($CDCl_3$): δ 8.20 (d, 4H), 8.15 (d, 4H), 7.39 (d, 4H), 7.00 (d, 4H), 6.05 (d of p, 2H), 5.43 (d of d, 1H), 5.33 (d of d, 2H), 4.63 (d of t, 4H).

Synthesis of ODBP-Ph-Odps. A 2 dram vial equipped with small stirrer and an Ar needle inlet was charged with ODBP-Ph-Oallyl (9.9 mg, 0.017 mmol), disiloxane (5.0 mg, 0.035 mmol), DCM (1 mL) and Platinum(0)-1,3-divinyl-1,1,3,3-tetramethyldisiloxane complex (1 drop) and heated to 45 °C for 24 hours. At the end of the reaction, the mixture was diluted in

methanol and chromatographed over silica-gel using 10:1:1 hexanes, acetone, DCM as eluent. The final product was minimal and only analyzed by microscopy and NMR. ^{1}H NMR ($CDCl_3$): δ 8.21 (d, 4H), 8.15 (d, 4H), 7.39 (d, 4H), 6.98 (d, 4H), 4.01 (t, 4H), 1.84 (p, 4H), 0.62 (m, 4H), 0.07 (s, 30H).

Synthesis of ODBP-Ph-OC$_5$Odm6. *Synthesis of 4-(benzyloxy)benzoyl chloride.* 4-benzyloxybenzoic acid (1) (2.4 g, 10.5 mmol) was dissolved in anhydrous CH_2Cl_2 (30 mL) and anhydrous DMF (3 drops) at 0 °C to which 2 N oxalyl chloride in dichloroethane (10.5 mL, 20.9 mmol) was added dropwise over 25 min. The reaction mixture was stirred at room temperature under Ar atmosphere for 5 hours. Solvent and excess reagents were removed under reduced pressure and product used without further purification and characterization for next step.

Synthesis of 4-(benzyloxy)-N'-(4-hydroxybenzoyl)benzohydrazide. 4-(benzyloxy)-benzoyl chloride from the above reaction and 4-hydroxybenzohydrazide were treated with $NaHCO_3$ (0.98 g, 10.5 mmol) in a mixture of dry THF (20 mL) and distilled H_2O (25 mL) for 4 hours at room temperature. White precipitate formed, was filtered, rinsed thoroughly with H_2O and dried to give final product (3.7 g, 97% overall yield). ^{1}H NMR (DMSO): δ10.24 (s, 1H), 10.16 (s, 1H), 10.10 (s, 1H), 7.88 (d, 2H), 7.78 (d, 2H), 7.48 – 7.33 (m, 5H), 7.12 (d, 2H), 6.83 (d, 2H), 5.18 (s, 2H).

Synthesis of 4-(5-(4-(benzyloxy)phenyl)-1,3,4-oxadiazol-2-yl)phenol, ODBP-OHBn. A mixture of 4-(benzyloxy)-N'-(4-hydroxybenzoyl)benzohydrazide (3.7g, 10.1 mmol), thionyl chloride (7.3 mL), pyridine (0.2 mL), and toluene (5 mL) was refluxed under Ar atmosphere for 8 hours. Reaction mixture was cooled to room temperature, quenched over ice, and stirred for about one hour. The resulting colorless precipitate was filtered, rinsed with H_2O,

and dried. Final product ODBP-OHBn was recrystallized from ethanol (2.5 g, 73% yield). ^{1}H NMR (DMSO): δ10.31 (s, 1H), 8.03 (d, 2H), 7.93 (d, 2H), 7.49 – 7.34 (m, 5H), 7.23 (d, 2H), 6.96 (d, 2H), 5.22 (s, 2H).

Synthesis of 4-(5-(4-(benzyloxy)phenyl)-1,3,4-oxadiazol-2-yl)phenyl-4-(pentyloxy)-benzoate, ODBP-OC$_5$Bn. 4-pentyloxybenzoic acid (0.14 g, 0.73 mmol) and ODBP-OHBn (0.25 g, 0.73 mmol) were treated with 1-(3-(dimethylamino)propyl)-3-ethylcarbodiimide hydrochloride (EDC) (0.14 g, 1 equiv.) and 4-(dimethylamino)pyridine (DMAP) (0.020 g, 20 mol%) in CH_2Cl_2 (50 mL) and were allowed to stir under Ar atmosphere at room temperature for 4 days. Solvent was removed under reduced pressure and recrystallized with CH_2Cl_2/MeOH to afford the final colorless product ODBP-OC$_5$Bn (0.33 g, 88%). ^{1}H NMR ($CDCl_3$): δ8.17 (d, 2H), 8.14 (d, 2H), 8.07 (d, 2H), 7.46 – 7.34 (m, 7H), 7.10 (d, 2H), 6.97 (d, 2H), 5.14 (s, 2H), 4.05 (t, 2H), 1.80 (pentet, 2H), 1.50 (sextet, 2H), 0.98 (t, 3H).

Synthesis of ODBP-OC$_5$OH. A scintillation vial was charged with ODBP-OC$_5$Bn (0.104 g, 0.195 mmol), Palladium on carbon (20.0 mg at 10% Pd), and DCM/Methanol (4 mL at 1:1). The system was pressurized with H_2 in a high-pressure bomb reactor to 60 psi and allowed to stir at room temperature for 24 hours. After the allotted time, the reaction mixture solution was filtered over celite, and the solvents were reduced in vacuo. The crude product was purified by silica-gel chromatography with hexanes, DCM, acetone (8:1:1) to afford ODBP-OC$_5$OH in 82% yield (70.5 mg). This product was identified by TLC and used for the next step without characterization.

Synthesis of ODBP-Ph-OC$_5$Odm6. 4-(2-methylhexan-2-yloxy)benzoic acid (18.6 mg, 0.0787 mmol) and ODBP-OC$_5$OH (35.0 mg, 0.0787 mmol) were treated with 1-(3-(dimethylamino)propyl)-3-ethylcarbodiimide hydrochloride (EDC) (15.1 mg, 1 equiv.) and

4-(dimethylamino)pyridine (DMAP) (1.9 mg, 20 mol%) in CH_2Cl_2 (5.0 mL) and were allowed to stir under Ar atmosphere at room temperature for 3 days. The reaction mixture was extracted once with water, and combined organics were dried over $MgSO_4$. The solvents were removed under reduced pressure, and the remaining crude product was recrystallized with CH_2Cl_2/MeOH to afford the final colorless product ODBP-Ph-OC_5Odm6 (26.6 mg, 51%). ^{1}H NMR ($CDCl_3$): δ 8.20 (d, 4H), 8.13 (d, 2H), 8.11 (d, 2H), 7.40 (d, 2H), 7.39 (d, 2H), 7.07 (d, 2H), 6.97 (d, 2H), 4.04 (t, 2H), 1.82 (p, 2H), 1.72 (m, 2H), 1.42 (m, 6H), 1.38 (s, 6H), 1.36 (m, 2H), 0.94 (t, 3H), 0.92 (t, 3H).

Synthesis of ODBP-Ph-OBn. 4-benzyloxybenzoic acid (33.7 mg, 0.148 mmol) and ODBP (15.0 mg, 0.0590 mmol) were treated with dicyclohexyl carbodiimide hydrochloride (DDC) (15.1 mg, 1.03 equiv.) and 4-(dimethylamino)pyridine (DMAP) (4.5 mg, 25 mol% by acid) in CH_2Cl_2 (10.0 mL) and were allowed to stir under Ar atmosphere at room temperature for 2 days. Upon completion, a white precipitate had formed and was filtered. The filtrate was rinsed with 10% HOAc (10 mL), rinsed with saturated NaCl (20 mL), and finally the organics were dried over $MgSO_4$. The final product ODBP-Ph-OBn was isolated as a white solid after being recrystallized from DCM/MeOH in 77% yield (30.6 mg). ^{1}H NMR ($CDCl_3$): δ 8.16 (d, 2H), 8.11 (d, 4H), 7.76 (d, 2H), 7.43 (s, 1H), 7.33 (d, 2H), 7.29 (d, 2H), 7.06 (d, 4H), 1.72 (t, 4H), 1.57 (m, 4H), 1.43 (m, 12H), 1.34 (sextet, 4H), 0.92 (t, 6H). – nz2130

Synthesis of ODBP-Ph-OBnC_4. *Synthesis of 1-(bromomethyl)-4-butylbenzene*. A 2-neck, 25 mL round bottom flask equipped with Ar inlet was charged with (4-butylphenyl)methanol (0.200 g, 1.22 mmol), CBr_4 (0.485 g, 1.462 mmol), triphenylphosphine PPh_3 (0.384 g, 1.46 mmol), and anhydrous THF (2 mL). After 6 hours of stirring at room temperature, a white

precipitate formed. The solid was filtered and rinsed thoroughly with hexanes. The filtrate was collected and passed through a small pipet column with hexanes to remove any remaining PPh_3 and $POPh_3$ by-product to yield 1-(bromomethyl)-4-butylbenzene as an oil, which was used without characterization and carried over to the next reaction.

Synthesis of methyl 4-(4-butylbenzyloxy)benzoate. A solution of 1-(bromomethyl)-4-butylbenzene (1.22 mmol), methyl 4-hydroxybenzoate (0.185 g, 1.22 mmol), and K_2CO_3 (0.850 g, 5 x excess) in DMF (5 mL) was prepared in a 100 mL round-bottom flask. The mixture was stirred at room temperature for 12 hours. At the end of the reaction, DMF was removed under reduced pressure and remaining crude product was dissolved in ethyl acetate, which was sequentially extracted with water and brine solutions. Combined organics were dried over $MgSO_4$, filtered and reduced to give methyl 4-(4-butylbenzyloxy)benzoate (0.366 g, 98% after two steps). ^{1}H NMR ($CDCl_3$): δ 7.95 (d, 2H), 7.32 (d, 2H), 7.18 (d, 2H), 6.96 (d, 2H), 5.06 (s, 2H), 3.85 (s, 3H), 2.56 (t, 2H), 1.55 (p, 2H), 1.32 (m, 2H), 0.86 (t, 3H).

Synthesis of 4-(4-butylbenzyloxy)benzoic acid. In a 50 mL, 1-neck round-bottom flask equipped with a condenser and Ar inlet, a solution of methyl 4-(4-butylbenzyloxy)benzoate (0.366 g, 1.22 mmol), KOH (2.0 g, excess), THF (5 mL), methanol (2 mL) and water (2 mL) was refluxed for 24 hours. Upon cooling the reaction mixture to room temperature, a precipitate formed, which was subsequently acidified with 2 M HCl solution. Once acidified, precipitate dissolved, but upon removal of organics, the final benzoic acid crashed out of solution, was filtered, rinsed with water and dried. The final 4-(4-butylbenzyloxy)benzoic acid was isolated in 82% yield (0.285 g). ^{1}H NMR ($CDCl_3$): δ 7.93 (d, 2H), 7.28 (d, 2H), 7.14 (d, 2H), 6.94 (d, 2H), 5.02 (s, 2H), 2.56 (t, 2H), 1.55 (p, 2H), 1.32 (m, 2H), 0.86 (t, 3H).

Synthesis of ODBP-Ph-OBnC$_4$. 4-(4-butylbenzyloxy)benzoic acid (41.9 mg, 0.148 mmol) and ODBP (15.0 mg, 0.0590 mmol) were treated with dicyclohexyl carbodiimide hydrochloride (DDC) (31.4 mg, 1.03 equiv.) and 4-(dimethylamino)pyridine (DMAP) (4.5 mg, 25 mol% by acid) in CH_2Cl_2 (10.0 mL) and were allowed to stir under Ar atmosphere at room temperature for 2 days. Upon completion, a white precipitate had formed and was filtered. The filtrate was rinsed with 10% HOAc (10 mL), rinsed with saturated NaCl (20 mL), and finally the organics were dried over $MgSO_4$. The final product ODBP-Ph-OBnC$_4$ was isolated as a white solid after being recrystallized from DCM/MeOH in 76% yield (35.3 mg). ^{1}H NMR ($CDCl_3$): δ 8.20 (d, 4H), 8.15 (d, 4H), 7.39 (d, 4H), 7.34 (d, 4H), 7.21 (d, 4H), 7.06 (d, 4H), 5.11 (s, 4H), 2.62 (t, 4H), 1.59 (p, 4H), 1.35 (sextet, 4H), 0.92 (t, 6H).

Synthesis of ODBP-OBn. A solution of ODBP (75.3 mg, 0.296 mmol), benzylbromide (112.2 mg, 0.656 mmol), K_2CO_3 (121.0 mg, 0.875 mmol) and anhydrous DMF (2.5 mL) were heated to 60 °C in a 25 mL. 2-neck round-bottom flask overnight. After completion of the reaction, DMF was removed under reduced pressure, and the crude product was dissolved in DCM and extracted with brine and water sequentially. The organics were combined, dried over $MgSO_4$, reduced and chromatographed with hexanes, DCM and acetone (8:1:1) as eluent. The isolated product ODBP-OBn was rotovapped to dryness as a white powder (93.1 mg, 98%). ^{1}H NMR ($CDCl_3$): δ 8.04 (d, 4H), 7.43 (t, 4H), 7.38 (t, 2H), 7.08 (d, 4H), 5.13 (s, 4H).

Synthesis of ODBP-OBnC$_4$. A 25 mL, 2-neck round-bottom flask equipped with Ar inlet and condenser was charged with 1-(bromomethyl)-4-butylbenzene (7.5 mg, 0.0272 mmol), ODBP (3.2 mg, 0.0124 mmol), K_2CO_3 (21.3 mg, 0.154 mmol) and acetone (3 mL) and set to reflux for 6 hours. The reaction mixture was diluted with water and extracted three times

with ethyl acetate. The combined organics were dried over $MgSO_4$ and reduced in vacuo. The final product ODBP-OBnC_4 was isolated after recrystallization from DCM/MeOH in 66% yield (4.5 mg). ^{1}H NMR ($CDCl_3$): δ 8.02 (d, 4H), 7.39 (d, 4H), 7.20 (d, 4H), 7.06 (d, 4H), 5.11 (s, 4H), 2.62 (t, 4H), 1.59 (p, 4H), 1.35 (sextet, 4H), 0.92 (t, 6H).

Synthesis of ODBP-OBn-OBn. A known procedure was followed for the two step synthesis of 1-(benzyloxy)-4-(bromomethyl)benzene.[32, 33] A 50 mL, 2-neck round-bottom flask equipped with Ar inlet and condenser was charged with 1-(benzyloxy)-4-(bromomethyl)benzene (52.8 mg, 0.190 mmol), ODBP (22.0 mg, 0.0865 mmol), K_2CO_3 (149.4 mg, 1.08 mmol) and acetone (20 mL) and set to reflux for 6 hours. The reaction mixture was diluted with water and extracted three times with ethyl acetate. The combined organics were dried over $MgSO_4$ and reduced in vacuo. The final product ODBP-OBn-OBn was isolated after recrystallization from DCM/MeOH in 88% yield (49.2 mg). ^{1}H NMR ($CDCl_3$): δ 8.02 (d, 4H), 7.50 (d, 4H), 7.40 (m, 6H), 7.06 (d, 4H), 7.00 (d, 4H), 6.92 (d, 4H), 5.11 (s, 8H).

Synthesis of ODBP-OBnOC$_8$. *Synthesis of 1-(bromomethyl)-4-(octyloxy)benzene*. A 2-neck, 25 mL round bottom flask equipped with Ar inlet was charged with (4-(octyloxy)phenyl)methanol (1.37 g, 5.79 mmol), CBr_4 (2.31 g, 6.95 mmol), triphenylphosphine PPh_3 (1.82 g, 6.95 mmol), and anhydrous THF (2 mL). After 6 hours of stirring at room temperature, a white precipitate formed. The solid was filtered and rinsed thoroughly with hexanes. The filtrate was collected and passed through a small pipet column with hexanes to remove any remaining PPh_3 and $POPh_3$ by-product to yield 1 Synthesis of 1-(bromomethyl)-4-(octyloxy)benzene as tacky solid, which was used without characterization and carried over to the next reaction.

Synthesis of ODBP-OBnOC$_8$. A 25 mL, 2-neck round-bottom flask equipped with Ar inlet was charged with 1-(bromomethyl)-4-(octyloxy)benzene (150.7 mg, 0.504 mmol), ODBP (51.2 mg, 0.201 mmol), K_2CO_3 (348.0 mg, 2.52 mmol) and DMF (6 mL) and allowed to stir at room temperature for 24 hours. The reaction was removed of its organic solvents under reduced pressure; the remaining solid was diluted with DCM and extracted with brine and water, sequentially. The organics were combined and dried over $MgSO_4$ and reduced in vacuo. The final product ODBP-OBnOC$_8$ was chromatographed with hexanes, DCM and acetone (8:1:1), which was then recrystallized from DCM/MeOH and isolated in 64% yield (89.1 mg). ^{1}H NMR ($CDCl_3$): δ 8.02 (d, 4H), 7.39 (d, 4H), 7.20 (d, 4H), 7.06 (d, 4H), 5.11 (s, 4H), 4.05 (t, 4H), 1.81 (p, 4H), 1.32 (overlapping m, 20H), 0.92 (t, 6H).

3.9 References

1. Reinitzer, F., *Montash. Chem.* **1888,** 9, 421-441.

2. Fisch, M. R., *Liquid Crystals, Laptops and Life*. World Scientific: Singapore, 2004.

3. Rasing, T.; Musevic, I., *Surfaces and Interfaces of Liquid Crystals*. Springer: Berlin, 2004.

4. de Gennes, P. G., *The Physics of Liquid Crystals*. Clarendon Press: Oxford, 1974; p 1-224.

5. Madsen, L. A.; Dingemans, T. J.; Nakata, M.; Samulski, E. T., Thermotropic Biaxial Nematic Liquid Crystals. *Physical Review Letters* **2004,** 92, (14), 145505.

6. Collings, P. J.; Hird, M., *Introduction to Liquid Crystals Chemistry and Physics*. Taylor & Francis Ltd.: Bristol, 1997.

7. Samulski, E. T., *Physical Properties of Polymers*. United Book Press: Baltimore, 1993.

8. Emsley, J. W., *Nuclear Magnetic Resonance of Liquid Crystals*. Reidel Publishing Company: Boston, 1985.

9. Hartshorne, N. H., *The Microscopy of Liquid Crystals*. Microscope Publications Ltd.: London, 1974.

10. Poon, C.-D.; Fung, B. M., Carbon-13 nuclear magnetic resonance of ferroelectric liquid crystals with off-magic-angle spinning. *The Journal of Chemical Physics* **1989,** 91, (12), 7392-7398.

11. Viney, C., *Transmitted Polarized Light Microscopy*. McCrone Research Institute: Chicago, 1990.

12. Chandrasekhar, S., *Liquid Crystals*. Cambridge University Press: New York, 1992.

13. Inoue, S., *Video Microscopy*. Plenum Press: New York, 1989.

14. Dierking, I., *Textures of Liquid Crystals*. WILEY-VCH: Verlag, 2003.

15. Gray, G. W., *Thermotropic Liquid Crystals*. John Wiley & Sons: New York, 1987.

16. Freiser, M. J., Ordered States of a Nematic Liquid. *Physical Review Letters* **1970,** 24, (19), 1041.

17. Chandrasekhar, S.; Nair, G. G.; Rao, D. S. S.; Prasad, S. K.; Praefcke, K.; Singer, D., *Mol. Cryst. Liq. Cryst.* **1996,** 288, 7-14.

18. Chandrasekhar, S.; Sadashiva, B. K.; Ratna, B. R., *Pramana* **1988,** 30, L491-L494.

19. Praefcke, K.; Kohne, B.; Singer, D.; Demus, D.; Pelzl, G.; Diele, S., Thermotropic biaxial nematic phases with negative optical character [1]. *Liquid Crystals* **1990,** 7, (4), 589 - 594.

20. Galerne, Y., *Mol. Cryst. Liq. Cryst.* **1998,** 323, 211-229.

21. Leube, H. F.; Finkelmann, H., *Makromol. Chem.* **1991,** 192.

22. Teixeira, P. I. C.; Masters, A. J.; Mulder, B. M., *Mol. Cryst. Liq. Cryst.* **1998,** 323.

23. Archarya, B.; Primak, A.; Dingemans, T. J.; Samulski, E. T.; Kumar, S., The elusive thermotropic biaxial nematic phase in bent-core molecules. *Pramana* **2003,** 61, (2), 231-237.

24. Demus, D.; Goodby, J.; Gray, G. W.; Spiess, H.-W.; Vill, V., *Physical Properties of Liquid Crystals*. WILEY-VCH: Verlag, 1999.

25. Hughes, J. R.; Kothe, G.; Luckhurst, G. R.; Malthete, J.; Neubert, M. E.; Shenouda, I.; Timimi, B. A.; Tittelbach, M., A deuterium nuclear magnetic resonance investigation of the symmetry and orientational order of the nematic phase of 4-[3,4,5-tris(4-dodecyloxybenzyloxy)benzoyloxy]-4[sup [prime]]- (4-dodecyloxybenzoyloxy)-1,1[sup [prime]]-biphenyl. A biaxial nematic? *The Journal of Chemical Physics* **1997,** 107, (21), 9252-9263.

26. Goldfarb, D.; Poupko, R.; Luz, Z.; Zimmermann, H., Deuterium NMR of biaxial discotic liquid crystals. *The Journal of Chemical Physics* **1983,** 79, (8), 4035-4047.

27. Fan, S. M.; Fletcher, I. D.; Gundogan, B.; Heaton, N. J.; Kothe, G.; Luckhurst, G. R.; Praefcke, K., The symmetry of the nematic phase of a thermotropic liquid crystal: biaxial or uniaxial? *Chemical Physics Letters* **1993,** 204, (5-6), 517-523.

28. Photinos, D. J.; Doane, J. W., *Mol. Cryst. Liq. Cryst.* **1981,** 76.

29. Kaneko, E., *Liquid Crystal TV Displays: Principles and Applications of Liquid Crystal Displays*. Scientific Publishers: Tokyo, 1987.

30. Gortz, V.; Goodby, J. W., Enantioselective segregation in achiral nematic liquid crystals. *Chemical Communications* **2005**, (26), 3262-3264.

31. Madsen, L. A.; Samulski, E. T., Addressing non-idealities in NMR experiments on rotating liquid crystals. *Liquid Crystals* **2005,** 32, (11), 1419 - 1425.

32. Lee, J.; Lee, J.-H.; Kim, S. Y.; Perry, N. A.; Lewin, N. E.; Ayres, J. A.; Blumberg, P. M., 2-Benzyl and 2-phenyl-3-hydroxypropyl pivalates as protein kinase C ligands. *Bioorganic & Medicinal Chemistry* **2006,** 14, (6), 2022-2031.

33. Oldfield, M. F.; Chen, L.; Botting, N. P., Synthesis of [3,4,8-13C3]daidzein. *Tetrahedron* **2004,** 60, (8), 1887-1893.

CHAPTER 4

Switchable Phase of an Unsymmetric Bent-Core Liquid Crystals Based on ODBP

4.1 Introduction to Switchable Phases

Over the past decade there have been numerous reports of anisotropic molecules possessing rigid bent-core shapes capable of forming liquid crystal phases. Their main appeal has mainly been a switchable, antiferroelectric and ferroelectric banana phase (designated as B_x), which was first discovered by Niori *et al*. in the banana-shaped molecules, 1,3-benzene bis[4-(4-*n*-alkoxyphenylliminomethyl)benzoate] (P-*n*-O-PIMB).[1] The ferroelectricity arises from the polar C_{2v} packing arrangement of the bent structures.[2] The molecules need not necessarily be chiral; several reports have shown achiral molecular systems to form chiral phases, i.e. ferroelectric liquid crystals.[3] In this high viscosity phase, the sample can very easily reorient in an electric field,[3] which draws interests for applications in electronics and optoelectronics (as materials for capacitors, light modulators, and light frequency converters).[4]

It has been shown throughout the literature that small changes in the chemical structure can significantly alter the phase behavior, especially those phases below the calamitic nematic and smectic C phase. This has led to the development of a myriad of novel banana molecules all derivatives of the parent P-*n*-O-PIMB series. Here, we report a structural modification to a previously reported biaxial nematic liquid crystal ODBP-Ph-C_7.[5,6] In this family of ODBP

compounds, the bending moiety of the molecule is achieved by a disubstituted 2,5-bis-(*p*-hydroxyphenyl)-1,3,4-oxadiazole (ODBP) heterocycle with an exocyclic bond angle of 134° and large electric dipole moment (~ 5 Debye). The resulting negative dielectric anisotropy of the ODBP core makes these compounds strong candidates for electro-optical switches.[7] Kang *et al*. recently observed an interesting polymorphism behavior in an oxadiazole-based molecule where the banana B_x phase formed is a fluid smectic phase that is chiral and optically isotropic.[8] They have concluded that the B_x phase arises from a layered structure where the molecules pack like a liquid and are tilted with respect to the layer; the helical twisting of the phase is produced from the ground-state B_2 phase with the homochiral SmC_AP_A structure. Previously, we reported a series of symmetric alkyl and alkoxy benzoate esters of the ODBP core of which ODBP-Ph-C_7 and ODBP-Ph-OC_{12} were shown to exhibit the elusive biaxial nematic phase.[6] In efforts to lower the onset of the biaxial nematic phase, we synthesized a series of unsymmetrical compounds having alkoxy benzoate ester and benzyloxy termini from an ODBP core. Paraskos *et al*. discovered in their desymmeterized thiophene-based bent-core mesogens a frustration in the lamellar superstructures that led to broader mesophases.[9] This may lead to a frustration in the lamellar superstructures. In this study, we report the synthesis and explore the phase behavior of several unsymmetrical ODBP-OC_nBn (n = 4, 5, 6, 7, 8, 9, 12) compounds by ^{2}H-NMR and X-ray diffraction.

4.2 Synthesis of ODBP-OC_nBn Series

The synthesis of the ODBP-OC_nBn series is illustrated in Figure 4.1. Synthesis of the symmetric ODBP core was previously reported by Samulski.[5] Here we focus on derivatizing 1,3,4-oxadiazole unsymmetrically. The parent compound **4.4** is prepared by coupling 4-

(benzyloxy)benzoyl chloride with the reactive 4-hydroxybenzohydrazide in nearly quantitative yield to give **4.3** which is then dehydrated using $SOCl_2$ to afford the five-membered oxadiazole heterocycle. The final compounds **4.5a-g** are made by the equimolar addition of the appropriate 4-alkoxy(*n* = 4, 5, 6, 7, 8, 9, 12)benzoic acid to **4.4** under EDC/DMAP coupling conditions. The yields are high, so the final compounds can readily be purified by recrystallization.

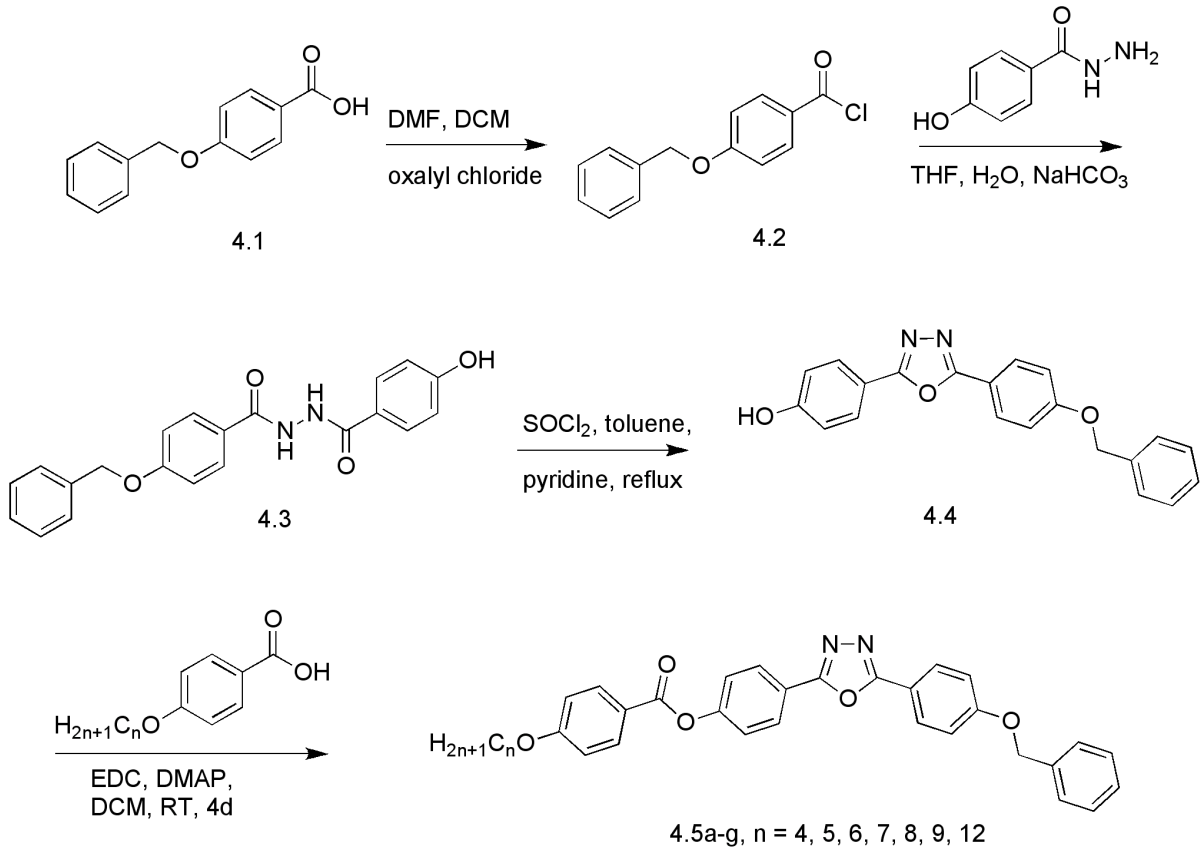

Figure 4.1. Synthesis of unsymmetric ODBP alkoxy derivatized liquid crystals, **4.5a** – **4.5g**.

4.3 Thermal Characterization

We originally sought out to make the biaxial nematic phase of ODBP-Ph-C_7 more accessible by an unsymmetric substitution of the 1,3,4-oxadiazole central ring. Goodby[10]

reported dissimilarly substituted materials based off the ODBP core with varying aliphatic chain lengths; however, he only observed a modest reduction in nematic onset temperature and did not report any measurements on their biaxiality. We have synthesized an unsymmetric analogue where one terminus maintains the same alkyloxybenzoic ester while the opposing terminus is a non-aliphatic benzyloxy group. Although the molecular structures as drawn appear to be traditional bent-core shapes, solid-state ^{2}H-NMR analyses of the OC_5 and OC_{12} compounds indicate clearly a uniaxial nematic. We propose that unlike the symmetric ODBP-Ph-C_7 originally reported to possess a biaxial order parameter, $\eta = 0.1$, the pendant benzyloxy group can freely rotate and assume a position indicative of a uniaxial shape.

Thermal Analysis. The DSC results of the homologous series ODBP-OC_nBn, where *n* ranges from 5 to 12, are presented in Figure 4.2. All compounds are liquid crystalline, containing at least an enantiotropic nematic phase. The mesophase onset temperatures for this series of compounds is significantly lower than the parent symmetric series. The respective DSC traces for each compound is shown in Figure 4.3; all traces are shown as second coolings at a rate of 10 °C/min. These temperatures, as well as the clearing points, decrease slightly with an odd-even effect as the aliphatic chain increases in length. Overall, the nematic window broadens with decreases with chain length. **4.5a** shows a crystal to crystal transition observable by optical microscopy at 50 °C while **4.5b-f** have only nematic phases. The last compound in the series, OC_{12} or **4.5g**, has multiple phases. Optical microscopy and X-ray studies indicate a smectic A phase as well as a higher ordered smectic G or J phase.

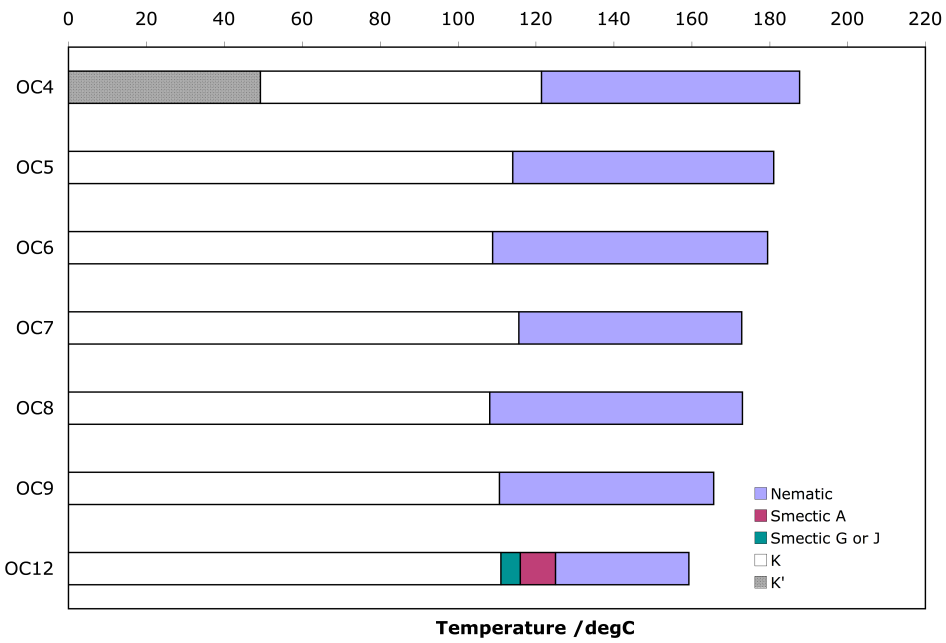

Figure 4.2. Transition maps showing the phase behavior of the ODBP-OC$_n$Bn liquid crystals.

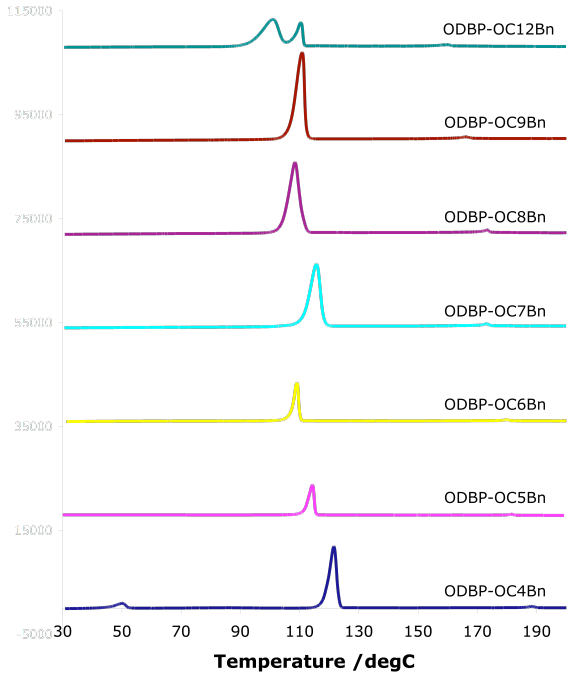

Figure 4.3. DSC traces for the ODBP-OC$_n$Bn homologous series upon second cooling at a rate of 10 °C/min. Inset shows DSC traces between 75 °C and 150 °C.

Microscopic Analysis. We used hot-stage optical microscopy to study the melt behavior of ODBP-OC_{12}Bn and gain insight into the phase type and phase stability as a function of the temperature. The sample was heated into the isotropic phase and cooled with 5 °C.min^{-1}, and their mesophase textures were observed (Figure 4.4). At 140 °C a nematic Schlieren texture, which exhibits mainly two-brush disclinations, could be observed. When cooling was continued, a focal conic texture, indicative of the SmA phase was formed. The SmA phase transformed into a higher ordered Smectic phase, which exhibits an unusual low birefringence texture. When observed under crossed polarizers rotated 10° past 90° there are only light and dark regions, but as the analyzer rotates to -10° to the other direction, the light regions become dark and dark become light (Figure 4.5). This phase has been seen in other highly ordered smectics, however, it is only stable over a 5 °C temperature range, and crystallization takes place almost immediately.

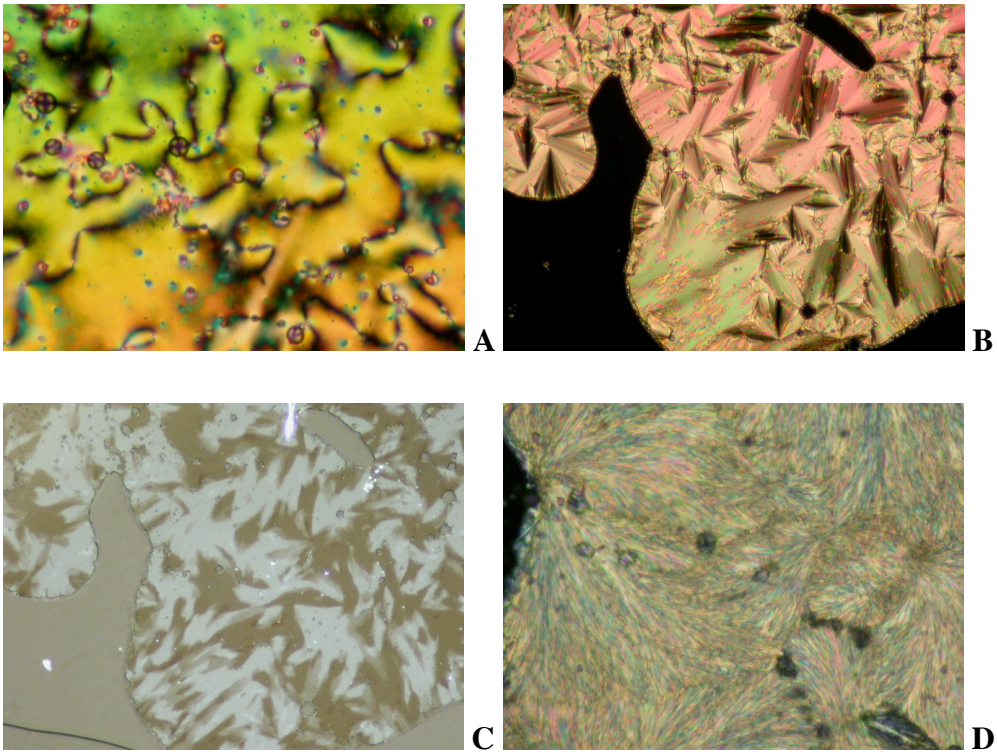

Figure 4.4. Microphotographs of ODBP-OC_{12}Bn, between crossed polarizers (20 X); ***A***– Nematic Schlieren texture at 140 °C, ***B***– Focal conic texture of the SmA phase at 117 °C. ***C***– Highly ordered Sx phase (J or G) at 115 °C. ***D***– Crystal phase at 110 °C.

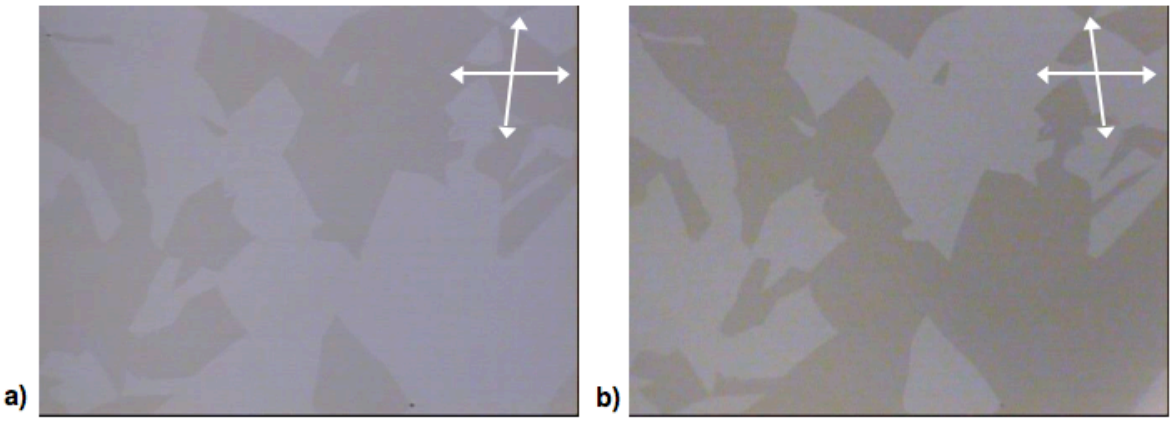

Figure 4.5. Microphotographs of the highly ordered Sx phase at 116 °C of ODBP-OC_{12}Bn between crossed polarizers +10° (a) and -10° (b) past 90° (10 X magnification). White arrows indicate positions of polarizer and analyzer.

X-ray Analysis. ODBP-OC_{12}Bn was also investigated using temperature dependent small-angle X-ray diffraction. This liquid crystal sample was prepared in a 1.0 mm quartz capillary, sealed and placed in a graphite furnace. The X-ray measurements were obtained after the sample was first heated to the isotropic phase. As the sample slowly cooled from the isotropic phase, a permanent magnet of ~4 T was applied to align the liquid crystal phase; the sample was kept in this field throughout the duration of the experiment. The diffraction patterns obtained at various temperatures are illustrated in Figure 4.6.

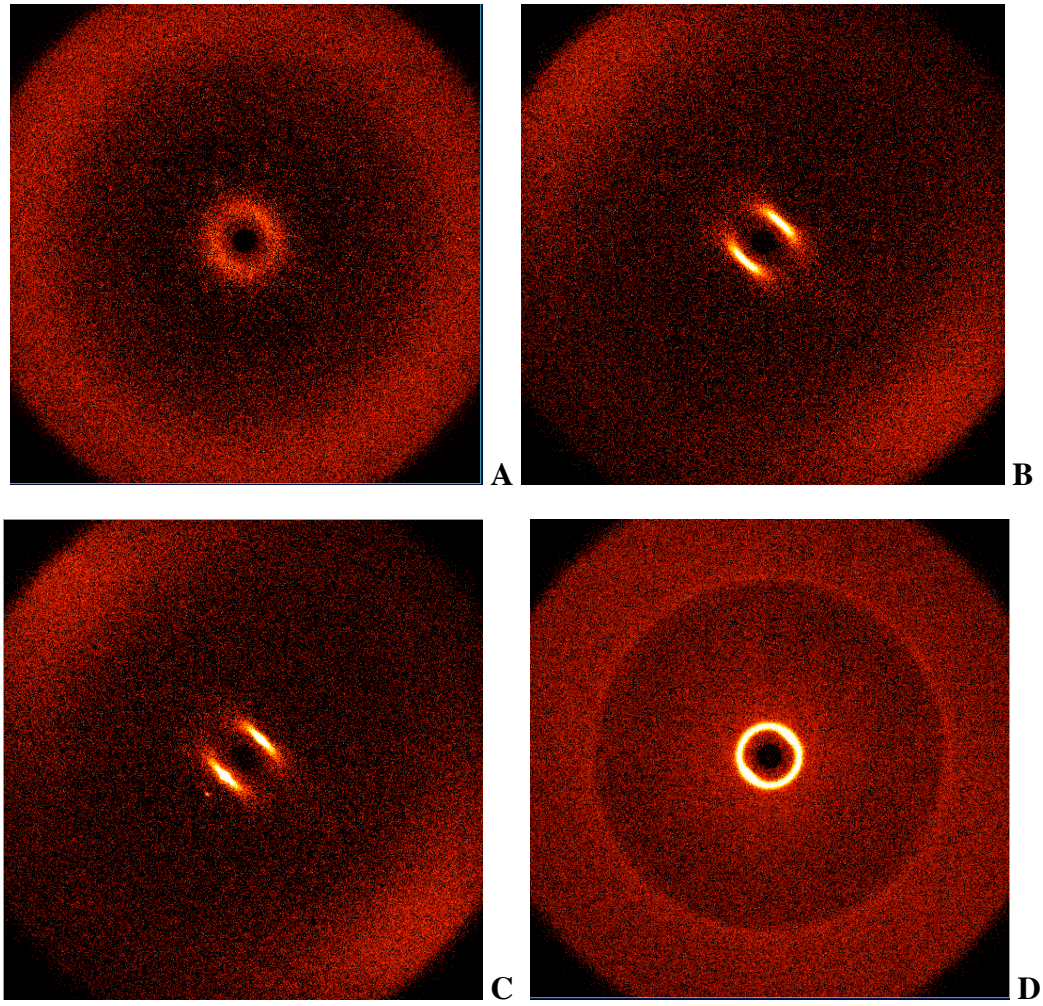

Figure 4.6. Diffraction patterns of ***A***– the isotropic phase at 170 °C, ***B***– the nematic phase at 140 °C, ***C***– The SmA phase at 117 °C, and ***D***– Sx phase (J or G) at 115 °C.

The results are summarized in Figure 4.6. The isotropic phase (at 170 °C) is identified by the absence of diffraction (Figure 4.6A). As the sample cooled farther into the nematic phase, a conventionally aligned nematic phase forms and diffraction pattern obtained at 140 °C (Figure 4.6B), which shows signs of a cybotactic structure. When cooling is continued, the nematic phase transforms into a well-aligned SmA phase. The small angle reflection (2θ ~ 2°) corresponds to a layer spacing (*d*) of 37.7 Å. This corresponds to the molecular length of this mesogen in its most extended conformation as estimated by *Spartan* (Figure 4.7). The SmA phase can therefore be indexed as a SmA_1 monolayer (Figure 4.8A). The SmA_1 phase cools into an unaligned liquid crystal phase, with a (001) reflection corresponding to a layer spacing of 33. 7 Å, indicating a slightly interdigitated smectic phase (possibly a G or J) (Figure 4.8B). Due to the lack of alignment of this phase it is difficult to be more specific about the exact nature of this phase, hence we have labeled this phase Sx. Proposed arrangements of this unsymmetric molecule in the smectic A and interdigitated smectic phases are illustrated in Figure 4.9.

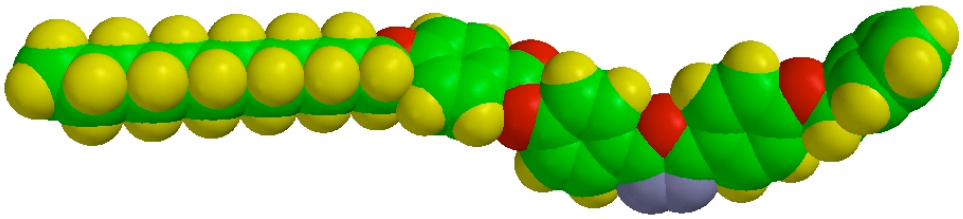

Figure 4.7. Molecular model of ODBP-OC12Bn proposed by *Spartan* as its most extended isomer.

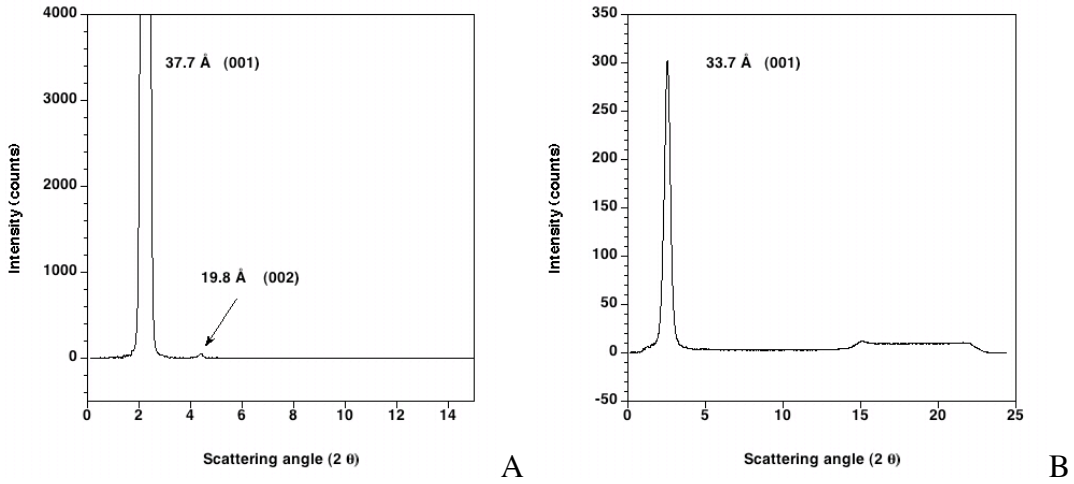

Figure 4.8. X-ray diffraction patterns of ODBP-OC_{12}Bn. ***A***– SmA_1 phase at 117 °C, ***B***– Sx phase (J or G) at 115 °C.

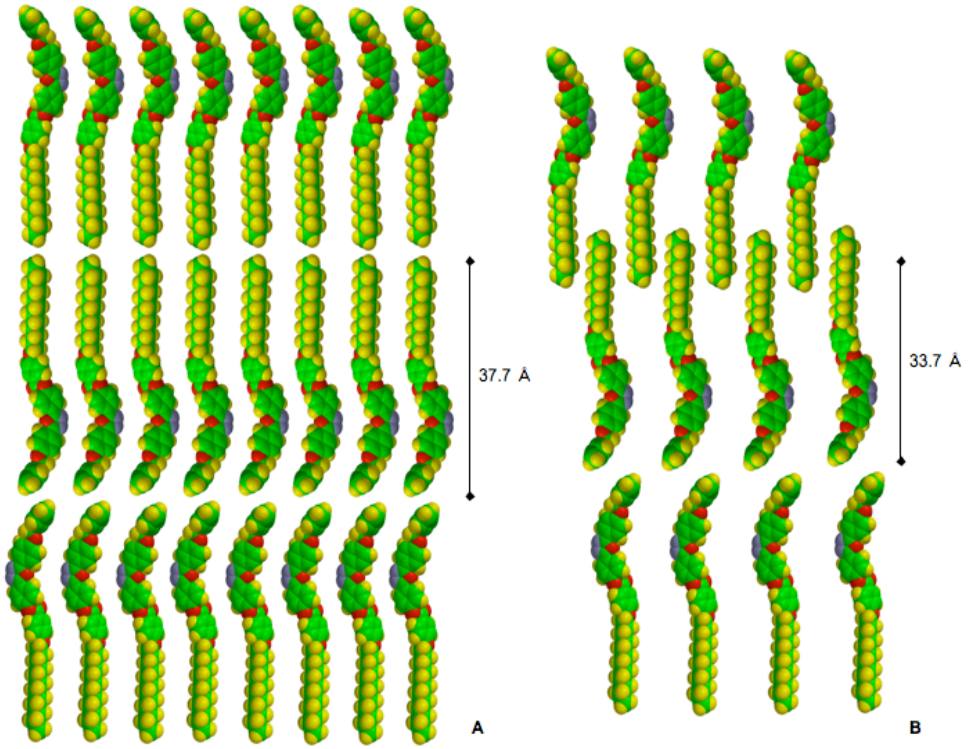

Figure 4.9. Diagram to show two possible arrangements of ODBP-OC_{12}Bn into smectic A layers (A) and interdigitated layers (B). Period lengths indicated in image correspond with layer spacings determined from X-ray analysis.

4.4 ^{2}H-NMR of ODBP-OC$_5$Bn

Our initial goal with this homologous series of compounds was to synthesize a nematic liquid crystal whose behavior exhibited biaxiality ($Q_{XX} \neq Q_{YY}$) at temperatures lower than the previously reported symmetric ODBP-Ph-OC12 and ODBP-Ph-C7. We chose ODBP-OC$_5$Bn to observe by solid-state ^{2}H-NMR spectroscopy as described by the method in Chapter 3. ODBP-OC$_5$Bn is not a perdeuterated compound, so the experiment was conducted by doping the sample with 1-2 wt% hexamethylbenzene-d_{18} (HMB) to serve as a solute probe molecule. The first experiment involved obtaining the NMR spectrum in the static case at a range of temperatures from 480 K to 280 K (Figure 4.10). The ^{2}H-doped sample exhibits a single line at 480 K, indicating an isotropic phase. As this sample cools, we observe a pair of lines split by ν_Q, where ν_Q is proportional to the motionally averaged component of the partially averaged quadrupole tensor $\boldsymbol{q}$ parallel to the major director $\boldsymbol{n}$. This splitting continues until the sample crystallizes, resulting in a single peak where the distribution of probe molecules yields an apparent isotropic-like phase.

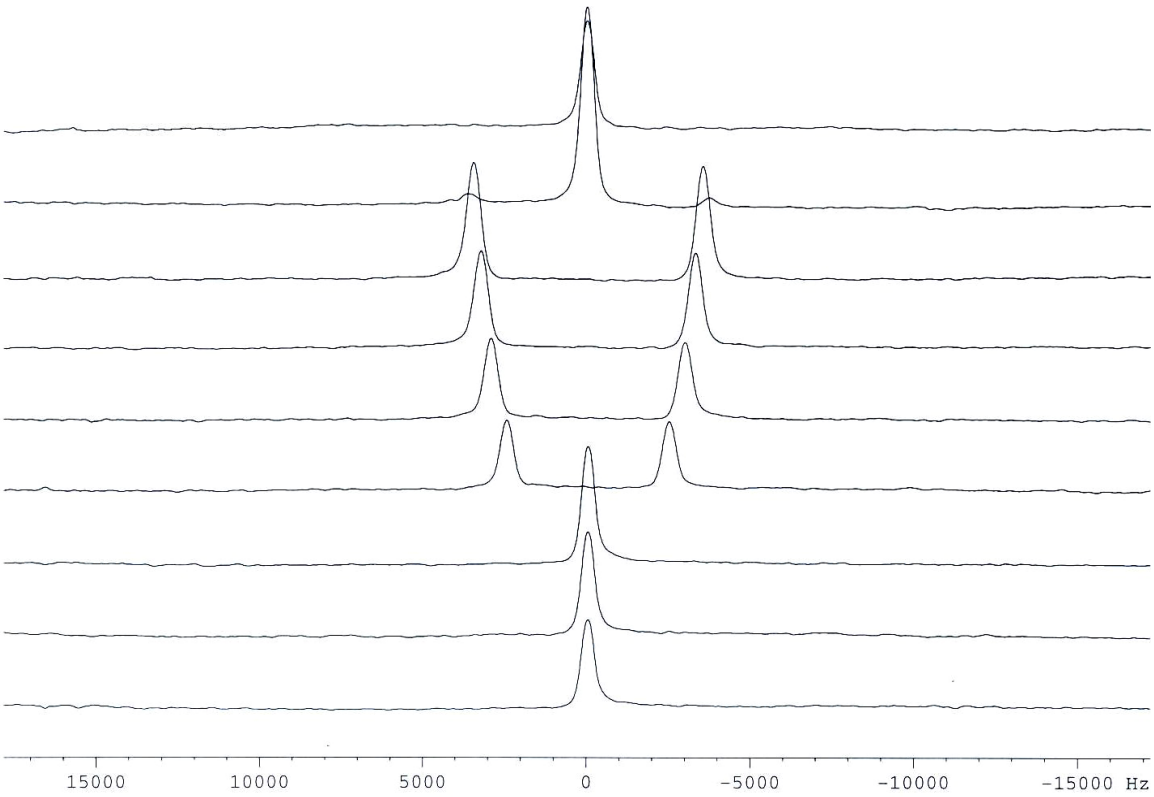

Figure 4.10. NMR data for a static sample of ODBP-OC_5Bn/HMB-d_{18} at temperatures ranging from 480 K (lower) to 280 K (upper).

When the sample was rotated about an axis normal to the magnetic field $\mathbf{B}_0$ at a rate of 166 Hz at 395 K (122 °C), the lower end of the nematic range, the NMR spectrum exhibits a two-dimensional "powder" pattern – a weighted average of the quadrupolar spectra for a planar distribution of $\boldsymbol{n}$. In a biaxial nematic we would expect to see a secondary alignment of the X component to minimize the magnetic free energy. However, we observed a uniaxial nematic with equivalent $X = Y = \frac{1}{2} Z$ components. This is evident in Figure 4.11 where we have overlaid the experimentally determined spectrum with the simulated spectrum. We measured a biaxiality parameter $\eta = 0.00 \pm 0.03$ for ODBP-OC_5Bn/HMB, i.e. ODBP-OC_5Bn is in fact a uniaxial nematic. We hypothesize that ODBP-OC_5Bn has a bent core, but if we consider

rotations about the benzyloxy ether bonds (Figure 4.12), we can envision a more calamitic-like molecular structure, which would lead to an entirely uniaxial nematic phase.

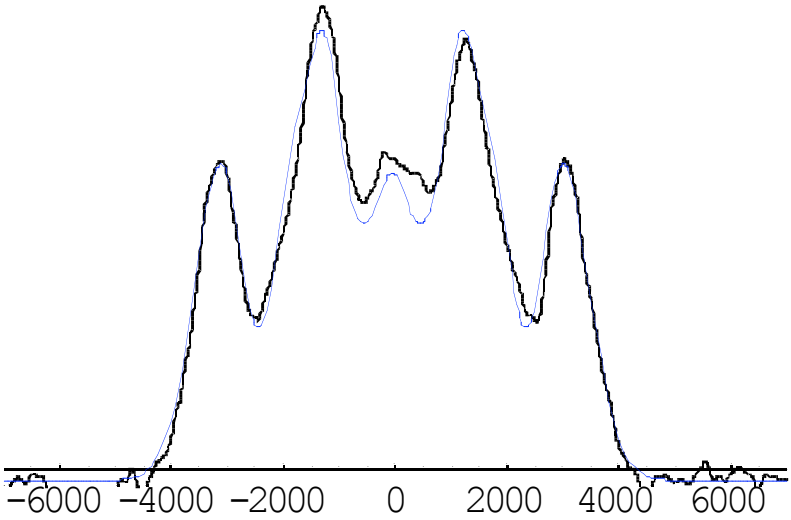

Figure 4.11. NMR data (black) and simulation (blue) for a rotating uniaxial nematic ODBP-OC_5Bn (x-axis is in Hz). Best fit obtained with biaxiality $\eta = 0.00 \pm 0.03$.

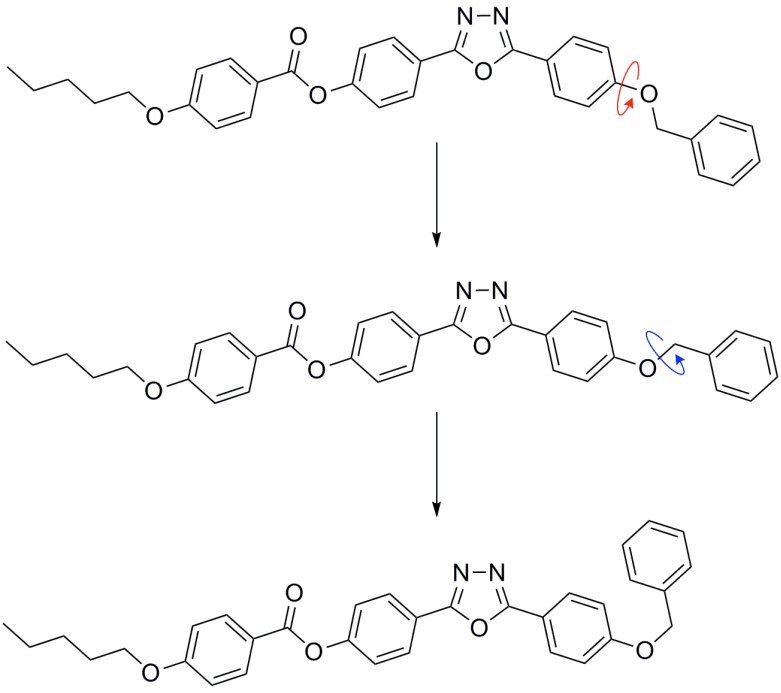

Figure 4.12. Schematic representation of the rotation about the benzyloxy ether bonds, demonstrating a more calamitic structure.

4.6 Concluding Remarks

We have successfully synthesized a homologous series of unsymmetric ODBP bent-core liquid crystals. Thermal analyses indicate that all compounds with singular alkyl termini ranging from butyloxy to dodecyloxy chains exhibit nematic phase behavior on average between 115 and 170 °C; the nematic window decreases with increasing carbons. As expected, the longer alkyl chain promoted stabilization of multiple smectic phase behaviors, which were meticulously characterized by optical microscopy and wide-angle X-ray diffraction. The lower lying, short-lived SmecticX phase of ODBP-OC_{12}Bn exhibited switching-like behavior – evident in other bent-core liquid crystal systems. We chose ODBP-OC_5Bn to explore its potential as a biaxial nematic liquid crystal because of its low nematic onset temperature and wide nematic range. By ^{2}H-NMR analysis we concluded that the opposing benzyloxy ether terminus governs the behavior of the nematic phase to procure a uniaxial nematic. This series is another example demonstrating the sensitivity of mesogenic phases by innocuous modifications to the molecular structure.

4.7 Experimental Section

General. Tetrahydrofuran (THF) and toluene were dried over and distilled from sodium/benzophenone prior to use. Pyridine was dried over and distilled from calcium hydride. Dichloromethane (CH_2Cl_2) was dried through molecular sieves. All other solvents and reagents were purchased from Aldrich and used without further purification. All of the reactions were carried out under argon with the use of standard inert-atmosphere Schlenk techniques. NMR spectra were recorded on a Bruker NMR 400 DRX spectrometer. ^{1}H-NMR were recorded at 400 MHz and referenced to the proton resonance resulting from the

incomplete deuteration of chloroform (δ 7.26) and dimethylsulfoxide (δ 2.50). Transition temperatures were determined by using a PerkinElmer Sapphire differential scanning calorimeter (DSC), calibrated with indium (99.99%) (m.p., 156.5 °C, ΔH = 28.315 J/g) and tin (99.99%) (m.p., 232.0 °C, ΔH = 54.824 J/g). The second heating (10 ^{o}C min^{-1}) as well as the cooling scans (10 °C min^{-1}) were recorded. In order to prevent the LCs from subliming out of the sample pans we used high-pressure DSC sample capsules (Seiko, AL 15). Mesophases were identified with a Nikon Microphot-FX polarizing microscope with orthoscopic and conoscopic equipment and a linkam hotstage. All products were analyzed at the Delft ChemTech mass spectroscopy facility with a VG 70 SE mass spectrometer. The accelerating voltage was 70 keV and M+ represents the molecular ion.

X-ray Analysis. ODBP-OC$_{12}$Bn was investigated using temperature dependent small-angle X-ray diffraction. A 1.0 mm quartz capillary was charged with the LC sample, sealed and placed in a graphite furnace. The sample was heated to the isotropic phase and slowly cooled. A permanent magnet of ~4 T was used to align the liquid crystal phase and the sample was kept in this field throughout the duration of the experiment.

^{2}H-NMR of ODBP-OC$_5$Bn.

Sample Preparation. A sample containing ODBP-OC$_5$Bn was prepared for ^{2}H-NMR by packing the LC material as a solid into a glass bulb. The glass bulb contains up to about 25 mg of sample and typically 1-2 wt% of the solute probe molecule HMB. To remove all oxygen and ensure the sample is completely contained within the bulb, the sample was slowly heated under vacuum and then subsequently sealed by flame torch under liquid nitrogen.

NMR Setup. A Bruker ^{2}H static solids probe (72 mm OD) was modified, according to an already reported schematic,[11] to include a rotation stage enclose in a fumed silica high temperature oven. A typical variable temperature static spectrum was obtained by first heating the sample, while in the probe, into the isotropic and then slowly cooled by one or two degree increments as the sample passes through the T_{NI}. A rotation spectrum was obtained by heating the sample into the lower temperature regime of the nematic phase. The act of spinning at this high temperature can induce a ± 2 °C uncertainty. After about 10k pulse-acquire scans, we obtained a 2D powder pattern that we fit using MATHEMATICA 6.0 according the previously discussed functions with varying values of η, and then minimized with a non-linear least-squares fit.

Synthesis of ODBP-OC$_n$Bn Series.

*Synthesis of 4-(benzyloxy)benzoyl chloride (**4.2**)*. 4-benzyloxybenzoic acid (1) (2.4 g, 10.5 mmol) was dissolved in anhydrous CH_2Cl_2 (30 mL) and anhydrous DMF (3 drops) at 0 °C to which 2 N oxalyl chloride in dichloroethane (10.5 mL, 20.9 mmol) was added dropwise over 25 min. The reaction mixture was stirred at room temperature under Ar atmosphere for 5 hours. Solvent and excess reagents were removed under reduced pressure and product used without further purification and characterization for next step.

*Synthesis of 4-(benzyloxy)-N'-(4-hydroxybenzoyl)benzohydrazide (**4.3**)*. 4-(benzyloxy)-benzoyl chloride (**4.1**) from the above reaction and 4-hydroxybenzohydrazide were treated with $NaHCO_3$ (0.98 g, 10.5 mmol) in a mixture of dry THF (20 mL) and distilled H_2O (25 mL) for 4 hours at room temperature. White precipitate formed, was filtered, rinsed thoroughly with H_2O and dried to give final product **4.3** (3.7 g, 97% overall yield). ^{1}H NMR

(DMSO): δ10.24 (s, 1H), 10.16 (s, 1H), 10.10 (s, 1H), 7.88 (d, 2H), 7.78 (d, 2H), 7.48 – 7.33 (m, 5H), 7.12 (d, 2H), 6.83 (d, 2H), 5.18 (s, 2H).

*Synthesis of 4-(5-(4-(benzyloxy)phenyl)-1,3,4-oxadiazol-2-yl)phenol, ODBP-OHBn (**4.4**).* A mixture of 4-(benzyloxy)-N'-(4-hydroxybenzoyl)benzohydrazide (3.7g, 10.1 mmol), thionyl chloride (7.3 mL), pyridine (0.2 mL), and toluene (5 mL) was refluxed under Ar atmosphere for 8 hours. Reaction mixture was cooled to room temperature, quenched over ice, and stirred for about one hour. The resulting colorless precipitate was filtered, rinsed with H_2O, and dried. Final product **4.4** was recrystallized from ethanol (2.5 g, 73% yield). ^{1}H NMR (DMSO): δ10.31 (s, 1H), 8.03 (d, 2H), 7.93 (d, 2H), 7.49 – 7.34 (m, 5H), 7.23 (d, 2H), 6.96 (d, 2H), 5.22 (s, 2H).

*Synthesis of 4-(5-(4-(benzyloxy)phenyl)-1,3,4-oxadiazol-2-yl)phenyl-4-(propyloxy)-benzoate, ODBP-OC$_4$Bn (**4.5a**).* Compounds **4.5a-g** were all synthesized in the same manner as ODBP-OC$_4$Bn. 4-propyloxybenzoic acid (0.14 g, 0.73 mmol) and ODBP-OHBn 4 (0.25 g, 0.73 mmol) were treated with 1-(3-(dimethylamino)propyl)-3-ethylcarbodiimide hydrochloride (EDC) (0.14 g, 1 equiv.) and 4-(dimethylamino)pyridine (DMAP) (0.020 g, 20 mol%) in CH_2Cl_2 (50 mL) and were allowed to stir under Ar atmosphere at room temperature for 4 days. Solvent was removed under reduced pressure and recrystallized with CH_2Cl_2/MeOH to afford the final colorless product **4.5a** (0.33 g, 88%). ^{1}H NMR ($CDCl_3$): δ8.17 (d, 2H), 8.14 (d, 2H), 8.07 (d, 2H), 7.46 – 7.34 (m, 7H), 7.10 (d, 2H), 6.97 (d, 2H), 5.14 (s, 2H), 4.05 (t, 2H), 1.80 (pentet, 2H), 1.50 (sextet, 2H), 0.98 (t, 3H).

*Synthesis of 4-(5-(4-(benzyloxy)phenyl)-1,3,4-oxadiazol-2-yl)phenyl-4-(pentyloxy)-benzoate, ODBP-OC$_5$Bn (**4.5b**).* Reaction of **4.4** (0.50 g, 1.5 mmol) with 4-pentyloxybenzoic acid (0.30 mg, 1.5 mmol) gave **4.5b** (0.56 mg, 72%). ^{1}H NMR ($CDCl_3$): δ8.17 (d, 2H), 8.14

(d, 2H), 8.07 (d, 2H), 7.45 – 7.34 (m, 7H), 7.10 (d, 2H), 6.97 (d, 2H), 5.14 (s, 2H), 4.04 (t, 2H), 1.81 (pentet, 2H), 1.53 – 1.39 (m, 2H), 1.35 – 1.25 (m, 2H), 0.93 (t, 3H).

*Synthesis of 4-(5-(4-(benzyloxy)phenyl)-1,3,4-oxadiazol-2-yl)phenyl-4-(hexyloxy)-benzoate, ODBP-OC$_6$Bn (**4.5c**).* Reaction of **4.4** (0.25 g, 0.73 mmol) with 4-hexyloxybenzoic acid (0.16 mg, 0.73 mmol) gave **4.5c** (0.35 mg, 87%). ^{1}H NMR ($CDCl_3$): δ8.17 (d, 2H), 8.14 (d, 2H), 8.07 (d, 2H), 7.45 – 7.34 (m, 7H), 7.10 (d, 2H), 6.97 (d, 2H), 5.14 (s, 2H), 4.04 (t, 2H), 1.81 (pentet, 2H), 1.53 – 1.42 (m, 2H), 1.37 – 1.32 (m, 4H), 0.90 (t, 3H).

*Synthesis of 4-(5-(4-(benzyloxy)phenyl)-1,3,4-oxadiazol-2-yl)phenyl-4-(heptyloxy)-benzoate, ODBP-OC$_7$Bn (**4.5d**).* Reaction of **4.4** (0.25 g, 0.73 mmol) with 4-heptyloxybenzoic acid (0.16 mg, 0.73 mmol) gave **4.5d** (0.35 mg, 86%). ^{1}H NMR ($CDCl_3$): δ8.17 (d, 2H), 8.14 (d, 2H), 8.07 (d, 2H), 7.46 – 7.33 (m, 7H), 7.10 (d, 2H), 6.97 (d, 2H), 5.14 (s, 2H), 4.04 (t, 2H), 1.81 (pentet, 2H), 1.49 – 1.41 (m, 2H), 1.40 – 1.28 (m, 6H), 0.89 (t, 3H).

*Synthesis of 4-(5-(4-(benzyloxy)phenyl)-1,3,4-oxadiazol-2-yl)phenyl-4-(octyloxy)-benzoate, ODBP-OC$_8$Bn (**4.5e**).* Reaction of **4.4** (0.25 g, 0.73 mmol) with 4-octyloxybenzoic acid (0.16 mg, 0.73 mmol) gave **4.5e** (0.36 mg, 86%). ^{1}H NMR ($CDCl_3$): δ8.17 (d, 2H), 8.14 (d, 2H), 8.07 (d, 2H), 7.46 – 7.34 (m, 7H), 7.10 (d, 2H), 6.97 (d, 2H), 5.14 (s, 2H), 4.04 (t, 2H), 1.81 (pentet, 2H), 1.48 – 1.42 (m, 2H), 1.41 – 1.23 (m, 8H), 0.88 (t, 3H).

*Synthesis of 4-(5-(4-(benzyloxy)phenyl)-1,3,4-oxadiazol-2-yl)phenyl-4-(nonyloxy)-benzoate, ODBP-OC$_9$Bn (**4.5f**).* Reaction of **4.4** (0.25 g, 0.73 mmol) with 4-nonyloxybenzoic acid (0.16 mg, 0.73 mmol) gave **4.5f** (0.37 mg, 86%). ^{1}H NMR ($CDCl_3$): δ8.17 (d, 2H), 8.11

(d, 2H), 8.07 (d, 2H), 7.45 – 7.34 (m, 7H), 7.10 (d, 2H), 6.97 (d, 2H), 5.14 (s, 2H), 4.04 (t, 2H), 1.81 (pentet, 2H), 1.50 – 1.42 (m, 2H), 1.39 – 1.23 (m, 10H), 0.87 (t, 3H).

*Synthesis of 4-(5-(4-(benzyloxy)phenyl)-1,3,4-oxadiazol-2-yl)phenyl-4-(dodecyloxy)-benzoate, ODBP-OC_{12}Bn (**4.5g**).* Reaction of **4.4** (0.25 g, 0.73 mmol) with 4-dodecyloxybenzoic acid (0.16 mg, 0.73 mmol) gave **4.5g** (0.41 mg, 89%). ^{1}H NMR ($CDCl_3$): δ8.17 (d, 2H), 8.14 (d, 2H), 8.07 (d, 2H), 7.45 – 7.34 (m, 7H), 7.10 (d, 2H), 6.97 (d, 2H), 5.14 (s, 2H), 4.04 (t, 2H), 1.81 (pentet, 2H), 1.50 – 1.42 (m, 2H), 1.40 – 1.21 (m, 16H), 0.90 (t, 3H).

4.8 References

1. Niori, T.; Sekine, T.; Watanabe, J.; Furukawa, T.; Takezoe, H., Distinct ferroelectric smectic liquid crystals consisting of banana shaped achiral molecules. *J. Mater. Chem.* **1996,** 6, 1231-1233.

2. Gerhard Pelzl, S. D. W. W., Banana-Shaped Compounds†-†A New Field of Liquid Crystals. *Advanced Materials* **1999,** 11, (9), 707-724.

3. Schroder, M. W.; Diele, S.; Pelzl, G.; Dunemann, U.; Kresse, H.; Weissflog, W., Different nematic phases and a switchable SmCP phase formed by homologues of a new class of asymmetric bent-core mesogens. *Journal of Materials Chemistry* **2003,** 13, (8), 1877-1882.

4. Lagerwall, S. T., *Ferroelectric and antiferroelectric liquid crystals*. WILEY-VCH: Weinheim; New York, 1999.

5. Dingemans, T. J.; Samulski, E. T., Non-linear boomerang-shaped liquid crystals derived from 2,5-bis(p-hydroxyphenyl)-1,3,4-oxadiazole. *Liquid Crystals* **2000,** 27, (1), 131 - 136.

6. Madsen, L. A.; Dingemans, T. J.; Nakata, M.; Samulski, E. T., Thermotropic Biaxial Nematic Liquid Crystals. *Physical Review Letters* **2004,** 92, (14), 145505.

7. Dingemans, T. J.; Madsen, L. A.; Zafiropoulos, N. A.; Lin, W.; Samulski, E. T., Uniaxial and biaxial nematic liquid crystals. *Philosophical Transactions of the Royal Society A: Mathematical, Physical and Engineering Sciences* **2006,** 364, (1847), 2681-2696.

8. Kang, S.; Saito, Y.; Watanabe, N.; Tokita, M.; Takanishi, Y.; Takezoe, H.; Watanabe, J., Low-Birefringent, Chiral Banana Phase below Calamitic Nematic and/or Smectic C Phases in Oxadiazole Derivatives. *Journal of Physical Chemistry B* **2006,** 110, (11), 5205-5214.

9. Paraskos, A. J.; Swager, T. M., Effects of Desymmetrization on Thiophene-Based Bent-Rod Mesogens. *Chemistry of Materials* **2002,** 14, (11), 4543-4549.

10. Gortz, V.; Goodby, J. W., Enantioselective segregation in achiral nematic liquid crystals. *Chemical Communications* **2005**, (26), 3262-3264.

11. Madsen, L. A.; Samulski, E. T., Addressing non-idealities in NMR experiments on rotating liquid crystals. *Liquid Crystals* **2005,** 32, (11), 1419 - 1425.

CHAPTER 5

Mesoscopic Behaviors of Nanoscale Metal-Organic Frameworks

5.1 Fundamentals of Particle Dispersions

The organization of inorganic nanocrystals presents a new and challenging area in the field of nanotechnology. Nanoparticles are a newly explored and researched material that possesses chemical and physical properties not like their bulk counterparts. When extended over two- and three-dimensional (2D and 3D) superlattices, this ordered array may find applications in electronics, semiconductors, optics, catalysis and magnetism. Inorganic nanocrystals have been shown to self-assemble into compact hexagonal networks, rings, lines, stripes, columns, and in large "supra" crystals (crystalline lattice comprised of nanoparticle unit components). The potential applications that arise from the structure-organization-function relationship of nanocrystals make these new materials very intriguing and deserving of a considerable amount of attention.

Interparticle interactions need to be addressed when attempting to self-assemble them into a 2D or 3D lattice structure. The most pervasive interaction is the van der Waals force, which at the nanometer scale cause these uncharged particles to aggregate.[1] In order to stabilize and prevent aggregation of particles, it is necessary to balance the repulsive and attractive forces. The interparticle electrostatics can be balanced by charge-balancing the surface, essentially creating a charge-neutral, high electric potential double layer where

Coulombic repulsions would prevent aggregation. To stabilize particles they are commonly surface functionalized with long alkyl chains to keep the particles farther away from the distance in which the attractive forces are dominant. The stability of a colloidal suspension is governed by the total interparticle potential energy U_{total}:

$$U_{total} = U_{vdW} + U_{dd} + U_{elec} + U_{steric}$$

where U_{vdW}, U_{dd}, U_{elec}, and U_{steric} are the attractive potential energy due to long-range van der Waals interactions, the attractive potential energy due to long-range dipolar interactions between magnetic particles, the repulsive potential energy resulting from electrostatic interactions between like-charged particle surfaces, and the repulsive potential energy resulting from steric interactions between particles, respectively.[1]

There are several forces leading to an efficient and well-ordered array of nanoparticles: solvation forces, substrate effect and capillary forces. Firstly, the use of appropriate solvents is required for high particle stabilization, i.e. the particles must have high solvent dispersibility. Long-range order can be obtained by judiciously choosing a substrate that will contribute to a low overall interparticle potential energy U_{total}. The particle-substrate interaction, which takes into account the nature of the nanoparticle, the solvent and the substrate, can be expressed in terms of the U_{vdW} as

$$U_{vdW} = -\frac{A_{p-o-s}}{6}\left\{\frac{d}{\left(2r_{ij}-d\right)} + \frac{d}{\left(2r_{ij}+d\right)} + \ln\left(\frac{\left(2r_{ij}-d\right)}{\left(2r_{ij}+d\right)}\right)\right\}$$

where r_{ij} is the distance from the particle (i) center to the wall (j). When this separation distance ($r_{ij} = d/2 + l$) is minimized, the interaction energy becomes:

$$U_{vdW} = -\frac{A_{p-o-s}}{12}\left(\frac{d}{l}\right)$$

Capillary forces are a driving interaction that can bring together particles as the solvent evaporates. This sort of interaction depends on the contact angle (ϕ) of the solvent meniscus (surface tension γ) between two neighboring particles with diameter d and is defined as

$$F = 2\pi(d\gamma)\cos\phi$$

As F increases, the forces driving two particles together are greater than those involving particle-particle and particle-substrate interactions. Overall, these forces can drive the organization of nanoparticles.[1]

Other methods, external forces and constraints, have been explored to induce nanoparticle organization. These methods include application of electric and magnetic fields, which takes advantage of the particles dipolar forces, and fluid flow alignment. However, these methods were not used in this work and therefore will not be discussed.

5.2 Onsager Model of Anisotropic Nanoparticles

In Chapter 3 we extensively discussed the behavior of thermotropic liquid crystals at the molecular level where typical liquid crystals are pure organic compounds having shape anisotropy that leads to intermediate phase behaviors. In 1925, Zocher,[2] a German physicist, discovered that an aqueous suspension of vanadium pentoxide (V_2O_5) ribbons exhibited mesophase-like behavior. His observations fell in line with what was being reported for thermotropic organic liquid crystals and inferred from their results that the V_2O_5 colloids must be constituted from high aspect ratio objects mutually oriented in the same direction.[3] Later, it was found that this aqueous dispersion was in fact forming a nematic phase, having orientational order but lacking translational order in a fluid phases and exhibiting nematic-like texture when observed between crossed polarizers. Mineral liquid crystals were later

coined to describe colloidal suspensions. Because of the inherent similarities between molecular LCs and colloidal suspensions, techniques such as alignment under electric and magnetic fields and shear flow are used to manipulate these dispersions. Their bulk organization can then be observed by such physical methods as small angle X-ray scattering (SAXS). At low angles, this technique is less sensitive to the detailed atomic structure than the particle shape and its organization on length scales ranging from 3 to 300 nm.[3] Electron microscopies such as SEM and TEM are very useful technique in characterizing dimensions and organization of particles.

The idea of forming mesophases from a dispersion of anisotropic objects was theoretically explored by Lars Onsager, a physical chemist, in the mid 1900s. In 1949, he published a statistical model aimed at understanding the nematic order of a suspension of rodlike tobacco mosaic virus (TMV).[4] In his model he illustrates a competition between two types of entropies: the orientational entropy of the rods and the packing entropy related to the excluded volume interactions. The fact that certain dispersions can form nematic phases is due to a loss in orientational entropy and a gain in packing entropy. According to Onsager, the model system for rodlike particles abides by the following:

- High aspect ratio: for a particle with length L and diameter D, $L >> D$.
- Excluded volume interactions that are independent of temperature.
- Isotropic to nematic phase transition is first-order in coexistence, i.e. a biphasic state can exist between volume fractions ϕ_n and ϕ_i where they are defined as

$$\phi_n = 4.2 D/L \quad \text{and} \quad \phi_i = 3.3 D/L$$

- The nematic order parameter at the transition is large ($S \geq 0.8$, defined in Chapter 3).

Essentially, stabilization of a nematic phase from anisotropic rods requires volume fractions inversely proportional to the aspect ratio and equally as important high dispersibility of the particles in solution at a given volume fraction. Onsager's model has also been applied to semiflexible rods as well as disc-like particles where the theory still holds.

Recently, the Alivisatos group reported the synthesis and organization of highly monodisperse CdSe nanorods with length and diameter of 40 and 4.0 nm, respectively.[5] These rods were prepared in a hot surfactant that became incorporated onto the CdSe surface, rendering the particles hydrophobic and highly dispersible in anhydrous cyclohexane. At a volume fraction of about 50% the mixture demonstrated both liquid crystalline and isotropic phases. Indicative of liquid crystallinity are disclinations, which were observed in strengths of both ½ and 1 in the texture upon viewing through crossed polarizers. These defects are commonly observed in the Schlieren texture of the nematic phase.

5.3 Nanoscale Metal-Organic Frameworks

In this work we are exploring the potential for nanoscale metal-organic frameworks (NMOFs) to form liquid crystalline phases and to utilize that physical characteristic to create an ordered array of luminescent nanorods. Metal-organic frameworks – an extended network of metal ions and tailorable organic linkers – are an interesting class of materials which have led to applications in gas storage[6], non-linear optics[7], and catalysis[8]. The Lin group has recently reported a method to synthesize MOFs on the nanoscale by a reverse (water-in-oil) microemulsion synthesis, using lanthanides (Gd, Tb and Eu) as the metal ions and 1,4-benzenedicarboxylate as the organic linker.[9, 10] Details of the synthesis will be discussed later on in this section in addition to how particles of higher aspect were obtained by controlling

the initial conditions of the microemulsion. Nanorods of high aspect ratio were of most value for obtaining liquid crystalline NMOFs (LC-NMOF). We have explored a variety of methods to create an extended array of organized nanocrystals on the large scale:

1) Hydrophobic surface treatment of NMOFs and dispersion in organic solvents.
2) *In situ* synthesis of NMOF within an ordered lyotropic liquid crystal.

The lanthanide/1,4-benzediacarboxylate NMOF crystallizes in a non-cubic spacegroup $P\bar{1}$, where Ln = Eu^{3+} or Tb^{3+}. The Eu- and Tb-based nanorods are luminescent in the red (615 nm) and green (543 nm) regions, respectively. Our objective is to develop an ordered array on a large scale of these luminescent nanocrystals and demonstrate their polarization-dependence luminescence when the incident UV light or luminescence is polarized. The ability to generate and control linearly polarized luminescence is important in many electrooptical devices.

5.4 Background on Surfactant Stabilized Assemblies

In Chapter 3 we eluded to lyotropic liquid crystals (LLC) where amphiphilic molecules with "head" and "tail" moieties can self-assemble into anisotropic shapes. LLCs are concentration dependent phases, typically a mixture of at least two or more components. The amphiphile typically has an ionic or polar head group and a long-chain aliphatic tail that associate with the aqueous and organic components of the mixture, respectively. Various geometries can be accommodated with regard to the surfactant, organic solvent as well as any additional co-surfactants. In this work we have focused on cetyltrimethylammonium bromide (CTAB) cationic surfactant (Figure 5.1), whose phase diagrams for variety of constituents have been extensively measured.

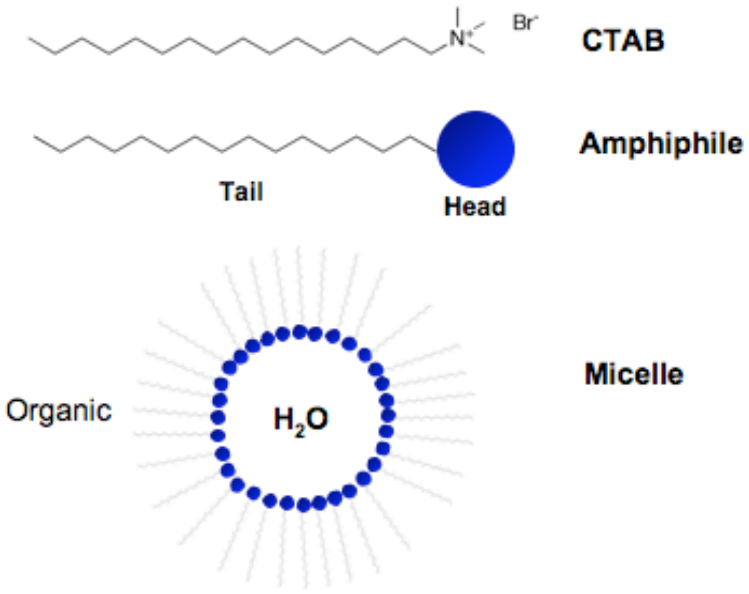

Figure 5.1. Pictorial representation of a CTAB amphiphilic molecule that organizes into a stable micelle under certain surfactant/water/organic ratios.

The ternary phase diagram for CTAB (and co-surfactant *n*-pentanol), water, and hexane gives concentrations necessary to stabilize different geometries of CTAB (Figure 5.2). For instance, CTAB directed assemblies are used to synthesize the MCM-41 and MCM-48 mesoporous silicas that were used in Chapter 2. By controlling the ratio, prior to addition of TEOS, the surfactant can self-assemble into either columnar networks or interconnected channels to afford MCM-41 and MCM-48, respectively. At high concentrations of surfactant, according to the phase diagram, birefringent, or liquid crystalline, phases can form. The most common LC phases for lyotropics are the thermodynamically stable hexagonal and lamellar structures where columns and sheets of water are stabilized by high volume fractions of surfactant, co-surfactant and non-polar solvent.

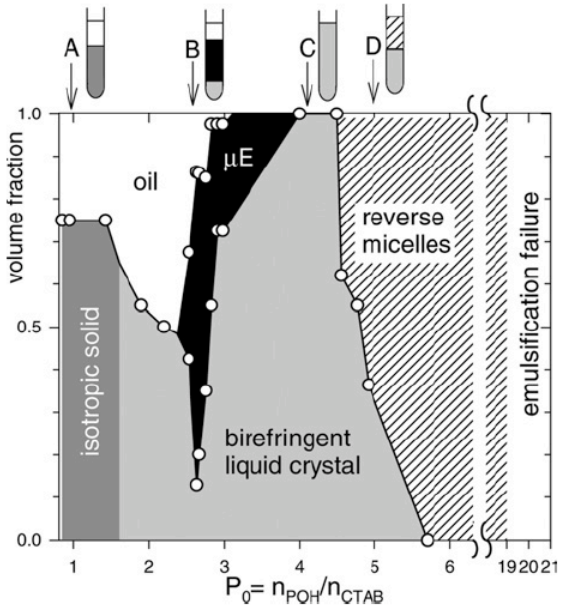

Figure 5.2. Volume fractions of different phases of mixture of CTAB, water and hexane at fixed mole ratios 1:80:47 with *n*-pentanol.[11]

Another very common surfactant organization is the micelle or water-in-oil (w/o) microemulsion. The hydrophobic/hydrophilic nature of surfactant molecules results in an enrichment of these molecules at the interface between aqueous and hydrocarbon solvent. A predominantly hydrocarbon rich mixture will force the hydrophilic heads to seek each other or water droplets in order to minimize surface and interface energies. This segregation is spontaneous and thermodynamically favorable. As the amount of surfactant increases in a hydrocarbon solvent, the surface tension decreases linearly to a point where the surface tension stabilizes. This point is known as the critical micellar concetration (CMC). At the CMC, the surfactant aggregates are spherical in shape and isotropically distributed in solution, but as surfactant concentration increases, the geometry transfers to rod-like shapes. These geometries are important in the synthesis of nanoparticles. Microemulsions are controlled by the concentration of water to surfactant, known as the *w*-value =

[H_2O]/[surfactant]. With increasing *w*-value in a surfactant mixture described above, the micelles tend to form tubular structures.[12] Microemulsions have been used for the synthesis of a variety of nanoparticles, including CdSe and $BaCrO_4$ nanorods.[13-15]

The Lin group has previously demonstrated the synthesis of NMOFs via a reverse microemulsion synthesis to afford high aspect ratio particles.[9, 10] In this work, we have explored the synthesis of NMOFs in other confined geometries, the hexagonal and lamellar phases using the same solution components as the microemulsion. By *in situ* synthesis of NMOFs within this confined and highly ordered space, we expect to achieve simultaneous growth and alignment of these crystalline nanorods.

5.5 Langmuir-Blodgett Technique

Organic films of monolayer thicknesses are of use in components in many practical and commercial applications such as sensors, detectors, displays and electronic circuit components.[16] There are a variety of techniques available to deposit a solid material on any desired substrate: thermal evaporation, sputtering, electrodeposition, molecular beam epitaxy, adsorption from solution, Langmuir-Blodgett (LB) technique and self-assembly. The LB technique provides a very promising method for controlling monolayer thickness, homogeneous depositions over large areas, and delivering multiple layers on a single substrate; all of which can in theory be done on any substrate.

The phenomenological behavior of water with oil was studied by the Babylonians and Greeks centuries ago. But it was not until 1774 when Benjamin Franklin reported to the British Royal Society that oil "though not more than a teaspoonful" would spread and calm Clapman pond.[17] Quantitatively, 2 mL of an oil would spread over an area of half an acre

and the resulting thickness would be no more than 2 nm, a single monolayer. Nearly 100 years later, Lord Rayleigh suspected that an oil film on water would extend to a layer one molecule thick. At the same time in 1891, Agnes Pockles studied the behavior of various oils and developed a method for actually preparing a monolayer. Her work[18] eventually set the stage for further monolayer studies on fatty acids, esters, and alcohols.

In the 1910s and 1920s, Irving Langmuir was the first to perform systematic studies on floating monolayers of fatty acids.[19] He reported in 1920 the ability to transfer a monolayer onto a solid surface. Several years after this report, Katherine Blodgett published a detailed description on a build-up of monolayer assemblies.[20] These assemblies or films are commonly referred to as Langmuir-Blodgett (LB) films.[21] The experimental and theoretical concepts developed by Langmuir and Blodgett underlie today's understanding of monolayers and multilayes at the air-liquid interface as well as their transfer onto a solid surface.[17]

The Langmuir-Blodgett method was the first and simplest technique to provide a means to constructing ordered assemblies at the molecular and mesoscopic levels. A typical LB film is created at the air-water interface. Molecules, particles, or more generally, objects, in a liquid will have a certain attraction for one another. The degree of attraction is known as cohesion.[22] In the bulk each object has equivalent forces acting upon in all directions. However, a small proportion of those objects exist at the surface, where they are exposed to air or any other gas phase. These objects at the surface have net attractive forces towards the bulk, resulting in a minimization of the gas-liquid interfacial area (Figure 5.3).

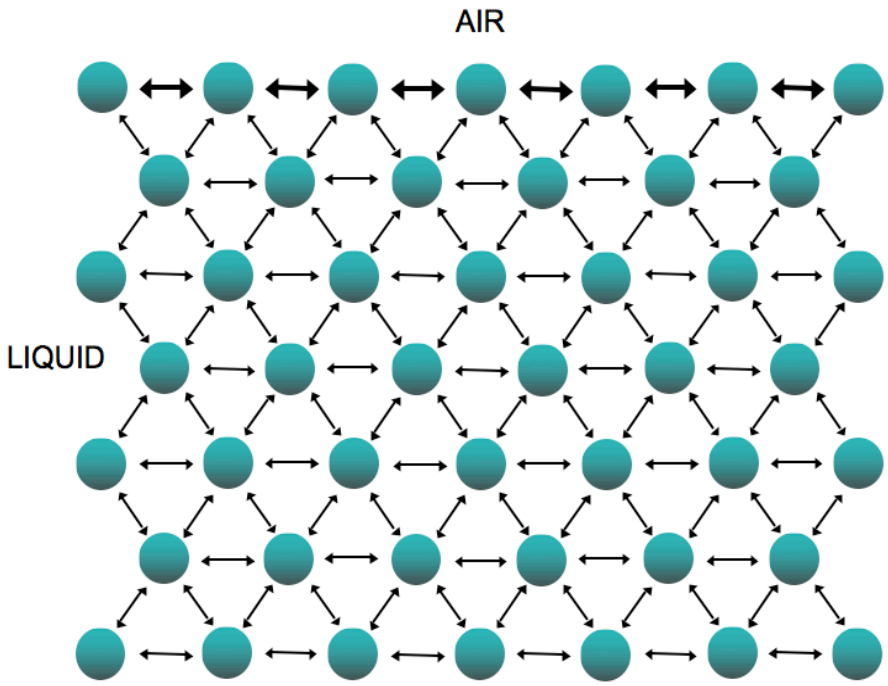

Figure 5.3. Schematic illustration of the net attractive forces incurred on objects in a liquid in the bulk and at the surface.

The net effect of the above scenario is an increase of free energy at the surface, which is usually quantified as energy/area or force/length (surface tension). Surface tension is a measure of the cohesive energy at the surface in terms of dynes/cm or mN/m. For example, water is a polar liquid with strong intermolecular attractions (H-bonding), leading in high surface tension. This explains why water will typically form a meniscus against certain solids. Materials that are capable of floating on the water surface (known as the subphase) will most often lower the overall surface tension. This is the premise for how LB films are formed.

Agnes Pockles was the first to design a trough used in the preparation of LB films, which consisted of a rectangular trough filled with water to a point where the surface tension of the water causes a 0.5 cm high meniscus above the trough. A schematic of the modern trough is

illustrated in Figure 5.4. The trough is usually made with Teflon® to prevent leakage of the subphase over the edge, and the system is equipped with computer-controlled barriers that respond to surface pressures measured by the Wilhelmy plate that suspends from a balance. The substrate used for transferring the LB films is suspended adjacent to the Wilhelmy plate to ensure that the presence of a constant pressure while the transfer is taking place. During a typical transfer, surface pressures will lower as the sample is removed from the monolayer but the set pressure is maintained by simultaneous barrier compression. A dilute sample for deposition is prepared in a highly volatile solvent. When this solution is deposited on the water surface, the mixture will spread and the solvent will evaporate. At this stage the barriers are at their farthest positions – low pressure. The barriers are slowly compressed and decompressed to obtain an isotherm with suitable hysteresis. At lower pressures, a monolayer will have random wholes, known as the "gas" phase, but as the available surface area decreases, transition from gas (G) – liquid expanded (L_1) – liquid condensed (L_2) – solid state (S), the forces will cause the particles to arrange in an ordered fashion as a function of pressure. Compression past the monolayer solid state can cause a rapid decrease in surface pressure, indicating horizontal breakage of the monolayer film and possibly the formation of a multilayer.

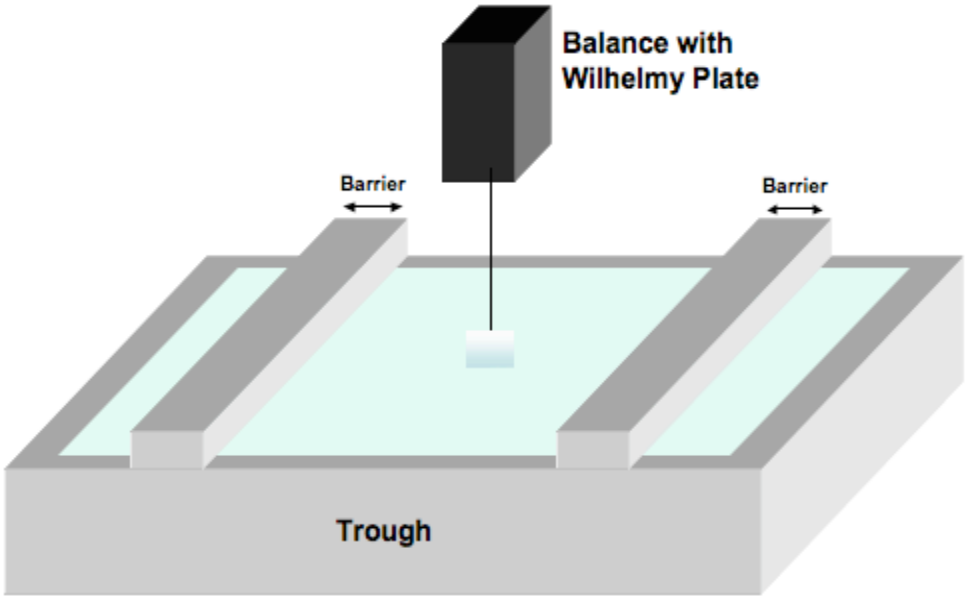

Figure 5.4. Schematic illustration of a Langmuir-Blodgett trough apparatus with Wilhelmy plate electrobalance and computer-controlled barriers.

Many groups have studied the behaviors of a myriad of amphiphilic molecules at the air-water interface. The hydrophobic/hydrophilic interactions of these molecules make them desirable candidates for the study and preparation of LB films. However, little research has been performed on LB films of nanoparticles, particularly high aspect ratio nanorods. The Yang group successfully used the LB technique to assemble one-dimensional nanorods into textures resembling liquid crystals.[23-25] When this sample was compressed to higher surface densities, the particles reoriented and aligned parallel to the trough barrier, forming a closely packed monolayer.

The goal of this project was to render the previously reported and described $Ln(BDC)_{1.5}(H_2O)_2$ nanorods of high aspect ratio hydrophobic through a variety of surface modifications. By dispersing these particles in non-polar solvent and depositing on an LB trough, we plan to compress these particles on the water surface and obtain macroscopic

organization. We wish to explore the polarized luminescence behavior of this large-scale assembly of nanocrystalline materials.

5.6 Shear-Flow Alignment of Anisotropic Particles

It has been shown that high aspect ratio materials when dispersed in a liquid media at high concentrations will reorient in the direction of a shear that is applied to a sample. This concept is known as shear flow. Fluids are typically known to support shear stresses. In a standard shear flow where the fluid is sandwiched between two plates, the lower plate remains stationary as the upper plate moves in a uniform velocity V under the influence of a weight.[28] A fluid comprised of anisotropic materials, like a nematic liquid crystal, will have a director that aligns at an angle θ to the flow direction,

$$\theta = \frac{1}{2}\cos^{-1}\left(\frac{1}{\lambda}\right) \text{ and } \lambda = -(\gamma_2/\gamma_1)$$

where γ_1 and γ_2 are phenomenological volume torque coefficients. Therefore, since $|\lambda|$ is greater than 1 for all nematics,[29] their directors will flow at some small angle to the flow direction. A schematic illustrating the stresses induced during a shear are illustrated in Figure 5.5.

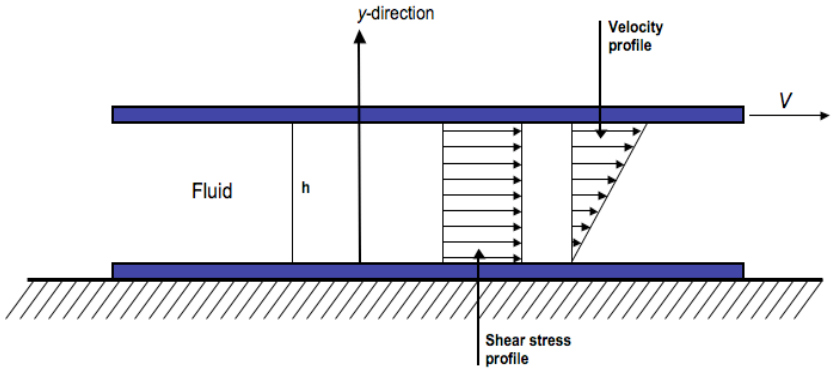

Figure 5.5. Schematic illustration of a fluid under shear flow.

5.7 Synthesis of Hydrophobic NMOFs

We have explored two means for making $Ln(BDC)_{1.5}(H_2O)_2$ nanorods hydrophobic. In order to minimize any electrostatic interactions between particles and reduce aggregation, it was imperative to functionalize the particles with aliphatic alkyl chains of at least 8 carbons. The two methods include 1) a multiple step process where bare particles are first modified

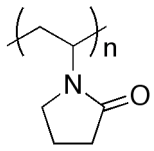

poly(vinyl-pyrrolidone), PVP

with a coating of poly(vinyl-pyrrolidone) (PVP, MW = 40k) and then subsequently treated with TEOS under sol-gel conditions to give a thin silica coating which renders the particles amenable for condensation of various alkyl trialkoxy silanes, and 2) in a one step process the lanthanide metal ions at the surface of the NMOF are terminated with a long-chain fatty acid, such as stearic acid (C_{18}).

5.7.1 Synthesis by Multi-step Surface Modifications

NMOFs of the composition $Ln(BDC)_{1.5}(H_2O)_2$ were synthesized according to previously reported reverse microemulsion syntheses where Ln = Tb^{3+} (100%) with w = 22.5 and where Ln = Gd^{3+} (95%) and Eu^{3+} (5%) with w = 15.0.[9, 10] These particles were synthesized by stirring together two separate optically transparent reverse microemulsions (in a mixture of cationic cetyltrimethylammonium bromide (CTAB)/iso-octane/*n*-hexanol/water) of $LnCl_3$ and bis(methylammonium)benzene-1,4-dicarboxylate in a 2:3 molar ratio for two hours. Bare $Tb(BDC)_{1.5}(H_2O)_2$ and $Gd_{0.95}Eu_{0.05}(BDC)_{1.5}(H_2O)_2$ particles were isolated, after two successive centrifugations and ethanol redispersions, at this stage for characterization by

scanning electron microscopy (Figure 5.6) and TGA. In it is interesting to note that during sample preparation for SEM the un-coated $Gd_{0.95}Eu_{0.05}(BDC)_{1.5}(H_2O)_2$ particles spontaneously formed ethanol evaporation-promoted aggregates (Figure 5.7). These aggregates of nanorods resemble common liquid crystal-like arrangements with high orientation order (nematic phase) as well as positional order (smectic A phase).

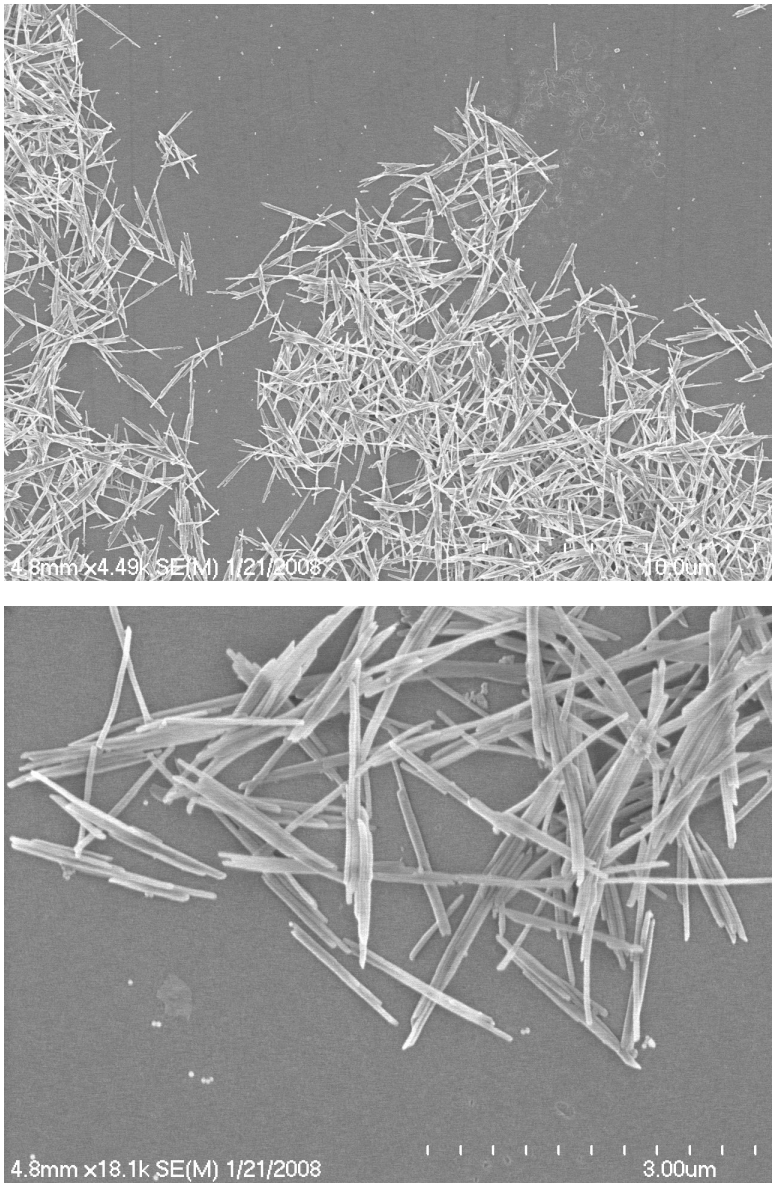

Figure 5.6. SEM images of $Tb(BDC)_{1.5}(H_2O)_2$ nanorods synthesized with $w = 22.5$.

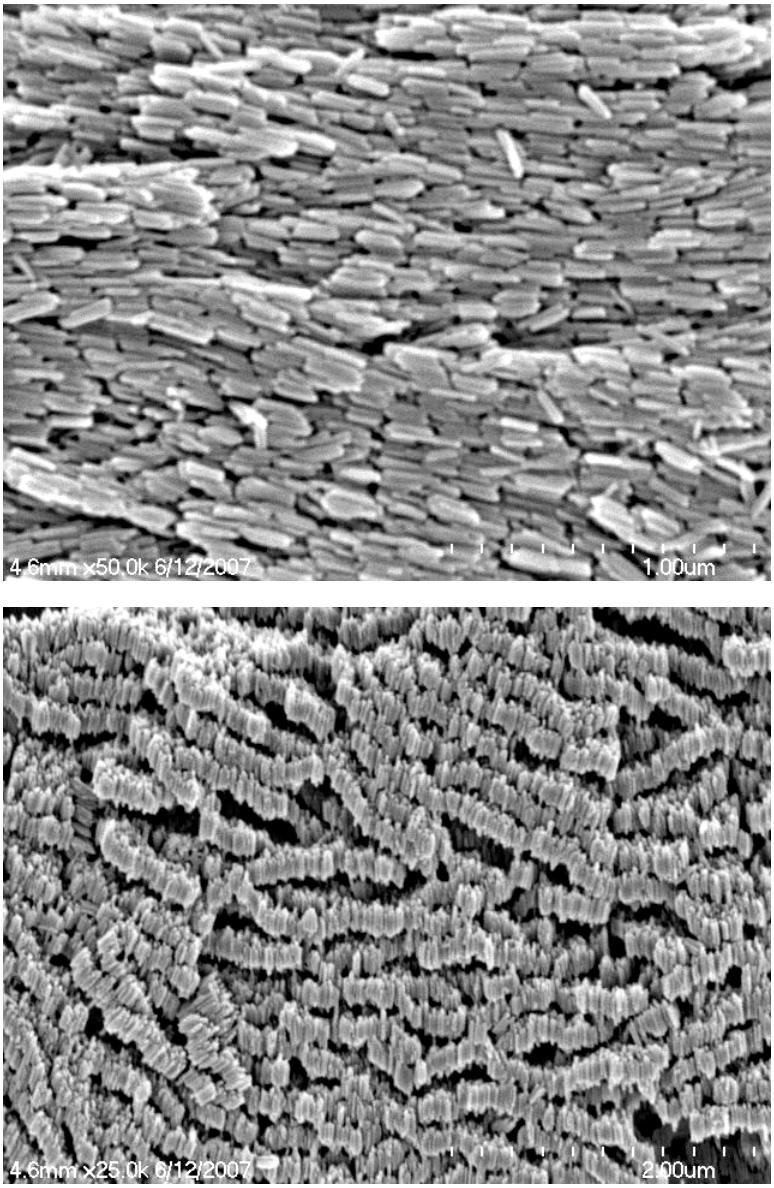

Figure 5.7. SEM images of $Gd_{0.95}Eu_{0.05}(BDC)_{1.5}(H_2O)_2$ nanords with w = 15 organized into nematic (top) and smectic A (bottom) arrangements.

PVP-functionalized particles were prepared by adding an aqueous solution of PVP (0.005 M) to the microemulsion *in situ*. The mixture was allowed to stir for an additional 12 hours after which the particles were isolated by centrifugation. SEM exhibits high dispersibility of these particles upon evaporation from ethanol suspensions (Figure 5.8). The PVP-functionalized $Gd_{0.95}Eu_{0.05}(BDC)_{1.5}(H_2O)_2$ with w = 15 were then subsequently coated with

silica SiO_2 via sol-gel processing. A dilute suspension of the particles in basic ethanol (4 % v/v of NH_3) was prepared. An initial addition of tetraethyl orthosilicate (TEOS) was added to this suspension to displace PVP and prime the particles for further additions of TEOS. To prevent unwanted secondary nucleation of TEOS, the particles were isolated after one hour and exposed again to another round of sol-gel treatment. For $Gd_{0.95}Eu_{0.05}(BDC)_{1.5}(H_2O)_2$ particles a silica shell of about 5-6 nm was obtained and observed by SEM (Figure 5.9).

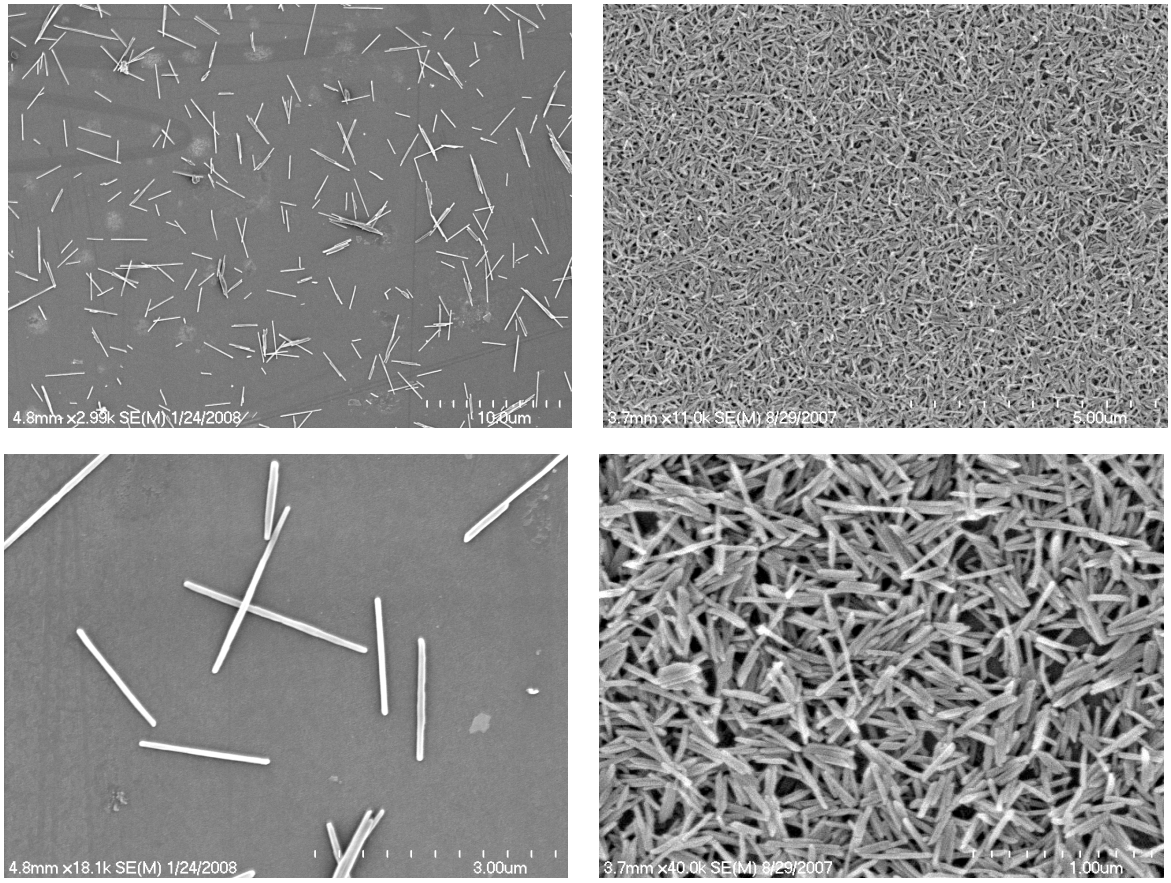

Figure 5.8. SEM images of PVP-coated $Tb(BDC)_{1.5}(H_2O)_2$ nanorods of w = 22.5 (left) and $Gd_{0.95}Eu_{0.05}(BDC)_{1.5}(H_2O)_2$ nanorods of w = 15 (right).

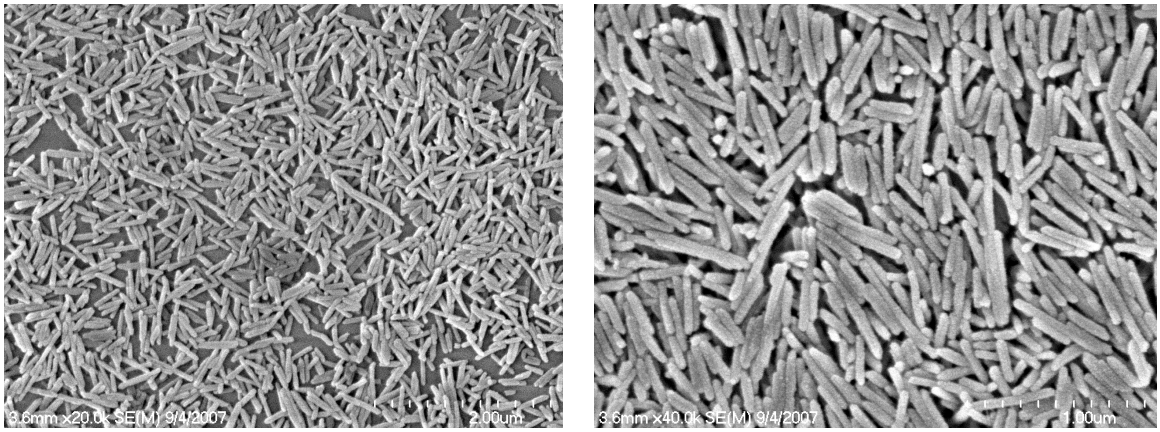

Figure 5.9. SEM images of $Gd_{0.95}Eu_{0.05}(BDC)_{1.5}(H_2O)_2@SiO_2$ nanorods of $w = 15$.

To render the $Gd_{0.95}Eu_{0.05}(BDC)_{1.5}(H_2O)_2@SiO_2$ nanorods hydrophobic and therefore dispersible in organic solvents, triethoxy(octyl)silane was condensed onto the surface by refluxing this silane and the particles in toluene for eight hours (Figure 5.10). These particles were isolated by centrifugation and shown to form stable suspensions in iso-octane and cyclohexane; they were later used in LB and shear flow alignment experiments.

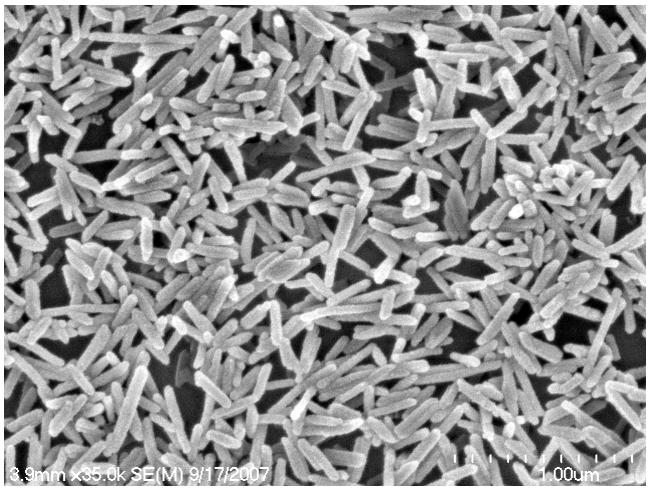

Figure 5.10. SEM images of $Gd_{0.95}Eu_{0.05}(BDC)_{1.5}(H_2O)_2@SiO_2$-$C_8$ nanorods of $w = 15$.

5.7.2 Synthesis by One-step Surface Modification

In this method we took advantage of the crystallization pathway in which these NMOFs form. Crystallization of deprotonated benzene dicarboxylate and Tb^{3+} metal ions is a fast process; in fact, bulk precipitate of these two components generates crystalline $Tb(BDC)_{1.5}(H_2O)_2$ upon mixing. Individual nanoparticles of $Tb(BDC)_{1.5}(H_2O)_2$ have faces terminated with accessible Tb sites, some of which are involved in coordination to the bulk while others have vacant sites for water coordination. By exposing these particles after isolation from the microemulsion to a solution of stearic acid in hexanes, we afford a particles whose Tb sites are now coordinated to the carboxylate end of this 18-carbon chain fatty acid. In this simple one-step treatment, we have made non-polar, organic dispersible NMOFs.

5.7.3 *In Situ* Synthesis of $Tb(BDC)_{1.5}(H_2O)_2$ within a Lyotropic Liquid Crystal.

$Tb(BDC)_{1.5}(H_2O)_2$ NMOFs were prepared within the hydrophilic channels of a hexagonal phase of a lyotropic liquid crystal (LLC) stabilized by similar components used for the reverse microemulsions, CTAB/hexanes/*n*-hexanol/H_2O (6.0 : 66.8 : 3.4 : 23.8). NMOF-containing LLCs were prepared by first preparing two separate lyotropics one containing $TbCl_3$ and the bis(methylammonium)benzene-1,4-dicarboxylate, respectively, in a 2:3 molar ratio. After 30 minutes of independent mixing, the two lyotropics were combined. A precipitate instantaneously formed that was later proven to be crystalline $Tb(BDC)_{1.5}(H_2O)_2$ by powder XRD. The texture of the LLC-NMOF when observed under crossed polarizers was indicative of a hexagonal phase for lyotropics (Figure 5.11).

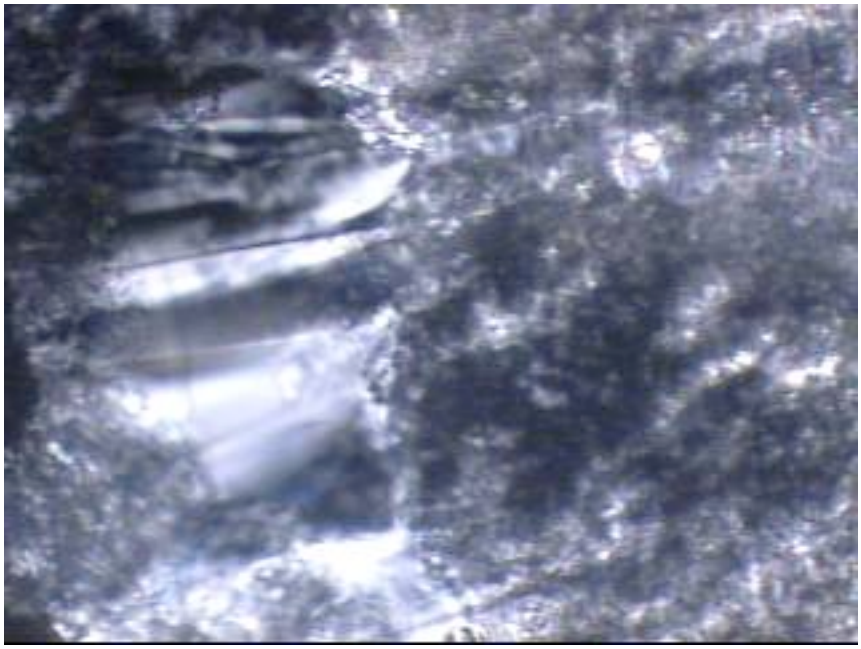

Figure 5.11. Birefringent texture of the hexagonal phase of LLC containing $Tb(BDC)_{1.5}(H_2O)_2$ nanoparticles observed between crossed polars at 10x magnification.

This sample was analyzed by SEM before and after extraction with ethanol. According to Figure 5.12a of the LLC-NMOF, there are clear indications of a columnar network as expected for the hexagonal phase. When the LLC-NMOF was extracted, the resulting particles are still anisotropic in shape, however, they are clearly not discrete, smooth and monodisperse nanorods as those prepared by the well-organized reverse microemulsion technique (Figure 5.12b).

a)

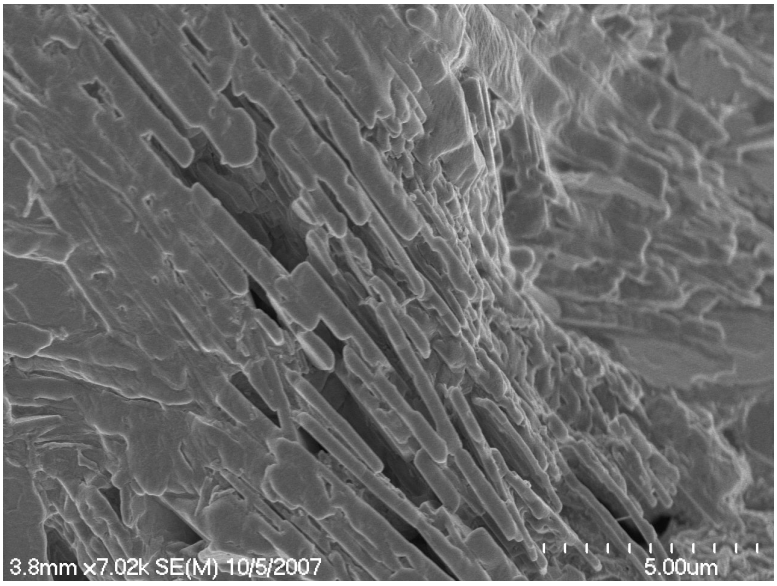

b)

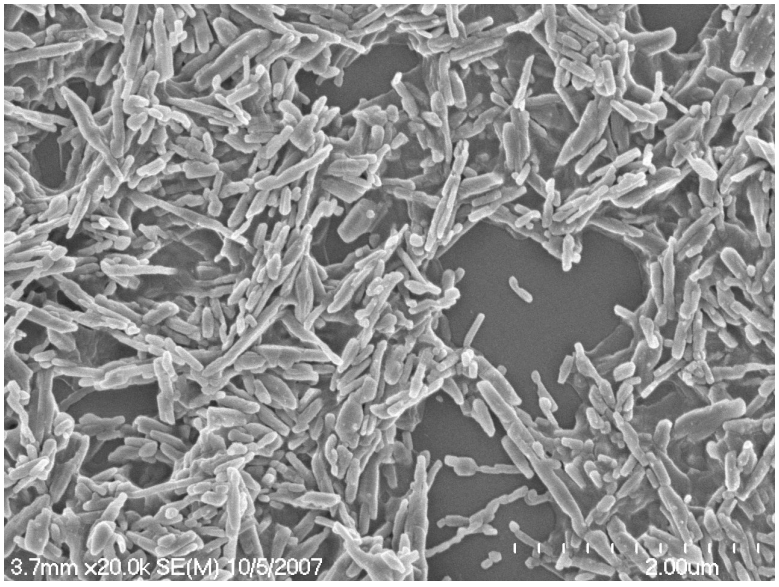

Figure 5.12. SEM images of the a) LLC-NMOF pre-extraction and b) post extraction.

5.8 Organized Arrays of NMOFs

The hydrophobic $Gd_{0.95}Eu_{0.05}(BDC)_{1.5}(H_2O)_2@SiO_2\text{-}C_8$ nanorods were deposited between two untreated glass slides and observed through crossed polarizers. A static birefringent texture was observed due to its high viscosity. At this very high volume fraction, the

particles have enough mobility to show liquid-like behavior. When a sample of $Gd_{0.95}Eu_{0.05}(BDC)_{1.5}(H_2O)_2@SiO_2$-$C_8$ is sheared between two slides, the resulting birefringence becomes directionally dependent. When the direction of the shear is parallel to one of the polarizers, we observe a maximum in transmitted light. As the sample rotates 45°, we approach the darkest state (Figure 5.13). When lower volume fractions are prepared using anhydrous cyclohexane (dry solvents are commonly used to prevent gelling), the viscosity decreases with increasing amount of cyclohexane to the point where the sample becomes isotropic and can no longer be sheared.

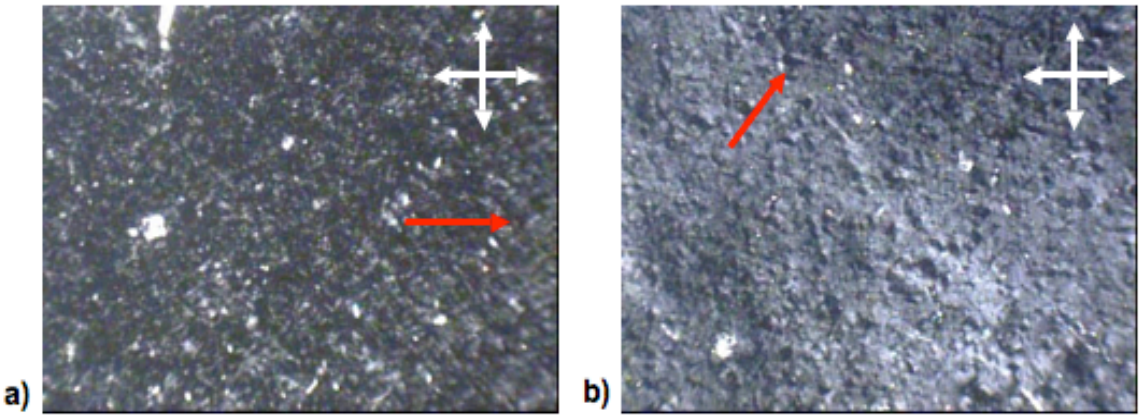

Figure 5.13. Sheared sample of $Gd_{0.95}Eu_{0.05}(BDC)_{1.5}(H_2O)_2@SiO_2$-$C_8$ between crossed polarizers with direction of shear a) parallel and b) 45° to polarizer.

The same nanoparticles were used to fabricate monolayer LB films on quartz substrates for luminescence studies. A nanorod colloidal suspension in iso-octane was spread dropwise (1.5 mL of 1.3 mg/mL concentration) on the water surface of a LB trough. The nanorod surface layer was compressed slowly while the surface pressure was monitored with a Wilhelmy plate. In Figure 5.14 the compressed surface containing $Gd_{0.95}Eu_{0.05}(BDC)_{1.5}$-$(H_2O)_2@SiO_2$-$C_8$ is illuminated with UV light and the red emission from the Eu-based

particles indicates their position at the surface and subsequent transfer to the quartz slide. With this deposition, the surface pressure increased with compression. At different stages of compression, nanorod assemblies were extracted and transferred onto quartz slides for analysis by SEM. At a low surface pressure of 1 mN/m, the nanorods assembled into random aggregates that scattered across the glass slide (Figure 5.15a). At a slightly higher pressure of 10 mN/m, the particles began to form micron sized islands where organization within each is random (Figure 5.15b). The surface coverage of the nanorods increased as the LB film was further compressed. The particles finally formed a continuous monolayer at 50 mN/m (Figures 5.15d). At a closer look, the particles showed signs of orientational order similar to a nematic phase and appear to align parallel to the barriers of the trough (Figure 5.15e). With further compression, nanorods began to stack upon each other in a multi-layer fashion. The buckling effects can attribute to the lack of orientational order during this process (Figure 5.15f).

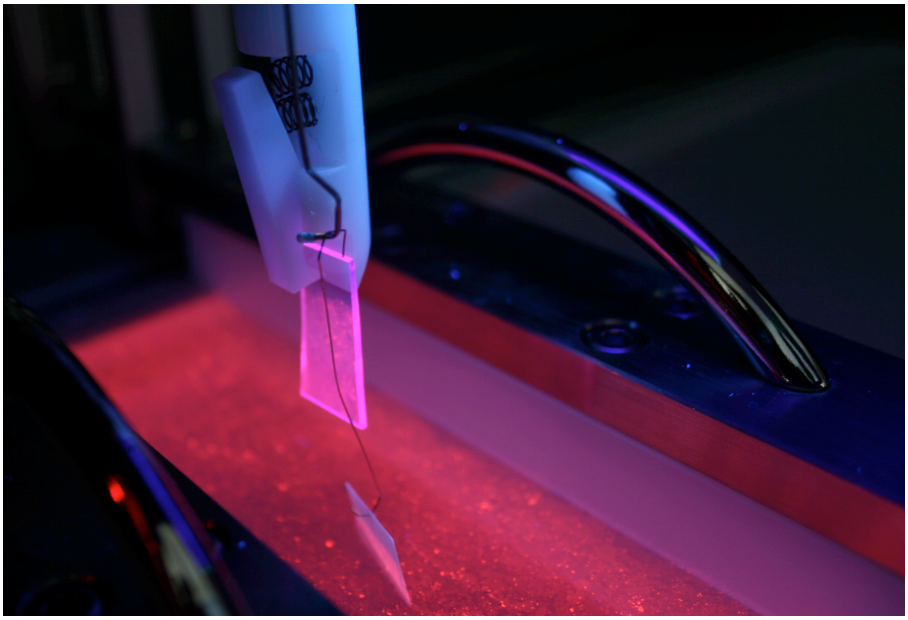

Figure 5.14. Photo of a compressed monolayer film of $Gd_{0.95}Eu_{0.05}(BDC)_{1.5}$-$(H_2O)_2$@$SiO_2$-$C_8$ on a water surface and LB monolayer transferred to the quartz substrate when illuminated red by UV light.

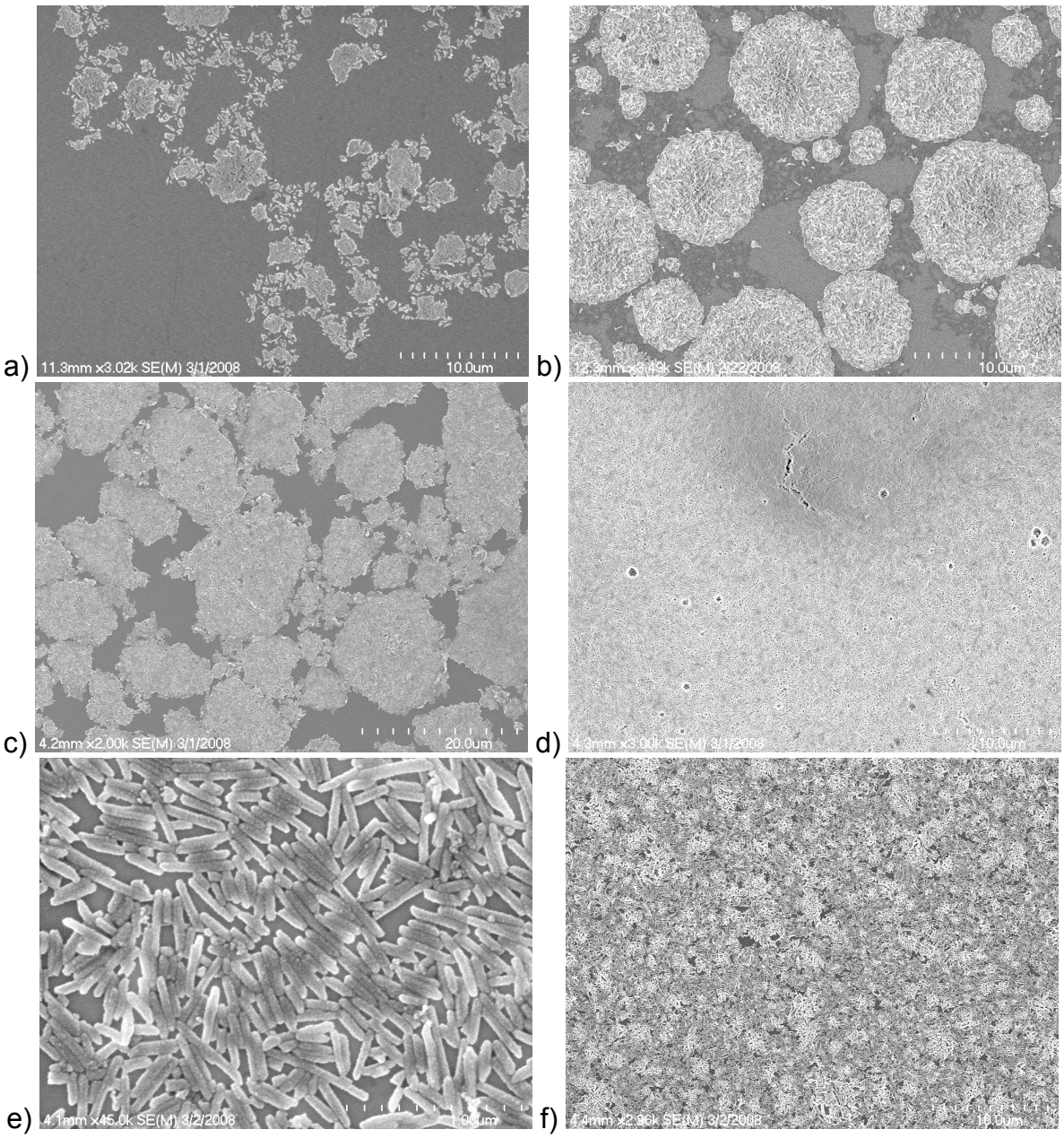

Figure 5.15. SEM images of the nanorod assemblies at the air-water interface at different stages of compression: a) 1 mN/m, b) 10 mN/m, c) 35 mN/m, d) 50 mN/m, e) zoomed in region of (d) and f) 65 mN/m.

We attempted to align the $Tb(BDC)_{1.5}(H_2O)_2$ NMOFs contained within the LLC by shearing the sample between two glass slides. Shearing the sample resulted in alignment along the direction of the shear. When observed under crossed polars equipped with plane

polarized transmitted light as well as an orthogonal un-polarized UV light source, the sample showed a bright state when the shear was parallel with one of the polarizers. When this site was rotated 45°, we observed the darkest state. Throughout the rotation green emission is observed from $Tb(BDC)_{1.5}(H_2O)_2$ (Figure 5.16). From these micrographs in conjunction with SEM images (Figure 5.17) taken of this sample, we can confirm the LLC does in fact contain luminescent $Tb(BDC)_{1.5}(H_2O)_2$ NMOF.

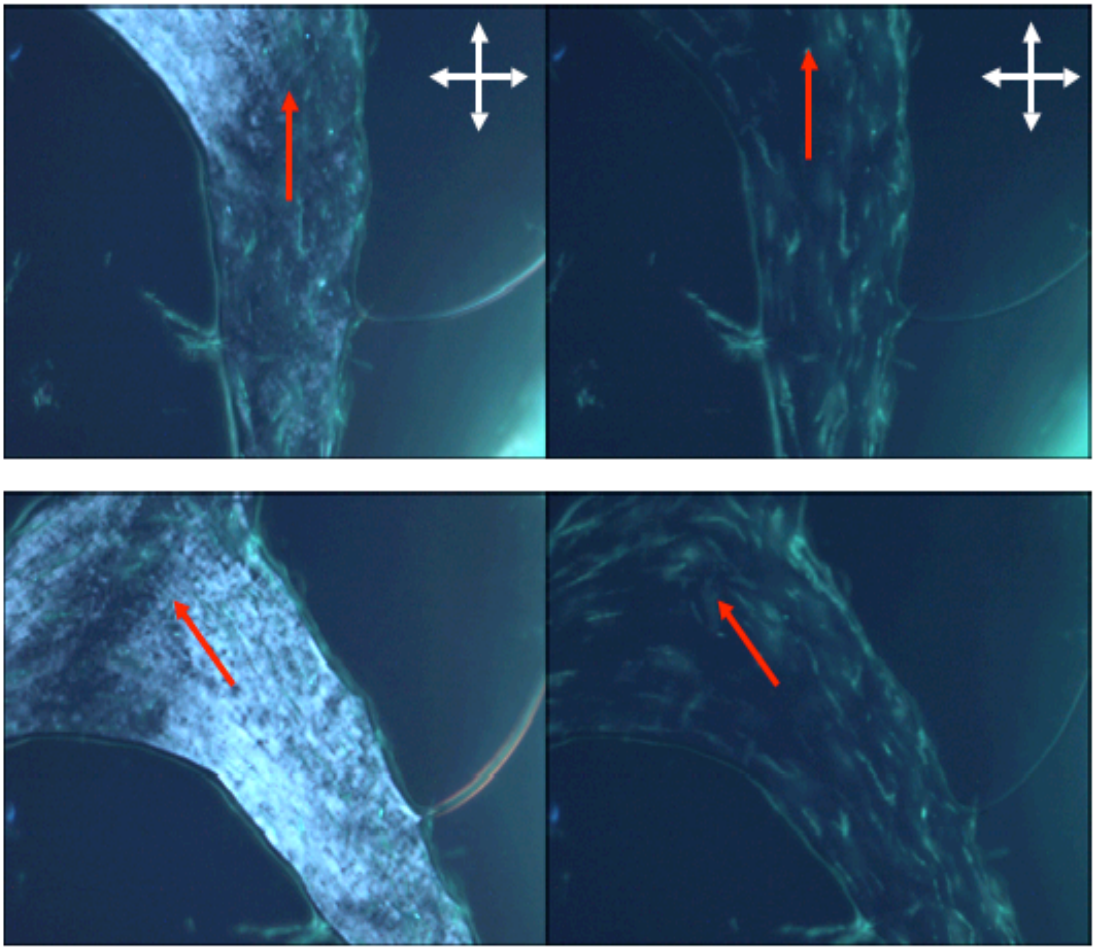

Figure 5.16. Optical micrographs of a sheared (indicated by red arrow) $Tb(BDC)_{1.5}(H_2O)_2$ LLC-NMOF between crossed polarizers with plane polarized light (left images) and with non-polarized UV light (right images). Lower images indicate rotated samples 45° to polarizer.

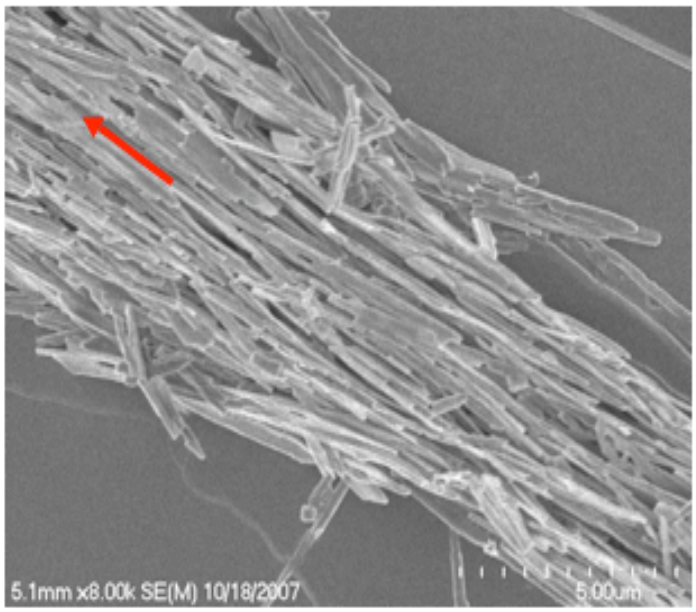

Figure 5.17. SEM image of a sheared LLC-NMOF sample containing $Tb(BDC)_{1.5}(H_2O)_2$ nanoparticles. Particles line along the direction of the shear (red arrow).

In order to test a polarized emission dependence of an ordered array of these particles, we observed a sheared LLC-NMOF sample containing $Tb(BDC)_{1.5}(H_2O)_2$ using unpolarized UV light. The metal-centered excitation from the particles passed through the polarizer in the optical path. The antenna effect of the ligand-metal system in a non-cubic environment will yield a change in the intensity of the observed excitation. The sheared LLC-NMOF exhibited a maximum excitation intensity when the shear was parallel with the polarizer and decreased when rotated away from 0°. We can conclude the anisotropic nature of the $P\bar{1}$ space group of $Tb(BDC)_{1.5}(H_2O)_2$ governs the way light emits from this assembly (Figure 5.18).

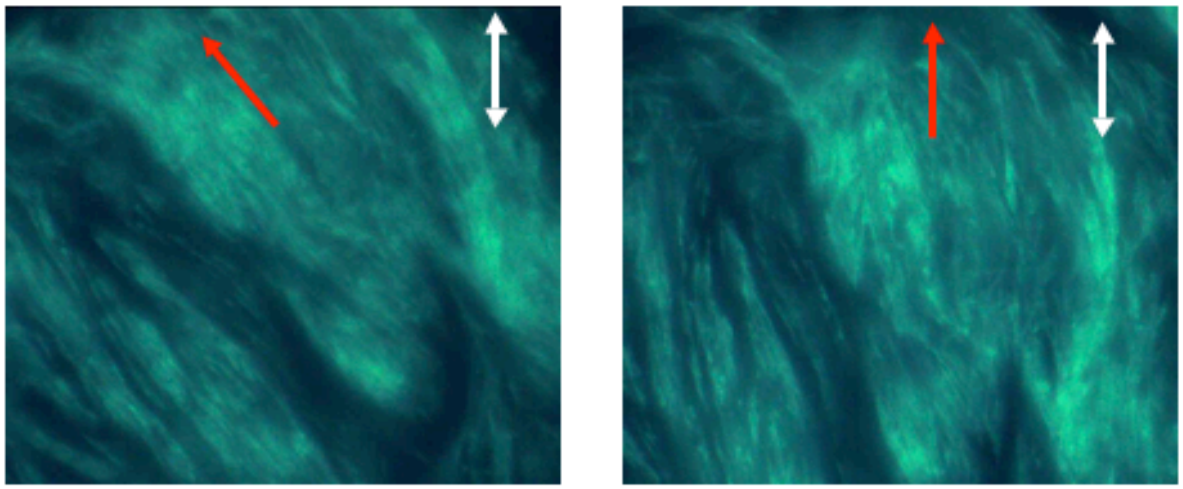

Figure 5.18. Optical micrographs of a sheared sample of an excited $Tb(BDC)_{1.5}(H_2O)_2$ LLC-NMOF with unpolarized UV light, excitation from particles passes through polarizer in the optical path. Maximum excitation intensity is observed when the sample is parallel 0° (right) to polarizer and decreases when sample stage is rotated (45°, left).

5.9 Concluding Remarks

We have explored the organization of high aspect ratio luminescent nanoscale metal-organic frameworks using a variety of techniques, including dispersing in organic solvent and aligning by shear, through compression by forming LB monolayers, and by shearing a NMOF-containing lyotropic liquid crystal. The assemblies were observed by SEM and the photoluminescence images were taken with optical microscopy combined with UV excitation. These particles provide an interesting opportunity to study organized assemblies of nanorods and their polarization-dependent luminescent behaviors.

5.10 Experimental Section

General. Cetyltrimethylammonium bromide (CTAB), $GdCl_3 \bullet 6H_2O$, $EuCl_3 \bullet 6H_2O$, $TbCl_3 \bullet 6H_2O$, terephthalic acid, *n*-hexanol, methylamine (40 wt% in water), poly(vinyl-pyrrolidone) (PVP, MW = 40k), tetraethyl orthosilicate (TEOS), and stearic acid were purchased from Aldrich and used without further purification. Cyclohexane was purchased from Aldrich and distilled over CaH_2. Triethyoxy(octyl)silane was purchased from Gelest. Thermogravimetric analysis (TGA) was performed using a Shimadzu TGA-50 equipped with a platinum pan and heated at a rate of 3 °C min^{-1} under air. A Hitachi 4700 field emission scanning electron microscope (SEM) was used to image particles and their respective assemblies. Prior to SEM imaging, the samples were sputter coated with Au using a Cressington 108 Auto Sputter Coater equipped with Au/Pd (80/20) target and MTM-10 thickness monitor. Mesoscopic behaviors were identified with a Nikon Microphot-FX polarizing microscope with orthoscopic and conoscopic equipment and a Linkam hotstage. Langmuir-Blodgett films were prepared using a KSV 500 trough (standard size, KSV Instruments, Ltd.) and KSV software.

Synthesis of $Ln(BDC)_{1.5}(H_2O)_2@SiO_2$-$C_8$ nanorods.

Synthesis of $Ln(BDC)_{1.5}(H_2O)_2@SiO_2$. The synthesis of $Tb(BDC)_{1.5}(H_2O)_2$ and $Gd_{0.95}Eu_{0.05}(BDC)_{1.5}(H_2O)_2$ bare nanorods of *w*-values equal to 22.5 and 15, respectively, with subsequent silica coating were prepared according to previously reported procedures.[9, 10]

Synthesis of $Gd_{0.95}Eu_{0.05}(BDC)_{1.5}(H_2O)_2@SiO_2$-$C_8$. A 25 mL 1-neck round bottom flask equipped with condenser was charged with $Gd_{0.95}Eu_{0.05}(BDC)_{1.5}(H_2O)_2@SiO_2$ (14.3 mg) and toluene (1.5 mL). Before addition of the silane, this suspension was sonicated for at least 15

minutes. To this suspension was added triethoxy(octyl)silane (2.83 mg, 20 wt% of particles), and the mixture was allowed to reflux for 8 hours. The particles were then centrifuged, rinsed with toluene to remove excess silane and then finally centrifuged and rinsed with ethanol (x2).

Synthesis of $Tb(BDC)_{1.5}(H_2O)_2$/Stearate(C_{18}).

A stock solution of stearic acid in hexanes was prepared (0.05 M). A concentrated dispersion of $Tb(BDC)_{1.5}(H_2O)_2$ particles in water was prepared (0.5 mg in 0.10 mL). To this dispersion was added an aliquot of the stearic acid solution (0.200 mL) and allowed to sonicate for 1 hour. After this time, the particles were shown to have transferred into the organic phase. The hexane layer was removed and centrifuged and rinsed twice with additional hexanes to remove any un-coordinated stearic acid and to afford $Tb(BDC)_{1.5}(H_2O)_2$/Stearate.

***In Situ* Preparation of $Tb(BDC)_{1.5}(H_2O)_2$ in a LLC.**

A stabilized lyotropic liquid crystal containing $Tb(BDC)_{1.5}(H_2O)_2$ within its channel was prepared from two independent LLCs. Two lyotropic LCs were prepared by mixing *n*-hexanol (209.6 μL), hexanes (5.10 mL), CTAB (0.300 g). To each LLC equivalent volumes of $TbCl_3 \bullet 6H_2O$ (1.190 mL of 0.15M) and BDC (1.190 mL of 0.20 M) were added. Each mixture was allowed to stir for 30 min at room temperature. A 1 mL aliquot from each LLC were taken and combined in a separate vial and allowed to stir for at least one hour before the oil component was allowed to separate from the birefringent component. The oil component

was found to not contain any $Tb(BDC)_{1.5}(H_2O)_2$. The birefringent component was used for further studies.

Preparation of $Gd_{0.95}Eu_{0.05}(BDC)_{1.5}(H_2O)_2@SiO_2$-$C_8$ Langmuir-Blodgett Films.

LB films of $Gd_{0.95}Eu_{0.05}(BDC)_{1.5}(H_2O)_2@SiO_2$-$C_8$ were prepared on clean quartz glass slides to be used later for luminescent studies. The LB trough was cleaned with *n*-butyl acetate and subsequently filled with water before calibration. A 1.3 mg/mL dispersion of particles in iso-octane was prepared by sonication for 1 hour. Approximately 1.5 mL of this dispersion was deposited on the water surface, and the solvent was allowed to evaporate for 30 minutes or until the pressure stabilized. The gas phase monolayer was compressed at a rate of 5.0 mm/min. Monolayers were transferred at the following pressures: 1 mN/m, 10 mN/m, 20 mN/m, 35 mN/m, 50 mN/m and 65 mN/m and at a dipping rate of 1.0 mm/min. The samples were allowed at least 3 hours to dry before use.

5.11 References

1. Pileni, M.-P., *Nanocrystals Forming Mesoscopic Structures*. WILEY-VCH: Weinheim, 2005.

2. Zocher, H., *Zeit. Anorg. Allg. Chem.* **1925,** 147.

3. Davidson, P.; Gabriel, J.-C. P., Mineral liquid crystals. *Current Opinion in Colloid & Interface Science* **2005,** 9, (6), 377-383.

4. Onsager, L., *Ann. N. Y. Acad. Sci.* **1949,** 51.

5. Li, L. s.; Walda, J.; Manna, L.; Alivisatos, A. P., Semiconductor Nanorod Liquid Crystals. *Nano Letters* **2002,** 2, (6), 557-560.

6. Matsuda, R.; Kitaura, R.; Kitagawa, S.; Kubota, Y.; Belosludov, R. V.; Kobayashi, T. C.; Sakamoto, H.; Chiba, T.; Takata, M.; Kawazoe, Y.; Mita, Y., Highly controlled acetylene accommodation in a metal-organic microporous material. *Nature* **2005,** 436, (7048), 238-241.

7. Evans, O. R.; Lin, W., Crystal Engineering of NLO Materials Based on Metal-Organic Coordination Networks. *Accounts of Chemical Research* **2002,** 35, (7), 511-522.

8. Wu, C. D.; Hu, A.; Zhang, L.; Lin, W., A Homochiral Porous Metal-Organic Framework for Highly Enantioselective Heterogeneous Asymmetric Catalysis. *Journal of the American Chemical Society* **2005,** 127, (25), 8940-8941.

9. Rieter, W. J.; Taylor, K. M. L.; An, H.; Lin, W.; Lin, W., Nanoscale Metal-Organic Frameworks as Potential Multimodal Contrast Enhancing Agents. *Journal of the American Chemical Society* **2006,** 128, (28), 9024-9025.

10. Rieter, W. J.; Taylor, K. M. L.; Lin, W., Surface Modification and Functionalization of Nanoscale Metal-Organic Frameworks for Controlled Release and Luminescence Sensing. *Journal of the American Chemical Society* **2007,** 129, (32), 9852-9853.

11. Palazzo, G.; Carbone, L.; Colafemmina, G.; Angelico, R.; Ceglie, A.; Giustini, M., The role of the cosurfactant in the CTAB/water/n-pentanol/n-hexane system: Pentanol effect on the phase equilibria and mesophase structure. *Physical Chemistry Chemical Physics* **2004,** 6, (7), 1423-1429.

12. Cao, G., *Nanostructures & Nanomaterials: Synthesis, Properties and Applications*. Imperial College Press: London, 2004.

13. Li, M.; Schnablegger, H.; Mann, S., Coupled synthesis and self-assembly of nanoparticles to give structures with controlled organization. *Nature* **1999,** 402, (6760), 393-395.

14. Peng, X.; Manna, L.; Yang, W.; Wickham, J.; Scher, E.; Kadavanich, A.; Alivisatos, A. P., Shape control of CdSe nanocrystals. *Nature* **2000,** 404, (6773), 59-61.

15. Steigerwald, M. L.; Alivisatos, A. P.; Gibson, J. M.; Harris, T. D.; Kortan, R.; Muller, A. J.; Thayer, A. M.; Duncan, T. M.; Douglass, D. C.; Brus, L. E., Surface derivatization and isolation of semiconductor cluster molecules. *Journal of the American Chemical Society* **1988,** 110, (10), 3046-3050.

16. Talham, D. R., Conducting and Magnetic Langmuir-Blodgett Films. *Chemical Reviews* **2004,** 104, (11), 5479-5502.

17. Tredgold, R. H., *Order in Thin Organic Films*. Cambridge University Press: Cambridge, 1994.

18. Pockles, A., *Nature* **1891,** 43, 437.

19. Langmuir, I., THE CONSTITUTION AND FUNDAMENTAL PROPERTIES OF SOLIDS AND LIQUIDS. II. LIQUIDS. *Journal of the American Chemical Society* **1917,** 39, (9), 1848-1906.

20. Blodgett, K. B., Films Built by Depositing Successive Monomolecular Layers on a Solid Surface. *Journal of the American Chemical Society* **1935,** 57, (6), 1007-1022.

21. Blodgett, K. B.; Langmuir, I., Built-Up Films of Barium Stearate and Their Optical Properties. *Phys. Rev*. **1937,** 51, 964-982.

22. Petty, M. C., *Langmuir-Blodgett Films*. Cambridge University Press: Cambridge, 1996.

23. Kwan, S.; Kim, F.; Akana, J.; Yang, P., Synthesis and assembly of BaWO4 nanorods. *Chemical Communications* **2001**, (5), 447-448.

24. Peidong Yang, F. K., Langmuir-Blodgett Assembly of One-Dimensional Nanostructures. *ChemPhysChem* **2002,** 3, (6), 503-506.

25. Yang, P., Nanotechnology: Wires on water. *Nature* **2003,** 425, (6955), 243-244.

26. Whang, D.; Jin, S.; Wu, Y.; Lieber, C. M., Large-Scale Hierarchical Organization of Nanowire Arrays for Integrated Nanosystems. *Nano Letters* **2003,** 3, (9), 1255-1259.

27. Tao, A.; Kim, F.; Hess, C.; Goldberger, J.; He, R.; Sun, Y.; Xia, Y.; Yang, P., Langmuir-Blodgett Silver Nanowire Monolayers for Molecular Sensing Using Surface-Enhanced Raman Spectroscopy. *Nano Letters* **2003,** 3, (9), 1229-1233.

28. Pnueli, D.; Gutfinger, C., *Fluid Mechanics*. Cambridge University Press: Cambridge, 1992.

29. Archer, L. A.; Larson, R. G., A molecular theory of flow alignment and tumbling in sheared nematic liquid crystals. *The Journal of Chemical Physics* **1995,** 103, (8), 3108-3111.